pamir
Poverty Alleviation by Mitigation of Integrated High-mountain Risk

BOKU

High-mountain hazard and risk assessment in the Pamir

Austrian Development Agency

Martin Mergili
Wolfgang Straka
Fabian E. Gruber
Jean F. Schneider
and collaborators

Imprint

High-mountain hazard and risk assessment in the Pamir

Final report of IAG-BOKU within the project PAMIR

IAG-BOKU

Institute of Applied Geology, University of Natural Resources and Life Sciences (BOKU), Peter-Jordan-Strasse 70, A-1190 Vienna, Austria

PAMIR

Poverty Alleviation by Mitigation of Integrated high-mountain Risk

under the European Union's Thematic Programme for Environment and Sustainable Management of natural resources, including energy, funded by the European Union and the Austrian Development Agency (ADA)

Lead authors

Martin Mergili, Wolfgang Straka, Fabian E. Gruber, Jean F. Schneider

Collaborators

Ikramuddin Bahram, Gisela Domej, Anatoli Ischuk, Nikolai Ischuk, Stefan Koch, Johannes P. Müller, Mullosami Samiev, Kumriniso Sayfulloeva, Christine Schönberger, Abdurrashid Tagoybekov, Baktybek Usen-Uluu, Christoph Waldhör, Ahmad Zaripov, Rajabali Zaripov, Fabian Znojemsky

Vienna, June 2013

The rights for the work presented in Appendix 1 to Appendix 7 are not exclusively held by the authors. These parts may therefore not be reproduced. All other parts of the work may be reproduced as long as proper reference to this report is given.

Preface

The Pamir is a high-mountain area of particular beauty. More importantly, it provides the resources necessary for the livelihood of the people living there for centuries. The extreme relief in combination with a changing cryosphere and repeated seismic activity, however, leads to the occurrence of rapid mass movement processes putting the population at risk. Whilst the people have learned to live with the risk emanating from frequent processes such as local rock falls or debris flows, they are not prepared for rare or singular high-magnitude events starting in the distant headwaters of the valleys. Such events may eradicate entire villages as the 2002 Dasht disaster has dramatically shown. Also from a scientific point of view, the prediction of this type of events in space and time is extremely challenging. The huge extent of the area in combination with the limited resources hampers the implementation of broad-scale risk reduction strategies. A basis for the prioritization of target areas for such strategies is therefore needed.

The present report and the attached maps, on the one hand, shall be considered as a very first attempt to provide such a basis in a reproducible way. Those communities more at risk with regard to specific hazardous processes are distinguished from those less at risk. On the other hand, the report highlights observed and expected changes in the high-mountain environment possibly leading to changed hazard conditions in the future. It builds on one decade of research by IAG-BOKU in the Pamir, with previous reports submitted in 2004 and 2010.

The present report starts with an Executive summary putting together the key findings of the work. Further details are provided in eight appendices: Appendix 1 outlines the results of a number of case studies. Appendix 2 – Appendix 7 are scientific articles – most of them published in highly-ranked journals, some in conference proceedings – outlining the methods and results of the underlying research. Comprehensive hazard indication maps for the entire study area are compiled in Appendix 8.

This report, including all its parts, was prepared with the intention to be useful for the implementation of risk reduction strategies. However, the authors are well aware that it is far from being perfect or complete. It relies on incomplete knowledge and data as well as on a number of ad-hoc assumptions which may be true or not. The interpretation and implementation of the content has to take into account that this report provides a generalized and possibly distorted view of the reality. Whilst the authors welcome all types of comments, critics, suggestions or discussion, they strictly refuse any responsibility for loss of life or property, or any other detrimental effects, caused by action or non-action related to the content of the present report.

Martin Mergili, Wolfgang Straka, Fabian E. Gruber, Jean F. Schneider and collaborators

Vienna, June 2013

Contents

Executive summary

of the high-mountain hazard and risk assessment 9

Appendix 1

Case studies 19

Appendix 2

Regional-scale analysis of lake outburst hazards in the South-Western Pamir, Tajikistan, based on remote sensing and GIS 55

Appendix 3

Glacial Lake Outburst Floods in the Pamir of Tajikistan: challenges in prediction and modelling 83

Appendix 4

Changes of the cryosphere and related geohazards in the high-mountain areas of Tajikistan and Austria: a comparison 101

Appendix 5

Spatio-temporal development of high-mountain lakes in the headwaters of the Amu Darya River (Central Asia) 127

Appendix 6

Regional-scale analysis of high-mountain multi-hazard and risk in the Pamir (Tajikistan) with GRASS GIS 151

Appendix 7

Impact of large landslides, mitigation measures 187

Appendix 8

Hazard and risk indication maps 207

Executive summary

of the high-mountain hazard and risk assessment

1 Scope and objectives

A 98,300 km² study area is considered, extending from 1670 m a.s.l. near Khala-i-Khumb to 7495 m at the top of Ismoili Somoni Peak. The area corresponds to the headwaters of the Amu Darya River (Fig. 1). It is described in more detail in Appendix 6 and comprises most catchments leading to the 181 target communities of the PAMIR project (see Fig. 1). We define the scope of the present report as follows:

1. To highlight changes of the high-mountain environment in the past 45 years and to build scenarios for future changes. The findings are put in the context of related hazardous processes the magnitude or frequency of which may be influenced by these changes. Appendix 4 and Appendix 5 focus on high-mountain environmental changes with a focus on glaciers, permafrost and lakes.
2. To provide regional-scale hazard and risk indication maps for high-mountain geohazards for the entire 98,300 km² study area with the purpose of facilitating the prioritization of target areas for risk mitigation. Even though some of the areas are far away from the PAMIR target villages, travel distances may be large and villages far from the source areas are affected. However, as an additional service, all 528 communities identified in the study area are considered. The hazard and risk indication maps are compiled in Appendix 8. Appendix 6 describes the methodology in detail whilst Appendix 2 and Appendix 3 provide some additional information.
3. To investigate in more detail possibly hazardous situations in the vicinity of the target communities and to come up with recommendations on how to deal with these hazards. Appendix 1 accounts for this in detail whilst Appendix 7 puts it in a larger context.

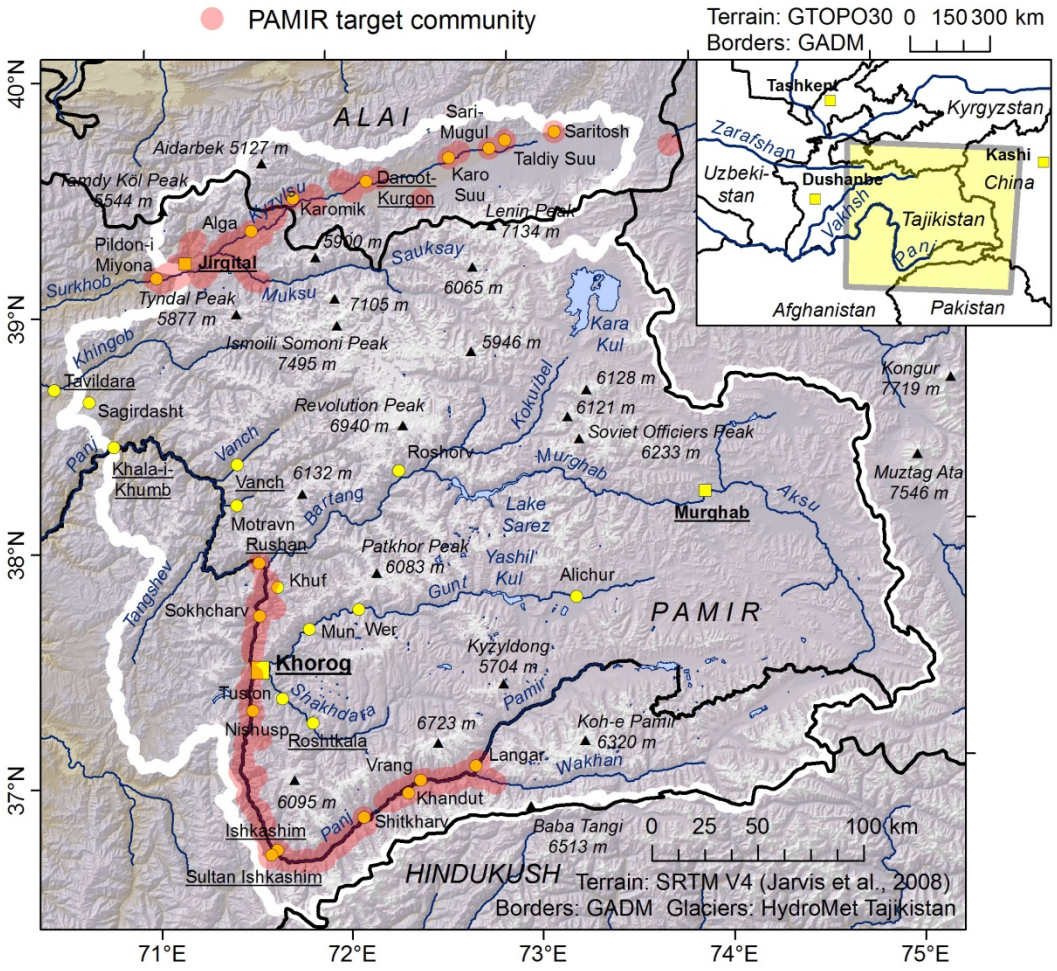

Fig. 1 Study area with PAMIR target communities.

The work presented here partly builds on the project Remote Geohazard Assessment in Tajikistan (TajHaz) carried out in 2009 and 2010. Even though the geographic focus was slightly different, some aspects also relevant here are outlined in more detail in the TajHaz final report (Schneider and Mergili, 2010).

Schneider, J.F., Mergili, M., et al., 2010. Remote Geohazards in High Mountain Areas of Tajikistan - Assessment of hazards connected to lake outburst floods and large landslide dams in selected areas of the Pamir and Alai mountains. FOCUS Humanitarian Assistance. 342 pp.

2 High-mountain environmental change

Besides a review of the available literature, multi-temporal remote sensing surveys of glaciers and glacial lakes as well as additional helicopter and field surveys were conducted. In addition, potential permafrost distribution maps for the present and the future were produced by adapting an empirical model developed in Switzerland. The scope, methods and results of these studies are compiled and discussed in Appendix 4 and Appendix 5.

The abundance of potential permafrost areas in the GBAO – particularly in the highlands of the eastern Pamir – leads to a tremendous potential loss in terms of absolute values, aggregating to roughly 20,000 km² in the case of a 4°C temperature increase (a realistic scenario for the year 2100). This value would, however, correspond to only 40% of the potential permafrost area of

the GBAO. Melting of permafrost on steep rock or debris slopes may increase the susceptibility to associated mass movement processes such as rock-ice avalanches or periglacial debris flows (see Appendix 4 and Appendix 6).

The observed retreat of the glaciers has led to the formation of numerous new glacial lakes. Other lakes in the area are embedded in older glacial landscapes (erosion lakes) or impounded behind block or debris dams (e.g., Lake Sarez). 1642 lakes are mapped in total, 652 out of them are glacial lakes. 73% of all lakes are located above 4000 m a.s.l. Glacial lakes, abundant in those areas where glacier tongues retreat over flat or moderately steep terrain, have experienced a significant growth, even though changes are often superimposed by short-term fluctuations. The analysis results also indicate a shifting of the growth of glacial lakes from the south western Pamir to the central and northern Pamir during the observation period. This trend is most likely associated with more elevated contribution areas in the central and northern Pamir. The lakes of the other types have remained constant in size in general (see Appendix 5). The dynamics of glacial and non-glacial lakes in combination with glacier and permafrost retreat substantially influences the susceptibility to sudden drainage and consequent lake outburst floods (see Appendix 2, Appendix 3 and Appendix 6).

3 Regional-scale patterns of hazard and risk

3.1 Methodology

A model framework relying on expert knowledge and empirical equations is used to derive the hazard and risk with regard to four types of high-mountain processes:

1. Rock slides – here, the term is understood in a broad sense also including rock falls, rock avalanches and rock-ice avalanches
2. Ice avalanches
3. Periglacial debris flows
4. Lake outburst floods

Process interactions are included as far as possible. The model framework, which is only suitable for the regional scale and not for in-detail studies, is described in detail in Appendix 6. It results in hazard and risk indication maps for the entire 98,300 km² study area. The maps for all four process types are compiled in Appendix 8. Besides the raster cell- or object-based delineation of possible source areas (susceptibility and hazard) and the raster-cell based identification of possible impact areas (impact hazard), each of the 528 communities is assigned a community risk indication score, derived from the impact hazard and the land use (see Appendix 6 and Appendix 8).

3.2 Results

The model results indicate that the total area with significant periglacial debris flow (PF) susceptibility/hazard is much larger than those for the other hazard types: 9.9% of the entire study area are designated as possible PF source areas. 42.7% out of this area are assigned the three higher susceptibility scores 4–6. This pattern indicates the ubiquity of hazardous areas on the one hand, but also the limited means of a sharper delineation on the other hand. In contrast,

the ice avalanche (IA) susceptibility and the lake outburst (LO) susceptibility are constrained in a much sharper way. 1.6% of the total study area are identified as susceptible to IA, 64.5% out of this area are assigned the susceptibility scores 4–6. 70.9% of all lakes are assigned susceptibility scores >0, 50.0% of these lakes the susceptibility scores 4–6. The rock slide (RS) susceptibility displays intermediate patterns in terms of the total area identified as susceptible (4.7% of the total study area). 16.2% of this area – a much lower value than those associated with the other process types – are assigned the susceptibility scores 4–6. The reason for this phenomenon is the limited area occupied by very steep slopes.

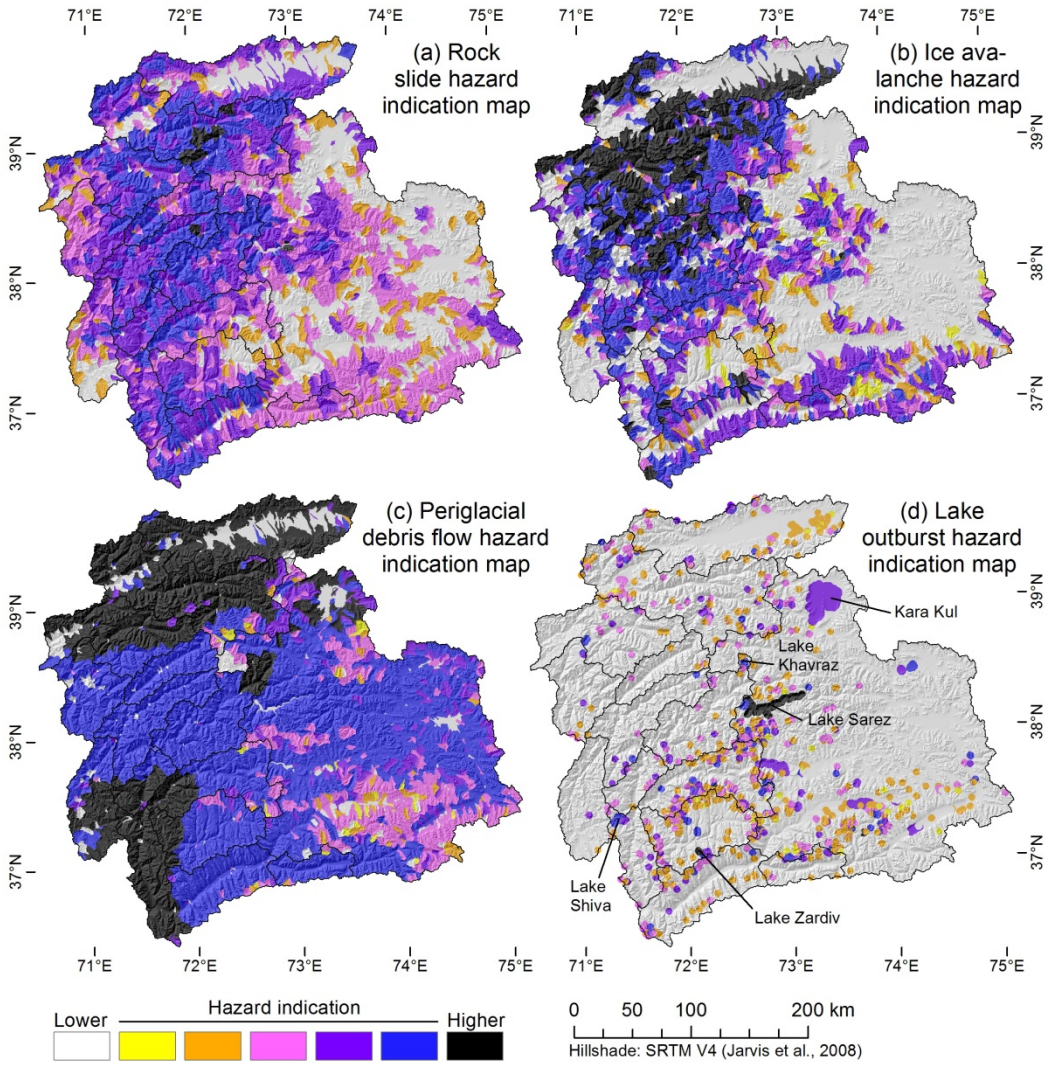

Fig. 2 Distribution of (a) rock slide, (b) ice avalanche, (c) periglacial debris flow and (d) lake outburst hazard indication over the entire study area. The maximum score is shown for each catchment.

The distribution of the raster cells or lakes identified as susceptible among the six hazard indication score classes depends on the susceptibility and the possible process magnitude. 38.1% of the RS and 68.4% of the IA are assigned the hazard indication scores 4–6. Comparatively few lakes (23.9%) are assigned the LO hazard indication scores 4–6. This phenomenon is explained by the large number of rather small but highly susceptible lakes.

Fig. 2 represents the hazard indication scores for each process type broken down to the level of small catchments. The maximum out of all raster cell-based hazard indication scores is shown for each catchment, except for the LO hazard where the value assigned to each lake is illustrated.

As expected, the RS hazard (see Fig. 2a) is highest in areas with a particularly steep topography in the northern and central Pamir. More localized high-hazard areas are distributed throughout the study area. The IA hazard (see Fig. 2b) is high in most glaciated areas, particularly in parts of the northern Pamir where large portions of steep glaciers are extremely abundant. Within these zones the inter-catchment differentiation of hazardous areas is rather poor.

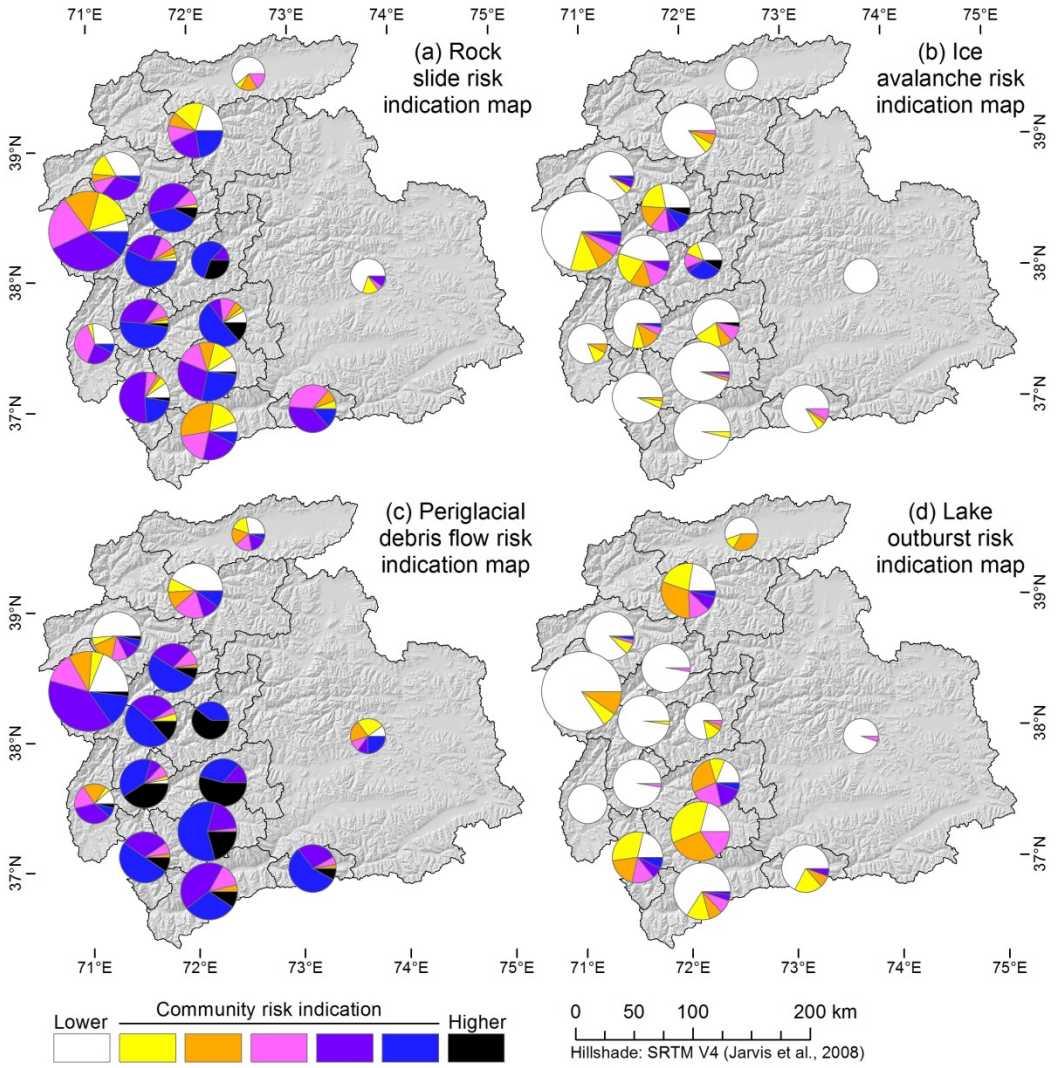

Fig. 3 Community risk indication map, generalized to 15 regions. For each region, the pie chart illustrates the relative abundance of the different community risk indication scores. The size of each chart is proportional to the number of communities it represents.

The PF hazard is poorly differentiated at the catchment scale: steep slopes near the permafrost boundary are almost ubiquitous in the study area, except for the elevated and comparatively gently inclined south eastern portion. The most notable regional pattern is therefore attributed to the seismic susceptibility. The patterns observed in Fig. 2c are further a consequence of the limited input information that can be reasonably applied at the regional scale. With regard to the LO hazard, the details concerning specific lakes are further discussed in Appendix 6. However,

the comparatively high hazard indication score of Kara Kul – where a closer look reveals no significant outburst hazard – suggests that the approach used tends to overestimate the hazard for large lakes.

The distribution of community risk over the study area reflects the patterns shown in Fig. 2 on the one hand and the distribution of the exposed communities on the other hand. Fig. 3 illustrates the relative frequency of the community risk indication score classes for 15 regions within the study area, each of them representing a catchment or section of a catchment. The eastern Pamir is considered as one single region due to the low number of communities there. Except for the very western part of the study area, the eastern Pamir and the Kyrgyz part of the study area (Chan-Alai Valley) in the north, all regions are dominated by communities with a significant rock slide risk, the highest scores are observed for the villages in the rugged Bartang and middle Panj valleys as well as in the Gunt Valley (see Fig. 3a). The hot spots of ice avalanche risk are identified in the Vanch and Bartang valleys, both deeply incised into glaciated mountain ranges (see Fig. 3b). This type of risk plays a less prominent role in the other regions. Also the risk of periglacial debris flows is highest in the deep gorges of the western Pamir, decreasing towards north where permafrost is less abundant (see Fig. 3c). However, the model predicts a significant PF risk for most communities throughout the study area. This is not the case for the risk caused by lake outburst floods, which is significant mainly in the south western Pamir and in part of the northern Pamir (see Fig. 3d). The LO community risk indication score $CR_{lo} = 6$ is not assigned to any village. Table 1 summarizes the relative frequency of villages assigned to each class with respect to all four hazard types.

Table 1 Per cent of communities assigned to each class of the community risk indication score. RS = rock slides, IA = ice avalanches, PF = periglacial debris flows, LO = lake outburst floods.

Process type	Community risk indication score						
	0	1	2	3	4	5	6
RS	12.1%	9.7%	8.6%	15.3%	27.5%	23.9%	2.9%
IA	75.2%	8.9%	5.7%	4.8%	2.2%	2.4%	0.8%
PF	11.5%	3.7%	6.1%	9.2%	24.4%	31.4%	13.9%
LO	65.6%	12.3%	11.6%	6.2%	2.9%	1.4%	0.0%

3.3 Scope and limitations of the regional-scale hazard and risk analysis results

The purpose of the regional-scale investigation presented above is to provide a reproducible basis for the prioritization of areas and communities where targeted hazard and risk assessment studies as well as monitoring, awareness-building and preparedness-raising at the community scale are required. Consequently, the maps shown in Fig. 2 and Fig. 3 as well as those provided in Appendix 8 may not be used as basis for more far-reaching measures and may not be seen as definite hazard and risk maps, but rather as **conceptual hazard and risk indication maps**. The hazard and risk indication score classes are therefore not given definite names such as *Moderate hazard*, *Extremely high risk* etc. but instead have to be interpreted in a relative context. Further, the

interpretation of the model results on the basis of raster cells is appropriate for scientific discussion, but not for the design of risk mitigation measures. Here the scale of communities, catchments or even regions is much more suitable. The interpretation of the model results has to take into account the characteristics of the scoring schemes as well as the limitations of the input data and the methodology used (see Appendix 6 for details).

Due to the design of the model, not all areas or villages with high hazard or risk scores are necessarily at hazard or at risk as not all of the key factors are included in the model. Consequently, the maps in Appendix 8 provide an idea about what can happen under the assumptions taken, but not about what will happen. On the other hand, also areas with low scores may be affected by hazardous processes as a consequence of deficiencies of the model framework. Processes such as non-periglacial debris flows, ordinary floods or landslides/rock slides starting from areas with a slope angle <45° are not considered. Next, the model is not suitable for the motion of outburst floods from large lakes, therefore the impact hazard and the community risk associated to such lakes may be underestimated (e.g., Lake Sarez or Rivakkul). Further, some types of process interactions are out of scope of the present study, such as the damming of lakes by mass movements and subsequent rapid drainage. The same is true for the entrainment of debris, modelling of which remains a challenge particularly at the scale of the present study. Finally, the approach used does not allow for an analytical overlay of the susceptibility, hazard, impact hazard and risk indication scores associated to each process type (see Appendix 6).

4 Case studies

Based on preliminary work and helicopter reconnaissance, ten areas of special interest were selected to be studies in the field by task forces selected among the collaborators and typically having four members each. Locations and names of these localities are presented by Fig. 1, Appendix 1. The findings of the field surveys, in turn, suggested the following six sites to merit detailed presentation (sections of Appendix 1 in parentheses): Tusion (Section 3), Lake Shiva (Section 4), Garm-chashma (Section 5), Dasht-sulaymon (Section 6), Shidz (Section 7), and Karomik (Section 8). These sites can represent the range of hazard types encountered. Four of the sites pose a certain degree of hazard to traffic or communities at present. The remaining two, namely Shidz and Dasht-sulaymon, were studied for magnitude of the prehistoric events observed there as well as the possibility to learn about the factors responsible, which are certainly no less effective today as they were in the past.

Basically there are three main reasons for the problems or potential problems identified (the sections refer to Appendix 1):

1. Tectonic forces, further explained in the introduction to Appendix 1, which create extreme topography with very steep slopes and deep undercutting by the rivers, as well as intense fracturing of rocks, and earthquakes. Certain geologic formations, e.g. slates and schists, which are easily weathered and frost-shattered or may have a downslope dip, are also important to take account of. The interplay of these factors are well illustrated by the sites of Karomik (a creeping to slowly flowing slope in disintegrated

schists; Section 8), and Dasht-sulaymon (a prehistoric rock avalanche of major proportions, originating in frost-shattered slates; Section 6).

2. Late Glacial ice retreat and "paraglacial" adjustment of the formerly glaciated landscape to Holocene conditions, which is not entirely completed in all places. Large accumulations of glacial and ice-marginal deposits, but also frost-shattered residual rocks, which had not been buried by the ice, and landslides on slopes relieved of ice-pressure and permafrost play the major part here, as exemplified by Tusion (Section 3). In the case of Lake Shiva (Section 4), despite the paraglacial process having attained closure by now, the combined moraine and landslide body damming up the lake is being affected by retrograde erosion, which may merit concern for the future. Shidz (Section 7) turned out to be of entirely glacial, contrary to a landslide, origin, and nicely illustrates the problems of distinction encountered by researchers when trying to classify events on the basis of limited information (without ground check).
3. Glacial retreat, currently enhanced by the well-known warming spell in Holocene climate evolution. The most tricky problem in this regard is to prognosticate the behaviour of glacial lakes being dammed up by till or ice-marginal sediments probably still intercalated with dead ice bodies, often buried by these sediments and not readily visible. Although it is possible to infer the presence of dead ice from geophysical data, there is no theoretically valid model describing the behaviour of such rock-ice masses. As a field example, we describe the glacial lake in the headwaters of Garm-chashma (Section 5).

As will become clear from the presentations in Appendix 1, in all the described instances, direct constructive measures to alleviate the hazard and by implication the risk are not available. Practical options are (a) risk avoidance, i.e. altering the course of a road or prohibiting housing development in certain areas, and (b) understanding the mechanism which is affecting a defined or suspected hazardous site, and monitoring by (visual or instrumental) observation any change that may signify an evolution of site behavior to the worse.

5 Conclusions and recommendations

The decision on suitable hazard mitigation strategies shall be founded on the following three statements:

1. The study area is large and many areas are at risk of high-mountain geohazard processes. Whilst, within the project, it was possible to distinguish those areas more hazardous/risky with regard to specific processes than others (see Appendix 6 and Appendix 8), the available data does not allow to predict where and when geohazard processes will happen and which areas/communities exactly they will affect.
2. No extremely hazardous situation calling for immediate drastic action – such as evacuation or resettlement – was detected. However, this situation is subject to change and possibly hazardous situations have to be monitored at regular intervals.
3. Due to the limited resources available in the study area and the high magnitude of the processes in discussion, technical measures towards reducing the hazard can only be

realized for specific cases. Instead, cost-efficient risk mitigation strategies directed towards the reduction of exposure and vulnerability should therefore be prioritized.

A combination of broad-scale hazard mitigation strategies is therefore recommended, focusing on the following three points:

1. Improving the awareness of the population by targeted workshops. Further, the curricula of the schools should pay appropriate attention to awareness-building with regard to geohazards.
2. Improving the preparedness of the communities. This includes the ability to correctly interpret warning signals and the knowledge on how to react in an appropriate way (e.g., the identification of safe places). Also here, workshops and the curricula of the schools are considered the most important instruments.
3. Installation of simple, easy to maintain emergency warning systems at selected sites.
4. Further strengthening of the organisational structures allowing for an appropriate response to emergency situations (see Appendix 7 for case studies regarding lakes formed by large landslides).

These activities shall be focused on the communities with higher risk indication scores (see Appendix 8). Further it is highly recommended to initiate and continue activities towards an improved knowledge on the high-mountain environment and its changes (see Appendix 4 and Appendix 5) such as:

1. Proper maintenance of existing and installation of additional meteorological and hydrological stations.
2. Regular monitoring of glacier fluctuations, the development of high-mountain lakes and permafrost.
3. Systematic study of sites known or suspected to be a source of risk to be avoided, in order to understand the responsible natural mechanisms and man-made factors (the national institutions capable of doing this are there), and regular visual or instrumental inspection to keep track of any evolution to the worse (not only man-made factors, but also natural mechanisms can change).

All these activities have to be carried out in a participative way, handing over part of the responsibility to the possibly affected communities. For this purpose we recommend to prepare a comprehensive brochure on how to recognize and to monitor possibly hazardous situations, how to interpret warning signals, how to prepare for hazardous events and how to react in case. This brochure should be distributed in the communities and – particularly – in the schools.

Appendix 1

1 Regional Geology

The Pamirs owe their present existence as a high mountain range to the collision of the Indian subcontinent with the Eurasian Plate and subsequent uplift, beginning ca. 50 million years ago (my). However, several tectonic zones and mountain ranges (Tian-shan, Altai, Kunlun-shan), including the High Pamirs, were originally formed as continental fragments accreted to the Siberian Shield during older collisional episodes, and only the Himalayas can been seen as a direct result of the latest plate collision.

Since the end of the Cretaceous, about 65 my ago, convergence between the Indian and Eurasian Plate has lead to north-directed subduction of the Tethys Ocean formerly separating the two continents, until the continents collided. Giant "rock slabs" were piled on top of each other and thereby attained, in addition, a complicated internal structure. The crust was thickened in the process, its lower parts subjected to medium- to high-grade metamorphism (gneiss, schist, quartzite, marble), as well as intruded by granitoid and some basaltic magmas (granite, diorite, gabbro). At last, the thickened crust was isostatically uplifted and the topmost parts (above sea level) dissected by erosion, to create the high mountain topography presently evident.

In case of the Pamirs, this extreme topography is in large part due to a right hand rotational trend of India during collision, thereby inducing the north-western part of the Indian Plate to act as a rigid indenter against the substructure of the Tarim and Tajik basins to the north, and even inducing south-directed continental subduction at the northern margin of the compressed area. Fig. 1and Fig. 2 illustrate the large-scale tectonic situation; further details can be found in Khain (1994) and Searle (2008).

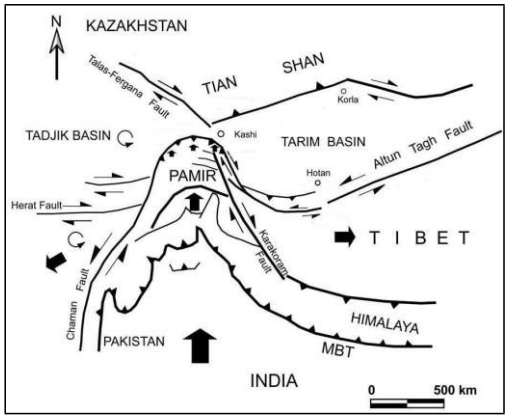

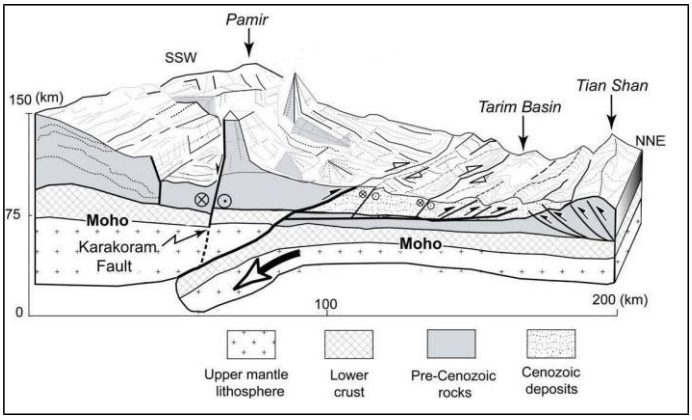

Fig. 1 (left): Plate tectonic setting of the Pamirs.

Fig. 2 (right): Structural tectonic interpretation to the north of the Pamirs.

Recent GPS data show a convergence rate between the Indian and the Eurasian Plate of 5–7 cm per year. In the Tajik Tian-shan, even 20 mm of shortening on the same timescale is reported (Searle, 2008). Uplift rates are higher than erosion rates, resulting in a net uplift on the order of 2.5–3.0 mm per year. Obviously, collision, crustal thickening, and uplift and topographic

steepening are still ongoing, which explains much of the slope instability prevalent, and in many places visible, throughout the investigated area.

Also, the High Pamirs and Hindu-kush are regions of deep earthquake activity (60–300 km acc. to Kondorskaja and Shebalin, 1977). Both the Tajik Basin to the west and the Tarim Basin to the east are seismically rather inactive, by comparison, but nevertheless transfer stress. The Pamir subduction Zone in the north (tangential to the Northern Pamirs, where it borders on the Tajik Depression) dips south and generates earthquakes of up to ca. 180 km of hypocentral depth. The Hindu-kush Zone in the south (around the Southern Pamirs and Hindu-kush) dips north and generates earthquakes of up to >250 km depth, thereby constituting the deepest-reaching continental seismic zone (Searle, 2008). Both subduction slabs seem to merge at depth, so that the big picture may be one of a crustal wedge pointing downward and receiving pressure from both sides (north and south), therefore rising upwards.

For a more detailed account of the seismic hazard in the study area please consult the report of the TajHaz project (Schneider and Mergili, 2010).

The High Pamirs can be subdivided into six tectonic zones (mainly acc. to Rukhentsev and Shvolman, 1982), which differ from commonly applied geographical zonation (cf. Fig. 3):

I	Darvaz/Trans-Alai (extern.)	IV	Rushan Zone
II	Northern Pamir	V	South-eastern Pamir
III	Central Pamir	VI	South-western Pamir

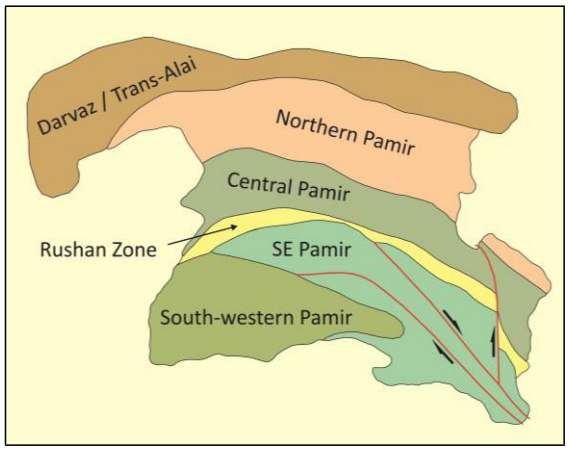

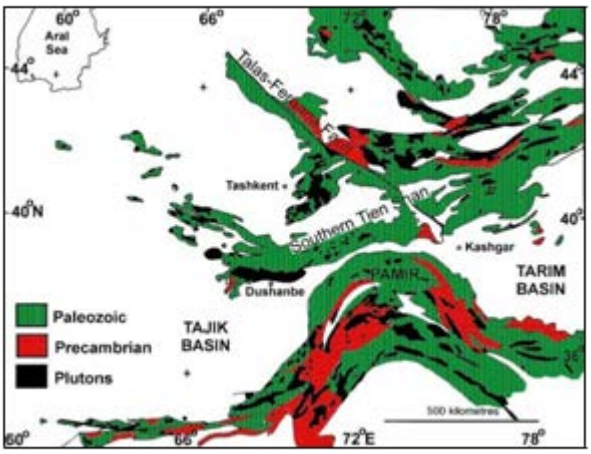

Fig. 3 (left): Geotectonic zonation of the Tajik High Pamirs.

Fig. 4 (right): Distribution of Paleozoic, Precambrian and plutonic rocks.

Details on the various tectonic zones are available, for example, in Khain (1994). The majority of sites chosen for field survey are within the South-western Pamir; the two described last (Shidz and Karomik) are located in the Central and Northern Pamir, respectively. The differences are subtle and mostly not relevant to this study. What is generally conspicuous is the abundance of Precambrian crystalline basement, Paleozoic originally sedimentary rocks in various stages of

metamorphism, and plutonic rocks with contact-metamorphic belts around them. This is illustrated by Fig. 4 (modified from Brookfield, 2000).

The Precambrian core complex dates back to the Archean era, 2700–2400 my (Karapetov, 1975). Gneiss, schist, and minor amphibolite, quartzite, etc. are in high-grade metamorphic state (up to granulite facies), and partly migmatized (beginning melt generation). A Proterozoic sequence, consisting mainly of paragneiss, amphibolitic schist and quartzite, lies on top, with metamorphic grade becoming less bottom-up. Structurally, this whole complex is characterized by granite-gneiss doming (later intrusions, still later metamorphized) and meridional folding (lateral squeezing). Mesozoic and Cenozoic granitoid plutons are widespread, the latest dating from the Miocene (20–15 my).

The core complex is transgressively covered by upper Paleozoic terrigeneous sedimentary rocks (Slavin, 1976), Mesozoic rocks are also to be found in places, but the only non-metamorphic sedimentary rocks to take into account in the present context are Quaternary (glacial) till and Holocene slope deposits (incl. rock glacier and slide masses). They are described in more detail in the following chapters.

2 Selection of case studies

Based on preliminary studies and helicopter reconnaissance, several areas were chosen for field survey, to be executed by teams of typically four persons. The selected areas, which are indicated as yellow blobs in Fig. 5, were studied in more or less detail, depending on time constraints, accessibility and available methods.

Not all of the sites offered insight significant enough to be presented here in some detail, but those which did are treated in the following chapters. These are the sites of Tusion (Chapter A1.1), Lake Shiva (A1.2), Garm-chashma (A1.3), Dasht-sulaymon (A1.4), Shidz (A1.5), and Karomik (A1.6).

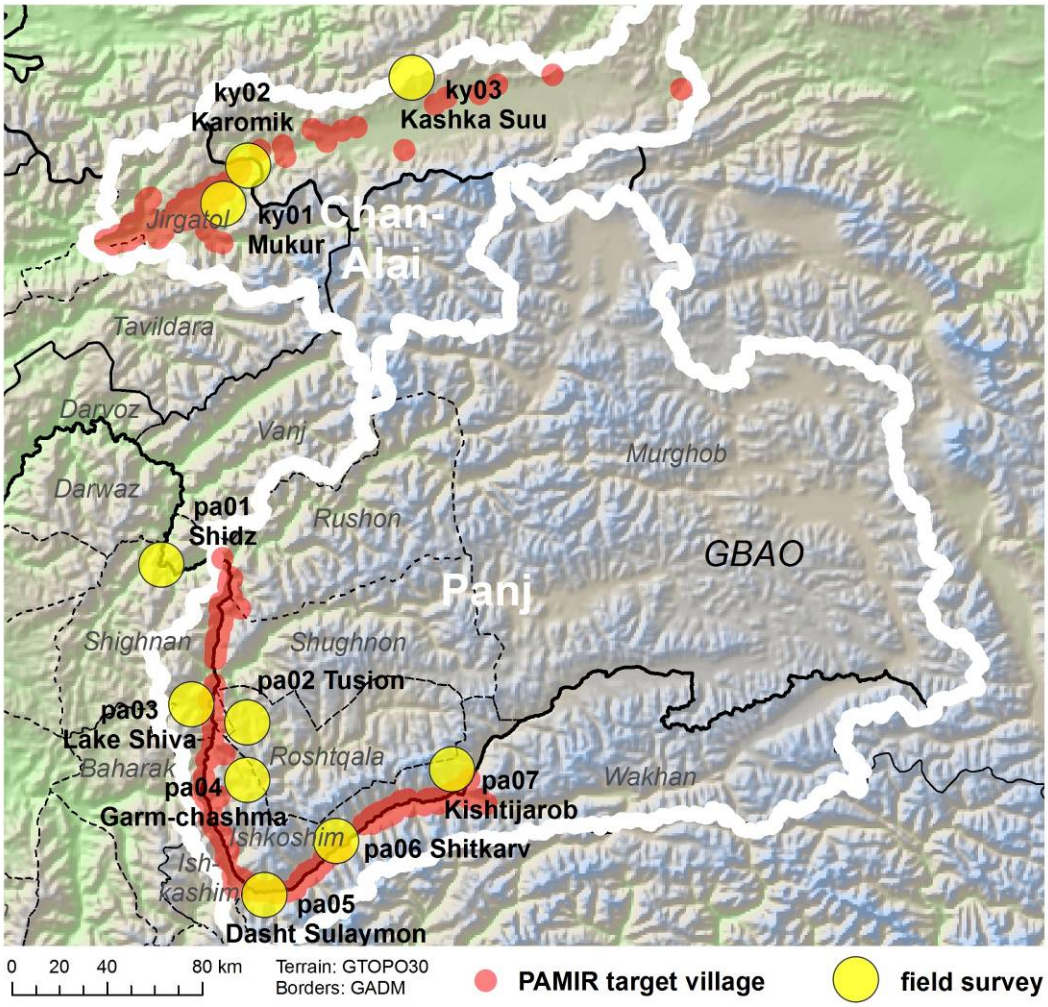

Fig. 5: Study areas surveyed in the field in detail.

3 Tusion

3.1 General information

The village of Tusion is located at the western side of the Sharfdara Valley immediately upstream of its confluence with the Shakhdara Valley. The Shakhdara is the main river and catchment in Rostqala subdistrict of GBAO, and the Sharfdara is a left-hand tributary of it. The mouth of the tributary steeply slopes into the main valley, over an altitude differential of 100–150 m, and thereby enters in the way of a glacial perched valley. (The only access road to the village of Tusion winds up over this topographic step.) The water sources feeding the Sharfdara are glaciers and glacial lakes in the far back catchment area. There, four glacial lakes have been detected by remote sensing. The average slope of the river profile between these lakes and the Sharfdara river mouth is 4–5° (Schneider et al., 2004).

Tusion includes five village parts (Delokh, Lakhshik, Langar, Namadrosh, and Shosh), ranging between 2500 and 2800 m a.s.l. Of these, three parts are currently affected by landslides, namely Delokh, Shosh, and Lakhshik. Fig. 6 illustrates this scenery.

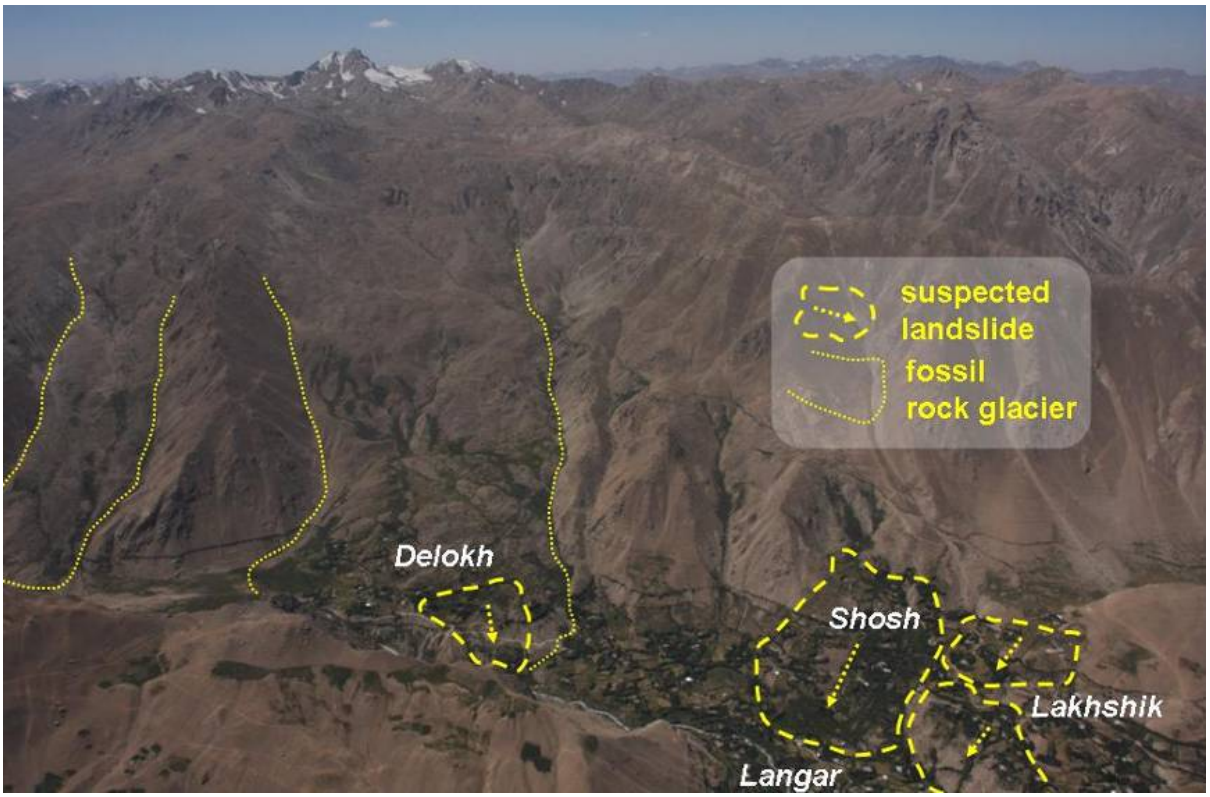

Fig. 6: Helicopter view of the village of Tusion with location of fossil rock glaciers and suspected landslides, based on first results from helicopter reconnaissance.

3.2 Geological situation

Geologic maps show the Sharfdara Valley embedded in a late Jurassic to early Cretaceous intrusive complex, the Pamir-Shugnan Complex. The dominant lithology is granitic (S-granite containing both of the common micas, biotite as well as muscovite, and leuco-granite). Some of

the magmatic rocks are criss-crossed by aplitic and pegmatitic veins. In the upper course of the Sharfdara rocks are originally sedimentary and have been subjected to greenschist facies metamorphosis. Paragneiss and calcitic to dolomitic slates dominate. Two details from available geological maps are shown in Fig. 7 and A8 below.

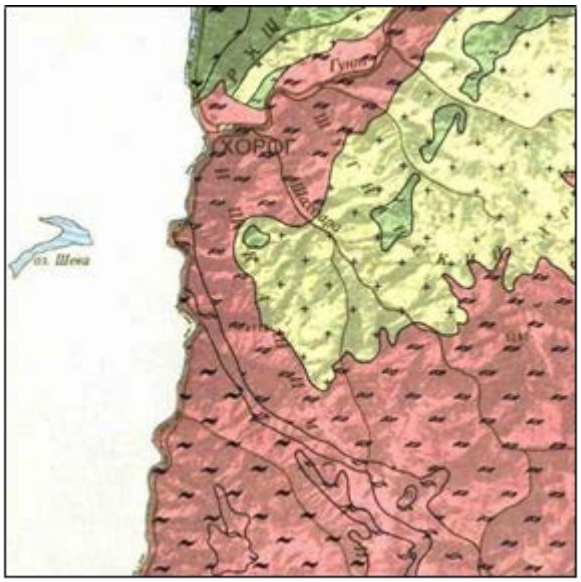

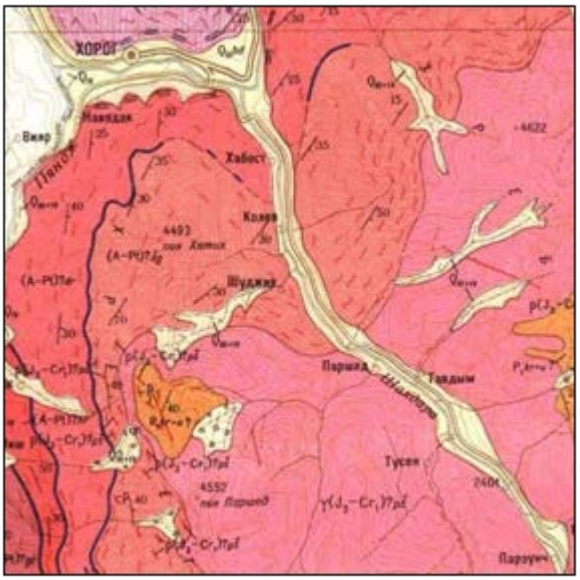

Fig. 7 (left): Geologic map of the region southeast of Khorog, with Tusion in the center of the picture, showing the granitic core complex (++) and greenschist facies metamorphic cover sequences (~~).

Fig. 8 (right): Geologic map of the area around the Shakhdara lower reaches (Tusion near the lower right), with Jurassic to early Cretaceous granitic plutons shown in pink ($\gamma(J_3\text{-}Cr_1)$).

Quaternary deposits are of upper Pleistocene to Holocene origin. In Fig. 9 the inferred extent of Middle and Late Quaternary ice covers are indicated by green and violet lines, respectively. It is obvious that the Middle Quaternary glaciation is thought to have been more extensive than the Late Quaternary one, however, both are shown to be restricted to the topographic depressions, essentially just filling up the valleys. Strangely, in the Shakhdara main valley no glaciation is indicated by available Quaternary geological maps. Probably more realistic is a scenario as presented later (Fig. 13).

The reddish areas in Fig. 9 indicate Late Pleistocene and Holocene soft rocks, which on the basis of our field survey are interpreted as frost-shattered or otherwise decomposed residual rock, Late Glacial ice marginal sediments and rock glaciers, often relocated and interfingering because of downslope creep and sliding (in Russian terminology eluvial, diluvial and colluvial). Major tectonic discontinuities, one of which is assumed to pass through Tusion (cf. Fig. 10), could not be verified because of the extensive Quaternary and residual sediment cover.

As most of the slope material is quite loose and disconnected, the occurrence of landslides in not only very likely but also frequent. The regional extent of known gravitational slope movements is illustrated by Fig. 11. In the lower Sharfdara Valley two areas are of interest: A big landslide in Delokh and another one of complex genesis in the area of Shosh and Lakhshik, which should be subdivided into two or three distinct creep or slide masses as already indicated in Fig. 6.

Another possible hazard is debris flows, but they are comparatively rare in the Sharfdara, and occur only after rapid snowmelt in the far back of the catchment, mostly between May and July

(cf. Fig. 12). Water that does not leave the catchment via river drainage is either stored as ice in the high mountains or in fractured groundwater aquifers. Rising groundwater within slopes may be a factor periodically weakening cohesion of the soft rock cover, especially where fine-grained glacial deposits are affected, thereby contributing to creep and sliding. For lack of long-term data on slope movements, there was no way to verify this idea in the present context.

Fig. 9 (left): Present glacial (light blue) and Quaternary deposits around Tusion, Upper Pleistocene (light grey, gIII) and Upper Pleistocene to Holocene (reddish brown, cIII+IV).

Fig. 10 (right): Engineering geological map showing clastic and residual rock material (green and brown) within crystalline rocks (red), red lines delineate major discontinuities.

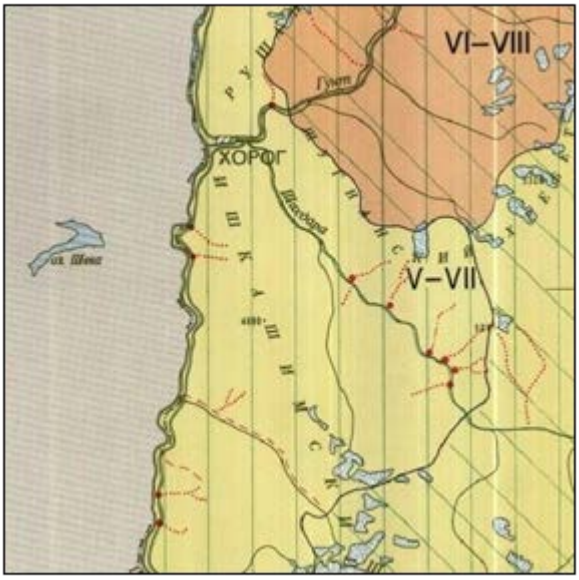

Fig. 11 (left): Landslide indication map showing known areas of gravitational slope deformation (continuous red lines) and such areas of mixed genesis (dashed red lines).

Fig. 12 (right): Survey map of known debris flow hazard, with areas moderately endangered by debris flows after rapid snowmelt (mostly between May and July) shown in yellow.

3.3 Soft rock cover and landslides

Part of the area is covered by till. Its origin is certainly due, for the most part, to the Last Glacial ice cover and Late Glacial retreat. The extent of Last Glacial Maximum ice, inferred from till distribution and morphological features (roche moutonnée and similar), is illustrated in Fig. 13.

Fig. 13: Inferred ice cover in the valleys of the Shakhdara (main valley), the Sharfdara (upper left tributary), and the Khidorjevdara (upper right tributary). The site of Tusion is left of center.

As the visible morphological effects of glaciation are of an erosive nature, (over-consolidated) basal till was expected to be of minor significance, and no such deposits were actually found. By implication, almost all glacial sediments in the area should be of ice marginal origin or have been deposited by ablation. The bulk of the soft rock cover seems to have been of local origin, that is, shattered or decomposed rock mass entrained by the moving ice or accumulating at its margins. After ice retreat the residual slope materials and loose sediment cover, having been relieved from the ice pressure, began to move into a more stable position (a kind of landscape adjustment also called paraglacial). The process is largely, but not entirely completed.

In the southern part of Tusion, two masses of residual rock exist, the origin of which is not entirely clear (see Fig. 6, left side). The most likely hypothesis is that they represent fossil rock glaciers: When the glaciers retreated from the area at the end of the last ice age, the ice-bearing till could have mobilized and formed these rock glaciers, which are certainly not active any more. The village part of Delokh is situated in the very lower portion of the presumed northern rock glacier.

Another option we cannot ignore is that of a landslide origin of the mass, which then should have dammed up the river for a period of time. While, on the one hand, we did not find

indication of any upstream lake deposits, on the other hand the presence of much fine-grained material within the Delokh displaced rock mass could speak against the rock glacier hypothesis, on the grounds that the fines should have been largely washed away at melt-out.

There is no indication that these entire masses are still moving. However, in past decades more localized mass movements have occurred in Delokh and also in the village parts of Shosh and Lakhshik, all of them in residual rock, originally composed of till and the rock glacier mentioned above. Therefore, these three areas were investigated in more detail. The situation as we see it, based on the field survey, is illustrated by Fig. 14.

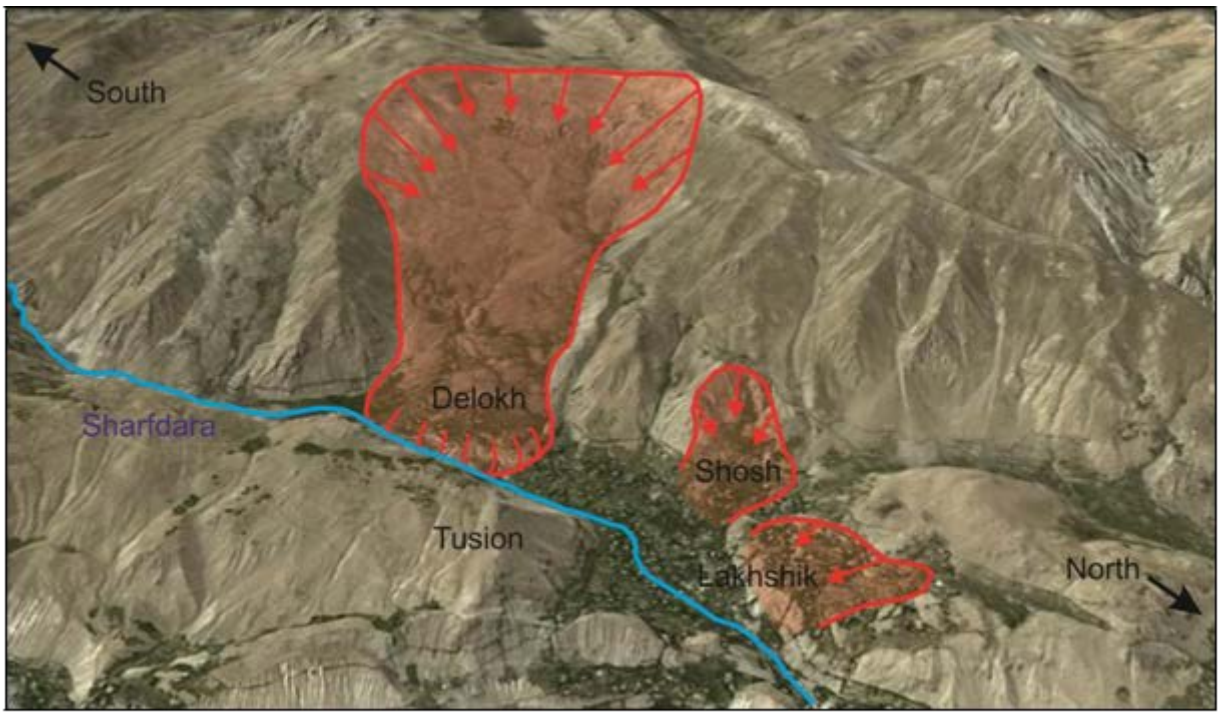

Fig. 14: Graphic overview, based on a Google Earth image, of the three investigated areas of rock mass instability, Delokh, Lakhshik, and Shosh.

The sliding planes of the present landslides are suspected at depths of ca. 10 m and more. The movements do not occur suddenly, but slowly and unevenly, possibly stepwise, over long periods of time. Therefore, people are not immediately at risk, but the movements do result at last in the damage, some of it profound, of buildings, infrastructures and agricultural areas. Part of these movements, to be sure, can be attributed to leaking irrigation channels altering the water budget of slopes.

FOCUS Humanitarian Assistance has carried out investigations and mitigation works during the last ten years, particularly regarding a better maintenance of the irrigation channels, so that the situation has improved. However, the general situation is not yet really understood, and the question whether and how reactivations could occur has not answered in a satisfactory manner.

3.4 Geophysical survey

In summer 2011, geophysical surveys were carried out by the PAMIR project team, in order to get a better understanding of the internal structure of the slope, in particular with respect to the sliding planes, and thereby also to better understand the slope mechanisms and options for appropriate mitigation strategies.

The applied method was a combined refraction seismic and geo-electric profiling campaign in the village parts of Delokh, Shosh, Lakhshik and Langar. The layout spreads are indicated in **Fig. 15**. The methodology was a robust engineering approach, and is described in great detail, including theory, data gathering, processing, and interpretation, by Domej (2012).

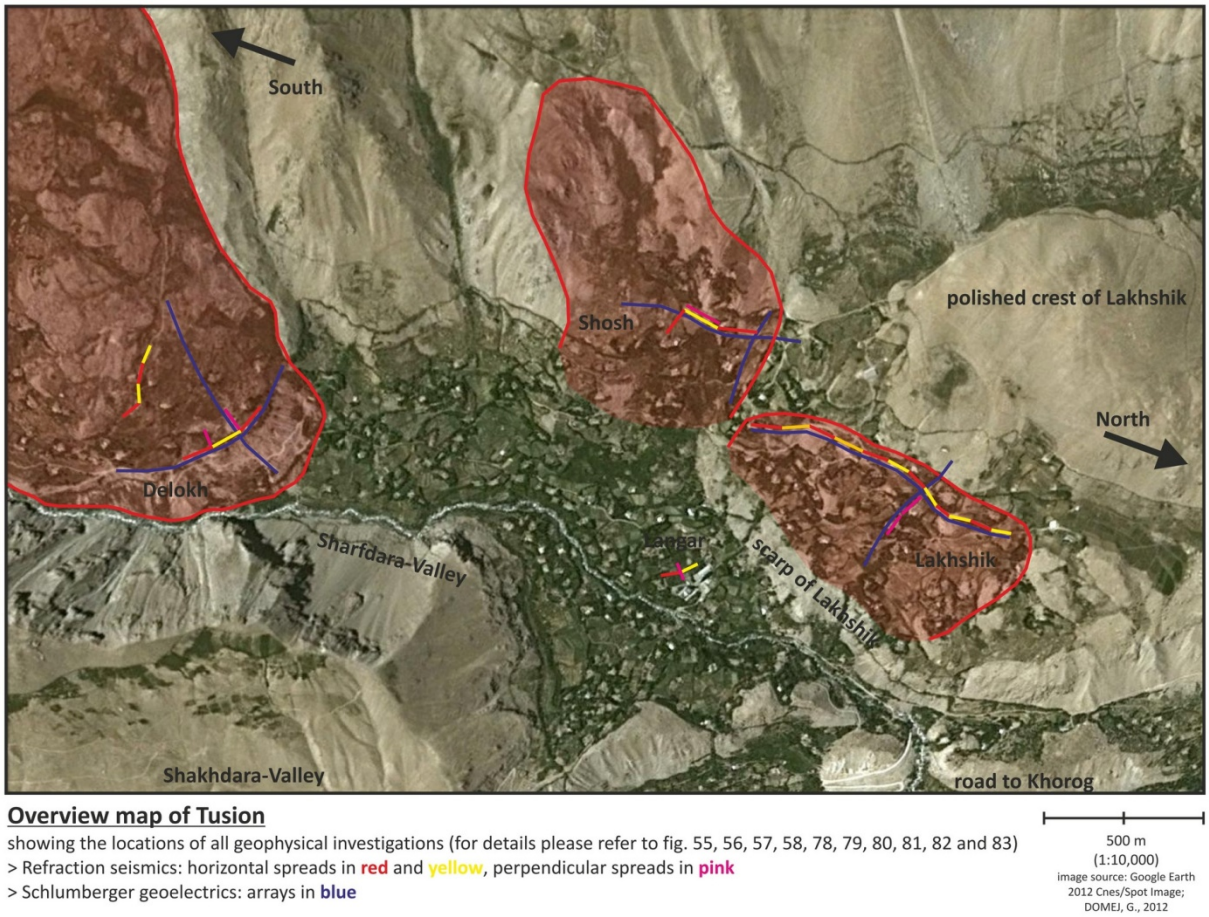

Fig. 15: Geophysical profiling spreads, superimposed on a Google Earth image with the three displaced rock masses indicated as red areas.

It became possible to gain some insight into the underground structure and the properties of the displaced rock masses at the sites of interest. A most significant unexpected observation during evaluation was the possibility of finding out about the relation between weathered horizons and water content. Within both the displaced rock masses in Delokh, as well as Lakhshik and Shosh, the top of a highly decomposed lower rock layer, overlain by a more loosened upper layer, likely delineates the zone of preferred creeping or sliding. This boundary was detected seismically as a refractor (density increase), and in geo-electrics by a major decrease in resistivity, basically at the same level. This was interpreted as a result of two circumstances:

- Firstly, the layer bearing more water is the uppermost actual deposition layer of the mass movement beneath the topsoil and some coarse interlayers. Thus recent motion and lower overlying pressure might have a loosening effect on the talus material and water infiltrates easily in the empty space in between.
- Secondly, this uppermost deposition layer is the most affected one to weathering due to its exposure. Since the whole region is characterized by crystalline rock, also the talus deposits must consist of this rock type. During the process of weathering and decomposition it turns to clay and clay bearing phases, which have the property of being a good conductor. Thus resistivities are particularly low in weathered horizons.

Although the genesis of the mass movements may differ in detail, in all areas a weathered zone is overlain by coarser and more permeable material and a meter or two of topsoil. It is presumed that the layering is a product of recent movements, affected in places by anthropogenic factors like irrigation. The uppermost layer moves on the lower one, which permanently holds some water. The preferred zone of creep or sliding on top of this lower, partly saturated layer generally runs ca. 10–15 m deep. Hard rock was nowhere evident in the profiles. Fig. 16 shows one example of the interpretations achieved by careful matching of seismic and geo-electric models.

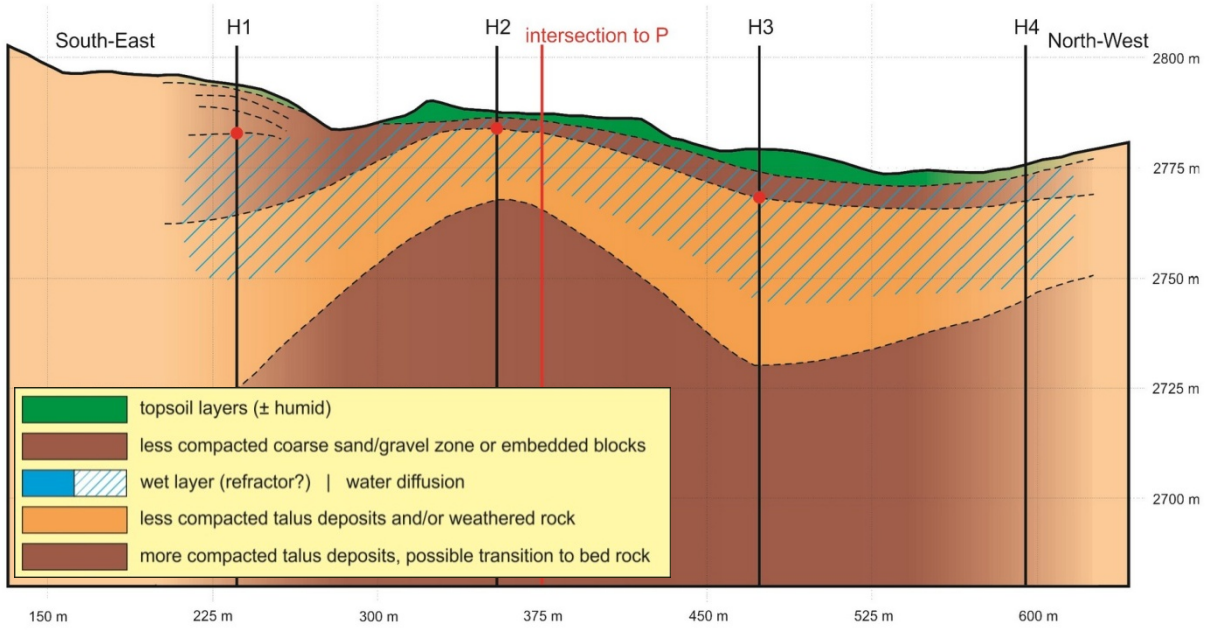

Fig. 16: Example interpreted cross section from Delokh, H1 through H4 indicate geo-electric profiling sites. The intersection with the longitudinal profile (P) is also indicated.

The landslide or rock glacier of Delokh is a case example of slope instability after glacial retreat and melt-out of permafrost. Large amounts of frost-shattered crystalline rock originated in the catchment, up to ca. 4.0 km away from the valley bottom. The displaced mass must have had a tendency to block the Sharfdara drainage, and fluviatile incision created a steep front toward the rivulet, where tens of meters of loose material crop out. Continued undercutting of this slope still poses a severe problem and contributes to the formation of secondary slides and characteristically uneven surface features.

Geophysics was carried out at the landslide foot where most of the residential area is located, and on the plateau above that area, which is used for small scale agriculture and animal husbandry. Sliding surfaces in these areas were found to be in 6–8 m and 8–10 m, respectively, between deeply weathered but rather consolidated talus deposits and the uppermost rather loose soil cover which is prone to the observed secondary sliding. The detailed examination of layer properties pointed to infiltrating water from irrigation channels as the main trigger for reactivation of previously dislocated mass and pre-existing sliding surfaces. Suspected seepage from damaged pipelines in the south-eastern part of Delokh is confirmed by the geophysical results.

So it seems that water supplied for gardening on the Delokh plateau is partly responsible for the persistent overall water content of the lowest parts of the slide mass. Moreover, ca. 1.0 km upslope there are permanent springs spread out over a wide area, probably originating from an aquifer within the main body of displaced rock, perhaps even from ice still melting out. On a larger scale, small displacements of fences and cracks on houses are readily visible, nonetheless large-scale stability can be assumed for now. However, one cannot be assured that further uncontrolled seepage will not reactivate the well-developed sliding planes on a larger scale, too. Also, large-scale sliding may sometime be triggered by river erosion and concurrent undercutting of the bottom slope, especially during major floods, effects that cannot be strictly prognosticated, except by continuous visual or instrumental observation.

The present mass movement in Lakhshik and Shosh is, in contrast to Delokh, interpreted to be a deep seated soil creep. The ground is believed to consist of lateral moraine from a glacier moving the Sharfdara downstream. The rounded mountain crest near Lakhshik must have been a natural obstacle to glacier flow, so the Last Glacial ice moved over and around it, and polished the crest in the sense of a roche moutonnée (see Fig. 15). Because the bottom should have received less ice load downstream as well as upstream the ice flow, today's area of Lakhshik and Shosh were a preferred area of till deposition.

On average, sliding planes detected here run some 10–15 m deep. They are defined by the border between a lower layer of deeply and intensely decomposed rock, and the uppermost topsoil and other incoherent layers through which water can seep in and be backed up by the deeper more decomposed layers, which are thought to act as an aquitard. We think that the upper layers were loosened and became more permeable in the course of rather recent slope movements. Detailed analysis of material properties, underground structures and distribution of water suggests that in Lakhshik most infiltration originates from the two poorly insulated branches of the Shoburhon channel above the village. Also, smaller temporary irrigation channels contribute to infiltration and could be an additional water source leading to regular saturation at preferred sliding zone.

In Shosh the situation is very similar. Six permanent springs beneath the Shoburhon Channel are evidence to the water seepage. Shosh is the only village part where major displacements of houses and fences are reported regularly.

4 Lake Shiva

Lake Shiva is a lake with a maximum length of approx. 9 km in Shighnan Province, Northeast Afghanistan, approx. 70 km east-northeast of Faizabad, and approx. 16 km southwest of Khorog. It was created by natural damming of the valley of Arakht. The valley is drained by a torrent of the same name, a tributary to the river Panj which, in that region, constitutes the border between Afghanistan and Tajikistan. There are also two small lakes (0.9 and 0.2 km max. length), roughly one kilometre away, at the southern end of the natural dam, and another circular lake (0.2 km diameter) on the eastern, downstream side of the dam. The latter lake originates from water seeping through the dam, and is the source of Arakht torrent (Fig. 17).

Fig. 17: Google Earth image of Lake Shiva and surrounding region. Yellow line: Afghan-Tajik state border, following the Panj River. The lake is dammed at its eastern end. On the eastern side of the dam a small circular lake marks the source of Arakht rivulet, which flows to the SE and into the Panj.

A preliminary geological hazard assessment of the lake and dam has been done in the context of the on-going project by means of helicopter survey, satellite image interpretation and ground check by a team of researchers during this summer's field campaign. No immediate hazard was detected, but a partial collapse due to retrogressive and piping erosion at some time in the future cannot be ruled out. Subsequent flood wave modelling of two partial collapse scenarios have shown that in either case, in addition to all the villages on the way, the city of Khorog, being located not too far down the Panj Valley, could be affected (Fig. 18).

Time constraints did not permit a detailed field investigation of the dam, the catchment and the downstream area. Therefore, an extension to PAMIR project will be proposed. For now, results of helicopter and field survey of the dam on August 14, 2011, can be summarized as follows.

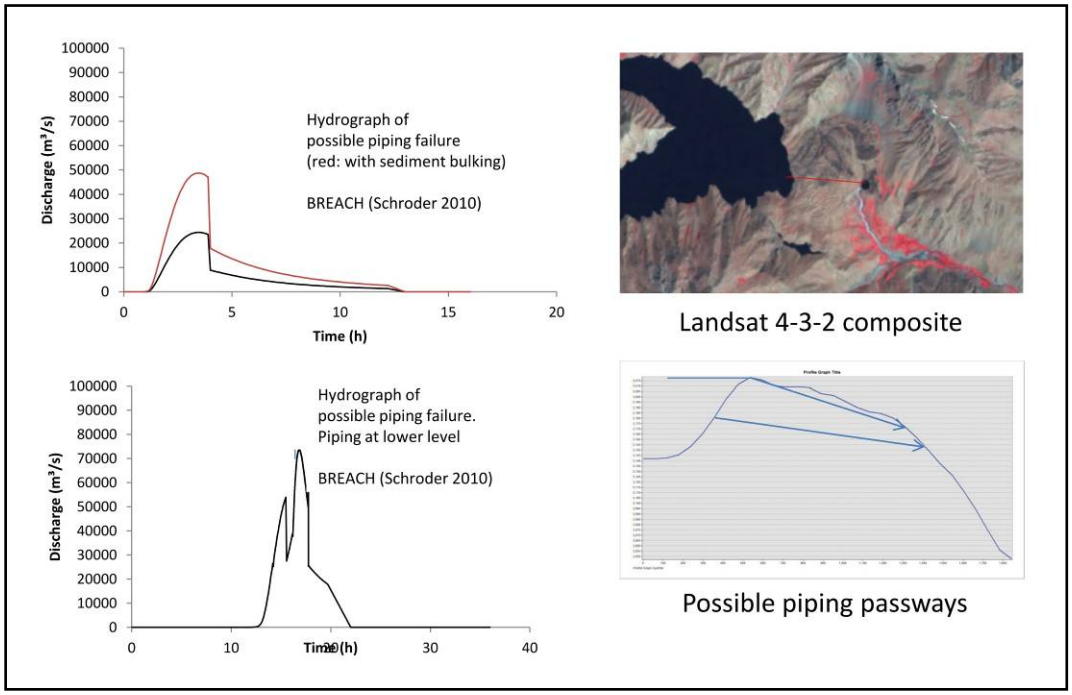

Fig. 18: Flood wave modeling results for two published scenarios of Lake Shiva partial breach and outburst flood. In either case, if for a short time, very large discharge rates (an order of magnitude more than a fairly big river like the Danube in Vienna) can be created, which would cause flooding as far away as Khorog.

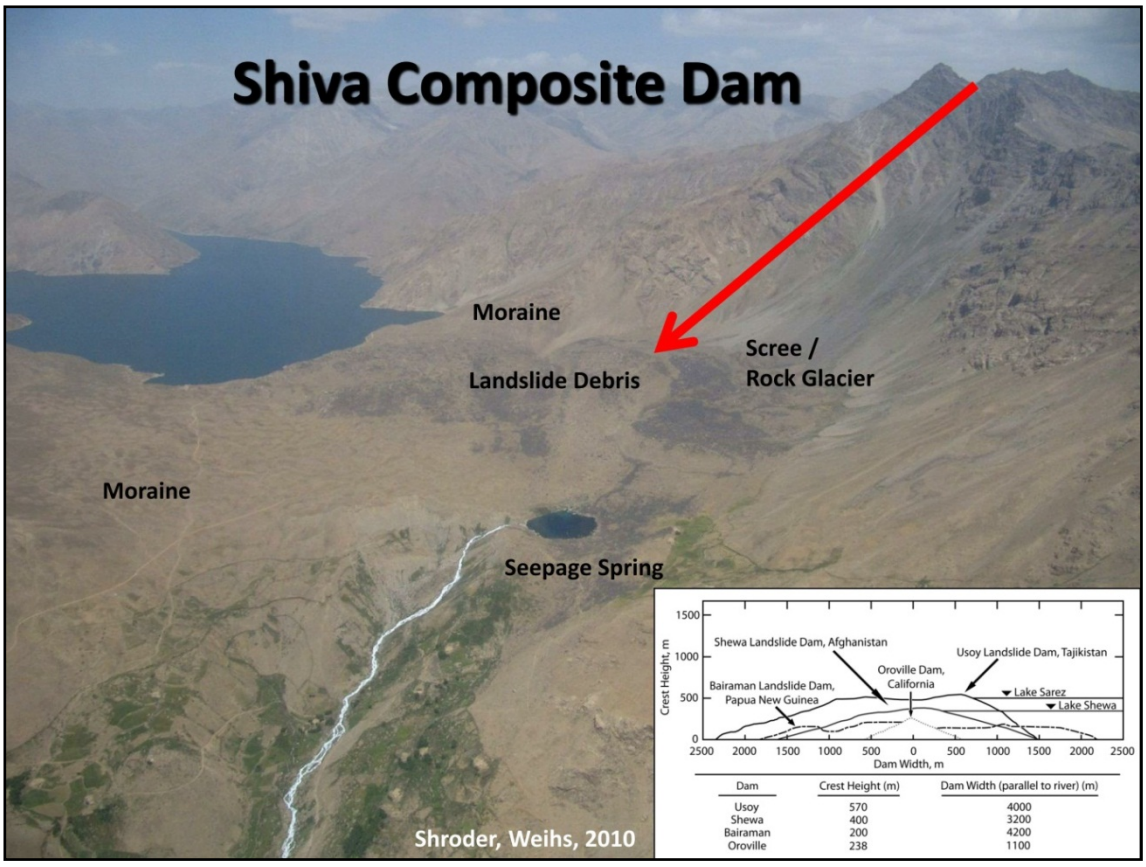

Fig. 19: Helicopter reconnaissance picture of Shiva Lake and composite dam, view to the west. Red arrow indicates landslide. The depression spring (circular lake, diameter approx. 200 m) and headwater of Arakht torrent in the foreground; to the left of the lake the unstable due to seepage (cf. Fig. 20), with a band of much smaller springs (notice spots of green vegetation). The landslide debris and former rock glacier are easily distinguished from the moraine by their dark brown color, due to rock varnish covering most of the blocks.

The dam is a minimum of 1.6 km wide. According to Shroder and Weihs (2010), "an assumption has been made by many people heretofore that Lake Shewa [sic] was dammed by a glacial moraine", and they attempt to show that "in fact, […] Lake Shewa was actually impounded by a series of massive, rock avalanches", or rather, of at least three landslides and a rock glacier.

However, our own field assessment led us to believe that the abovementioned older opinions are basically correct, and that the main part actually is a morainic dam, presumably representing at least two late-glacial stages. The ridges created by those stages leave a depression between them, which is where the two smaller lakes near the southern end of the dam are situated. The large morainic part of the dam has a surface morphology reminiscent of hummocky moraine, and consists of crushed, rather light-colored local gneisses. There is a wide range of grain sizes (up to approx. 1.0 m), with a substantial sand fraction, and many larger, platy components seem to be aligned in a way that suggests topography-parallel material flow, or that at any rate would not be expected in a landslide mass.

What is more, from satellite imagery it is possible to ascertain one implication of the aforesaid interpretation, namely that only substantial glacial ice flow from the local catchment can explain a terminal moraine of this size. The nearby Panj Valley bears no signs of intense glacial reworking, although Last Glacial Maximum ice from local glaciers might have accumulated there. In contrast, the Shiva catchment does show such indications, in the form of parabolic valley cross-sections and high-mountain corries. We have refrained from mapping these indicators, but illustrate this in Fig. 20.

Fig. 20: Google Earth image of Shiva lake and surroundings, looking WNW. In front of the lake the composite dam, beyond the lake, right in the center, one example of parabolic valley cross-section, beyond that a range of corries with small snow fields. A single (grey-colored) mountain with corries on top is visible in the far distance, above center. It is surrounded by mountains without any signs of glacial reworking.

Fig. 21: View to the east across Shiva composite dam. Morainic dam, with gentle or hummocky morphology, bordering the lake to the left, and in the right-side middle ground. The landslide mass seems rugged, with uncountable blocks of darker color. Right of center it reaches the lake and may have filled up a hypothetical meltwater canyon there.

In the northern part of the dam, the till interdigitates with a landslide mass. On the surface of that mass there are many large fractured, but not altogether fragmented, rock bodies. They consist of gneisses with a significant biotite and amphibole content, thereby showing darker colors than the bulk of till described before. These rocks outcrop on the slopes to the north, where the landslide rushed down from (see Fig. 19), presumably while the landscape had to accommodate the loss of its ice cover at the end of the last ice age (paraglacial environment). Perhaps a partial breach of the morainic dam by glacial meltwater did occur back then, but if so, the gorge is now covered by landslide debris. In Fig. 21, left side, the difference in appearance between till (moraine) in the foreground and landslide mass in the back is conspicuous.

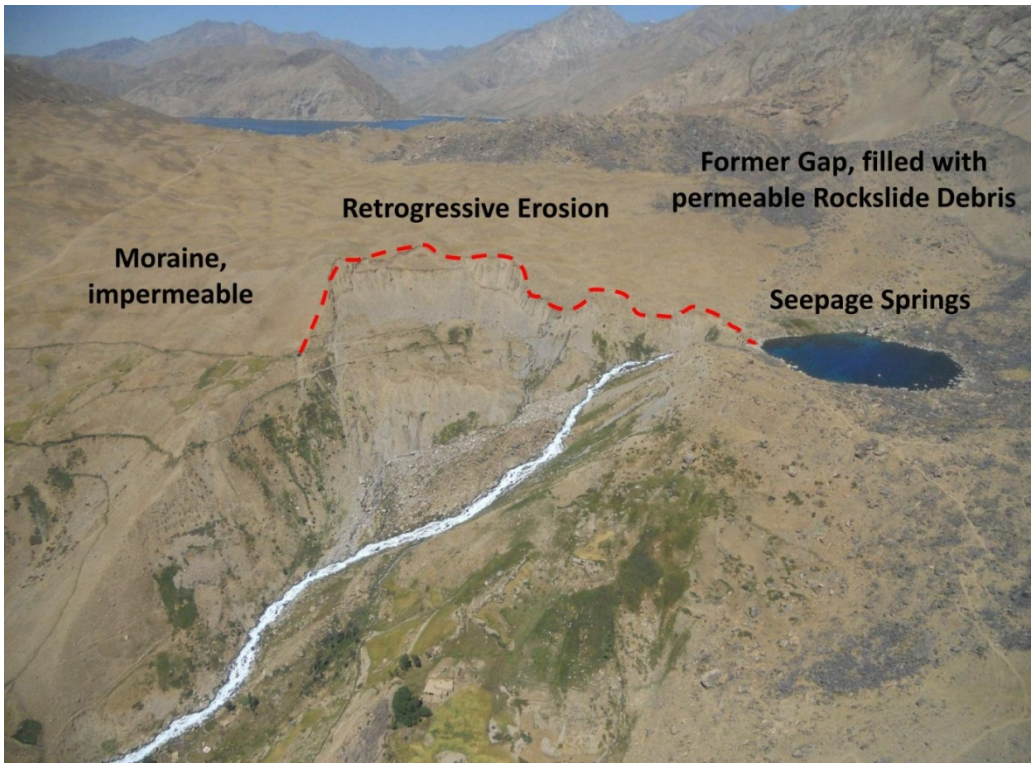

Fig. 22: Helicopter view of the air side of the central part of Shiva composite dam, with the large circular depression spring and headwaters of Arakht rivulet. To the left of the spring, retrogressive slumping of till and consequent erosion, due to seepage, presumably from the landslide-covered area in the back. The small springs in this area show themselves by vegetated spots, and they seem to be used even for irrigation.

The dam has consolidated since Late Glacial times, and obviously has never been overtopped in the shape it is now (after the possible first breakout), by the water dammed up behind it. Instead, all the water supplied by the catchment made it through the dam by virtue of seepage, and for the most part, we think, became channelled through the permeable material supplied by the landslide. On the downstream side of the dam, most of the seepage emerges in a stable depression spring, thereby creating the small circular lake.

However, there is not only the big, stable depression spring, but several additional springs on the downstream slope of the dam, to the south of the main spring. This indicates seepage through the comparatively impermeable till, which constitutes the major part of the dam. This already has led to retrogressive erosion of the – currently rather small – part of the dam affected by the seepage, and it is obvious that repeated slumping is taking place and that the slope instability is active (Fig. 22). In case this is expected to go on, the dam – in the long run – could be weakened by erosion of its narrowest part, and also undermined by more concentrated seepage (piping).

Furthermore, Shroder and Weihs (2010) describe the dam site as situated at the crossing of two active tectonic lines, which could trigger local earthquakes.

Therefore, on the one hand, a comprehensive risk assessment for rural and urban planning to be based on in the future, as well as specific monitoring and possibly an early warning system are called for. On the other hand, the existing stable seepage, emerging in a big perennial spring, offers a chance for electric power generation on a local scale, without having to build a pressure pipeline through the dam. For the purpose of long-term hazard assessment, as well as planning for the water works, a detailed evaluation of the geotechnical behavior of the dam is recommended.

5 Garm-chashma

The study area of Garm-chashma is located in the south-western Pamir in a tributary valley on the orographic right side of the Panj Valley between Ishkashim and Khorog. The entire catchment has a surface area of 237 km². The main river is mainly fed by meltwater and follows the V-shaped valley southeast up to 5744 m a.s.l. (Fig. 23).

The lake under investigation (Fig. 24) is located at an altitude of 4413 m a.s.l. in a steep tributary valley (with slopes up to 70°) south of the river. Embedded in dead ice, the lake is surrounded by steep slopes, moraine structures and the debris covered ablation zone of the glacier. At present the accumulation area of the glacier has approx. the same size as the ablation zone, so the glacier is in the progress of degradation.

Fig. 23: Google Earth image of the area around Garm-chashma. Yellow line: State border to Afghanistan, following the Panj Valley. Purple line: Helicopter survey route, August 7, 2011. The route passes Garm-chashma township to the NNW of the image center, and circles around the glacial lake to the SE.

The lake has a surface area of 13,600 m² and an estimated volume of less than 15,000 m³. It is located on a mass of dead ice, which also dams the lake (Fig. 25), with a sub glacial drainage underneath. The freeboard between the lake level and the crest of the ice ridge is about six meters. Regarding the geometry of the dam, the hazard of a sudden drainage is rather low. However, older lake sediments indicate a former lake level, which is 2.5 m higher (Fig. 26). This difference does not seem to represent seasonal fluctuations, because other lakes in the same area with comparable characteristics have not shown this effect.

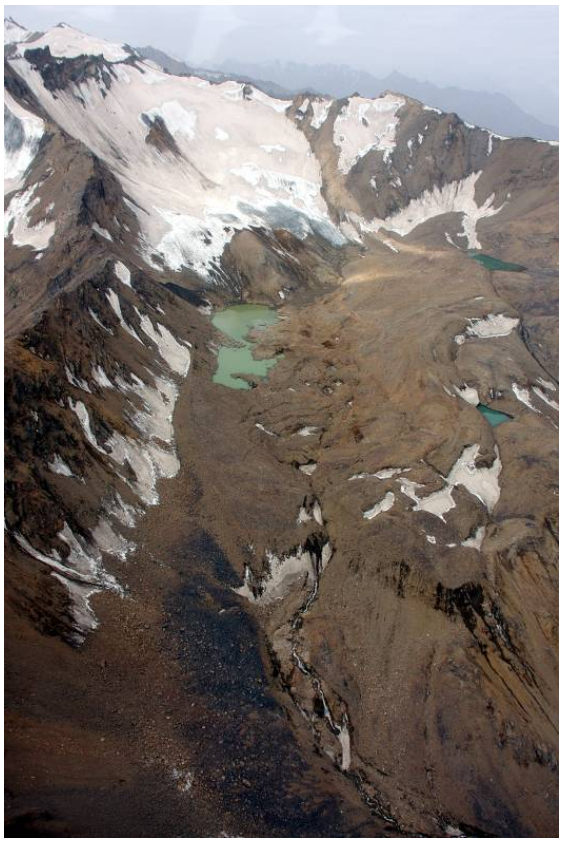

Fig. 24: Lake overview from helicopter survey (view to the SSW).

Fig. 25: Distal end of lake, embedded and backed up by dead ice.

Fig. 26 (left): Lake sediments, 2.5 m above current lake level.

Fig. 27 (right): Erosion channel, caused by GLOF.

The former lake level rather indicates a glacial lake outburst flood which occurred on August 5, 2008. The former lake level was used to derive an outburst volume of 75500 m³. In the intermediate area of the transition zone of the 2008 GLOF, the erosion channel is 20 m wide and 8 m deep (Fig. 27). Blocks of up to 4 m³ large were observed in the channel. Assuming that they are remnants of the GLOF, its peak discharge was estimated between 30 and 50 m³/s. Most of the entrained material was deposited on a debris cone at 3357 m a.s.l. The vertical difference from the glacial lake to the debris cone are therefore 1056 m with an average slope of 28°.

The 2008 event had no direct impact on the population. But it is assumed that the debris cone formed by the deposit impounded the river (Fig. 28). A six meters deep lake formed within two days, then the dam failed. This second outburst event caused minor damage by destroying small bridges of local importance and destabilizing some slopes on the way to agricultural areas (see Fig. 27).

The environment of the glacial lake is in a sensitive balance, different scenarios for a further increase of the lake level are possible. Furthermore, there are some triggering factors possibly affecting the lake and contributing to a dam break. Such are ice and rock avalanches, melting of stagnant ice within the lake area or earthquakes. Therefore it is recommended to examine the lake in more detail and to engage in regular monitoring.

The damage potential in the valley is significant, if not high. Herdsman would be immediately affected by GLOFs. Further downstream there are houses of farmers and some of their fields are located closely to the river. The highest damage potential is certainly concentrated in the village of Garm-chashma, which consists of almost 30 one-story houses and some multi-story houses. The village is known for a thriving tourism sector. A sanatorium and associated hot spring attract thousands of people each year (Fig. 29). The place is famous all over the country for its healing effects on skin diseases. There are at least two more smaller villages further downstream, and a military checkpoint at the junction of the main road through the Panj Valley with the secondary road to Garm-chashma.

Fig. 28 (left): View from debris cone to the broke dam (left) and old lake structures (right).

Fig. 29 (right): Hot spring in Garm-chashma township; bathing basin and calcareous sinter deposits. The slope in the background is in a creeping movement. Approx. 2.0 km upstream (to the left) there are springs at the valley bottom, delivering CO_2-rich, slightly thermal water.

6 Dasht-sulaymon

The Panj Valley, forming the border between Tajikistan and Afghanistan (Wakhan Corridor), is partly blocked by the deposit of a debris avalanche at Dasht-Sulayman, upstream of the town of Ishkashim. The origin of the landslide is located in the mountain range to the south (Fig. 30).

Fig. 30: Google Earth image of catchment and debris avalanche of Dasht-sulaymon. North is to the right. Yellow line: State border to Tajikistan, following the Panj River. Purple line: Helicopter survey route, August 7, 2011. The catchment is left of center, the distal end of the debris mass is to the lower right, seemingly lying on top of a pre-existing alluvial fan. To the west (upper half of the picture) there is another catchment, still with some glacial debris in place, and supplying an alluvial fan adjacent to the abovementioned one. In-between the two, the dark grey debris, which is presently deposited from the eastern catchment, can be seen.

Figs. A31 and A32 are panoramic views of the distal part of the landslide mass from the opposite side of the Panj Valley, and down from the mouth of the tributary which supplied the material. In Fig. 31, the remaining parts of the pre-existing alluvial fan can be seen on both sides of the lobe, and the distal fan material (basically the same as in the slide mass), which is interfingering with cobbles and boulders deposited by the river, is indicated by streaks of boulders visible at the bottom of the slide mass. To the left there are additional lake deposits (banded silts and sands), covered by grass and grain fields. In front of the slide mass and to the right there are boulder fields, the boulders being well rounded and many blackened by rock varnish, which means they have been exposed for a very long time (thousands of years perhaps). If the likely interpretation of the boulder fields as a lag deposit is correct, all this points to the outbreak of a lake dammed up behind the slide mass, somewhere in prehistoric times. Historical as well as geochronological evidence is missing, though.

In Fig. 32, left and right of the avalanche lobe the pressure ridges can be seen that were pushed up when the avalanche ploughed through the alluvial fan. On the right-hand ridge there are the ruins of a medieval fortification. The question of the mechanism necessary to achieve massive scour instead of lateral spread on top of the alluvial fan can be answered only hypothetically. The most likely option, in our opinion, is that the alluvial fan contained much groundwater, perhaps meltwater from the same catchment (which could also have mobilized the landslide), so that the sudden overload at arrival of the avalanche on the fan could weaken the apparent cohesion of the

underlying debris. It became entrained by the avalanche and the avalanche in turn developed into a wet rock and debris flow, confined to a broad channel and surging further as it would otherwise have, eventually against the opposite side of the valley. A depression thereby developed between the pressure ridges; the valley was blocked and a lake was dammed up. The grating of the bedrock on the opposite side of the valley, resulting from the subsequent lake outbreak, can also be seen in the figure, beyond the distal end of the avalanche lobe.

Fig. 31 (upper) and Fig. 32 (lower): Distal part of the Dasht-sulaymon landslide mass (rock avalanche and debris flow) and surroundings; panoramic views from the opposite side of the Panj Valley, and down from the mouth of the tributary which supplied the source material. As can be seen in the upper picture, much material has been left in the canyon connecting the tributary catchment and the main valley. Significant amounts of it are glacial advance sediments and glacial till. Further detailed explanations are given in the text.

Fig. 33 illustrates the character of the avalanche material. It is a diamictite, partly grain- and partly matrix-supported, consisting of angular fragments of black slate in all grain sizes between silt and boulder, mostly up to ca. 0.5 m maximum length. Larger boulders were later washed out at the surface and seem to be concentrated there. Many larger platy fragments are imbricated (slightly inclined in up-flow direction), but otherwise the texture is chaotic. The lighter-coloured silt fraction has probably been entrained from glacial till.

Locally, on the steep sides of the lower reaches of the tributary valley (the left side especially), a sedimentary sequence of glacial advance, temporary lake, and ground or ablation moraine deposits can be observed (Fig. 34). The glacial advance came from the main valley, and the associated deposits contain sub-rounded fragments of light-coloured gneiss, the like of which is probably present in the western part of the local catchment (they may also come from outside, but cf. light-coloured scree in the upper part of Fig. 30). The temporary lakes were dammed up in

front of the advancing ice, and the horizontally banded silts, having filled up the lakes, were overridden by the ice and covered by till, which was dominated by local rocks, with some of the larger fragments sub-rounded and striated.

Fig. 33: Detail of the rock avalanche material, from a fluvial channel on the right side of the tributary valley, ca. 100 m up from the apex of the alluvial fan in the Panj Valley. The foot rule to the right shows 1.2 m of length.

Fig. 34: Sedimentary sequence on the left side of the tributary valley, ca. 500 m up from the apex of the alluvial fan in the Panj Valley. A thick lens of yellowish light brown, horizontally banded silt is visible just below the middle, inserted between lower glacial advance deposits and upper glacial till (which is also seen higher up, attached to the steep slope, which consists of paragneiss with a tight cleavage).

Ground and ablation moraine, which often have been dislocated further during the Holocene in the way of a rock glacier, were certainly present in the uppermost catchment, but have been washed out and built up the alluvial fan before the rock avalanche occurred. The avalanche

originated in the eastern part of the catchment (lower central part of Fig. 30, where the dark colours indicate the outcrop of the source rock). The slates are dipping to the west, more steeply than the slope, so as to assure overall slope stability, but are heavily frost-shattered. They broke loose in a rock avalanche, entraining glacial till on the way down the tributary valley.

No larger amounts of till and only scree are now left in the uppermost catchment (cf. Fig. 30), but some like material is still there in the adjacent catchment to the west. If mobilized, it may trigger a comparatively minor debris flow and reach the small village of Uchdrag.

Figs. A35 and A36 once again illustrates blockage of the Panj and subsequent lake breakout, resulting in a flood wave washing the (comparative) fines away and leaving residual boulders (lag deposit) behind.

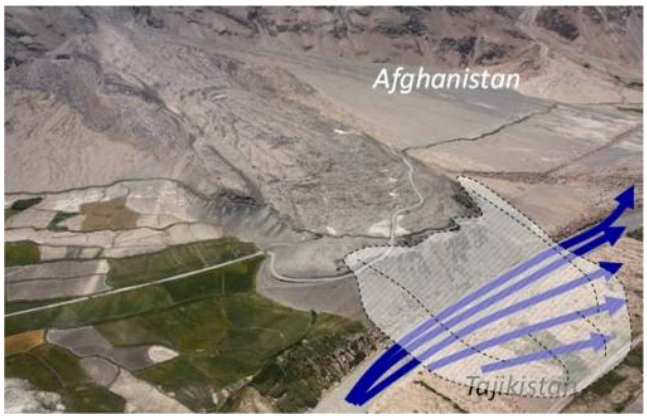

Fig. 35 (left): Rock avalanche at Dasht-Sulayman, upstream Ishkashim in the Wakhan Corridor, Afghanistan. Interpretation on the basis of picture taken during helicopter reconnaissance on August 7, 2011, showing front lobe of the rock avalanche from the NE, and graphical indication of the landslide dam temporarily blocking the Panj, and subsequent lake outburst, which left behind residual boulders, littering a large area in front of and downstream of the present front lobe. A thin cover of lake sediments underlies the cultivated area.

Fig. 36 (right): Washed-out boulders cover the orographic right side of the Panj River in front of the distal end of the rock avalanche in its present form. They are remnants of the lake outburst flood, and many are encrusted by rock varnish, attesting to a long period of time since the disaster (many hundreds to several thousands of years).

7 Shidz

Shidz is a village on the orographic right side of the Panj, ca. 80 km downstream of Khorog. It is located at the foot of a large body of loose, coarse rock debris, which fills the bottom of a slope recession just before a sharp left river bend. This rock body lies on top of granitoid rocks (augengneiss, which is seen in outcrop up to approx. 2030 m a.s.l., i.e. ca. 65 m above the river), and is approx. 300 m thick, as far as can be inferred from the steep erosive front, looking toward the river. The upper edge of the frontal face is around 2350 m a.s.l. (ca. 385 m above the river), and at approx. the same altitude on the opposite side of the valley there is a horizontal ledge, which is taken as indication that the whole mass originally spanned the entire cross-section of the valley and has been eroded by river action. The top surface of the remaining rock mass extends over an area of approx. 1.8 by 1.5 km, and is partly covered by angular boulders, many of which are blackened by rock varnish. The origin of this mass is in question. Fig. 37 illustrates how the mass is embedded in the landscape.

Fig. 37: Overview of the topographic situation at Shidz, in the Panj Valley, on the basis of a screenshot from Google Earth, looking east. The soft rock mass in question is just left of center. Other landscape elements that are indicated are referred to later in the text. To the right (left, Afghan side of the Panj) the mouth of a tributary is visible, with a lake of greenish color in it. This lake is artificially dammed up. Approx. 4.0 km upstream of the investigated area the Panj takes a sudden turn to the right. The sharp ridge on the inside of the river bend attests to the minor degree of glacial flow in the valley, if any, during the Last Glacial Maximum.

The bedrock geology is dominated by rather light-colored granite and granodiorite, altered – in most outcrops we have seen – to granitoid gneiss, indicated by preferred orientation of the mica platelets. There are aplitic as well as pegmatitic veins, and repeatedly in the scree there are fragments of light- and dark-colored rocks to be found, as well as some boulders with streaks and layers of both varieties. The light-colored parts have the character of plagiogranite (plagioclase,

less alkali-feldspar, and quartz), the dark-colored parts often look like biotite (or amphibole) schist, and actually consist of biotite (coarse-grained, macroscopically black Fe-rich biotite, in x-ray diffractometry transitions to Mg-rich phlogopite), plagioclase (anorthite-rich), minor quartz and hornblende, and traces of chlorite as secondary alteration product. This suite of rocks is interpreted as migmatitic (deep regional metamorphosis, up to near melting conditions), and the aplitic and pegmatitic veins could have been injected by "leucosome", i.e. the light-colored melt created first from partial melting (another, less likely, possibility is that leucosome dominates, which would lead to widespread near magmatic texture).

The adjacent slope to the south, bordering against the rocks described above along a SW–NE-trending fault, is built of interlayering schists and light-colored (granite) gneisses, which could not be studied in more detail. Generalized results of geologic mapping and bedrock geology are illustrated by Figs. A38 and A39. The scenery from a vantage point to the SE is shown by Figs. A40 and A41.

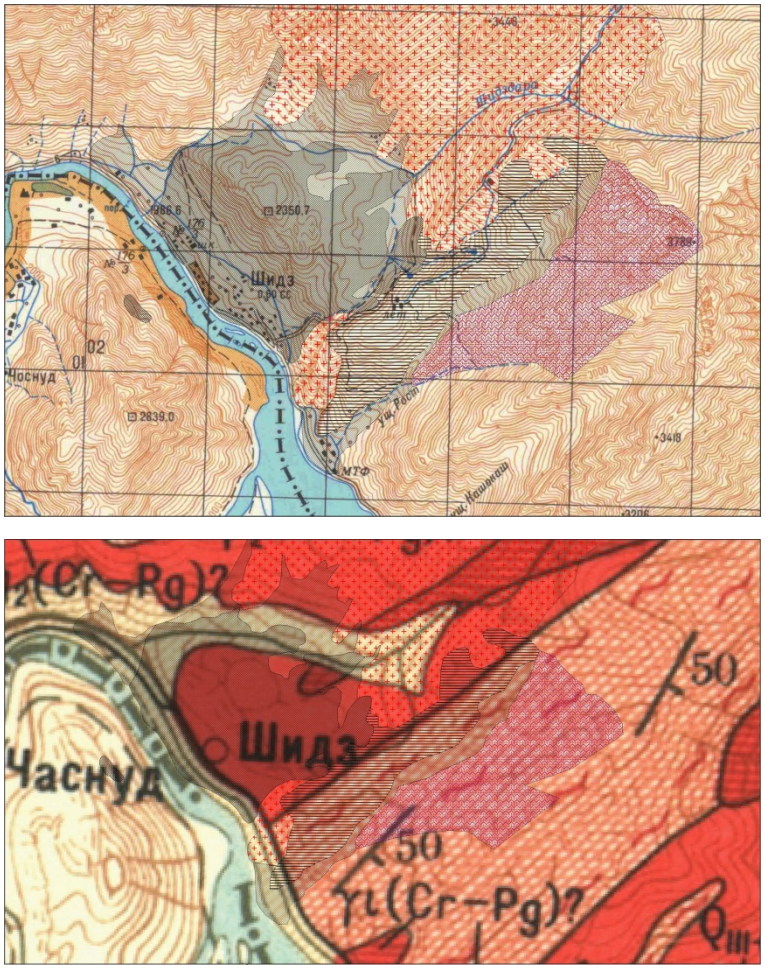

Fig. 38 (upper): Section of the regional topographic map 1:100.000 (the gridlines are 1.0 km apart), Shidz township is left of center, with results of geologic mapping by Nikolai Ischuk and colleages, represented by signatures indicating terminal moraine (dark grey), scree (light grey), lateral moraine (grey horizontal hatches), granite gneiss and related (red crosses), and interlayered gneiss and schist (purple cross-hatches).

Fig. 39 (lower): Roughly same area as shown by the regional geological map, with granitoid rocks (dark red), partly migmatized (additional horizontal hatches), and gneiss/schist complex (red cross-hatches and swung dashes). Soft rocks other than alluvial and colluvial are not represented. To improve comparability with Fig. 38, respective signatures there are repeated as a transparent overlay.

Fig. 40 (upper): Panoramic view, center looking NW. Large moraine littered with blackened boulders in the center, beyond that the Panj Valey (left river band with greenery), local lateral moraine in the foreground.

Fig. 41 (lower): Similar view from a vantage point to the SW. Right in the center Shidz village, lying on the Panj, in the left middle ground the bedrock spur mentioned in the text, beyond that the mouth of a large tributary (possible supplier of an LGM local glacier) with a greenish-looking, artificially dammed-up lake

Fig. 42: Major rock types found in soft and bedrock at Shidz. Upper left, grey migmatized gneiss (in the back a boulder with boudinaged amphibolite layer), white plagiogranite in the foreground. Upper right, granodiorite gneiss with pegmatite vein. Lower left, till in lateral moraine, dominated by white granite gneiss. Lower right, glaciofluvial gravel on the left side of the Panj near Shidz, crude cross-bedding, dipping ca. 15° to the right (downstream).

The boulder and debris mass in question contains fragments in all sizes of a range of rocks like those described above (cf. Fig. 42, upper part), and also some probably exotic ones, like meta-gabbro (diopside, anorthite-rich plagioclase, phlogopite; one boulder rounded, possibly glacially striated), tightly layered paragneiss, garnet-bearing amphibolite, and mica-bearing quartzite. There may be a crude sequence of rock types, the lower parts of the mass being dominated by light-colored granite gneiss and orthogneiss with alkali feldspar blasts (augengneiss, the footwall of the mass!), and the upper parts containing increasing amounts of light- and dark-colored fragments of migmatitic origin. Above approx. 2200 m a.s.l. (i.e. in the top 150 m) there is a high concentration of large angular boulders, some as large as a family house. In the southern part of the upper surface, many of these boulders have rock varnish on them.

The southern end of the slope recession accommodating the boulder mass is created by a bedrock spur. The local gneiss is fractured and hydrothermally altered in places, which may be both related to the fault zone crossing the valley at this place. The fracturing may also be due to glacial loading, which is plausible in this position, if only there was a major glacier flowing down

the Panj Valley during the Last Glacial Maximum. From the bedrock spur to the northeast there extends a ridge, in the typical shape of a lateral moraine. The contours become blurred high up on the slope. It consists entirely of a – partly matrix-supported – mass of very light-colored gneiss fragments, which we think originated in the local catchment (Fig. 42, lower left). The moraine is terraced on the southern side in approx. 3430 m a.s.l. (ca. 465 m above the Panj), corresponding to the – equally cultivated – small terrace approx. 3.5 km to the southwest, on the ridge between the two local tributaries on the Afghan side. Interestingly, the northern slope of the moraine is the steeper one, without a (glacial or fluvial) terrace, so normally this would be the side of the depositing glacier.

The elongated depression between the lateral moraine and the large rock mass in question is covered by silt and fine sand. The flat top of these sediments is at approx. 2300 m a.s.l. (ca. 340 m above the river). There is no surface drainage out of the small basin. To the northwest there are two other cultivated sand flats at the same elevation, the northernmost having an erosion edge looking toward the main valley. In places, the silt and sand clearly does not extend into open cavities between the large boulders, which indicates that ice must have been present to prevent the fines from being washed into the boulder mass.

Approx. 10.5 km downstream on the left side of the Panj there is another loose rock mass, also filling up a slope recession "protected" against valley flow by a bedrock spur, and rather flat-topped approx. 420 m above the river. Nearby, on the right side, it is a similar-looking mass topped by an alluvial fan, flattening out at approx. 260 m above the river. The first one seems to correspond rather well with the accumulation level at Shidz (385 m above the river). Therefore, sedimentary accumulation levels in Shidz and surroundings can be observed in approx. 260, 340, 400 (385–420), and 465 m above the present river. This could be a sequence of late-glacial retreat stages. Confirmation of this hypothesis should refer to an accepted system of glacial stages and corresponding ice-marginal and fluvial terraces. Judging from the literature (Ehlers et al., 2011), studies have been published on Late Glacial stages in neighboring countries, but our results are not on a scale necessary to extend and verify those results in the present context.

Going back to the immediate question of the origin of the boulder mass at Shidz, an option worth of consideration is certainly landslide. It could only have come from the local catchment, because a remote event would have left some additional traces, which are nowhere to be found (on the basis of remote sensing images). The mass originally must have had a total volume of approx. 400 Mio. m^3, which should have left a corresponding scar on the adjacent slope in case of a landslide origin. But the shape of the higher parts of this slope is rather convex than concave, and there are only minor scars and none of an appropriate size (Fig. 43). In view of this fact, and of observations already referred to (local bedrock fragments at the bottom of the mass, some exotic boulders higher up, ice in the interstices when the sand flats were created, facing steep side of adjacent lateral moraine), we conclude that the debris and boulder mass at Shidz is of a glacial origin, probably of moraine type.

The source of the lateral moraine is entirely local, while parts of the large moraine probably has a distant source. When this material was still embedded in the glacial ice, the ice body backed the lateral moraine to the north, explaining its steep northern side.

Fig. 43: Google Earth view of the scenery, looking NW. The yellow line is the GPS-tracked survey path taken on August 21, 2011, circling over and around the interesting boulder mass and lateral moraine (in the foreground). Clearly there isn't any scarp on the slope to the right sufficient to explain the boulder mass as a landslide. Also, the shape of the slope here is convex rather than concave, perhaps reflecting the origin of the bedrock as a granite intrusion.

There are two options for the origin of the ice having deposited the large moraine: (a) Local glaciers, from the tributaries immediately to the NE, which now supplies a debris cone proximal to the southern part of the large moraine (dark-looking because of much rock varnish), and to the SW, on the opposite, Afghan side; (b) a larger ice flow in the Panj Valley, being supplied by a host of local glaciers. The latter is conceivable because a large ice flow could very well have dumped some of its debris load in the shadow zone behind the bedrock spur at the southern end of the moraine. A large ice body in the Panj, whether or not flowing downstream, is assumed anyway, because the accumulations (terrace level) at 465 m above the present river can best be explained in that manner. What is more, the Late Glacial retreat of an ice mass in the Panj would initially have allowed the local glaciers to (once again) advance into the main valley and deposit moraines there. The accumulation level of around 400 m above the present river can then be understood as the one corresponding to this first stage of retreat.

The lower terraces have probably a glaciofluvial origin. A good example of the sediments involved is offered by the gravel ridge on the inside of the sharp left turn of the Panj immediately west of the area in question. It consists of gravel and "floating" boulders, similar to very coarse till, but has a crude bedding, consistently dipping ca. 15° downstream (see Fig. 42, lower right). The bedding is cut off by the erosive slope (dipping 40°) on the lee side. Similar longitudinal ridges are present further downstream.

Finally, we mention that clear morphological signs of intense glacial ice flow in the Panj Valley (parabolic valley cross section, truncated interfluve spurs, smoothing of rugged slopes, different-looking till veneer on lower slopes), are clearly present only in the upper section, down to approx. 30 km north of Ishkashim. If Last Glacial Maximum ice masses, supplied by local glaciers, were

present further north in the Panj, without necessarily coalescing into a single ice stream, while still blocking drainage to some degree, then lake and subsequent glaciofluvial deposits were to be expected in-between the former ice bodies. Thick banded silt deposits, a clear indication of a former presence of lakes (which must have been backed up by some downstream obstacle, be it ice, moraine, or landslide), have been observed by the project team where Arakht rivulet (coming down from Shiva lake) enters the Panj from the left, and on the other side north of this location. No indications of large landslide masses were found, which could explain this.

Fig. 44: Collaborators taking a well-deserved rest (Mullosami Samiev, Abdurrashid Tagoybekov, Nikolai Ischuk, Fabian Znojemsky, Christoph Waldhör).

8 Karamik

Karamik is a village in Kyrgystan and a border post of the same name on the Tajik side, approx. 50 km ENE of the town of Jirghatol on the Muksu river. Karamik lies on the right (northern) side of Kyzyl-suu river, a tributary to the Musku. The cross-border road uses the northern side of Kyzyl-suu Valley, roughly 200 m above the river. Between the customs houses on both sides of the border it is a dirt road, and regularly affected by sagging downslope movement, which makes repair works necessary practically every year. A project survey team got permission for a guided drive on the road up to the border, and to work for another day in the field, on the mountain crest above the cross-border road (accessible by another, smaller dirt road). Time did not permit to create a veritable engineering-geological map, but the situation became sufficiently clear when mapping results are complemented with information from helicopter reconnaissance and the existing geological map (Google Earth doesn't offer good imagery in this case). A topographic map with significant results of mapping is presented in Fig. 45.

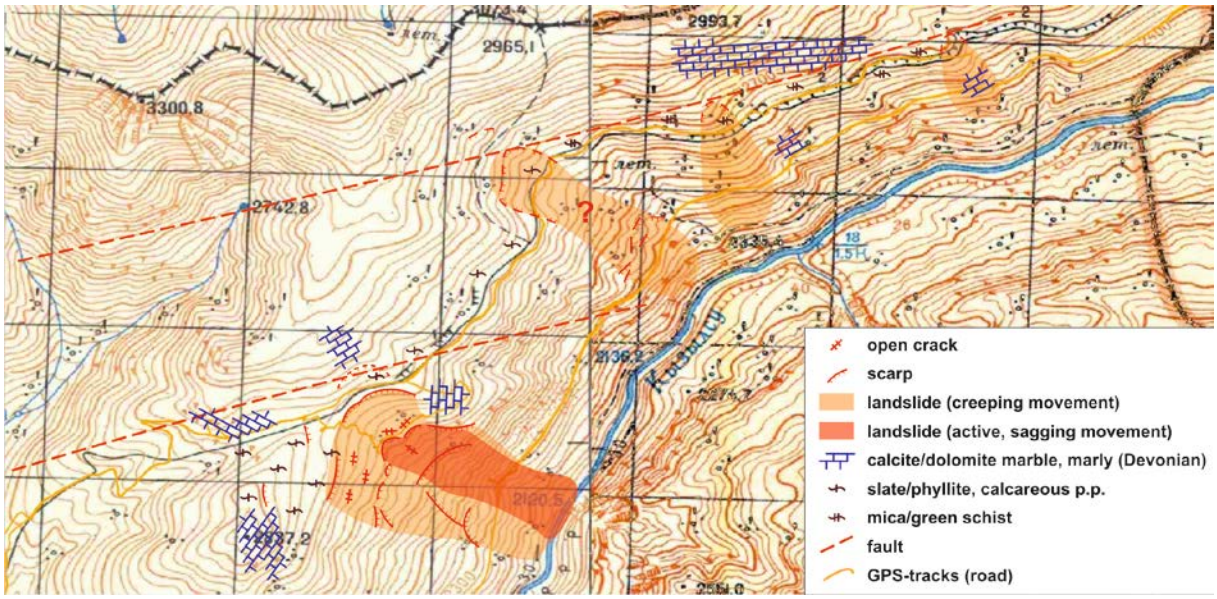

Fig. 45: Topographic map of the area north of the Tajik border post of Karamik, just inside the border with Kyrgystan (visible near the right and upper edge of the image, Karamik itself is not visible). The cross-border road and the smaller access road to the mountains are recognizable from the GPS-tracks shown as thick yellow lines. The attitudes of the limestone/marble signatures (looking like brickwork) indicate the strike of the formations as observed. If there is discernable bedding, the dip is downslope (toward the river). Incipient or supposed scarps are delineated by stitched lines (instead of solid).

Geologically, the entire area of interest is in a Devonian, slightly metamorphic, originally sedimentary sequence. It consists of (a) phyllites and mica schists, the latter being greenish in parts (muscovite-chlorite-schist or green schist), rich in small streaks and knobs of quartz, and often tightly folded ("crenulated", in the mm- to cm-range), and (b) thick layers of grey (marly) calcite and dolomite marble. There is no consistent layering (bedding) or cleavage; if clearly visible, the dip is moderate or steep between south and east. On the opposite side of the valley there is an imbricated sequence of various Cretaceous and Lower Tertiary sedimentary rocks. This points to a major tectonic boundary, which the Kyzyl-suu valley is obviously following in the area. Marble outcrops along the cross-border road show intense fracturing, presumably a consequence of vicinity to the major fault zone. In addition, there are two other faults running

through the mountain crest in question, in a WSW–ENE direction. The course of the Kyzyl-suu river seems to be influenced by this fault direction, where it comes near the state border.

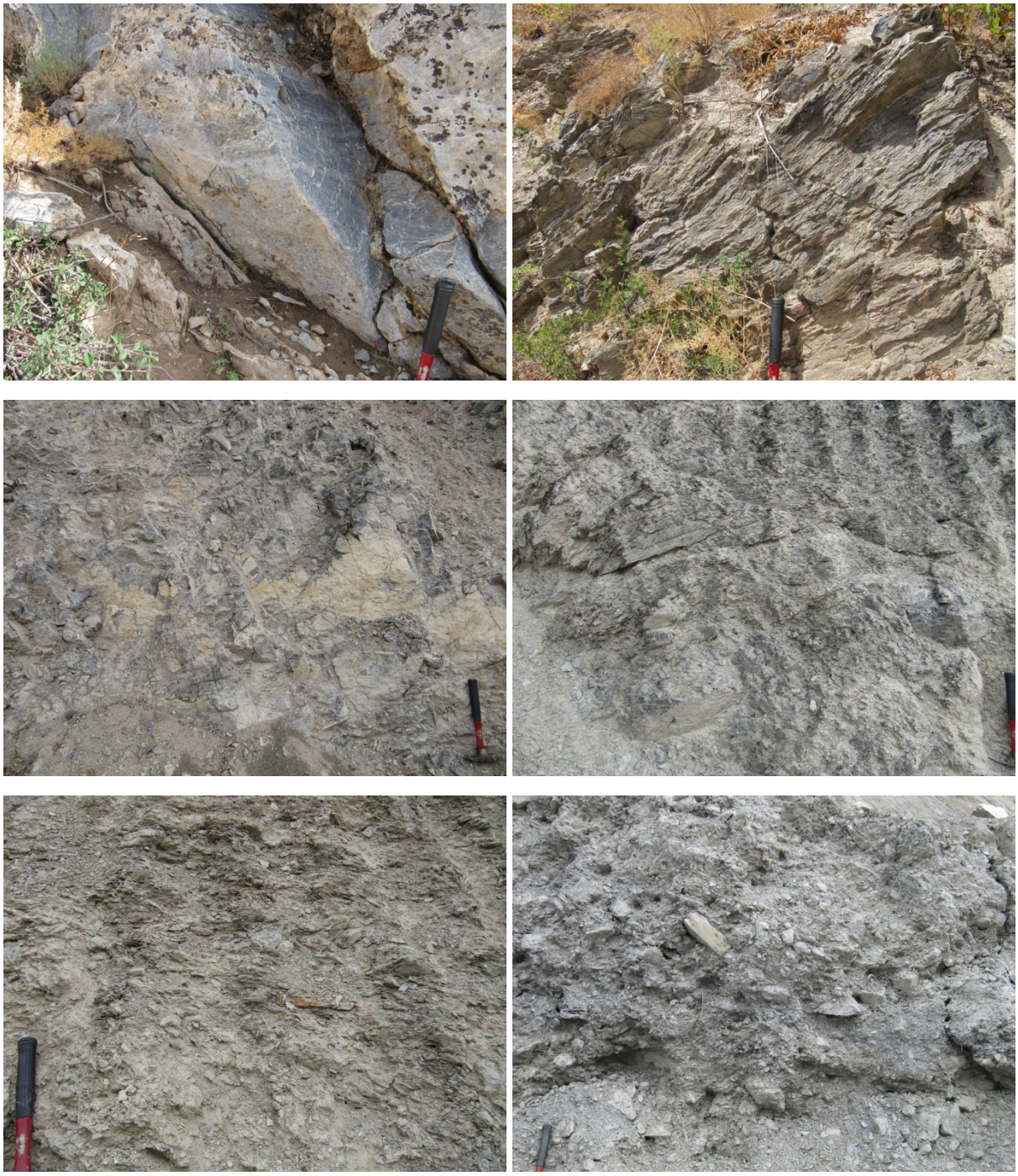

Fig. 46: Outcrop pictures (hammer for scale comparison), illustrating a sequence of disintegration from intact rock (upper row) to completely loose rock mass deposited from a debris flow. Upper left: Calcite marble, partly dolomitized; yellowish rock face in the center is covered by hardened fault gouge (kataklasite). Upper right: Phyllitic slate, with much quartz of silt and fine-sand size (perhaps properly identified as meta-siltite), slightly calcareous, pervaded by quartz streaks elongated in the cleavage plane (dipping to the left). Middle left: Calcite/dolomite marble like before, heavily fractured. Middle right: As before, completely fractured, with fault running through picture from top left to middle right. Lower left: Disintegrated rock mass, consisting of marble (mostly) and meta-sandstone/siltstone fragments; wavy layering due to creeping slope movement. Lower right: Matrix-supported, chaotic rock mass, with fragments of all rock types described, in a sandy matrix; if water-saturated, this mass would flow rather than slide or creep.

Several geological factors referred to above facilitate slope instability: Slate and schist (mica-rich) with a downslope dip is prone to disintegration by weathering, and provide potential sliding planes on a small scale, but in abundance, often leading to deep-seated creep. (Just to quote another example, in the so-called Greywacke Zone of the Northern Calcareous Alps of Europe, because of similar geological build-up, including Devonian formations, slopes are in a creeping movement practically everywhere.) In addition, even if the layering or cleavage is dipping favorably with respect to overall slope stability (often steeper than the slope in our case), the rocks are heavily fractured, especially near the major fault zones. Once the cleavage planes or fractures are opened by incipient mass movement, weathering agents have easier access into the rock mass, and the process becomes self-enhancing. If disintegration becomes pervasive, the mechanism can change from a creeping or sagging to a (perhaps slowly) flowing movement. The sequence of disintegration, as observed in the present case, is illustrated by Fig. 46.

Fig. 47 is a helicopter view (looking north) of that part of the valley side, which is permanently active (the large slide area in the lower part of Fig. 45; for a closer view of some of the scarps and crevices see Fig. 48). Three degrees of activity can be distinguished: (1) A central, most active part, in permanent slow flow, or sagging, in the latter case depending on moisture content, which under the given climate should repeatedly approach saturation. (2) A wider area encompassing the central part, which is in permanent creep or unevenly sagging like before, but not in a flowing movement. (3) Extension zone, working itself higher up the slope, above the uppermost major scarps. These zones are circumscribed in the picture by the red lines.

Fig. 47: Helicopter view (looking north) of the central, most active part of the moving slope at Karamik (between customs house and border to Kyrgystan). The red lines delineate the (1) central sagging/flowing, (2) outer creeping, and (3) extension zone of the landslide as described in the text.

Looking again at Fig. 45 above, the distribution of mapped elements suggests that the upslope extension of the major slide as well as three other areas of deep-seated creep indicated there is somehow related to the fault zones as shown by the published geological map. It also suggests that the permanently active slide will extend into all parts of the slope where slates and phyllites dominate, while the marble ridges offer more resistance, while still being prone to creep due to a high degree of tectonic fracturing.

In the experience of the authors there is nothing to stop these processes, once they have begun. As far as technical advice is called for, there has to be made a decision as to do anything at all, or rather to avoid the problem. In case of prolonged rainfalls which would lead to saturation of the central active slide mass, its movement could time and again accelerate into a debris flow. Also, there is a degree of risk from rather small-scale rock fall, where the road passes steep slopes in calcareous rocks, and debris sliding down the road-cuts. Other events running traffic into imminent danger are not to be expected.

Thinking of constructive measures, widening the road to accommodate higher traffic loads would aggravate the problem by further undercutting the active slope, and cannot be recommended. Likewise, a protection gallery against rock fall and debris slide is meaningless, because the deep-seated creep would affect the gallery, too. If the cross-border road would gain importance such as to compare to a first-order highway, there are two technical concepts which have been proven to work in practice: (a) A bridge-type foundation for the road, along-side the slope, with elliptical or button hole-shaped well foundations for the trusses; (b) an circumvention tunnel through solid rock inside the mountain. Both methods are very expensive. Another option would seem to use the southern (instead of the northern) side of the valley. Unfortunately this is a no-go either, because sagging (sackung-type) mass movements are present along the valley side opposite the area of interest virtually in its entirety. This is obvious from the almost continuous sequence of bulges protruding from all the slope foots.

Fig. 48: Major scarps (left) and open cracks (right) in the upper part of the slope shown in Fig. 46, both views to the west.

9 References

Brookfield, M.E., 2000. Geological development and Phanerozoic crustal accretion in the western segment of the southern Tien Shan (Kyrgyzstan, Uzbekistan and Tajikistan). Tectonophysics, vol. 328, p. 1–14.

Ehlers, J., Gibbard, P. L., & Hughes, P. D. (eds.), 2011. Quaternary Glaciations – Extent and Chronology: A Closer Look. (Developments in Quaternary Science, Vol. 15.) Elsevier.

Domej, G., 2012. Geophysical Investigations on a System of Active Landslides in the Village of Tusion (Pamir, Tajikistan). Master thesis, Univ. Natural Resources and Life Sciences, Vienna. 109 pp.

Khain, V.E., 1994. Geology of Northern Eurasia (Ex-USSR). (Beiträge zur regionalen Geologie der Erde, Bd. 24.) Gebrüder Borntraeger, Berlin–Stuttgart, p. 221–235.

Kordonskaya, N.W., Shebalin, N.W., 1977. Neuer Starkbeben-Katalog für das Territorium der UdSSR von den ältesten Zeiten bis zum Jahre 1975. Nauka, Moskau, 536 pp.

Karapetov, S.S., et al., 1975. On some important features of structure and evolution of the Afghan-Pamir segment of the Alpine fold belt. Bulletin of the Moscow University of Geology, nr. 3, p. 38–46.

Ruzhentsev, S.V., Shvolman, V.A., 1982. The Pamirs. In: MAHEL, M., 1982. Alpine Structural Elements: Carpathian-Balkan-Caucasus-Pamir Orogene Zone. Publishing House of the Slovak Academy of Science, Bratislava, 126 pp.

Schneider, J.F., 2011. Hazards and chances of natural landslide dams. Presentation: Sarez Conference, September 27–29, 2011, Dushanbe, Tajikistan.

Schneider, J.F., Mergili, M., et al., 2010. Remote Geohazards in High Mountain Areas of Tajikistan - Assessment of hazards connected to lake outburst floods and large landslide dams in selected areas of the Pamir and Alai mountains. FOCUS Humanitarian Assistance. 342 pp.

Searle, M., 2008. Geology of Tajikistan. In: Middleton, R., Thomas, H., 2008. Tajikistan and the High Pamirs, Odyssey Books & Guides, Illustrated Edition. Hong Kong, p. 236–240.

Slavin, V.I., 1976. Tectonics of Afghanistan. Nedra, Moscow, 205 pp.

Shroder, J.F., and Weihs, B.J., 2010. Geomorphology of the Lake Shewa landslide dam, Badakhshan, Afghanistan, using remote sensing data. Geografiska Annaler A, vol. 92, p. 469–483.

Appendix 2

Regional-scale analysis of lake outburst hazards in the South-Western Pamir, Tajikistan, based on remote sensing and GIS

Research article

Mergili, M., Schneider, J.F. (2011): Regional-scale analysis of lake outburst hazards in the southwestern Pamir, Tajikistan, based on remote sensing and GIS. Natural Hazards and Earth System Sciences 11: 1447-1462. doi:10.5194/nhess-11-1447-2011

Original article: http://www.nat-hazards-earth-syst-sci.net/11/1447/2011/nhess-11-1447-2011.pdf

Abstract

This paper presents an analysis of the hazards emanating from the sudden drainage of alpine lakes in the South-Western Tajik Pamir. In the last 40 years, several new lakes have formed in the front of retreating glacier tongues, and existing lakes have grown. Other lakes are dammed by landslide deposits or older moraines. In 2002, sudden drainage of a glacial lake in the area has triggered a catastrophic debris flow. Building on existing approaches, a rating scheme was devised allowing a quick regional-scale identification of potentially hazardous lakes and possible impact areas. This approach relies on GIS, remote sensing and empirical modelling, largely based on medium-resolution international datasets. Out of the 428 lakes mapped in the area, 6 were rated very hazardous and 34 hazardous. This classification was used for the selection of lakes requiring in-depth investigation. Selected cases are presented and discussed in order to understand the potentials and limitations of the approach used. Such an understanding is essential for an appropriate application of the methodology for risk mitigation purposes.

1 Introduction

Natural dams of different size and origin exist in mountain areas all over the world (Costa and Schuster, 1988). They often retain lakes which, in the case of a dam failure, may drain as powerful floods. If the failed dam is a glacier or a feature of a glacially shaped landscape, such events are called Glacial Lake Outburst Floods (GLOFs). Sudden drainage of glacial lakes has been reported from the Himalayas, the mountains of Central Asia, the North American mountains, the South American Andes, New Zealand and the Alps. (e.g. Clarke, 1982; Hewitt, 1982; Haeberli, 1983; Watanabe and Rothacher, 1996; Richardson and Reynolds, 2000; Vilímek et al., 2005; Narama et al., 2010). Climate change, with its impact on the glacial extent, the hydrological cycle and the condition of ice-bearing dams, may condition the occurrence of GLOFs in manifold ways and on different time scales (Evans and Clague, 1994; IPCC, 2007; Dussaillant, 2009; Haeberli et al., 2010a).

But also other types of lakes – particularly such dammed by landslide deposits – may be subjected to sudden drainage (Mergili and Schneider, 2010). Lake outburst floods (referred to as LOFs in the present paper, including both glacial and non-glacial lakes) often have a highly destructive potential. A large amount of water is released within a short time, with a high capacity to erode loose debris, potentially leading to a powerful flow with a long travel distance. Peak discharges are often some magnitudes higher than in the case of "normal" floods (Cenderelli and Wohl, 2001).

LOFs can evolve in different ways, possible causes are:

(1) landslides, rock/ice avalanches or calving glaciers that produce flood waves in a pro- or supra-glacial lake which may overtop and possibly breach glacial, morainic or landslide dams (Tinti et al., 1999);

(2) rising lake levels, leading to progressive incision and destabilization of a dam;

(3) hydrostatic failure of ice dams or enhanced ground water flow (piping), which can cause sudden outflow of accumulated water (Iturrizaga, 2005a, b);

(4) degradation of glacier dams or ice cores in morainic dams leading to loss of stability and to subsidence resulting in internal failure or progressive erosion if a certain threshold is reached.

Richardson and Reynolds (2000) and Haeberli et al. (2010a) provide overviews of conditioning and triggering factors of lake outburst floods, dam failure mechanisms and process interactions as well as case studies.

Even though lakes can be identified relatively easily with remote sensing tools and field work (e.g. Huggel et al., 2004b; Kääb et al., 2005; Quincey et al., 2007), the selection of potentially hazardous lakes, the prediction of outburst floods and modelling of the motion and reach of specific LOFs still remain a challenge (Kargel et al., 2010; Mergili et al., accepted). Changes in flow behaviour (e.g. from clear water flow to hyperconcentrated flow and debris flow or reverse) imply some difficulties when using computer models to predict LOF velocities and travel distances.

This paper presents a lake outburst susceptibility and hazard analysis for a selected area of the South-Western Pamir, focusing on the regional scale: GIS and Remote Sensing approaches are applied, allowing a quick identification of potentially hazardous lakes and possible impact areas over a large area. The results of such a study facilitate the selection of sites requiring more detailed studies and serve as a baseline for risk mitigation strategies in the region. It is attempted to push the methodology for this type of analysis forward, building on existing approaches (e.g. Reynolds, 2003; Huggel et al., 2004a).

2 Study area

The study presented covers the Gunt and Shakhdara valleys in the South-Western Tajik Pamir (Fig. 1). It covers a total surface area of 8,430 km². The Gunt River originates in the highlands of the Eastern Pamir and joins the Panj River near the town of Khorog (2075 m a.s.l.). The Shakhdara Valley is a Southern tributary of the Gunt Valley with the confluence just upstream from Khorog. From North to South, the valleys are separated by the Rushan Range (culminating at 6068 m a.s.l.), the Shugnan Range (5708 m) and the Shakhdara Range (6723 m), all stretching in an East-West direction. The North-South stretching Ishkashim Range (6095 m) follows directly North-West of the Shakhdara Range. In terms of geology, gneisses dominate the area, with remnants of a former sedimentary cover particularly in the Northern portion. The area is seismically active with frequent earthquakes (e.g. Babaev and Mirzoev, 1976).

The area covers the districts of Shugnan (Gunt Valley) and Roshtkala (Shakhdara Valley) under the Gorno-Badakhshan Autonomous Oblast of the Republic of Tajikistan with the regional centre of Khorog. Except for Khorog, the population largely depends on agriculture and pastoralism. Industry, services, and tourism are poorly developed. The permanent settlements concentrate close to the valley bottom and depend on irrigation with melt water. Transhumance to distant summer pastures in the upper valleys is common (Kassam, 2009).

The climate is semi-arid to arid, with an annual mean precipitation of 288 mm. Most of it occurs during winter and spring. The average annual air temperature is 9.2 °C (Khorog; 1970 – 2008). High-altitude meteorological data is missing. The major mountain ranges are glacierized, but most of the glaciers are in a stage of retreat. Many glacier tongues are covered by debris, so that it is hard to delineate their extent from satellite imagery or superficial field surveys.

Whilst many glaciers in the Northern Pamir have shown a variable behaviour during the previous decades (Mergili et al., submitted) or surge at certain intervals (e.g. Kotlyakov et al., 2008), the glaciers in the South-Western Pamir have been shrinking for several decades. Numerous lakes have formed in the front or on the top of retreating glacier tongues, and several more are retained by holocene landslide or moraine dams and in depressions within the glacially shaped terrain.

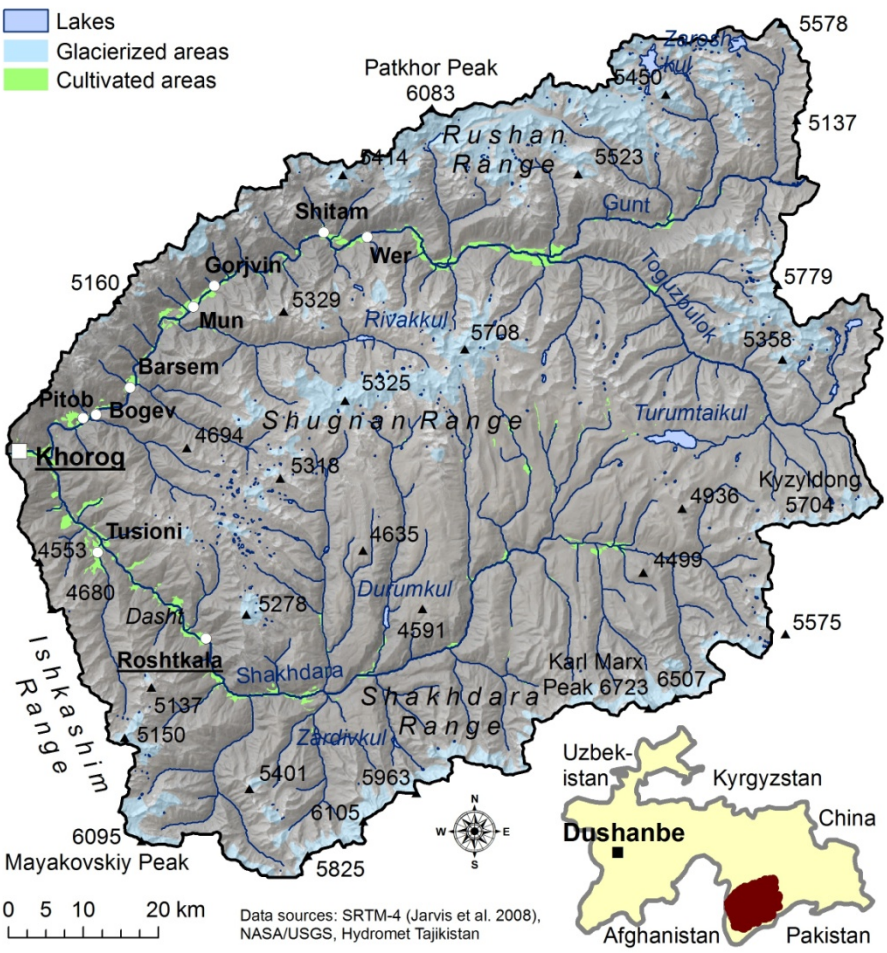

Fig. 1. The study area.

Altogether, 428 lakes were identified in the study area (including only those with a surface area ≥ 2500 m²). The majority of the lakes is found in the direct forefield of the recent glaciers and on the undulating highlands shaped by Pleistocenic glaciers. 90 per cent of all lakes are located between 4200 – 4900 m a.s.l. Some of the larger lakes, however, dammed by holocene landslides and/or terminal moraines from the Pleistocene, are located at lower elevation (e.g. Rivakkul, Durumkul, Zardivkul). No lakes at all were identified below 3341 m a.s.l.

3 The Dasht 2002 event

On August 7, 2002, the village of Dasht (Shakhdara Valley) was hit by a GLOF. 10.5 km upstream in the headwaters of the valley, a lake with a surface of 37,000 m², located on the decaying tongue of a debris-covered glacier, had suddenly released an estimated volume of 320,000 m³ of water. Multitemporal analysis of Landsat imagery showed that the lake had existed for less than two years prior to drainage (Mergili et al., submitted). The outburst occurred beneath the glacier surface. The most likely interpretation of the observed features is that a drainage channel within the glacier was suddenly blocked at the end of 2000 or in the beginning of 2001, allowing the development of the lake. With increasing lake size and therefore pressure, the blockage failed and the lake drained suddenly.

The volume of debris deposited on the cone was estimated 1.0 – 1.5 million m³, meaning that the ratio between entrained debris and water would be 3 – 5. This is a very high value compared to the ratio of 2 – 3 suggested by Huggel et al. (2004b). However, an even higher ratio than observed for Dasht was reported by Breien et al. (2008) for a GLOF in Norway. Possibly, subglacial water reservoirs connected to the superficial lake were involved in both events.

These figures show that the characteristics of the Dasht event underwent pronounced changes during the flow, converting from clear water runoff to a hyperconcentrated flow and finally to a granular debris flow. The event destroyed a large portion of the village of Dasht, killed dozens of people and dammed the Shakhdara river. It was reported that the flood wave arrived at Dasht in three stages, a phenomenon that can be explained by temporary backwater in the canyon of the lower transitional zone due to blockage of large boulders transported by the GLOF or by lateral slope failures followed by vigorous breakthroughs (Schneider et al., 2004). According to local people from the village of Baroj on the opposite side of the valley, the travel time from the onset of the process to Dasht was at least 45 minutes.

The Dasht event was the only major GLOF reported from the Pamir in the past decades. However, several events are known from the Tien Shan, most recently the outbursts of the Archa-Bashy glacier lake in 1998 and of the western Zyndan glacier lake in 2008 (Narama et al., 2010).

4 Lake inventory preparation

The study relies primarily on remotely sensed data. In order to obtain a multi-temporal coverage of the entire study area, the following sets of satellite images were collected:

(1) declassified Corona images (1968; pixel size <5 m)

(2) Landsat ETM+ images (2000 – 2003; pixel size 15 m pan-sharpened)

(3) ASTER images (2000 – 2009; pixel size: 15 m)

In addition, the SRTM-4 digital elevation model (Jarvis et al., 2008; approx. 90 m pixel size) was used. Despite its coarser resolution, it appeared to better represent the real terrain than ASTER DEMs, a finding in line with Kääb et al. (2005).

All lakes in the area were mapped for three time windows: 1968 (Corona imagery), 2001/02 (ASTER and pan-sharpened Landsat ETM+ imagery), and 2007/08 (ASTER imagery). Except for 1968, it was not possible to cover the entire area with cloud- and snow-free scenes from one single year, let alone day. Verification and the collection of additional information for each lake was supported by high-resolution Google Earth scenes.

Dam material, type of drainage and the presence of glaciers calving into the lake were recorded for each lake. Seepage through the dam was assumed for all lakes without a clearly recognizable surface drainage. Even though combinations and temporal changes of both types of lake drainage are common, a detailed analysis of this phenomenon is hardly applicable at the regional scale. Lake area A (m²) was derived and the freeboard F (m) was computed as difference between the DEM with filled sinks and the elevation of the lake (value of original DEM for the lake centroid).

Table 1 summarizes the key parameters assigned to each mapped lake. All lakes with $A < 2500$ m² in 2007/08 were excluded from the further analysis.

Regression functions relating lake volume to lake area were suggested e.g. by O'Connor et al. (2001) and Huggel et al. (2002), and used by Allen et al. (2009). However, computing lake volume directly from lake area is problematic. The area is immanent to the volume and autocorrelation effects reduce the large scatter in the relation of measured area and depth and lead to an overestimation of the information quality (Huggel et al., 2002). Therefore, average lake depth was first derived from lake area using an empirical relationship developed by Huggel et al. (2002):

$$D = 1.04 \cdot 10^{-1} A^{0.42} \quad (1)$$

In a next step, lake volume V (m³) was derived from lake area and average lake depth:

$$V = D \cdot A = 1.04 \cdot 10^{-1} A^{1.42} \quad (2)$$

Lake area development was expressed as the lake area in 1968 resp. 2001/02, related to the area in 2007/08:

$$r_{A1} = \frac{A_{1968}}{A_{2007/08}} \quad (3)$$

$$r_{A2} = \frac{A_{2001/02}}{A_{2007/08}} \quad (4)$$

Values below 1 indicate a growth, values above 1 a shrinkage of the lake. Values of 0 mean that the lake did not yet exist in 1968 resp. 2001/02. Lakes existing in 1968 and/or 2001/02, but not in 2007/08, were disregarded in the analysis.

As lake outburst floods are often related to major earthquakes, a surrogate for the seismic hazard was introduced: the maximum possible Peak Ground Acceleration PGA_{max} (cm/s²) was considered useful for this purpose. It was derived from a published map of active faults of Tajikistan (Babaev et al., 1984) and empirical relationships relating PGA_{max} to the maximum earthquake magnitude assigned to the fault and the distance to the fault axis (Abdrakhmatov et al., 2003).

5 Hazard analysis

5.1 Work flow

The hazard analysis procedure applied to the regional scale is illustrated in Fig. 2. It aims at the identification of potentially hazardous lakes and possible impact areas of LOFs as a baseline for in-detail studies and risk mitigation procedures. The concept includes the hazard

(1) of each lake to produce an outburst flood (lake outburst hazard *H*);

(2) of each pixel to be affected by an outburst flood from a certain lake (impact hazard *HI*).

The general difficulty of establishing frequencies for rare or singular events like lake outburst floods in combination with sparse historical data in the study area made a strictly quantitative approach inapplicable. The concept of susceptibility – understood as the tendency of a lake to

produce an outburst flood resp. the tendency of an outburst flood to reach a certain area or pixel – is used instead. It is combined with the maximum possible magnitude in order to derive a measure for the hazard. The developed and employed system of scoring and rating partly refers to work done by Reynolds (2003) and Huggel et al. (2004a) and is explained in the following sections.

The entire work flow is realized as a system of a shell and a C script making use of GRASS GIS, which is an Open Source Geographic Information Software, for the spatial analysis components. The major spatial modelling tasks include the topographic Susceptibility Index *TSI* (see next section), the dam geometry and the area of impact. The DEM, a raster map with a unique ID for each lake, and a text file with the parameters listed in Table 1 for each lake are used as input. The output consists of a table with the lake outburst susceptibility and hazard ratings for each lake as well as raster maps with lake-specific impact susceptibility and hazard ratings for each pixel.

The procedure is applied with a pixel size of 60 m. The results are verified by testing the output of the entire procedure against the information available for the Dasht 2002 event and by in-depth investigations of selected cases. For this purpose, several helicopter and field missions were carried out in 2003 and 2009 in order to ensure a close and up-to-date survey of the lakes and valleys of interest.

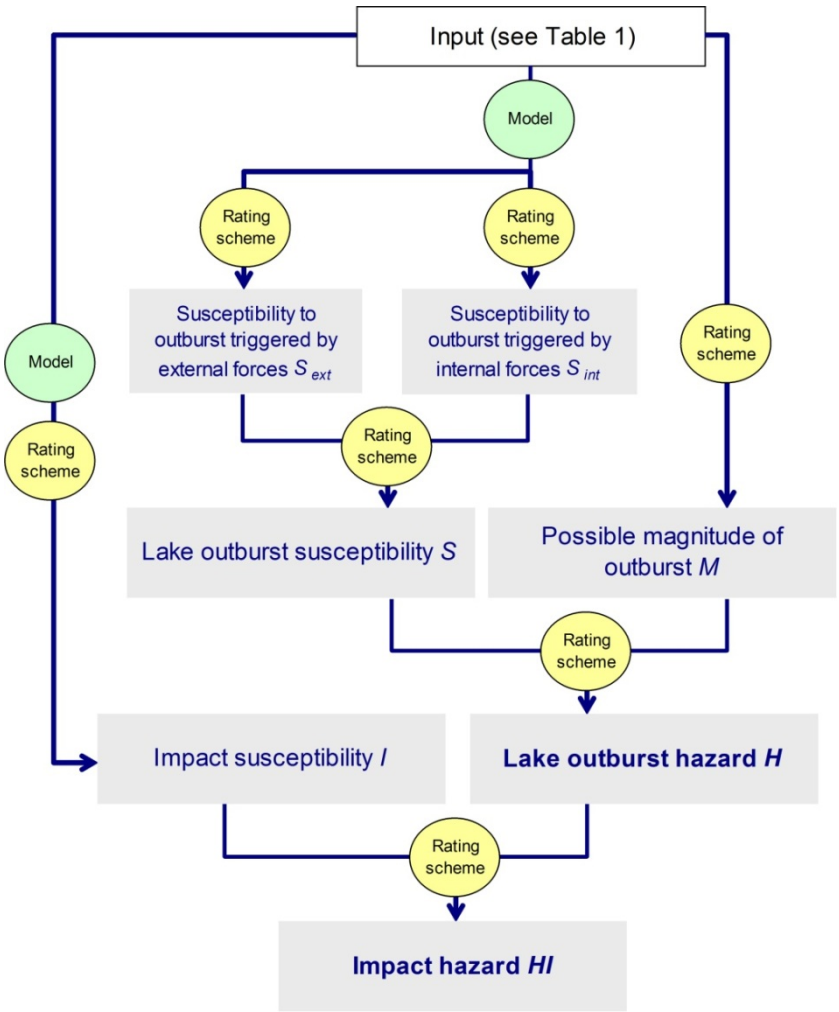

Fig. 2. Work flow of the regional-scale hazard analysis.

Table 1. Parameters used as input for the regional-scale lake outburst hazard analysis (see Fig. 2).

Parameter	Shortcut	Unit	Source
Lake drainage		boolean	Qualitative interpretation of satellite imagery (ASTER, WorldView, GoogleEarth)
Dam type		nominal	
Possible calving into lake		boolean	
Elevation a.s.l.	z	m	Computed from lake centroid and DEM
Freeboard	F	m	
Lake area	A	m²	Derived from mapped lakes
Average lake depth	D	m	Empirical relationship with lake area (Eq. 1)
Lake volume	V	m³	Derivation from lake area and average lake depth (Eq. 2)
Lake area development 1968 – 2007/08	r_{A1}	ratio	Comparison of lake areas derived by multitemporal analysis of satellite imagery
Lake area development 2001/02 – 2007/08	r_{A2}		
Maximum Peak Ground Acceleration	PGA_{max}	m/s²	Map of active faults and published relationships (Babaev and Mirzoev, 1984; Abdrakhmatov et al., 2003)

5.2 Lake outburst susceptibility and hazard

5.2.1 Susceptibility to lake outburst triggered by external forces

The susceptibility to each lake to produce an outburst flood triggered by any kind of mass movement interfering with the lake or by an earthquake is investigated. The event at Laguna 513 in the Cordillera Blanca (Perú; Haeberli et al., 2010b), where an ice avalanche from far upslope caused a destructive flood wave on April 11, 2010, has shown the need to include the entire catchment in such an analysis, and not only the portion directly adjacent to the lake. The topographic susceptibility index *TSI* is introduced in order to account for this need: each pixel within the catchment of the lake is assigned to one of 25 predefined classes, based on the local slope and the average slope of the steepest path to the lake. Depending on the class, a topographic susceptibility rating *TSR* (with possible values 0 – 10) is assigned to the pixel, describing the tendency of the lake to be affected by a mass movement originating from the respective pixel. The rating builds on a combination of classes of local slope for the onset and of the average slope of the potential flow path between onset area and lake for the motion of mass movements, following thresholds given e.g. by Corominas et al. (2003). In order to derive *TSI* for the entire catchment, the sum of the *TSR*s for each class is weighted by the surface area assigned to the respective class (possible weights: 1 – 4). The weighted indices for each class are then summed up. The resulting maximum possible *TSI* is 212. This concept does not account for the

local geological conditions, but provides a valuable estimate where impacts are basically possible and where they are not.

TSI is the base for the rating of the susceptibility to lake outburst triggered by external forces S_{ext} (Table 2). The possibility of ice calving into the lake is accounted for by increasing S_{ext} by 1 for lakes with directly adjacent glaciers.

Regarding the probability of triggering events, too little high-altitude meteo data are available to be included in the rating. The Maximum Peak Ground Acceleration PGA_{max} is used to account for the seismic hazard. *PGA* thresholds for the triggering of mass movements in different areas show a large scatter. The values of $0.5 - 2$ m/s² found out by Wang et al. (2010) for the Wenchuan 2008 earthquake relate to the extremely landslide-prone slopes of that area and are not applicable to the South-Western Pamir. Murphy et al. (2002) suggested thresholds between 4.5 and 20.4 m/s² for the rocky slopes of the Tachia Valley in Taiwan. Holding to these findings, S_{ext} is increased by 1 for $PGA_{max} \geq 5$ m/s².

The freeboard F (m) is computed from the DEM. For lakes with $F \geq 25$ m, the rating is decreased by 1 in order to derive the final rating (see Table 2). Therefore, S_{ext} could take values between 0 and 4 (negative values are considered as 0).

Table 2. Rating scheme for susceptibility to outburst triggered by external forces S_{ext}. Initial values of S_{ext} are determined from the topographic susceptibility index. These values are then increased or decreased according to the possibility of calving, seismic hazard and freeboard.

Criterion	Class	Definition	S_{ext}
Topographic susceptibility index	1 Low	$TSI < 10$	0
	2 Medium	$TSI \geq 10 - < 40$	1
	3 High	$TSI \geq 40$	2
Calving into lake	1 No calving possible	mapped	±0
	2 Calving possible	mapped	+1
Seismic hazard	1 Low	$PGA_{max} < 500$ cm/s²	±0
	2 High	$PGA_{max} \geq 500$ cm/s²	+1
Freeboard	1 High	$F > 25$ m	-1
	2 Low	$F \leq 25$ m	±0

5.2.2 Susceptibility to lake outburst triggered by internal forces

As directly measured quantitative data is not applicable at the regional scale, a qualitative rating for the Susceptibility to lake outburst by internal forces (dam failure) S_{int} has to be introduced, building on the following key parameters: (1) dam material; (2) lake drainage, (3) lake area development, and (4) dam geometry. Table 3 shows the applied rating scheme.

Dams with seepage are rated more susceptible to failure than dams with surface runoff only, and growing lakes are rated more susceptible than stable or shrinking ones. All lakes with a size of ≤ 80 per cent of the 2007/2008 surface area in either 1968 or 2001/02 are classified as growing.

Dam geometry is expressed as an idealized average downstream slope of the dam: the dam width W is defined as the Euclidean distance between the lake outlet and the closest pixel along the downstream flow path with a lower elevation than the average lake bottom, using the average lake depth D. The tangent of the average slope of the dam in outflow direction, $\tan \beta$, is then derived as D/W. For very small downstream average slopes $\tan \beta \leq 0.02$, the rating is decreased by 1 (see Table 3).

Also S_{int} could take values between 0 and 4, negative values are considered as 0.

Table 3. Rating scheme for Susceptibility to lake outburst triggered by internal forces S_{int}. Initial values of S_{int} are determined from the dam material. These values are then increased or decreased according to lake drainage, lake area development and downstream slope of dam.

Criterion	Class	Definition	S_{int}
Dam material	1 Embedded lake	mapped	0
	2 Block dam	mapped	0
	3 Debris dam	mapped	1
	4 Rocky swell dam	mapped	0
	5 Glacier or fresh moraine dam	mapped	2
Lake drainage	1 Clearly recognizable surface drainage	mapped	±0
	2 No clearly recognizable surface drainage	mapped	+1
Lake area development	1 Stable or shrinking	r_{A1} and $r_{A2} > 0.8$	±0
	2 Growing	r_{A1} or $r_{A2} \leq 0.8$	+1
Downstream slope of dam	1 Gentle	$\tan \beta < 0.02$	-1
	2 Steep	$\tan \beta \geq 0.02$	±0

5.2.3 Derivation of lake outburst susceptibility and hazard

The ratings for S_{int} and S_{ext} are combined using the rating scheme shown in Table 4. In order to derive a measure for the hazard, the resulting lake outburst susceptibility S is combined with a measure for the potential event magnitude M. Lake volume V or the expected peak discharge of an outburst flood Q_p would be most suitable, but they are derived by empirical equations only

and are highly uncertain. The lake volume is directly related to the lake area A (see Eq. 1 and Eq. 2). Therefore, the well-known lake area appears to be the best surrogate for *M*. The rating for the lake outburst hazard *H* is derived by combining the outburst susceptibility *S* of each lake with its area class. The applied scheme is shown in Fig. 3.

Table 4. Lake outburst susceptibility rating *S*: combination of S_{ext} and S_{int}.

$S_{int}\downarrow$ $S_{ext}\rightarrow$	0	1	2	3	4
0	0	1	2	3	4
1	1	2	3	3	4
2	2	3	3	4	5
3	3	3	4	4	5
4	4	4	5	5	6

M ↓ *S* →	0 Ne	1 Lo	2 Mo	3 Me	4 Hi	5 Vh	6 Eh
A < 5,000 m²	0 Ne	0 Ne	0 Ne	0 Ne	0 Ne	0 Ne	0 Ne
A = 5,000 – <20,000 m²	0 Ne	1 Lo	1 Lo	2 Mo	2 Mo	2 Mo	3 Me
A = 20,000 – <40,000 m²	0 Ne	1 Lo	2 Mo	3 Me	3 Me	3 Me	4 Hi
A = 40,000 – <100,000 m²	0 Ne	2 Mo	3 Me	3 Me	3 Me	4 Hi	4 Hi
A = 100,000 – <250,000 m²	0 Ne	2 Mo	3 Me	4 Hi	4 Hi	5 Vh	5 Vh
A = 250,000 – <1,000,000 m²	0 Ne	2 Mo	3 Me	4 Hi	5 Vh	5 Vh	6 Eh
A ≥ 1,000,000 m²	0 Ne	3 Me	4 Hi	4 Hi	5 Vh	6 Eh	6 Eh

Fig. 3. Lake outburst hazard *H*: combination of lake area as surrogate for the possible lake outburst magnitude *M* and susceptibility *S*. Ne = negligible, Lo = low, Mo = moderate, Me = medium, Hi = high, Vh = very high, Eh = extremely high.

5.3 Impact susceptibility and hazard

5.3.1 Impact susceptibility

Impact susceptibility *I* is understood as the tendency of an outburst flood from a defined lake to affect a certain area resp. pixel. It disregards the lake outburst hazard *H* which is included in the next step (impact hazard *HI*).

On the regional scale, empirical-statistical relationships are suitable for relating the travel distance *L* or the average slope of reach ω of a flow to the involved volume *V* or the peak discharge Q_p, or just defining a global ω. Table 5 shows some of these relationships developed for debris flows in general and lake outburst floods in particular.

Corominas et al. (2003) found an average angle of reach of $\omega = 21°$ for debris flows on unobstructed flow paths. Rickenmann (1999) related the horizontal travel distance L (m) to the bulk volume of the flow *V* (m³) and the vertical distance *Z* (m) (see Table 5). The results obtained by these rules show a large scatter among themselves and generally underestimate the

travel distance of LOFs (Mergili et al., accepted; Fig. 4). Haeberli (1983) suggested $\omega = 11°$ specifically for GLOFs, which was applied by Huggel et al. (2003) in combination with the Modified Single Flow direction model (MSF).

Several authors have proposed empirical relationships for deriving the peak discharge Q_p (m³/s) – required as input for the relationship T3 in Table 5 – based on outburst volume V (m³) and dam height resp. lake depth D (m) as predictors, see e.g. Crosta et al. (2006) for an overview. In the present study, the outburst volume was set equal to the lake volume (worst-case assumption). Table 6 summarizes various approaches, mainly regression functions. Huggel et al. (2004a) emphasized the importance to distinguish between different types of dams. t in the relationship Q8 stands for the duration of the outburst, Huggel et al. (2004a) suggest to set $t = 1000$ s as a first approximation.

Table 5. Empirical relationships potentially suitable for estimating the travel distance of lake outburst floods.

	Relationship	References	Remarks
T1	$L = 1.9V^{0.16}Z^{0.83}$	Rickenmann (1999)	for debris flows in general
T2	$\omega = 11°$	Haeberli (1983), Huggel et al. (2003), Huggel et al. (2004a)	for debris flows from GLOFs, applied with $\omega = 8°$ in the present paper
T3	$\omega = 18Q_p^{-0.07}$	Huggel (2004)	worst case for debris flows from GLOFs
T4	$\omega \geq 2°$	Haeberli (1983), Huggel et al. (2004a)	for floods from GLOFs

After the deposition of the debris or mud carried by the LOF, or if not much sediment is entrained at all, the flood may propagate much farther: Haeberli (1983) suggested an average angle of reach of 2 – 3°, but also travel distances exceeding 200 km were reported (e.g. Hewitt, 1982).

In order to achieve a robust estimate of the travel distance of potential LOFs, the approaches T1 – T4 shown in Table 5 are combined. The approach of Corominas et al. (2003) is disregarded as it is apparently not at all suitable for LOFs. The susceptibility of each pixel to be affected by an outburst flood from the respective lake is computed as follows, making use of GRASS GIS:

(1) The lake outburst flood is considered as one single mass point, starting from the outlet of the respective lake. It is routed downstream following a random walk approach weighted for the local slope angle. In order to cover all possible pathways, 800 random walks are performed for each lake.

(2) At the start of each random walk, the empirical relationship defining the travel distance is determined randomly, choosing among T1 – T4 (see Table 5). This means that ±200 random walks are performed according to each of the relationships. For T1, the volume V is randomly

varied between one time and four times the lake volume in order to account for bulking with sediment. Regarding T3, Q_p is chosen randomly from Table 6 for each random walk. Q1 – Q9 are used for glacial lakes (Type 5 in Table 3). For all other lakes, only the relationships Q1 – Q7 are used. This leads to the representation of all the relationships in the results (±25 – 30 random walks per relationship).

Table 6. Empirical equations relating peak discharge Q_p to outburst volume V and lake depth resp. dam height D. ϱ_w = density of water (kg/m³), g = gravity (m/s²). The relationships Q1 to Q7 were developed for landslide dams, Q8 is valid for moraine dams and Q9 for the subglacial drainage of ice-dammed lakes. The examples refer to the computed peak discharges of the Dasht event 2002 (lake area: 37,000 m²) and a hypothetic complete drainage of Rivakkul (1.2 km²). Values in brackets refer to drainage modes not relevant for the respective lake and are shown for comparison only.

	Equation for Q_p (m³/s)	Reference	Example Q_p Dasht 2002	Example Q_p Rivakkul
Q1	$672\left(10^{-6}V\right)^{0.56}$	Costa (1985)	(354 m³/s)	5562 m³/s
Q2	$6.3D^{1.59}$		(194 m³/s)	1955 m³/s
Q3	$181\left(10^{-6}V \cdot D\right)^{0.43}$		(280 m³/s)	4329 m³/s
Q4	$1.58 \cdot 10^{-2}\left(\rho_W \cdot g \cdot V \cdot D\right)^{0.41}$	Costa and Schuster (1988)	(299 m³/s)	4072 m³/s
Q5	$1.6V^{0.46}$	Walder and O'Connor (1997)	(544 m³/s)	5225 m³/s
Q6	$6.7D^{1.73}$		(278 m³/s)	3446 m³/s
Q7	$9.9 \cdot 10^{-1}\left(V \cdot D\right)^{0.40}$		(373 m³/s)	4766 m³/s
Q8	$2V/t$	Huggel et al. (2002)	(638 m³/s)	(87,124 m³/s)
Q9	$46\left(10^{-6}V\right)^{0.66}$	Walder and Costa (1996)	22 m³/s	(555 m³/s)

(3) An impact susceptibility rating I (0 negligible – 6 extremely high) is then assigned to each pixel, based on the number n of relationships T1 – T4 predicting an impact for the corresponding pixel, and on the average slope ω (Table 7). With $n = 1$, the corresponding relationship would always be T4, yielding the longest travel distance and the largest impact area. For these pixels, the possible type of impact is considered as a flood (no debris flow), and the impact susceptibility rating I is 1 low – 3 medium, depending on ω. If at least two of the relationships predict an impact on the pixel, also debris flow is considered as possible impact type, and the impact susceptibility is defined 4 high – 6 extremely high, depending on n.

Table 7. Impact susceptibility rating *I*. *n* stands for the number of relationships (see Table 5) predicting an impact on the considered pixel, ω stands for the average slope angle from the lake to the considered pixel. Since the relationship designed for floods predicts the longest travel distance and not all LOFs evolve into debris flows, the impact type for pixels with $n \geq 2$ can be flood or debris flow.

I	*n*	ω (degree)	type of impact
0 Negligible	0		
1 Low	1	<4	flood
2 Moderate		4 – <6	
3 Medium		≥6	
4 High	2	not applicable	debris flow or flood
5 Very high	3		
6 Extremely high	4		

5.3.2 Impact hazard

The ratings for lake outburst hazard *H* and impact susceptibility *I* are combined to a rating of the impact hazard *HI* according to the matrix shown in Fig. 4. A first step towards risk analysis is taken by an overlay of the impact hazard map with a map of settlements and cultivated areas. A further differentiation of this map regarding exposure and vulnerability would be required for a full regional-scale risk analysis.

H↓ *I*→	0 Ne	1 Lo	2 Mo	3 Me	4 Hi	5 Vh	6 Eh
0 Ne	0 Ne	0 Ne	0 Ne	0 Ne	0 Ne	0 Ne	0 Ne
1 Lo	0 Ne	1 Lo	1 Lo	2 Mo	2 Mo	2 Mo	3 Me
2 Mo	0 Ne	1 Lo	2 Mo	3 Me	3 Me	3 Me	4 Hi
3 Me	0 Ne	2 Mo	3 Me	3 Me	3 Me	4 Hi	4 Hi
4 Hi	0 Ne	2 Mo	3 Me	4 Hi	4 Hi	5 Vh	5 Vh
5 Vh	0 Ne	2 Mo	3 Me	4 Hi	5 Vh	5 Vh	6 Eh
6 Eh	0 Ne	3 Me	4 Hi	4 Hi	5 Vh	6 Eh	6 Eh

Fig. 4. Matrix for the impact hazard *HI* rating based on the ratings for lake outburst hazard rating *H* and impact susceptibility *I*. The abbreviations are explained in the legend of Fig. 3.

6 Evaluation with the Dasht 2002 event

The hazard analysis procedure is evaluated using the Dasht 2002 event. In its surface appearance, the lake did not differ substantially from many other glacial lakes in the study area. The lake outburst susceptibility is rated very high, the hazard – due to the limited size of the lake – as medium only.

All empirical models shown in Table 5 underestimate the travel distance of the debris flow of Dasht, which is characterized by ω = 9.3°. Whilst the resulting debris flow had reached the village of Dasht 10.5 km downstream from the lake, the empirical relationships predict the debris flow to stop already in the upper portion of the catchment (Fig. 5). The reasons for the long travel distance might be a mobilized subglacial water reservoir involved in the flow, a particular flow rheology, or backwater effects: according to field observations and interviews with the local population, a blockage of a narrow channel section occurred for at least two times, followed by vigorous releases of water, debris and mud (Schneider et al., 2004).

In order to get more conservative values – as desired in this type of analysis – a value of ω = 8° is used when applying relationship T2 to the South-Western Pamir (see Table 5).

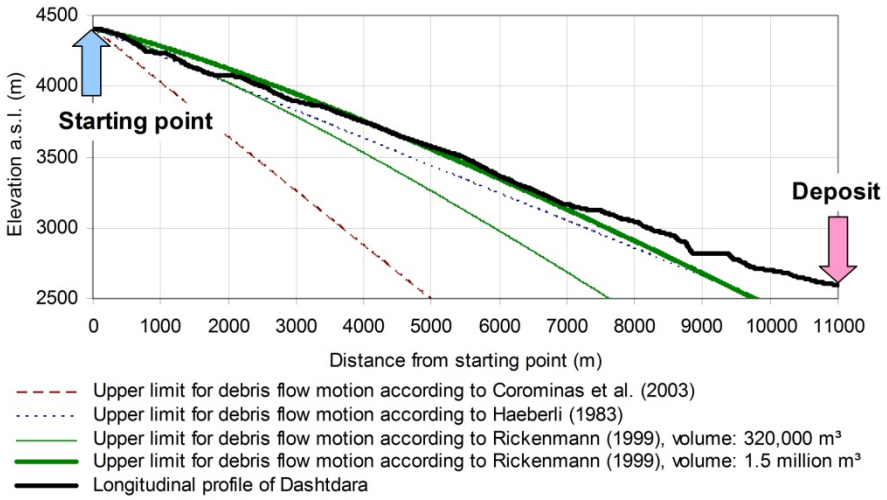

Fig. 5. Longitudinal profile of the flow path of the Dasht 2002 event with the upper limits of the flow paths according to different empirical relationships.

7 Results

7.1 Distribution and characteristics of lakes

For the period 2007/08, 428 lakes with A ≥ 2,500 m² are identified in the study area. 20 of them are just widened portions of rivers or shallow swampy lakes (recognized by topographic situation, colour and the existence of gravel bars) and are excluded from further analysis. Among the 408 remaining lakes, 187 are embedded in undulating landscapes most likely formed during the Pleistocene, at some distance from the recent glaciers, but still above 4000 m a.s.l (Type 1 in Table 3). 20 lakes have dams dominated by coarse blocks, representing Pleistocenic terminal moraines, landslide deposits or a combination of both (Type 2). 13 lakes are dammed by talus or debris cones (Type 3) and 16 by pronounced rocky swells (Type 4). The remaining 172 lakes represent glacial lakes in the strict sense: they are either directly embedded in the exposed ice, or dammed by debris-covered glacier tongues, rock glaciers or fresh moraines (Type 5). The transition between the latter three types is rather gradual than sharp and the identification requires geophysical methods not applicable at the regional scale. No distinction was therefore made between pro- and supraglacial lakes. Table 8 summarizes the numbers and some geometric characteristics of the different lake types.

Fig. 6 plots the altitudinal distribution of the lakes, organized by dam types. Less than 10 per cent of all lakes are found below 4200 m a.s.l., but two of them are larger than 1 km² (Durumkul and Rivakkul; Type 2). At approx. 4200 m a.s.l., the steep valley flanks give way to the undulating plains formed by Pleistocenic glaciers. The latter landscape hosts numerous lakes of Type 1. Turumtaikul and Zaroshkul are the largest representatives of this type. Above 4500 m a.s.l., in the zone of recent glaciers and fresh moraines, lakes of Type 5 become more abundant and dominate the zone from 4700 m upwards. The highest identified glacial lakes are located at 5060 m a.s.l. The highest density of lakes is found at 4500 – 4550 m a.s.l. Reasons are the large share of the land area in this class on the one hand (see Fig. 6) and the presence of favourable conditions for the development of lakes of Type 1 and 5 on the other hand.

Fig. 6 also shows the trends of lake development. Most glacial lakes (Type 5), located in a changing environment with active morphodynamics (Mergili et al., submitted), are growing, as are many lakes of Type 1.

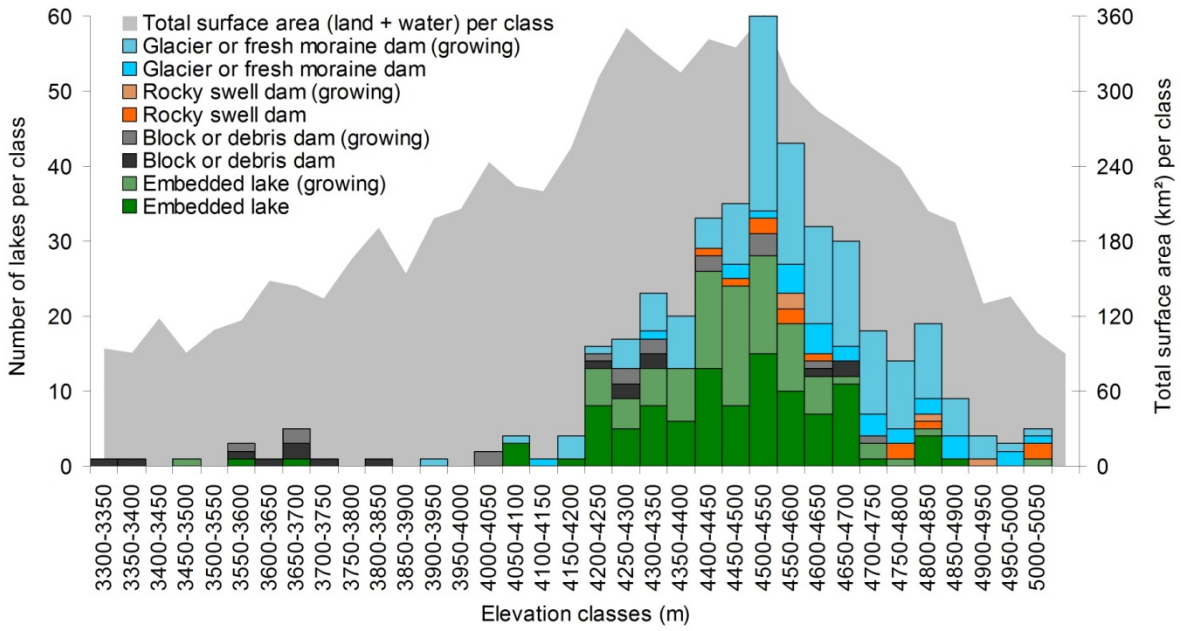

Fig. 6. Distribution of lake types and lake evolution plotted against elevation. The distribution of the total surface of the study area is shown as reference.

7.2 Lake outburst susceptibility

There is no significant differentiation of lake types regarding the susceptibility to lake outburst triggered by external forces S_{ext}, which rather depends on the topography and state of the adjacent slopes than on the dams themselves (Fig. 7a). Glacial lakes are most susceptible to outbursts triggered by internal forces, as prescribed by the rating scheme (Fig. 7b). In sum, glacial lakes are by far the most susceptible, with 66 cases of very high susceptibility (Class 5) and 85 cases of high susceptibility (Class 4). There are also 15 non-glacial lakes with high susceptibility. All other lakes are assigned to Class 3 (medium susceptibility) or lower (Fig. 7c).

7.3 Lake outburst hazard and Impact hazard

Among the 408 analyzed lakes, the lake outburst hazard H for 122 is classified as negligible (Class 0), for most of them due to their limited size of $A < 5{,}000$ m² (Fig. 7d). 35 lakes are assigned to Class 1 (low hazard), 124 to Class 2 (moderate hazard), 87 to Class 3 (medium hazard), 34 to Class 4 (high hazard) and 6 to Class 5 (very high hazard). No lakes are assigned to Class 6 (extremely high hazard). Glacial lakes are more prominent regarding susceptibility than hazard, as they are in average smaller than lakes of some of the other classes (see Table 8). In contrast, the large Durumkul with a surface area of 1.7 km² and Rivakkul with 1.2 km², dammed by deposits of large blocks (landslide deposits or Pleistocenic moraines), are both rated hazardous though moderate resp. medium lake outburst susceptibility.

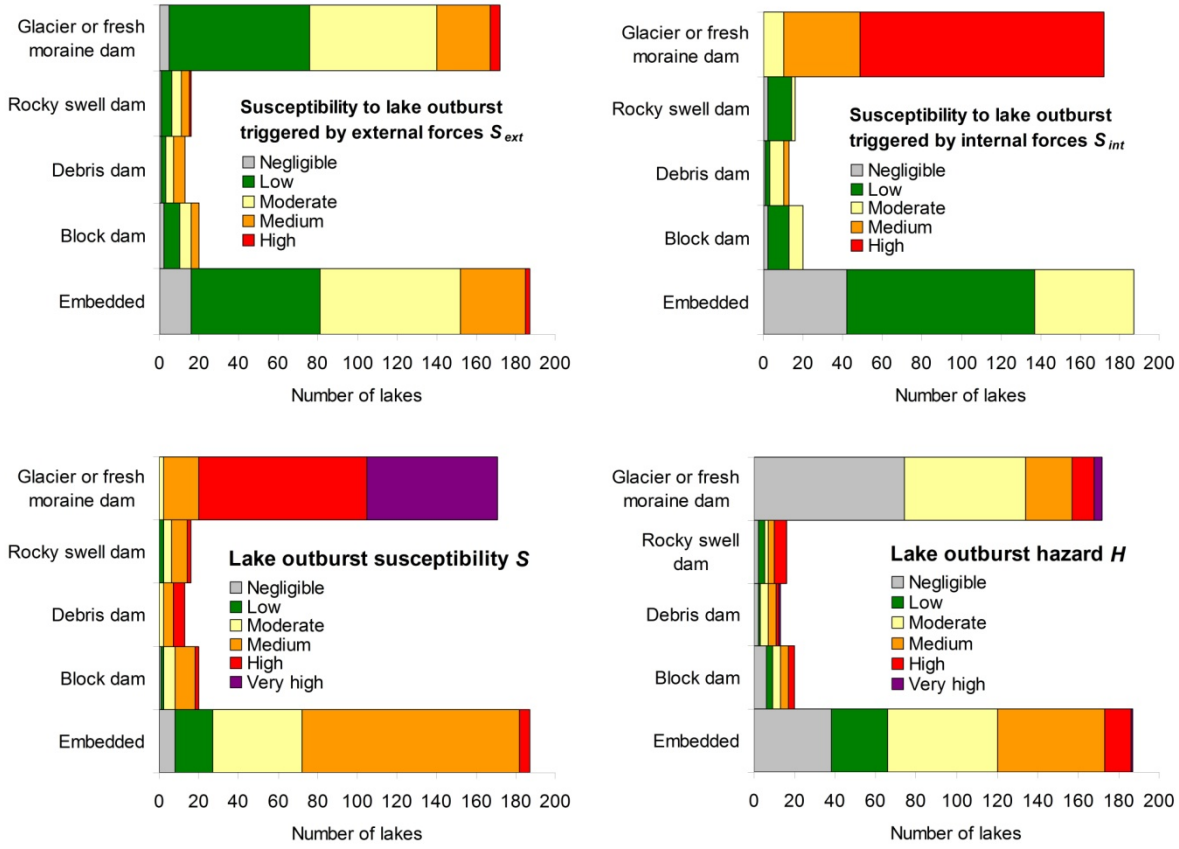

Fig. 7a. Susceptibility to lake outburst triggered by external forces S_{ext}.

Fig. 7b. Susceptibility to lake outburst triggered by internal forces S_{int}.

Fig 7c. Combined lake outburst susceptibility S.

Fig. 7d. Lake outburst hazard H.

Table 8. Lake statistics, organized by lake type. n_l = number of lakes, p_g = percentage of growing lakes, A_{avg} and A_{max} = average resp. maximum lake area, z_{min}, z_{avg} and z_{max} = minimum, average and maximum elevation a.s.l.

Lake type	n_l	p_g	A_{avg} (km²)	A_{max} (km²)	z_{min} (m)	z_{avg} (m)	z_{max} (m)

1 Embedded lake	187	45	0.143	8.99	3473	4460	5029
2 Block dam	20	55	0.205	1.68	3341	4076	4718
3 Debris dam	13	46	0.085	0.62	3590	4223	4686
4 Rocky swell dam	16	25	0.107	0.48	4418	4692	5021
5 Glacier or fresh moraine dam	172	83	0.018	0.41	3926	4608	5063

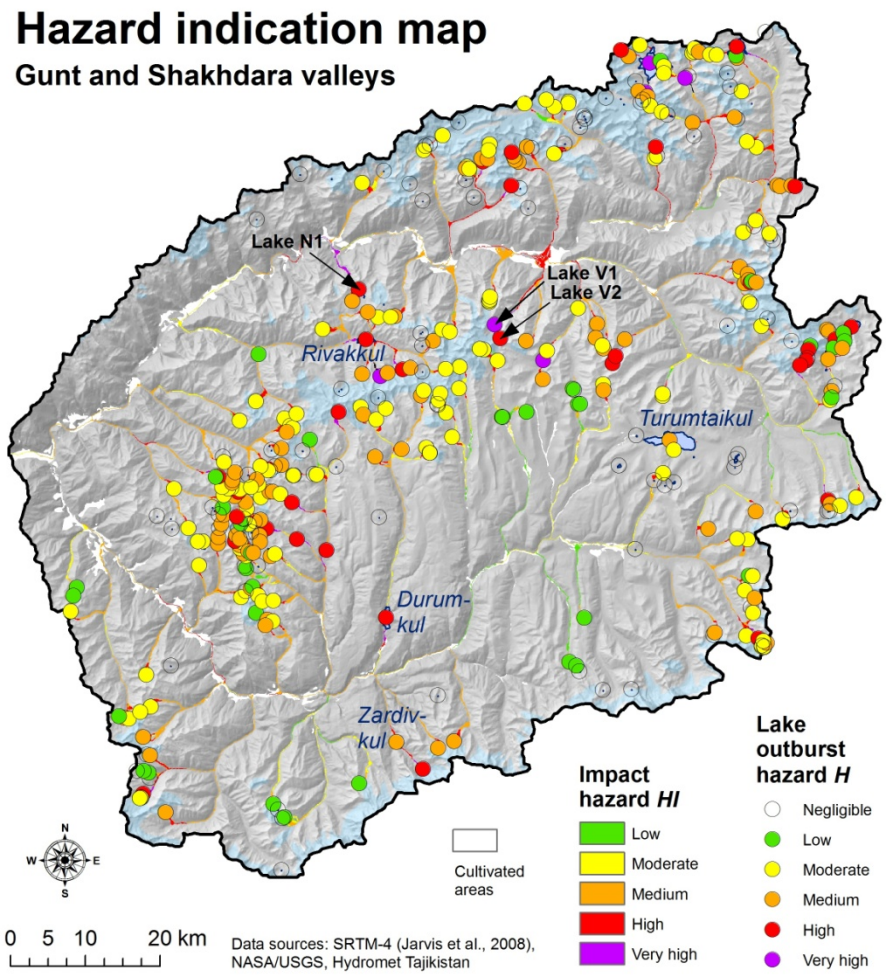

Fig. 8. Hazard indication map for the Gunt and Shakhdara valleys.

Fig. 8 shows the hazard indication map for the entire study area. The lake outburst hazard for each lake and the impact hazard for each pixel are shown. The maximum travel distances of potential debris flows and floods emanating from the lakes are plotted in Fig. 9. Only for 97 out of the 408 lakes, debris flows exceeding a travel distance of 2 km are predicted in the case of an outburst. The maximum value (15.5 km) is computed for Nimatskul (Lake N1 in Fig. 8; see next section). Flooding could proceed for more than 30 km in the case of 298 lakes, with a maximum of 75.5 km. However, it has to be kept in mind that the only criterion used for the travel distance of floods is the average slope of the flow path. Many lakes in the study area are too small to produce floods reaching that far.

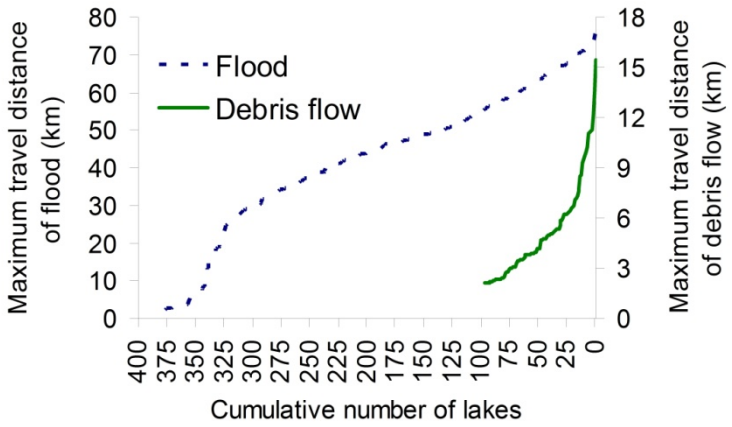

Fig. 9. Computed maximum travel distances of debris flows and floods from lake outbursts.

7.4 Case studies

The Dasht event is the only documented LOF in the study area. There is evidence for earlier outburst floods e.g. of Rivakkul (Schneider et al., 2004), but the observations are too vague to be used as reference.

The lakes identified as hazardous or very hazardous can be organized into two categories:

(1) growing glacial lakes (Type 5), mostly with seepage through the dam;

(2) large lakes of various types (Type 1, 2 and 4 according to Table 3).

Whilst it would be out of scope of the present paper to discuss all of those lakes in detail, one example of each type will be shown in order to illustrate the specific potentials and limitations of the regional-scale analysis procedure when zooming into a more detailed level.

A growing glacial lake (Lake V1) is located in the upper reaches of Varshedzdara at 4513 m a.s.l. (Fig. 10a and Fig. 10b; see Fig. 8), 11 km upstream of the village of Varshedz. In summer 2007, the lake had a surface area of 155,000 m². Lake outburst susceptibility and hazard are rated very high. Lake V1 serves as an example for many similar glacial lakes in the study area, most of which are, however, smaller. A second, larger lake (360,000 m²) of stable size (Lake V2) is located 2.5 km upstream from Lake V1, at 4,795 m a.s.l. It is dammed by a rocky swell partly covered by morainic material and bordered by steep, partly glacierized slopes. It has no permanent surface drainage. The lake outburst susceptibility was rated medium, the lake outburst hazard high. An ice avalanche into the lake would be the most likely scenario causing a flood wave. However, only a fraction of the lake would drain in such a case.

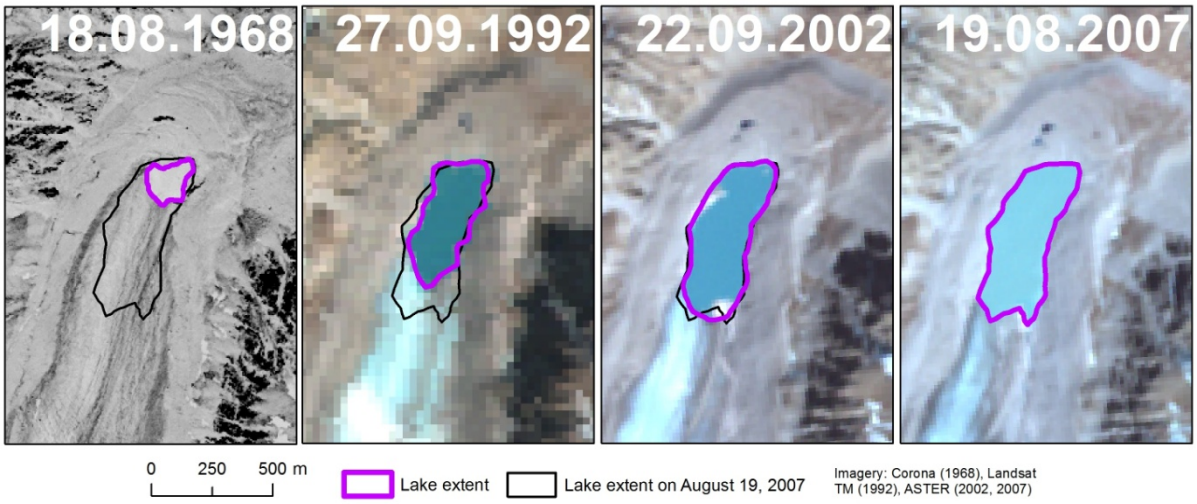

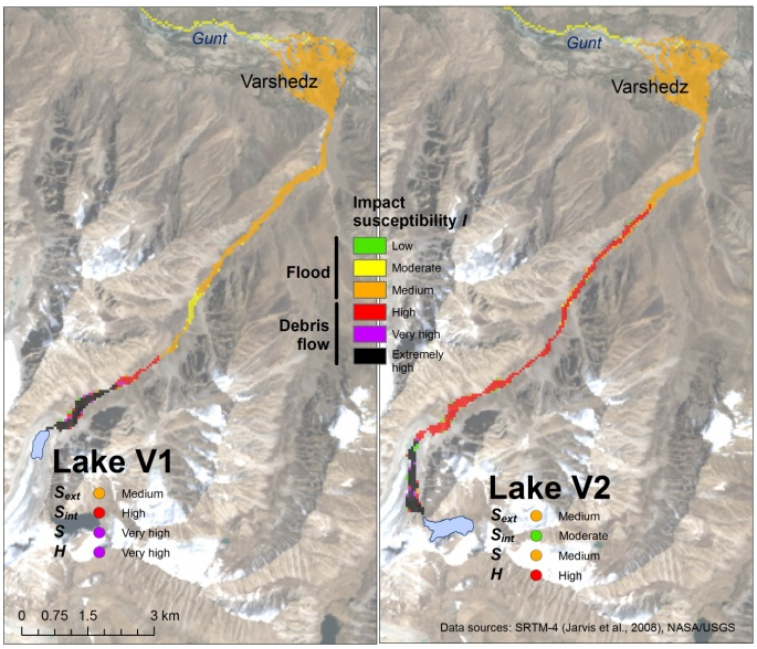

Fig. 10a. Aerial view of Lake V1 (August 2009).

Fig. 10b. Development of Lake V1 1968 – 2007.

Fig. 10c. Impact susceptibilities *I* for potential outbursts of Lake V1 and Lake V2.

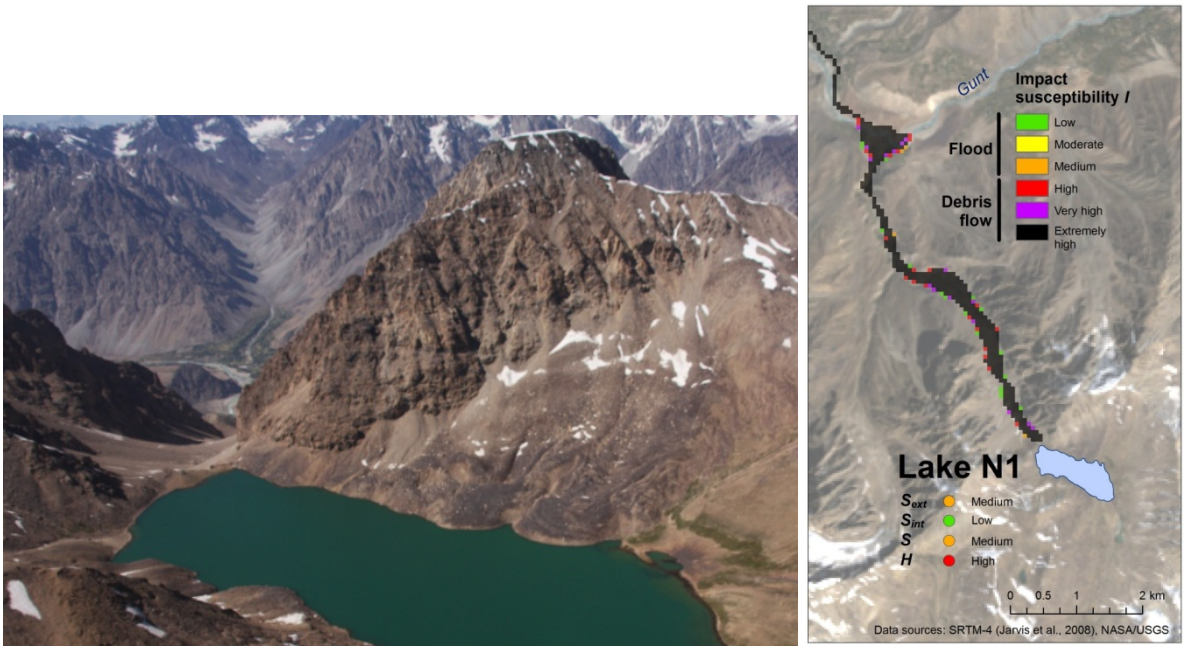

Fig. 11a. Aerial view of Lake N1 (Nimatskul) in August 2009, the Gunt Valley in the background. The viscous creep into the lake indicates that also the above rock wall is influenced by permafrost.

Fig. 11b. Modelled impact susceptibility *I* of a potential outburst of Nimatskul.

A LOF from Lake V2 would possibly hit Lake V1, which – depending on the specific characteristics of the flow – could either level out or amplify the flood. Such effects are not accounted for by the empirical approaches used for the impact susceptibility at the regional scale. Instead, travel distance, impact susceptibility and hazard are computed separately for each of the lakes. The empirical relationships suggest that a debris flow resulting from an outburst of Lake V1 or Lake V2 would not reach the village of Varshedz. A debris flow from Lake V2 would proceed farther (11.0 km) than one from Lake V1 (3.5 km) due to the larger maximum outburst volume and the steep initial slope. However, substantial flooding would have to be expected in the village of Varshedz (Fig. 10c). 43.9 km (Lake V1) resp. 50.1 km (Lake V2) are suggested as maximum travel distances of floods resulting from lake outbursts. When summing up the impact hazard *HI* for all pixels defined as settlement or agricultural area, Lake V1 and Lake V2 show much higher values than all the other lakes in the study area, mainly due to the location of the village of Varshedz directly on the debris cone where the flow would be supposed to spread.

Among all the lakes in the study area, Nimatskul (Lake N1; Fig. 11a) is closest to the villages in the main valley. Located at 4418 m a.s.l., the horizontal distance from the lake down to the Gunt Valley is only 5.9 km, with a vertical difference of 1600 m. The steep average slope of the flow path ($\omega = 15.2°$) and the availability of erodible material suggest that a possible outburst flood would most probably severely affect the villages near the outlet of the Nimatsdara (Fig. 11b).

The lake is dammed by a rocky swell and has a constant surface area of 475,000 m². Lake outburst susceptibility and hazard were rated medium resp. high. Sudden drainage of the lake may be caused by a powerful earthquake weakening the dam or leading to landslides into the lake. However, a closer on-site inspection of the slopes leading directly into the lake gave no evidence

of large-scale instabilities so that in reality, S_{ext} and H would be lower than suggested in the regional-scale analysis. Even though the slopes are obviously under permafrost conditions (see Fig. 11a), mass movements capable to displace a substantial portion of the lake would require a very powerful trigger. With some limitations, similar conclusions can be drawn for Durumkul and Rivakkul.

8 Discussion

Even though the population of the Pamir directly depends on the natural environment and a lot of traditional knowledge exists (Kassam, 2009), lake outburst hazards are often neglected: the source area is usually far away from the area of impact and events occur at very long time intervals or as singularities. The Dasht 2002 GLOF hit the village completely unexpected – there was no awareness of the hazard and no preparedness for the event (Schneider et al., 2004). Also in other mountain areas, deficiencies in risk communication are often responsible that natural processes evolve into disasters (Carey, 2005).

A regional-scale hazard analysis for the South-Western Pamir has been presented in order to highlight potentially hazardous lakes and possible impact areas, building largely on medium-resolution satellite imagery and elevation data. The predictive capacity of such an analysis is governed primarily by the applicability of various types of input data: satellite imagery and digital elevation models only provide information on surface features and patterns, not allowing for an insight beneath. Two aspects have turned out as the major limiting factors of regional-scale lake outburst hazard analyses:

(1) geological information. Rock types and major faults can be obtained from geological maps, but slope stability is often governed by small-scale dip directions and fault systems. Such features can be considered for single slopes or small catchments, but not at the regional scale. Therefore, no geological input was used for computing *TSI*;

(2) information on seepage through the dam and on its internal structure, particularly sediment consolidation, porosity (cavities) and subsurface ice content. Geophysical surveys (e.g. geoelectrics) are not feasible at a level broad enough to cover all relevant lakes.

Furthermore, the SRTM-4 DEM and the pixel size used (60 m) are insufficient to represent all relevant features: particularly for small lakes, the freeboard or the downstream slope of dams may be blurred. High-resolution DEMs are hardly applicable to regional-scale studies of this type, but a more thorough evaluation of the entire analysis procedure for a small test area with a high-resolution DEM and directly measured data (e.g. lake depth) would be an important next step.

The rating schemes used for the hazard analysis were tuned in a way to provide worst-case estimates, with the purpose of building a reproducible baseline regarding the site selection for in-depth investigations. In the case of Nimatskul (Lake N1), such an investigation led to a down-rating of the hazard. In contrast, the rating for Lake V2, with exactly the same values as for Lake N1, was confirmed in the field.

On the other hand, too conservative ratings had to be avoided. Due to its limited size, the lake in Dashtdara producing the 2002 disaster was rated very susceptible, but only medium hazardous.

Tuning the rating scheme in a way to yield a high or very high hazard for that lake would have led to such a classification of virtually all glacial lakes in the area, obstructing the purpose of the method for site selection. It is likely that superficially invisible factors (structure of the dam, englacial water reservoir) led to the high magnitude of the Dasht 2002 event. One can learn some major lessons by comparing the characteristics of that event to the analysis results:

(1) the Dasht lake did not appear more hazardous than many other glacial lakes in the area. This leads to the apparent conclusion that the location of specific outburst events is hard – or even impossible – to predict. The procedure shown up in the present paper gives way to a possible strategy of dealing with this problem: identifying potentially dangerous lakes and fostering a broad awareness-raising and preparedness-building connected with feasible technical measures (e.g. simple early warning systems) in possibly affected communities;

(2) hazardous glacial lakes may evolve within less than one year. This phenomenon was illustrated not only by the Dasht event, but also by the outburst of the western Zyndan glacier lake in the Tien-Shan (Kyrgyzstan) in 2008 (Narama et al., 2010). This means that a consequent monitoring of the glacial environment is required in order to keep updated on developing hazards. On the one hand, such a monitoring has to be performed by employing remote sensing techniques. On the other hand, the local communities have to be trained and encouraged to keep an eye on relevant environmental changes and developing lakes.

Empirical relationships were used for estimating the travel distances and impact areas of lake outburst floods. This is appropriate at the regional scale as physically-based models would require multiple input parameters not available over such a broad area. Mergili et al. (accepted) discuss the challenges and problems connected to physically-based modelling of the motion of lake outburst floods.

However, it should be emphasized that empirical relationships only provide a first estimate of the impact susceptibility which can serve as a baseline for in-depth studies. Specific process chains and interactions regarding the motion of the GLOF are not explicitly considered in the empirical relationships. Such include entrainment or deposition of sediment, change between different flow types (flood, hyperconcentrated flow, debris flow), the amplification or attenuation of flood waves by lakes on the flow path (e.g. Lake V1 in Fig. 10c) or backwater effects. In the case of Dasht, such interactions are thought to be responsible that the flow did not fit to the empirical rules derived from sets of other GLOFs (Haeberli, 1983; Huggel, 2004; Huggel et al., 2004a), but instead continued to the confluence of the Dashtdara with the Shakhdara Valley where lateral spreading was possible.

The global assumption that the entire lake would drain is realistic when considering small glacial lakes (in Dasht, it was the case), but not for larger lakes with rather stable dams where mass movements may cause an overflow. This problem leads to an overestimation of the lake outburst hazard of large lakes (e.g. Durumkul). Huggel et al. (2004a, b) have related expected outburst volumes to the impact volume – an adoption of this approach would require in-detail investigations for each lake.

An important aspect not explicitly accounted for in the hazard analysis procedure is permafrost, which may significantly influence lake outburst susceptibility and hazard (Haeberli et al., 2010a):

in the South-Western Pamir, almost all lakes are located in permafrost areas (Mergili et al., submitted) and a detailed analysis of the condition of the permafrost was out of scope. However, when applying the methodology presented to study regions with lakes both in permafrost and in permafrost-free areas, this aspect has to be included.

9 Conclusions

The regional-scale hazard analysis of lake outburst floods, as shown in the present paper for the South-Western Pamir, Tajikistan, has proven to be a valuable tool for a rapid and reproducible identification of potentially hazardous lakes and possible impact areas.

The analysis does not require specialized input data, it largely relies on internationally available medium-resolution satellite imagery and DEMs. This allows an application in remote or poorly developed areas with limited availability of local information. The neglect of such data, however, also limits the scope of the method: it is clearly confined to the identification of areas requiring more detailed investigations, e.g. field studies. The regional-scale analysis has to presume the unknown parameters as utmost unfavourable in order to come up with worst-case assumptions. This avoids to miss potentially hazardous lakes and situations during the site selection for detailed studies.

The Dasht 2002 event, the most destructive GLOF in the documented history of the South-Western Pamir, originated from a lake rated as very susceptible, but only medium hazardous in the regional-scale analysis. A closer on-site inspection did not reveal a substantial difference to other glacial lakes with such a rating, except for the short lifetime of the lake. This finding underlines the need to detect glacial lakes immediately after their emergence and to take adequate measures.

Also modelling of the travel distance of the Dasht 2002 GLOF showed the difficulties of putting lakes and events into prescribed schemes: it was impossible to reconstruct the reach of the flow by empirical rules based on previous events. This, in conjunction with the thoughts presented above, shows the importance of broad-scale risk mitigation strategies in potentially affected areas, including awareness-raising and preparedness-building within the local population, in combination with a regular monitoring of the glacial and periglacial environment.

Acknowledgements

The work presented in this paper was part of the project TajHaz (Remote Geohazards Assessment in Tajikistan) supported by FOCUS Humanitarian Assistance (an affiliate of the Aga Khan Development Network), the Swiss Agency for Development and Cooperation (SDC) and the UK Department for International Development (DFID). Special thanks go to Demian Schneider (University of Zurich) for valuable discussions and contributions and to Anatoli Ischuk (Tajik Institute of Earthquake Engineering and Seismology) for contributions to the calculation of PGA_{max}.

References

Abdrakhmatov, K., Havenith, H.-B., Delvaux, D., Jongmans, D., and Trefois, P.: Probabilistic PGA and Arias Intensity maps of Kyrgyzstan (Central Asia). J. Seismol., 7, 203–220, 2003.

Allen, S. K., Schneider, D., and Owens, I. F.: First approaches towards modelling glacial hazards in the Mount Cook region of New Zealand's Southern Alps. Nat. Haz. Earth Syst. Sci., 9, 481–499, 2009.

Babaev, A. M. and Mirzoev, K. M.: Basic principles of seismic zonation of the territory of Tajikistan. Vol.: The questions of the seismic zonation of the territory of Tajikistan, 3–31, Donish Publishing, Dushanbe, 1976.

Babaev, A. M., Lyskov, L. M., Mirzoev, K. M., Achilov, G. S., Lazaridi, L. K, and Rajabov, N. R.: Natural resources of Tajikistan. Seismic sources. 1:500000 scale map. GUGK USSR, 1984.

Breien H., De Blasio F. V., Elverhoi A., and Hoeg K.: Erosion and morphology of a debris flow caused by a glacial lake outburst flood, Western Norway. Landslides, 5(3), 271–280, 2008.

Carey M.: Living and dying with glaciers: people's historical vulnerability to avalanches and outburst floods in Peru. Glob. Plan. Change, 47, 122–134, 2005.

Cenderelli D. A. and Wohl E. E.: Peak discharge estimates of glacial lake outburst floods and "normal" climatic floods in Mount Everest region, Nepal. Geomorphology, 40, 57–90, 2001.

Clarke, G. K. C.: Glacier outburst floods from 'Hazard Lake', Yukon Territory, and the problem of flood magnitude prediction. J. Glac, 28(98), 3–21, 1982.

Corominas, J., Copons, R., Vilaplana, J. M., Altamir, J., and Amigó, J.: Integrated Landslide Susceptibility Analysis and Hazard Assessment in the Principality of Andorra. Nat. Haz., 30, 421–435, 2003.

Costa, J. E., and Schuster, R.L.: The formation and failure of natural dams. Geol. Soc. Am. Bull., 100, 1054–1068, 1988.

Costa, J. E.: Floods from Dam Failures. U.S. Geol. Surv. Open File Rep. 85-560, Denver, Colorado, 54 pp., 1985.

Crosta, G. B., Frattini, P., Fusi, N., and Sosio, R.: Formation, characterization and modelling of the 1987 Val Pola rock-avalanche dam (Italy). Italian J. Eng. Geol. Envir., Special Issue I, 145–150, 2006.

Dussaillant A., Benito G., Buytaert W., Carling P., Meier C. and Espinoza F.: Repeated glacial-lake outburst floods in Patagonia: an increasing hazard?. Nat. Haz., DOI 10.1007/s11069-009-9479-8, 2009.

Evans S. G. and Clague J. J.: Recent climatic change and catastrophic geomorphic processes in mountain environments. Geomorphology, 10(1-4), 107–128, 1994.

Evans S. G.: The maximum discharge of outburst floods caused by the breaching of man-made and natural dams. Can. Geotech. J., 23, 385–387, 1986.

Haeberli, W.: Frequency and characteristics of glacier floods in the Swiss Alps. Ann. Glac., 4, 85–90, 1983.

Haeberli, W., Clague, J. J., Huggel, C. and Kääb, A.: Hazards from lakes in high-mountain glacier and permafrost regions: Climate change effects and process interactions. Avances de la

Geomorphología en España, 2008-2010, XI Reunión Nacional de Geomorphología, Solsona, 439–446, 2010a.

Haeberli, W., Portocarrero, C. and Evans, S.: Nevado Hualcán, Laguna 513 y Carhuaz 2010 – Observaciones, evaluación y recomendaciones (un corto informe técnico luego de las reuniones y visita de campo en Julio 2010). Unpublished report on behalf of the Communidad Provincial de Carhuaz, 2010b.

Hewitt, K.: Natural dams and outburst floods in the Karakorum Himalaya. In: Glen J. W. (ed.): Hydrological aspects of alpine and high-mountain areas. IAHS Publication 138, 259–269, 1982.

Huggel, C., Haeberli, W., Kääb, A., Bieri, D., and Richardson, S.: Assessment procedures for glacial hazards in the Swiss Alps. Can. Geotech. J., 41(6), 1068–1083, 2004a.

Huggel, C., Kääb, A., and Salzmann, N.: GIS-based modeling of glacial hazards and their interactions using Landsat-TM and IKONOS imagery. Norwegian J. Geogr., 58, 761–773, 2004b.

Huggel, C., Kääb, A., Haeberli, W., and Krummenacher, B.: Regional-scale GIS-models for assessment of hazards from glacier lake outbursts: evaluation and application in the Swiss Alps. Nat. Haz. Earth Syst. Sci., 3, 647–662, 2003.

Huggel, C., Kääb, A., Haeberli, W., Teysseire, P., and Paul, F.: Remote sensing based assessment of hazards from glacier lake outbursts: a case study in the Swiss Alps, Can. Geotech. J., 39, 316–330, 2002.

Huggel, C.: Assessment of Glacial Hazards based on Remote Sensing and GIS Modeling. Dissertation at the University of Zurich, Schriftenreihe Physische Geographie Glaziologie und Geomorphodynamik, 88 pp., 2004.

IPCC: Climate Change 2007: The Physical Science Basis. Contribution of Working Group I to the Fourth Assessment Report of the Intergovernmental Panel on Climate Change [Solomon, S., Qin, D., Manning, M., Chen, Z., Marquis, M., Averyt, K. B., Tignor, M., and Miller, H.L. (eds.)]. Cambridge University Press, Cambridge, United Kingdom and New York, NY, USA, 996 pp, 2007.

Iturrizaga, L.: Historical Glacier-dammed Lakes and Outburst Floods in the Karambar Valley (Hindukush-Karakoram). GeoJournal, 62(3–4), 1–47, 2005a.

Iturrizaga, L.: New observations on present and prehistorical glacier-dammed lakes in the Shimshal valley (Karakoram Mountains). J. Asian Earth Sci., 25(4), 545–555, 2005b.

Jarvis, A., Reuter, H. I., Nelson, A., Guevara, E.: Hole-filled seamless SRTM data V4. International Centre for Tropical Agriculture (CIAT), available from http://srtm.csi.cgiar.org, 2008.

Kääb, A., Huggel, C., Fischer, L., Guex, S., Paul, F., Roer, I., Salzmann, N., Schlaefli, S., Schmutz, K., Schneider, D., Strozzi, T., and Weidmann, Y.: Remote sensing of glacier- and permafrost-related hazards in high mountains: an overview. Nat. Haz. Earth Syst. Sci., 5, 527–554, 2005.

Kargel, J. S., Leonard, G., Crippen, R. E., Delaney, K. B., Evans, S. G., Schneider, J. F.: Satellite Monitoring of Pakistan's Rockslide-Dammed Lake Gojal. EOS, 91(43), 394, 2010.

Kassam, K. A.: Viewing Change Through the Prism of Indigenous Human Ecology: Findings from the Afghan and Tajik Pamir. Hum. Ecol., 37, 677–690, 2009.

Mergili, M. and Schneider, J. F.: Large landslides related to earthquakes: a direct and indirect threat to Asian mountain communities. Abstract Volume of the Proceedings of the 6th Nepal Geological Congress, Kathmandu, November 15–17, 2010.

Mergili, M., Kopf, C., Müllebner, B., and Schneider, J. F.: Environmental changes and related geohazards in high-mountain areas of Tajikistan and Austria: a comparison. Submitted to Geogr. Ann., A: Phys. Geogr.

Mergili, M., Schneider, D., Worni, R., and Schneider, J. F.: Glacial Lake Outburst Floods (GLOFs): challenges in prediction and modelling. Accepted for the Proceedings of the 5th International Conference on Debris-Flow Hazards Mitigation: Mechanics, Prediction and Assessment, Padova, June 14–17, 2011.

Murphy, W., Petley, D. N., Bommer, J., and Mankelow, J. M.: Uncertainty in ground motion estimates for the evaluation of slope stability during earthquakes. Quarterly Journal of Engineering Geology and Hydrogeology, 35, 71–78, 2002.

Narama, C., Duishonakunov, M. , Kääb, A., Daiyrov M., and Abdrakhmatov, K.: The 24 July 2008 outburst flood at the western Zyndan glacier lake and recent regional changes in glacier lakes of the Teskey Ala-Too range, Tien Shan, Kyrgyzstan. Nat. Haz. Earth Syst. Sci., 10, 647–659, 2010.

O'Connor, J. E., Hardison, J. H., and Costa, J. E.: Debris flows from failures of Neoglacial-Age moraine dams in the Three Sisters and Mount Jefferson wilderness areas, Oregon, US Geological Survey Professional Paper, 1606, 93 pp., 2001.

Quincey D. J., Richardson S. D., Luckman A., Lucas R. M., Reynolds J. M., Hambrey M. J. and Glasser N. F.: Early recognition of glacial lake hazards in the Himalaya using remote sensing datasets. Glob. Plan. Change, 56(1-2), 137–152, 2007.

Reynolds, J.: Development of glacial hazard and risk minimisation protocols in rural environments. Guidelines for the management of glacial hazards and risks. Reynolds Geo-Sciences Independent Geological Consultants, Report No: R7816, Mold, United Kingdom, 2003.

Richardson, S. D. and Reynolds, J. M.: An overview of glacial hazards in the Himalayas. Quatern. Int., 65/66, 31–47, 2000.

Rickenmann, D.: Empirical Relationships for Debris Flows. Nat. Haz., 19, 47–77, 1999.

Schneider J. F., Gmeindl M., and Traxler, K.: Risk Assessment of Remote Geohazards in Central and Southern Pamir/GBAO, Tajikistan. Report to the Ministry of Emergency, Tajikistan and the Swiss Agency for Development and Cooperation (SDC), 2004.

Tinti, S., Maramai, A., and Cerutti, A. V.: The Miage Glacier in the Valley of Aosta (Western Alps, Italy) and the extraordinary detachment which occurred on August 9, 1996. Phys. Chem. Earth (A), 24(2), 157–161, 1999.

Vilímek, V., Zapata, M. L., Klimes, J., Patzelt, Z., and Santillán N.: Influence of glacial retreat on natural hazards of the Palcacocha Lake area, Peru. Landslides, 2(2), 107–115, 2005.

Walder J. S., Costa J. E.: Outburst floods from glacierdammed lakes: the effect of mode of lake drainage on flood magnitude. Earth Surf. Proc. Landforms, 21, 701–723, 1996.

Walder, J. S. and O'Connor, J. E.: Methods for Predicting Peak Discharge of Floods Caused by Failure of Natural and Constructed Earth Dams. Water Resour. Res., 33, 10, 2337–2348, 1997.

Wang, X., Nie, G., and Wang, D.: Reaearch on relationship between landslides and Paek Ground Accelerations induced by Wenchuan earthquake. Chinese Journal of Rock Mechanics and Engineering, 2010-01, DOI: CNKI:SUN:YSLX.0.2010-01-009, 2010.

Watanabe, T. and Rothacher, D.: The 1994 Lugge Tsho glacial lake outburst flood, Bhutan Himalaya. Mt. Res. Dev., 16, 77–81, 1996.

Appendix 3

Glacial Lake Outburst Floods in the Pamir of Tajikistan: challenges in prediction and modelling

Reviewed book chapter

Mergili, M., Schneider, D., Worni, R., Schneider, J.F. (2011): Glacial Lake Outburst Floods (GLOFs): challenges in prediction and modeling. In: Genevois, R., Hamilton, D. L., Prestininzi, A. (eds.): Proceedings of the 5th International Conference on Debris-Flow Hazards Mitigation: Mechanics, Prediction and Assessment, Padua, Italy, June 14-17, 2011. Italian Journal of Engineering Geology and Environment - Book: 973-982.

Abstract

Glacial lake outburst floods (GLOFs) are potentially highly dangerous events and have contributed to numerous disasters in history. Today, computer models are standard tools to estimate the magnitude of hazardous events in the future and to support risk mitigation. The present paper explores the potentials and limitations of modelling for predicting the motion of potential future GLOF events, based on examples from the Pamir (Tajikistan). Since the flow behaviour of GLOFs is in between debris flows and floods, different model approaches come into consideration, though none of them is perfectly suitable for GLOFs. RAMMS as a mass movement model and FLO-2D as a river hydraulics model were employed comparatively for the same areas. The friction parameters for RAMMS and rheologic parameters for FLO-2D were first calibrated by back-calculation with the well-documented Dasht event from summer 2002, and then applied to other areas. However, the applicability of such parameters to GLOFs of different volume and over a different topography remains questionable. The results may nevertheless be a valuable input for risk mitigation efforts, but due to the complex nature of GLOFs and the connected uncertainties, particular care is required when interpreting the model results. The critical points and potential approaches to deal with the limitations are discussed in the paper.

Keywords

Glacial lake outburst floods (GLOFs), Modelling, Central Asia

1 Introduction

Natural dams of different size and origin do exist in mountain areas all over the world (Costa & Schuster, 1988). They often retain lakes which, in the case of a dam failure, may drain as powerful floods. If the outbursting lake is located within the glacial or periglacial area, such events are called Glacial Lake Outburst Floods (GLOFs). They can evolve in different ways (Fig. 1), for example:

- rock/ice avalanches or calving glaciers that produce flood waves in a pro-, supra- or periglacial lake which may overtop and breach glacial or morainic dams (Tinti et al., 1999);
- rising pro-, supra-, sub- or periglacial lake levels, leading to overflow, progressive incision or mechanical rupture of a moraine or ice dam, as well as to retrogressive erosion of a moraine dam;
- enhanced ground water flow (piping) through moraines, or hydrostatic failure of ice dams which can cause sudden outflow of accumulated water (Iturrizaga, 2005a; 2005b);
- degradation of glacier dams or ice-cores in morainic dams leading to loss of stability and to subsidence resulting in internal failure or progressive erosion if a certain threshold is reached.

Richardson & Reynolds (2000) provide an overview of failure mechanisms and case studies. GLOFs often have a highly destructive potential because a large amount of water is released within a short time, with a high capacity to erode loose debris, potentially leading to a powerful flow with a long travel distance. Peak discharges are often some magnitudes higher than in the case of "normal" floods (Cenderelli & Wohl, 2001). The source area is usually far away from the area of impact and events occur at very long time intervals or as singularities, so that the population at risk is often not prepared for such events (Schneider et alii, 2004). Deficiencies in risk communication are often responsible that events evolve into disasters (Carey, 2005). A number of significant GLOFs resulting in fatalities and severe damage have occurred during the previous decades, particularly in the Himalayas, the mountains of Central Asia, the North American mountains, New Zealand, and the Alps. Case studies are provided e.g. by Clarke (1982); Hewitt (1982); Watanabe & Rothacher (1996); Richardson & Reynolds (2000); Schneider et alii (2004); and Vilimek et alii (2005). Climate change, with its impact on the glacial extent, the hydrological cycle and the condition of ice-bearing dams, may condition the occurrence of GLOFs in manifold ways and on different time scales (Evans & Clague, 1994; Dussaillant, 2009).

The present paper deals with computer modelling of the flow path of GLOFs. Using test areas in the Pamir (Tajikistan), the general potentials and limitations of such approaches as well as the suitability of different model concepts are explored and discussed. Particular emphasis is put on the capabilities of the models for the prediction of future events.

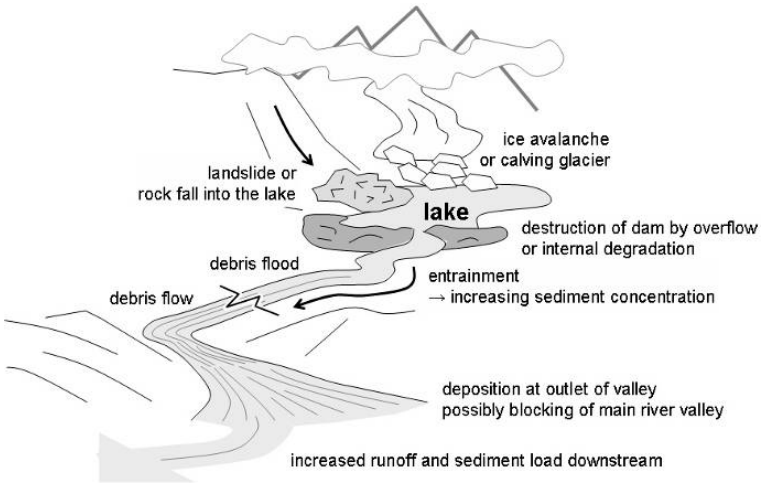

Fig. 1: Schematic representation of a glacial lake outburst flood (GLOF).

2 Background

In summer 2002, the village of Dasht (Shakhdara Valley, Pamir, Tajikistan; Fig. 2a) was hit by a GLOF. 10 km upstream in the headwaters of the valley, a supra-glacial lake had suddenly released an estimated volume of 250,000 m³ of water (Schneider et alii 2004). The volume of debris deposited on the cone was estimated 1.0 – 1.5 million m³, meaning that the ratio between entrained debris and water would be 4 – 6. This is a very high value compared to the ratio of 2 – 3 suggested by Huggel et alii (2004b). However, an even higher ratio than observed for Dasht was reported by Breien et alii (2008) for a GLOF in Norway. Possibly, subglacial water reservoirs connected to the superficial lake and highly saturated erodible material was involved in both events.

Fig. 2a (left): The debris cone resulting from the GLOF in Dasht in summer 2002, covering most of the village and damming a small lake upstream.

Fig. 2b (right): Lake dammed by a rock glacier in the upper Khavrazdara Valley.

It was reported that the flood wave arrived in Dasht in three stages, a phenomenon that can be explained by temporary backwater in the canyon of the lower transitional zone due to blockage of large boulders transported by the GLOF or by lateral slope failures followed by vigorous breakthroughs (Schneider et alii, 2004). The event destroyed a large portion of the village of Dasht, killed a few dozens of people, and dammed a small lake at the Shakhdara river. The event hit the village completely unexpected, as there was no awareness of the hazard and preparedness for the event.

Even though potentially hazardous supra-, pro- and periglacial lakes can be identified relatively easily with remote sensing tools and field work (e.g. Kaeaeb et alii, 2005; Quincey et alii, 2007), modelling and prediction of the motion and reach of GLOFs still remain a challenge. Like many other GLOFs, the characteristics of the Dasht event underwent pronounced changes during the flow, converting from normal runoff to a hyperconcentrated flow and finally to a granular debris flow. Changes in flow behaviour imply some difficulties when using computer models to predict the flow path and velocities of such events. Simple empirical rules for debris flows travel distances show a large scatter among themselves and generally underestimate the travel distance of GLOFs (Fig. 3). Corominas et alii (2003) assume an average runout angle of 21° for debris flows on unobstructed flow paths. Huggel et alii (2003), employing the Modified Single Flow direction model MSF, used an angle of 11° proposed by Haeberli (1983) as a minimum for observed granular debris flows. However, in the case of the Dasht event, both values underestimate the maximum travel distance of the debris flow which reached a runout angle as low as 9.3°. The debris flow actually did not stop before reaching the main valley. Rickenmann (1999) suggested the following empirical relationship for the travel distance of debris flows:

$$L = 1.9V^{0.16}Z^{0.83} \qquad \text{Eq. 1,}$$

where L is the travel distance of the flow, V is the involved volume, and Z is the loss of elevation. Using the release volume of 250,000 m^3 in Eq. 1, the Dasht travel distance is again strongly underestimated, while the estimated deposition volume of 1.5 million m^3 leads to a travel distance closer to the observation.

However, it is not the 'fault' of these empirical models not to fully capture the Dasht event, but rather a conceptual problem related to the characteristics of the event: The GLOF – as many others – was not a classical debris flow, it was characterized by several flow transformations (hyperconcentrated to debris flow and back).

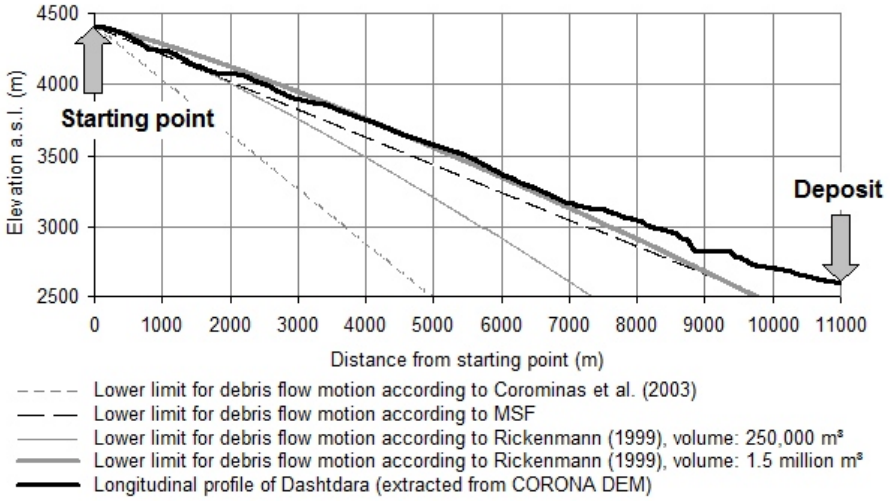

Fig. 3: Empirical approaches developed for the reach of debris flows and the observed travel path of the Dasht 2002 event.

Semi-deterministic approaches, using a friction model (e.g. Perla et alii, 1980 for snow avalanches) in combination with random walk routing techniques go one step further than strictly

empirical models and are often applied in combination with GIS (e.g. Gamma, 2000; Wichmann, 2006: Mergili et alii, 2008). They can be used for back-calculating GLOFs and other types of mass flows, but are only partly suitable for prediction purposes. Reliable physically based dynamic models are therefore required when trying to predict the motion of potential future mass flows (Hungr et alii 2005).

Several physically based model approaches and software packages are potentially suitable for GLOF runout modelling, some of which were developed within the mass movement research community, others within the river hydraulics community.

Many mass movement models go back to the Voellmy (1955) approach and were developed for snow avalanches, but are also applicable to other types of mass movements. A remaining problem is the entrainment of material that is an important characteristic of GLOFs (Breien et alii, 2008; Xu, 1988). Some models include entrainment modules, but rather on an empirical-statistical than on a physical base. Breien et alii (2008) emphasize the lack of appropriate data and knowledge on entrainment issues.

River hydraulics models commonly use flood routing algorithms based on volume conservation and a roughness parameter (usually Manning's n) for estimating the extent and the depth of river flow and flooding events. Most of the widely used software packages (e.g. FLO-2D, HecRAS) include modules for sediment transport, hyperconcentrated flows, and debris and mud flows. In contrast to mass movement models, they require input hydrographs. Therefore, they allow accounting more detailed for the onset mechanism, which plays a crucial role for the flow propagation and the magnitude of the resulting flood wave (Walder & Costa 1996). This type of model is particularly better suited for modelling the initial stage and flow path section of the event that depends more strongly on the input hydrograph. Bertolo & Wieczorek (2005) compare models following different concepts for the same set of debris flows. For an appropriate modelling of the motion of GLOFs, a combination of mass movement and river hydraulics models is suggested.

3 Objectives

The general objective of the study presented was to elaborate a way to estimate the travel distance and travel times of potential future GLOFs by comparing the results of two different models for mass flows. Each of them partially represents certain characteristics of GLOFs but cannot fully reproduce the flow behaviour. The results and the model settings and parameters suitable for GLOFs, but also the needs for further research and model development are highlighted, using examples from the Pamir (Tajikistan).

The paper concentrates on the movement of the flood wave itself, the breaching process of the dam is not considered. For the onset of the GLOF process, scenarios for the outburst volume and hydrograph, as well as for the finally deposited volume (including entrained debris) were elaborated. The scenarios are based on the lake volume, the dam characteristics, and the susceptibility to rock and ice avalanches into the lake.

4 Study areas and data

The modelling was performed for five study areas in Tajikistan (one for back-calculation, four for prediction; Fig. 4). All areas are located in the Pamir, a heavily glaciated high mountain area culminating in 7,495 m a.s.l. The lakes used in the case studies are distributed between 3,800 m and 4,800 m a.s.l.

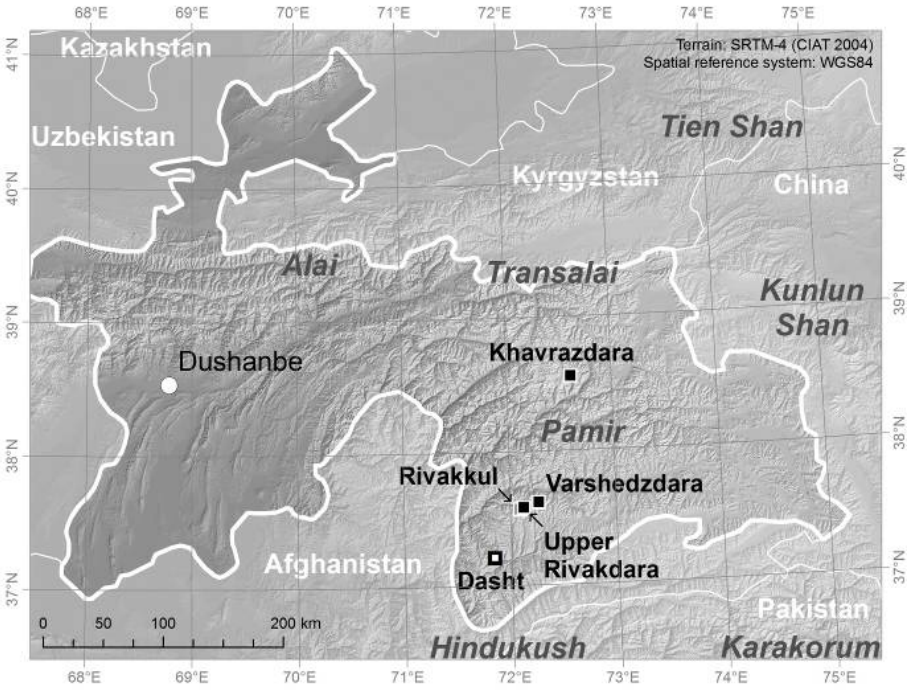

Fig. 4: Map of Tajikistan with the five selected areas for modelling.

The results for Khavrazdara, a Northern tributary of the Bartang Valley, will be discussed in detail below. 20 km upstream from the valley outlet, the tongue of a rock glacier dams a lake with a surface of 2 km², approximately, and an estimated volume of 40 million m³ (Fig. 2b). In the case of a climate-change-induced degradation of the rock glacier tongue, a breach of the dam followed by a flood wave down the valley is possible.

The following information was compiled for Khavrazdara as well as for all the other case studies:

- DEMs of different resolution were prepared for the investigation areas in order to allow the determination of the effect of resolution. SRTM-4 (90 m) was used as well as 10 m and 20 m DEMs derived from CORONA imagery and 5 m DEMs derived from WorldView1 imagery.
- Susceptible glacial lakes were identified using analysis of multitemporal satellite imagery, helicopter surveys, and field investigations. The surface of the relevant lakes was computed using ASTER imagery and the lake volumes were estimated.
- The peak discharges of potential outburst events were estimated from empirical rules (Evans 1986; Costa, 1988; Costa & Schuster, 1988; Manville, 2001; Huggel et alii, 2004a). Scenarios of outburst hydrographs were then created, based on the estimated peak discharge and the lake volume.

- The characteristics of the flow path and the area of deposition were mapped from satellite imagery, from the helicopter, and in the field (morphology of the valley, type of surface material, indicators for former outburst flood events).

5 Methods

The first model used is the physically based mass movement model RAMMS (Rapid Mass Movements), developed at the WSL Institute for Snow and Avalanche Research SLF Davos, Switzerland (see Christen et alii, 2010a, 2010b for a more detailed description and for case studies). The frictional resistance S is based on the Voellmy (1955) model that combines dry Coulomb friction μ with a velocity-squared dependent turbulent friction ξ.

$$S = \mu H g \cos\varphi + \frac{gU^2}{\xi} \qquad \text{Eq. 2,}$$

where g is the gravitational acceleration, H is the flow depth, φ the slope angle, and U is the depth-averaged flow velocity. The maximum velocity U_{max} is defined by Voellmy (1955) as:

$$U_{\max} = \sqrt{\xi H\left(\sin\varphi - \mu\cos\varphi\right)} \qquad \text{Eq. 3.}$$

If μ equals zero, Eq. 3 can be further transformed into the Chézy equation. Therefore, by applying low μ-values, an approximation to turbulent clear water open channel flow can be established.

RAMMS was originally designed to predict the maximum travel distance and velocity of snow avalanches. Calibrated parameters are available for this type of process. They are only valid for the front of the avalanche, so that the deposition geometry cannot be predicted in a straightforward way (Christen et alii, 2010a). The model is able to compute entrainment of material by the flow, governed by an empirically determined scaling factor and an entrainment law. RAMMS has recently been used for modelling other types of mass movements. Schneider et alii (accepted) successfully used it for the back-calculation of large rock-ice avalanches and Preuth et alii (in press) simulated various large rock avalanches in the European Alps. It has further been used for the simulation of debris flows in Switzerland (Naef et alii, 2006; Rickenmann et alii, 2006; Armento et alii, 2008) but not yet for modelling GLOFs.

The second model – FLO-2D – was developed by J. O'Brien (e.g. O'Brien et alii, 1993; O'Brien, 2001). It is a volume conserving model for flow routing of clear water floods, hyperconcentrated flows, or debris flows over floodplains or through confined channels. Topography, input hydrograph, and resistance to flow determine the flow behaviour. Case studies are provided e.g. by Huebl & Steinwendtner (2001) or Bertolo & Wieczorek (2005). For clear water flow, the governing equations are

$$\frac{\partial h}{\partial t} + \frac{\partial hU}{\partial x} = i \qquad \text{Eq. 4,}$$

$$S_f = \alpha - \frac{\partial h}{\partial x} - \frac{U}{g}\frac{\partial U}{\partial x} - \frac{1}{g}\frac{\partial U}{\partial t} \qquad \text{Eq. 5,}$$

where h is the flow depth, U is the depth-averaged flow velocity in one flow direction x, i is rainfall intensity, S_f is the friction slope component (based on Manning's Equation), and a is the bed slope.

Both programs – RAMMS and FLO-2D – need a DEM as input. RAMMS further requires the spatial distribution and depth of the release volume, the coefficients and possible areas for entrainment, and the friction parameters μ and ξ. FLO-2D needs an input hydrograph and values of Manning's n. When using FLO-2D for debris flow modelling the rheologic flow parameters viscosity and yield stress must be specified.

The following work flow was applied for the modelling:

1. Back-calculation of a well-documented recent GLOF: the Dasht event from summer 2002 was used to test the models and to find suitable parameter values. Travel distance, the spatial distribution of the deposit, and the travel time from the start to the deposit were used as reference for the calibration;
2. Scenarios of possible future outburst events of selected lakes (see Table 1 for an example) were elaborated. Outburst volumes, peak discharges, and flow rheologies were varied among the different scenarios. The friction parameters of RAMMS with the best fit for Dasht were taken as a reference, but adapted according to the outburst volumes and water content so that the worst case scenario reached the former debris flow fan of the main valley (compare Discussion and Conclusions).
3. The scenarios were run with RAMMS and FLO-2D. The resolution of the DEM and the computation were varied in order to estimate the influence of this setting on the model results.

6 Results

6.1 Back-calculation for Dasht

First, the Dasht (2002) event was back-calculated using RAMMS (Fig. 5). The purpose was to calibrate the model for this type of event and to find suitable values for the friction parameters μ and ξ. The model was run on the CORONA DEM (10 m), and on the SRTM-4 DEM (90 m) with a calculation resolution of 20 m in order to figure out the influence of different levels of smoothing of the terrain. Friction parameters of $\mu = 0.14$ and $\xi = 1{,}300$ proved to be the best guess for reconstructing the event, though it was necessary to assume lower values of μ (0.01) and higher values of ξ (2,000) in the flat starting area (representing the lake surface) in order to initiate the movement. The velocities and the extent of spreading in the area of deposit were larger when using the SRTM DEM (smoother terrain). The simulated travel time from the onset of the flow to the village was 55 minutes with the SRTM DEM and 76 minutes with the CORONA DEM. These values correspond reasonably with local reports concerning the time difference between the acoustic detection of the GLOF and its arrival at the village.

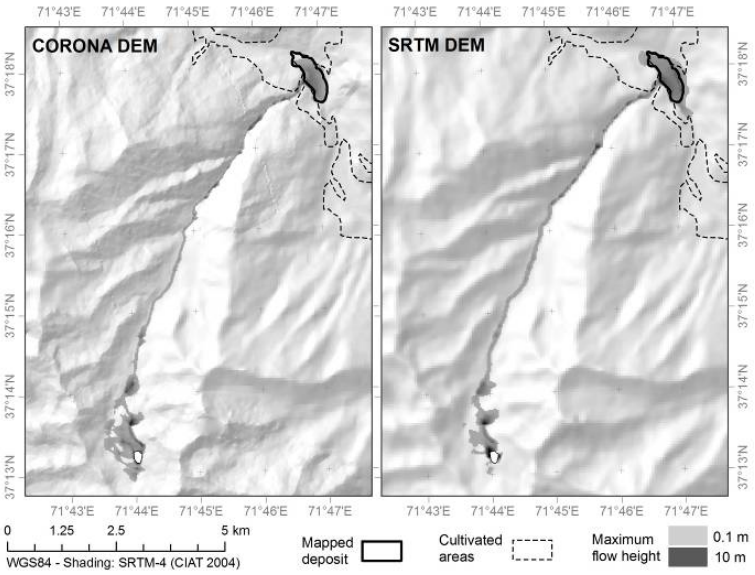

Fig. 5: Back-calculation of the Dasht 2002 event using RAMMS.

As the GLOF event in Dasht propagated as a debris flow, this case study was used to define the rheologic parameters for debris flow modelling in FLO-2D. It was found that values for viscosity η = 279 poises and yield stress τ = 798 dynes/cm^2 represented best the debris flow in Dasht. Consequently these values were also used in the scenario modelling. FLO-2D was run on the CORONA DEM only. The simulated travel time, flow heights and extent matched well with the field observations.

6.2 Khavrazdara

Different scenarios for lake outburst floods were then computed for Khavrazdara, Varshedzdara, Upper Rivakdara, and Rivakkul (see Fig. 4). The modelling results for Khavrazdara (see Fig. 2b) are discussed in detail.

The scenarios defined for an outburst flood in Khavrazdara are shown in Table 1. A cell size of 20 m was used for the RAMMS simulations and 40 m for the FLO-2D simulations, respectively. Whilst the GLOFs simulated with FLO-2D reached the outlet of the valley, the RAMMS simulations indicated a stop of the flow in the middle portion of the valley when using the friction parameters calibrated with the Dasht event. It was then tested how much the friction would have to be reduced to allow the flow to reach the valley outlet and to cover the debris cone there. Friction values of μ = 0.04 and ξ = 1,000 were found to be suitable. Decreased μ-values of μ = 0.03 were used to account for the lower sediment concentration expected in the upper section (before entrainment takes place), whilst increased values of μ = 0.05 were applied to account for the higher sediment concentration expected in the lower section. ξ–values were held constant for the entire flow path. The spatial distribution of the maximum flow height simulated with RAMMS and FLO-2D for selected scenarios is illustrated in Fig. 6.

With FLO-2D all scenarios were modelled as a hyperconcentrated flow with a volumetric sediment concentration of 20% on the one hand, and as a debris flow with volumetric sediment concentrations up to 50% on the other hand. Applying a range of different flow rheologies is a strategy to deal with the uncertainty regarding the flow type produced by the released water from

a lake. The amount of water is the same in both flow types, but the debris flow is bulked with much more material. This is why its total flow volume and peak discharge are higher than for hyperconcentrated flows of the same outburst scenario. As the peak discharge has the highest influence on calculated maximum flow depths, and the higher viscosity results in lower flow velocities, inundation depths are higher when modelling the GLOF as a debris flow.

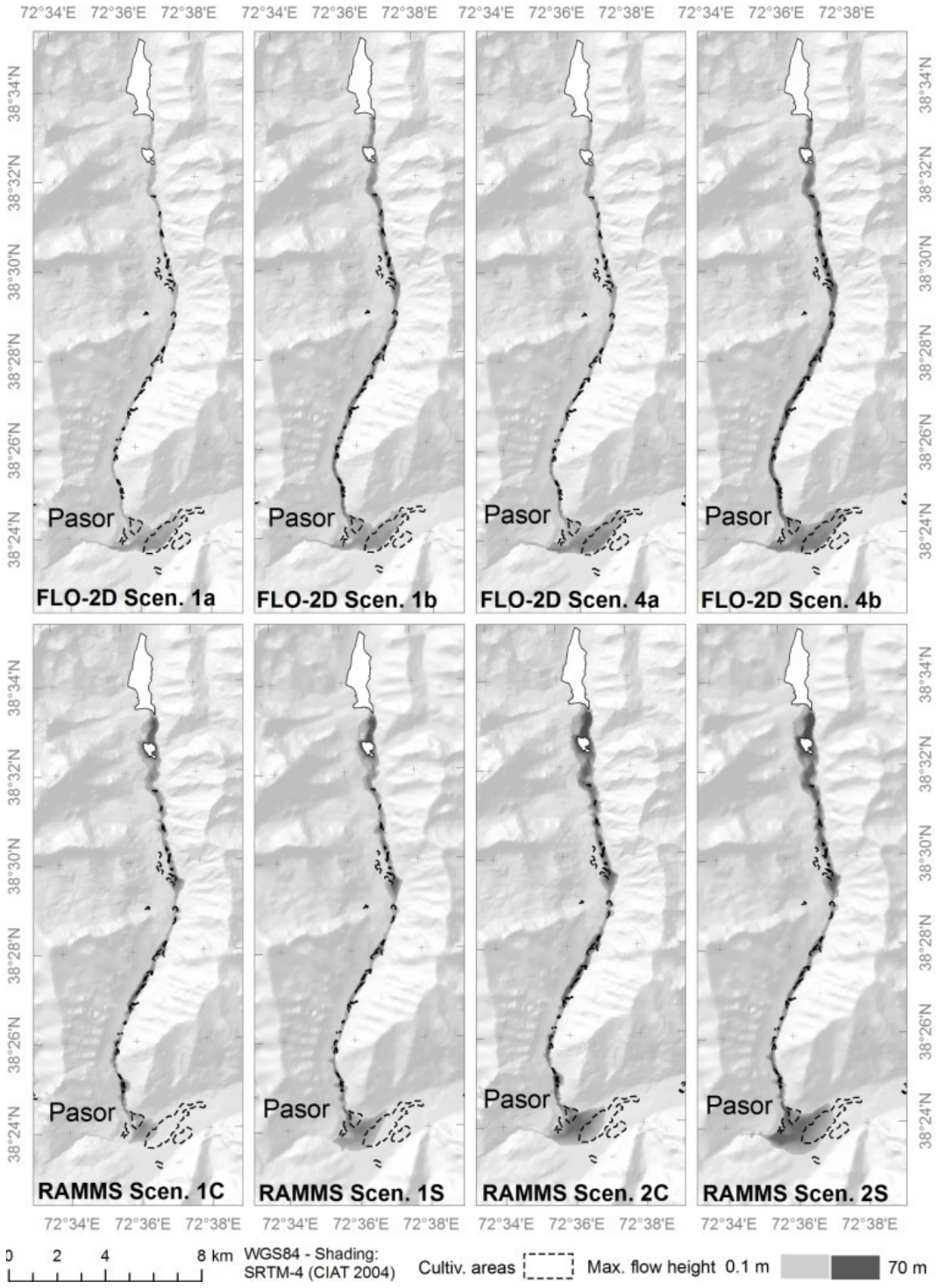

Fig. 6: Maximum flow depth computed with FLO-2D and RAMMS for different lake outburst scenarios of Khavrazdara.

Table 1: Modelling of a potential GLOF from the large lake in the upper Khavrazdara: Scenarios, involved volumes, maximum discharge, and travel times to the village of Pasor (outlet of the valley). Hflw = Hyperconcentrated flow, Dflw = Debris flow, C = CORONA DEM , S = SRTM-4 DEM, N/A = Not applicable.

Scenario	Starting volume	Deposition volume	Maximum discharge	Travel time
	10^6 m³	10^6 m³	m³/s	minutes
FLO-2D (all simulations on CORONA DEM)				
1a Hflw	15	19	2500	210
1b Dflw	15	23	4000	210
2a Hflw	15	20	10000	72
2b Dflw	15	25	16000	90
3a Hflw	30	38	2500	255
3b Dflw	30	47	4000	270
4a Hflw	30	38	10000	90
4b Dflw	30	48	16000	90
RAMMS				
1 C	15	45	N/A	99
1 S	15	45	N/A	73
2 C	30	90	N/A	70
2 S	30	90	N/A	48

According to the simulation, the flow would reach the village of Pasor at the outlet of the valley between 48 minutes and 4.5 hours after the onset, depending on the scenario (see Table 1; average velocity between 1 and 6 m/s, respectively). This wide range shows the uncertainties connected to the scenarios, topographic data and parameters used. The maximum velocity ranges around 10 m/s over most of the valley, with much higher values yielded in the upper portion, particularly by RAMMS. The influence of the DEM resolution on the model results is considerable: finer DEM resolutions generally lead to a rougher surface which significantly reduces the flow velocity and hence the reach of the debris flow (see also Christen et alii, 2010a). The smoother the original terrain is, the less this effect is observed.

7 Discussion and conclusions

The present study illustrates that modelling of GLOFs remains a challenge. Each case study area has its individual characteristics and the results provided by different model approaches

sometimes diverged considerably. These differences are not surprising as the two models follow disparate concepts, each requiring a specific definition of the initial conditions (sudden release of mass vs. discharge curve). In order to homogenize the results and to account for the generally larger amount of water, the friction parameters used in RAMMS had to be reduced considerably in comparison to those used for the Dasht event. This is of very high importance when the results are interpreted or shown to local authorities. However, adapting the friction parameters individually for each study area in a way that the simulated flow reaches the area of interest (often the valley outlet) provides useful information in two ways:

- A comparison of the assumed friction parameter values with those derived from the back-calculation of documented events allows an assessment of how realistic the assumed parameters are, and therefore the likelihood of the flow to reach the outlet of the respective tributary valley. Table 2 shows the friction parameters used in the RAMMS calculation, based on the assumption that the flow would reach the outlet of the respective valley.
- Approximate travel times to the outlet can be derived, given that the assumed parameters are considered as realistic.

Table 2: Involved volumes, valley characteristics, and friction parameters chosen for the RAMMS simulation. L = Length of valley; ΔZ = *Loss of elevation;* φ_{avg} = *average inclination.* [a] start volume [b] end volume * 1st section of flow path (upper) ** 2nd section of flow path (middle) *** 3rd section of flow path (lower)

Area	Volume	L	ΔZ	φ_{avg}	μ	ξ
	10^6 m³	m	m	degree		
Dasht	0.25[a], 1.50[b]	11,000	1,800	9.8	0.14	1,300
Khavrazdara	15 – 30[a], 45 – 90[b]	19,000	1,050	3.2	0.03*, 0.04**, 0.05***	1,000
Varshedzdara Lower Lake	0.5 – 1[a], 1.5 – 3[b]	11,500	1,350	6.7	0.09	1,350
Varshedzdara Upper Lake	2 – 5[a], 6 – 15[b]	13,500	1,650	7.0	0.08*, 0.10**, 0.12***	1,500*, 1,250**, 1,000***
Upper Rivakdara	0.37 – 0.73[a], 0.82 – 1.6[b]	4,800	700	8.3	0.08*, 0.09**, 0.10***	1,500*, 1,350**, 1,200***
Rivakkul	9.4 – 23.3[a], 31.6 – 58.5[b]	26,000	1,300	2.9	0.03	1200

A special characteristic of the RAMMS model is the sudden release of the start volume (mass), that well represents a sudden mechanical failure of a lake dam or the overtopping of a large impact wave. However, this is not always the way how GLOFs are triggered and may therefore lead to exaggerated flow heights and widths in the upper flow section. In contrast, the ability to erode material from the ground is an important feature of RAMMS because it accounts for the often observed fact that start and end volumes differ significantly (Berti et alii, 1999, Breien et alii, 2008).

In general, RAMMS predicts higher values of flow depth in the uppermost section of the flow path than FLO-2D. This is due to the sudden release of the mass (see above). FLO-2D makes use of an input hydrograph that distributes the release volume over a given time period, leading to lower flow depths for given total volumes. This can better reproduce a dam failure due to progressive incision.

RAMMS predicts the stop of the flow and the deposition of the mass on the debris cone whilst FLO-2D tends to predict a continuation of the flow along the stream path of the main valley. The potential impact areas derived with RAMMS are therefore smaller and the inundation depths are larger than those calculated with FLO-2D.

Partially good correspondence is found in the flow durations to the outlet of the valley. Table 1 shows that the range of the flow durations calculated with RAMMS are similar to those derived from the FLO-2D calculations, at least regarding the – more critical – lower boundary. This is remarkable because they are computed completely independently (the adaptation of μ and ξ is a purely frictional issue).

One has to conclude that, considering all relevant aspects, the simulation of the motion of potential future GLOFs remains a big challenge. Problems are in particular:

- The knowledge about the onset of the process is often limited (properties of dam, type of dam breach, understanding of process chains and interactions).
- The volume of water involved in the outburst flood is unclear. The lake bathymetry is often unknown and may change rapidly, whilst the ratio of water actually bursting out has to be estimated. Furthermore many lakes burst out within a short time after their development without being detected as potential source of hazard (Narama et alii, 2010). Continuous monitoring is required to keep updated on the existing hazards.
- Uncertainties related to erosion and deposition are a big unresolved issue. Erosion of the dam and the bed as well as concomitant deposition can strongly change the rheology and the moving volume of the flow. These changes have a direct impact on the spreading and reach.
- The flow transformation processes of the natural phenomena are a challenge for the models (and in general for any assessment). Software developed by the hydrological community is specialized to simulate floods or hyperconcentrated flows with input hydrographs on moderately steep flow channels and with lower sediment loads. In contrast to this, programs for rapid mass movements are better suited for steeper slopes

and sudden failure of the initial volume. The typical characteristics of GLOFs are in between and vary for different channel sections. Sediment transport models properly computing erosion and deposition are rather designed for less steep slopes, so that they are hardly applicable to GLOFs. Furthermore, the outburst scenario is very critical.

Flood dynamics are quite well understood and model results can therefore be considered as confident. In contrast, debris flow modelling is a based on empirical components and the results are therefore more inaccurate compared to modelling pure water or hyperconcentrated flows.

Nevertheless it is important not to model only the outburst scenarios as hyperconcentrated flows, but also as debris flows. With such a modelling strategy a range of expectable flow rheologies can be covered. This increases the robustness of the results and does not pretend a wrong accuracy.

Existing programs also largely fail to simulate process interactions and transformations such as the development of a hyperconcentrated flow into a debris flow, the effects of multiple flood waves (including the modified topography after the first wave), or the effects of short-term storage of water and debris by self-induced blockage of the valley.

Considering all these points, it has to be concluded that up to now, no well suitable modelling approaches do exist for GLOFs, as these represent highly variable phenomena and often exhibit a behaviour in between debris flows and floods. However, applying a combination of different model approaches, as attempted in the study presented, helps to estimate realistic process magnitudes, areas of impact, maximum velocities, and travel times. As a general conclusion for any kind of modelling effort, a responsible interpretation of the results and a controlled knowledge transfer to local authorithies is crucial.

Acknowledgements

The studies were supported by the FOCUS Humanitarian Assistance, an affiliate of the Aga Khan Development Network, by the Swiss Agency for Development and Cooperation (SDC), and the British Department for International Development (DFID). Special thanks go to Christian Huggel for his highly valuable comments on the draft manuscript.

References

Armento M.C., Genevois R. & Tecca P.R. (2008) - Comparison of numerical models of two debris flows in the Cortina d'Ampezzo area, Dolomites, Italy. Landslides, 5: 143-150.

Berti M. & Simoni A. (2007) - Prediction of debris flow inundation areas using empirical mobility relationships. Geomorphology, 90: 144-161.

Berti M., Genevois R., Simoni A. & Tecca P.R. (1999) - Field observations of a debris flow event in the Dolomites. Geomorphology, 29: 265-274.

Bertolo P. & Wieczorek G.F. (2005) - Calibration of numerical models for small debris flows in Yosemite Valley, California, USA. Nat. Haz. Earth Syst. Sci., 5: 993-1001.

Breien H., De Blasio F.V., Elverhoi A. & Hoeg K. (2008) - Erosion and morphology of a debris flow caused by a glacial lake outburst flood, Western Norway. Landslides, 5(3): 271-280.

Carey M. (2005) - Living and dying with glaciers: people's historical vulnerability to avalanches and outburst floods in Peru. Glob. Plan. Change, 47: 122-134.

Cenderelli D.A. & Wohl E.E. (2001) - Peak discharge estimates of glacial lake outburst floods and "normal" climatic floods in Mount Everest region, Nepal. Geomorphology, 40: 57-90.

Christen C., Bartelt P. & Kowalski J. (2010a) - Back calculation of the In den Arelen avalanche with RAMMS: interpretation of model results. Ann. Glac., 51(54): 161-168.

Christen M., Kowalski J. & Bartelt, B. (2010b) – RAMMS: Numerical simulation of dense snow avalanches in three-dimensional terrain. Cold Reg. Sci. Technol., 63,1-14.

CIAT (International Centre for Tropical Agriculture) (2004) - Void-filled seamless SRTM data V1, available from the CGIAR-CSI SRTM 90 m Database. http://srtm.csi.cgiar.org

Clarke G.K.C. (1982) - Glacier outburst floods from 'Hazard Lake,' Yukon Territory, and the problem of flood magnitude prediction. J. Glac, 28(98): 3-21.

Corominas J., Copons R., Vilaplana J.M., Altamir J. & Amigó J. (2003) - Integrated Landslide Susceptibility Analysis and Hazard Assessment in the Principality of Andorra. Nat. Haz., 30: 421-435.

Costa J.E. & Schuster R.L. (1988) - The formation and failure of natural dams. Geol. Soc. Am. Bull., 7: 1054–1068.

Costa J.E. (1988) - Floods from dam failures. In: Baker V.R. (1988, ed.) - Flood Geomorphology: 439–463, Wiley, New York.

Dussaillant A., Benito G., Buytaert W., Carling P., Meier C. & Espinoza F. (2009) - Repeated glacial-lake outburst floods in Patagonia: an increasing hazard?. Nat. Haz., DOI 10.1007/s11069-009-9479-8.

Evans S.G. & Clague J.J. (1994) - Recent climatic change and catastrophic geomorphic processes in mountain environments. Geomorphology 10(1-4): 107-128.

Evans S.G. (1986) - The maximum discharge of outburst floods caused by the breaching of man-made and natural dams. Can. Geotech. J., 23: 385-387.

Frey H., Haeberli W., Linsbauer A., Huggel C. & Paul F. (2010) - A multi-level strategy for anticipating future glacier lake formation and associated hazard potentials. Nat. Haz. Earth Syst. Sci., 10: 339-352.

Gamma P. (2000) - dfwalk – Ein Murgang-Simulationsprogramm zur Gefahrenzonierung. Geographica Bernensia G66. 144 pp. [in German]

Haeberli W. (1983) - Frequency and characteristics of glacier floods in the Swiss Alps. Ann. Glac., 4: 85-90.

Hewitt K. (1982) - Natural dams and outburst floods in the Karakorum Himalaya. In: Glen J.W. (1982, ed.) - Hydrological aspects of alpine and high-mountain areas. IAHS Publication 138: 259-269.

Huebl J & Steinwendtner H. (2001) - Two-dimensional simulation of two viscous debris flows in Austria. Phys. Chem. Earth (C), 26: 639-644.

Huggel C., Haeberli W., Kaeaeb A., Bieri D. & Richardson S. (2004a) - An assessment procedure for glacial hazards in the Swiss Alps. Can. Geotech. J., 41(6): 1068-1083.

Huggel C., Kaeaeb A. & Salzmann N. (2004b) - GIS-based modeling of glacial hazards and their interactions using Landsat-TM and IKONOS imagery. Norsk Geografisk tidsskrift / Norwegian J. Geogr., 58: 761-773.

Huggel C., Kaeaeb A., Haeberli W. & Krummenacher B. (2003) - Regional-scale GIS-models for assessment of hazards from glacier lake outbursts: evaluation and application in the Swiss Alps. Nat. Haz. Earth Syst. Sci., 3: 647-662.

Hungr O., Corominas J. & Eberhardt E. (2005) - State of the Art paper: Estimating landslide motion mechanism, travel distance and velocity. In: Hungr O., Fell R., Couture R., Eberhardt E. (2005, eds.) - Landslide Risk Management. Proceedings of the International Conference on Landslide Risk Management, Vancouver, Canada, 31 May – 3 June 2005, 129-158.

IPCC (2007) - Climate Change 2007: Synthesis Report, Intergovernmental Panel on Climate Change, 26-73.

Iturrizaga L. (2005a) - Historical Glacier-dammed Lakes and Outburst Floods in the Karambar Valley (Hindukush-Karakoram). GeoJournal, 62(3 - 4): 1-47.

Iturrizaga L. (2005b) - New observations on present and prehistorical glacier-dammed lakes in the Shimshal valley (Karakoram Mountains). J. Asian Earth Sci., 25(4): 545-555.

Iverson R.M., Schilling S.P. & Vallance J.W. (1998) - Objective delineation of lahar-inundation hazard zones. GSA Bull., 110(8), 972-984.

Kaeaeb A., Huggel C., Fischer L., Guex S., Paul F., Roer I., Salzmann N., Schlaefli S., Schmutz K., Schneider D., Strozzi T. & Weidmann Y. (2005) - Remote sensing of glacier- and permafrost-related hazards in high mountains: an overview. Nat. Haz. Earth Syst. Sci., 5: 527-554.

Manville V. (2001) - Techniques for evaluating the size of potential dam-break floods from natural dams. Institute of Geological and Nuclear Sciences Science Report 2001/28, 72 pp.

Mergili M., Fellin W., Moreiras S.M. & Stoetter J. (2008) - Integrated modelling of debris flows in the Central Andes based on Open Source GIS. Geophys. Res. Abstr., 10. [abstract]

Naef D., Rickenmann D., Rutschmann P. & McArdell B.W. (2006) - Comparison of flow resistance relations for debris flows using a one-dimensional finite element simulation model. Nat. Haz. Earth Syst. Sci., 6: 155-165.

Narama C., Duishonakunov M., Kaeaeb A., Dairov M. & Abdrakhmatov K. (2009) - The 24 July 2008 outburst flood from western Zyndan glacier lake, Tien Shan, Kyrgyzstan. Nat. Haz. Earth Syst. Sci., doi:10.5194/nhess-10-647-2010.

O'Brien J.S. (2001) - FLO-2D Users Manual. Nutrioso, Arizona. 83 pp. and appendices.

O'Brien J.S., Julien, P.Y. & Fullerton W.T. (1993) - Two-dimensional water flood and mudflow simulation, J. Hydraul. Eng., 119: 244-261.

Perla, R., Cheng, T. T., McClung, D.M. (1980): A Two-Parameter Model of Snow Avalanche Motion. Journal of Glaciology, 26: 197-207.

Preuth T., Bartelt P., Korup O. & McArdell B.W. (in press) - Fragmentation and frictional relaxation in rock avalanches. J. Geophys. Res.

Quincey D.J., Richardson S.D., Luckman A., Lucas R.M., Reynolds J.M., Hambrey M.J. & Glasser N.F. (2007) - Early recognition of glacial lake hazards in the Himalaya using remote sensing datasets. Glob. Plan. Change, 56(1-2): 137-152.

Richardson S.D. & Reynolds J.M. (2000) - An overview of glacial hazards in the Himalayas. Quatern. Int., 65/66: 31–47.

Rickenmann D. (1999) - Empirical Relationships for Debris Flows. Nat. Haz., 19: 47–77.

Rickenmann D., Laigle D., McArdell B.W. & Huebl J. (2006) - Comparison of 2D debris-flow simulation models with field events. Computational Geosciences, 10: 241-264.

Schneider D., Bartelt P., Caplan-Auerbach J., Christen M., Huggel C., & McArdell B. W. (accepted) - Insights into rock-ice avalanche dynamics by combined analysis of seismic recordings and a numerical avalanche model. J. Geophys. Res.

Schneider J. F., Gmeindl M. & Traxler K. (2004) - Risk Assessment of Remote Geohazards in Central and Southern Pamir/GBAO, Tajikistan. Report to the Ministry of Emergency, Tajikistan and the Swiss Agency for Development and Cooperation (SDC).

Tinti, S., Maramai, A. & Cerutti A.V. (1999) - The Miage Glacier in the Valley of Aosta (Western Alps, Italy) and the extraordinary detachment which occurred on August 9, 1996. Phys. Chem. Earth (A), 24(2), 157-161.

Vilímek V., Zapata M.L., Klimes J., Patzelt Z., & Santillán N. (2005) - Influence of glacial retreat on natural hazards of the Palcacocha Lake area, Peru. Landslides, 2(2): 107-115.

Voellmy A. (1955) - Ueber die Zerstoerungskraft von Lawinen. Schweizerische Bauzeitung, 73: 159-162, 212-217, 246-249, 280-285. [in German]

Walder J.S. & Costa J.E. (1996) - Outburst floods from glacierdammed lakes: the effect of mode of lake drainage on flood magnitude. Earth Surf. Proc. Landforms, 21: 701-723.

Watanabe T. & Rothacher D. (1996) - The 1994 Lugge Tsho glacial lake outburst flood, Bhutan Himalaya. Mt. Res. Dev., 16: 77-81.

Wichmann V. (2006) - Modellierung geomorphologischer Prozesse in einem alpinen Einzugsgebiet. Abgrenzung und Klassifizierung der Wirkungsraeume von Sturzprozessen und Muren mit einem GIS. Eichstaetter Geographische Arbeiten 15. 231 pp. [in German]

Xu D. (1988) - Characteristics of debris flow caused by outburst of glacial lake in Boqu river, Xizang, China, 1981. GeoJournal, 17(4), 569-580.

Appendix 4

Changes of the cryosphere and related geohazards in the high-mountain areas of Tajikistan and Austria: a comparison

Research article

Mergili, M., Kopf, C., Müllebner, B., Schneider, J.F. (2012): Changes of the cryosphere in the high-mountain areas of Tajikistan and Austria: a comparison. Geografiska Annaler, Series A 94(1): 79-96. doi:10.1111/j.1468-0459.2011.00450.x

Original article: http://onlinelibrary.wiley.com/doi/10.1111/j.1468-0459.2011.00450.x/abstract

Abstract

The present paper quantifies recent glacier changes and possible future permafrost retreat in the Austrian Alps and the Pamir and Alai Mountains of Tajikistan (Central Asia), two mountainous areas with striking differences in climate and hypsometry, but also in economy and research history. The aim of the comparative study is to improve the understanding of regional differences as a baseline for further research and for a differentiated evaluation of possible socio-economic implications. Besides a review of the available literature, multi-temporal remote sensing of glaciers of selected areas as well as additional helicopter and field surveys were conducted. The Tajik glaciers displayed a differentiated behaviour during the investigation period 1968–2009, with a strong trend to retreat at least since 2002. More than 100 pro- and supraglacial lakes have been forming or growing in the southwestern Pamir. Destructive outburst floods of such lakes have occurred there in the recent past. Almost all Austrian glaciers are in an advanced stage of retreat, a trend which continues at enhanced rates. Comparatively few glacial lakes exist in the direct forefields of the glaciers. Potential permafrost distribution maps for the present and the future were produced for Tajikistan and Austria by adapting an empirical model developed in Switzerland. In absolute terms, the highest loss was predicted for the Pamir. The expected relative loss in the same area is moderate compared to the rest of Tajikistan and particularly to Austria, where the model predicted the disappearance of more than 90% of the potential permafrost until the end of the 21st century.

Keywords

Austria, climate change, glaciers, high-mountain geomorphology, permafrost, Tajikistan

1 Introduction

High-mountain areas are particularly sensitive environments and therefore serve as early indicators for changes – or, on the long term, fluctuations – of climate. Such indicators include snow, glaciers, permafrost, ecosystems and the water cycle (e.g. Beniston 2003; Huber et al. 2005).

Worldwide, there is overwhelming evidence for an accelerated retreat of glaciers over the last few decades, involving the tropics (e.g. Kaser 1999), humid and arid mid-latitudes (e.g. Lambrecht and Kuhn 2007) and the polar regions (e.g. Cook et al. 2005). Much of this retreat has been attributed to the evident climate warming (IPCC 2007). However, glacial retreat is not occurring at the same rate and with the same characteristics worldwide. Recently, some valley glaciers have advanced particularly in humid areas strongly influenced by oceanic oscillations, for example in New Zealand and Norway (Hooker and Fitzharris 1999; Chinn et al. 2005). In detail, glaciers may alternate between advance and retreat as a complex and lagged response to climate signals (Aniya et al. 1997).

Glacier fluctuations contribute a great deal to environmental changes in high-mountain areas worldwide, but also alpine permafrost plays an important role. Much research on permafrost has been done in the former Soviet Union (Nekrasov and Klimovsky 1978), in Canada and in Switzerland. Alpine permafrost and its changes are more difficult to explore than glaciers and their changes. Various types of modelling techniques are therefore used, ranging from data-intensive local approaches for soil temperature dynamics to heuristic methods for the permafrost distribution at the regional and national scales (see Harris et al. 2009 for a review).

The interest in glacier and permafrost change is of practical as well as scientific relevance. The meltwater from glaciers contributes to the water budget of mountain areas and their forelands. Particularly in the valleys of arid mountain areas, it is highly important for the livelihood of the people (e.g. irrigation, hydropower generation), whilst its importance diminishes in humid areas and with increasing distance from the glaciers (Hagg and Braun 2005; Kaser and Grosshauser 2010).

The fluctuation of glaciers often results in the formation of glacial lakes. Tweed and Russell (1999) distinguished nine types of ice-dammed lakes. Some of these lakes are prone to sudden outbursts (Glacial Lake Outburst Floods or GLOFs). GLOFs can evolve in different ways, for example by rock/ice avalanches or ice fronts calving into lakes (Tinti et al. 1999; Haeberli et al. 2010b), rising lake levels leading to overflow, progressive incision, mechanical rupture or retrogressive erosion of a dam, hydrostatic failure (Iturrizaga 2005) or degradation of glacier dams or ice-cores in morainic dams. Richardson and Reynolds (2000) provide an overview of failure mechanisms and case studies. GLOFs often have a highly destructive potential because a large amount of water is released within a short time, with a high capacity to entrain loose debris, potentially leading to a powerful flood with a long travel distance. Glacial lakes have produced GLOFs e.g. in the Himalayas of Nepal and Bhutan (Bajracharya et al. 2007), the Karakorum (Wang et al. 2009), the Pamir (Mergili and Schneider 2011), the Tien Shan (Narama et al. 2010), the Andes (Harrison et al. 2006; Haeberli et al. 2010b) and the western Alps (Huggel et al. 2002).

It is now well documented that permafrost dynamics are a prominent preparatory factor for the occurrence of mass movements, but until recently, this fact has not been widely recognized (e.g. Haeberli 1992). Thawing of permafrost may affect slope stability, for example by fracturing of rocks during freeze-thaw cycles, by increased availability of physically active water or by changed topography (e.g. Haeberli et. al. 1997). Several studies on climate change-induced dynamics of permafrost and related geohazards have been conducted. Intensive and detailed research was carried out at selected sites in the Swiss and Italian Alps (e.g. Monte Rosa) including measurements and modelling of permafrost temperatures and related rock fall events, rock-ice avalanches, slides and debris flows (see Harris et al. 2009 for a comprehensive list of references).

The present paper focuses on the comparison of glacier and permafrost changes in the last 40 years, and on hazards related to these changes, in Austria and Tajikistan, the latter located in the Central Asian mountains (Pamir, Alai). The similarities and differences between the two countries – and also between different regions within each country – are highlighted and the most striking needs for further research are discussed.

2 Study areas

2.1 Geographic settings

Tajikistan and Austria are both mountainous countries with the same order of magnitude in surface area and population. There are, however, some marked differences between the two countries, both from a socio-economic and from a physical point of view (Table 1). According to the United Nations (UNdata), only 5.5% of the employed people in Austria worked in agriculture in 2005, compared to 55.5% in Tajikistan.

The climate in Austria is temperate and largely humid with warm summers and moderately cold winters. Tajikistan, though also temperate on average, experiences a much more continental climate with hot summers and cold winters, with sparse precipitation rather concentrated in the winter months (Table 2). Both countries have experienced a positive trend of mean annual air temperature (MAAT) since 1970. In Tajikistan, most of the warming can be assigned to the period after 1995. According to the 4th IPCC report (IPCC 2007), the median of the projected increase of the MAAT from 1980–1999 to 2080–2099 is 3.7 °C for Tajikistan and 3.5 °C for Austria.

Table 1. Selected key parameters of Tajikistan and Austria according to the United Nations (UNdata) and the United Nations Development Programme (UNDP). HDI = Human Development Index.

	Surface area (km^2)	Population 2008	GDP per capita 2008 (US$)	GDP growth rate 2008 (per cent)	HDI 2010 (rank)
Tajikistan	143,100	6.836 mio.	362.7	7.9	0.580 (112)
Austria	83,871	8.337 mio.	49,596.4	1.8	0.851 (25)

Fig. 1. Overview maps of Tajikistan and Austria with distribution of glaciers according to the WGI. Areas selected for detailed studies and location of mountain ranges, glaciers and glacial lakes mentioned in the text are shown.

60–65 per cent of Austria is occupied by the Alps, culminating at 3,798 m a.s.l. The average elevation of the country is 950 m a.s.l. Tajikistan is embedded in the Central Asian system of mountain ranges, sharing part of the Alai and most of the Pamir. The highest peak of Tajikistan is Pik Ismoili Somoni at 7,495 m a.s.l., the country's average elevation is 2,970 m a.s.l. (Fig. 1). Due to the extensive highland of the eastern Pamir, the average elevation of the Gorno-Badakhshan Autonomous Oblast (GBAO) is 4,240 m a.s.l.

Both countries host fragile high-mountains geosystems subjected to environmental changes – or, on the long term, fluctuations – induced by both climate and socio-economic factors. These geosystems are interrelated and include, among others, the glacial and the periglacial system.

Table 2. Climate characteristics of selected sites in Tajikistan (T) and Austria (A). Data: Central Institute for Meteorology and Geodynamics, Austria, HISTALP (2009) and Agency of Hydrometeorology, Tajikistan. MAAT = Mean annual air temperature 1971–2000 (Fedchenko: 1971–1995), MAP = Mean annual precipitation 1971–2000 (Fedchenko: 1971–1995). Trend 1 is from 1970–1995, trend 2 from 1970–2008.

	Elev. a.s.l. (m)	MAAT	Mean max/min air temperature (°C)	MAAT trend1 / trend2 (°C)	MAP (mm)	Nov. - April precipitation (per cent)
Khorog (T)	2075	9.1	22.1 / -4.8	-3.75 / +0.67	291	78.0
Dekhavz (T)	2561	4.5	15.4 / -6.9	+0.36 / +2.25	318	42.3
Fedchenko (T)	4169	-6.8	4.1 / -17.1	+0.27 / -	1280	42.2
Innsbruck (A)	578	8.9	24.9 / 3.7	+5.5 / +4.7	883	34.3
Sonnblick (A)	3105	-7.5	0.2 / -14.4	+4.3 / +3.4	1673	50.1

2.2 State of research in Austria

Direct information on selected Austrian glaciers is available back to the 17th century from reports, paintings and drawings (Nicolussi 1990; Hall et al. 2003). Topographic maps including glacier extent were first prepared at the end of the 19th century. The first systematic glacier inventory of Austria was compiled in 1969, using aerial photographs (Patzelt 1980). A second inventory was prepared in the late 1990s, so that a complete account of glacier changes in the last three decades of the 20th century exists (Lambrecht and Kuhn 2007). The most comprehensive available data are the annual Glacier Reports published by the Austrian Alpine Club (Österreichischer Alpenverein 1972–2010). They compile systematic annual measurements of length changes of approx. 100 Austrian glaciers. Detailed long-term monitoring has been performed particularly for the Pasterze Glacier in western Carinthia (e.g. Hall et al. 2001; Gspurnig et al. 2004) and the Hintereisferner in Tyrol (e.g. Kuhn et al. 1999).

In Austria, research on permafrost has less of a tradition than that on glaciers. Whilst in Switzerland the early work of Wilfried Haeberli dates back to the 1970s (e.g. Haeberli 1975), Austrian permafrost research started no earlier than 1980 (Lieb 1998). Conventional methods to distinguish permafrost areas from areas free of permafrost have been applied for a number of study sites in the Austrian Alps. Such approaches include temperature measurements at the base of the winter snow cover or of spring water, drillholes, geophysical methods (ground-penetrating radar, seismic sounding, geoelectrics), or geomorphologic interpretation (Krainer 2007). Only recently have attempts been made to extrapolate these findings to larger areas, i.e. the entire Austrian Alps (Ebohon 2007), amending relationships developed by Haeberli (1975) for Switzerland. Only indirect evidence exists for permafrost retreat and related hazards: Krainer (2007) reported problems with increasing rock fall activity and subsidence in permafrost areas of

Austria, which indicate a thicker active layer as well as melting of ice in the cracks of steep rock walls, most probably associated with climate change.

2.3 State of research in Tajikistan

The earliest reports on Tajik glaciers date back to the late 19th and early 20th century, when various explorers visited the high-mountain areas of Central Asia (The Great Game, Middleton and Thomas 2008). During the Soviet period, systematic mapping of the glaciers took place. The glaciers of the Pamir were inventoried in the period 1968–1973 as part of the Soviet Glacier Inventory (Kotlyakov 1980). Detailed studies were conducted in the 1960s and 1970s for the Fedchenko Glacier and the Abramov Glacier (on Kyrgyz territory close to the Tajik border, Kotlyakov 1980). After independence, and particularly during the Civil War from 1992–1997, research diminished. Meteorological and hydrologic measurements were discontinued. The main sources of glacier data are the World Glacier Inventory WGI (NSIDC 1999–2009) and the GLIMS database (Armstrong et al. 2005). Some attention was and is still put on surging glaciers (e.g. Dolgoushin and Osipova 1975; Kotlyakov et al. 2008) as well as on glacial lakes and connected hazards (Mergili and Schneider 2011).

Direct data on permafrost distribution, properties and impacts in Tajikistan are very scarce. More work, particularly from A.P. Gobunov and his team, exists on the adjacent Tien Shan of Kyrgyzstan and Kazakhstan (see Marchenko et al. 2007 for more references). Müllebner (2010) modelled the potential permafrost distribution for selected areas of Tajikistan with two contrasting methods: first, by adapting the elevation thresholds for Switzerland (Haeberli 1975) to the regional climate and second, by using a combination of temperature thresholds and incoming solar radiation (adapting a method suggested by Krummenacher et al. 2003). The resulting lower permafrost boundaries of both methods correspond well.

3 Data and Methods

3.1 The glacial environment

The research presented in this paper focuses on changes and fluctuations in the glacial and periglacial environment since the late 1960s. The first systematic glacier inventory of Austria was compiled in 1969 (Patzelt 1978, 1980) and the first appropriate sets of satellite imagery (Corona) for Tajikistan date back to 1968.

Basic geometric data on the glaciers in the two countries (surface area, Equilibrium Line Altitude ELA, elevation of the upper and lower boundary) were extracted from the World Glacier Inventory (WGI) provided by the NSIDC (1999–2009). Though very comprehensive, a major drawback or the WGI is the temporal inconsistence of the databases. The data for Austria, from 1998, are the same as used for the new Austrian Glacier Inventory (Lambrecht and Kuhn 2007). For Tajikistan, data sources from the 1940s to 1960s were used. Therefore, the WGI was only employed for the general characterization of the glaciers in the two countries.

Since much fewer detailed and recent measurements are available for Tajikistan, original research of the present work focuses on this country. The areas for detailed studies were chosen in a way to represent a wide range of climatic, topographic and altitudinal conditions representative for the

country. Three study areas were selected in different parts of the Pamir: northern Pamir, Shugnan Range and Rushan Range (see Fig. 1). The glaciers in these areas were systematically mapped from multitemporal satellite imagery:

- declassified Corona imagery from 1968 and 1969. The analogue images are available for the entire territory of Tajikistan and provide an excellent database for mapping the glacial status of the late 1960s. The effective cell size of the scanned images is ≤5 m. Drawbacks are that the imagery is only available in greyscale and the considerable geometric distortion, particularly in mountainous terrain.
- ASTER imagery from 2002 and 2007 to 2009. With a cell size of 15 m and several channels in the visible and infrared spectrum, it is the most cost-efficient medium-resolution dataset available for the period since 2000.

Only areas with exposed ice were mapped, considering their changes as a reasonable surrogate for the change of the total glacier surface. Even though remote sensing-based approaches for mapping the extent of debris-covered glaciers exist (Paul et al. 2004; Bolch et al. 2008), change detection remains a challenge since the transition between debris-covered glacier tongues and ice-bearing till is hard to identify and often fuzzy. More specialized approaches (e.g. DInSAR or geoelectrics) would be required for such a purpose.

A qualitative confidence measure was assigned to each mapped glacier (3–High; 2–Medium; 1–Low), primarily depending on the snow cover of the glacier in the respective image. Only glaciers with high or medium confidence were used for the analysis of glacier fluctuations.

For the southwestern Pamir, a multitemporal inventory of glacial lakes was prepared from the set of images mentioned above. Helicopter surveys and field visits in summer 2003 and 2009 served as verification of the findings from the remote sensing survey. The hazard of Glacial Lake Outburst Floods (GLOFs) from these lakes was analyzed using a rating scheme for the regional scale (Mergili and Schneider 2011).

Additional work was conducted in the Upper Zarafshan Valley in the Alai Mountains of northern Tajikistan, which occupies a lower altitudinal range than the Pamir (see Fig. 1). The positions of the termini of four selected glaciers were measured in cooperation with the Tajik Agency of Hydrometeorology, employing a geodetic approach. Including unpublished data on discontinued periodic measurements from the 1920s to 1991 held by the Agency of Hydrometeorology, series of glacier length changes 1927–2009 were derived.

The findings from the comparison of the 1969 and the 1998 Austrian Glacier Inventories presented by Lambrecht and Kuhn (2007) were used to compare the situations in Tajikistan and in Austria. No systematic account of Austrian glacier surface and volume changes was yet available for the period since the late 1990s. Cumulative glacier length changes, averaged by mountain range, were derived from the glacier reports 1971–2009 (Österreichischer Alpenverein 1972–2010).

3.2 The periglacial environment

Periglacial research presented in the paper focuses on the modelling of potential present and future permafrost distribution.

The approach developed by Haeberli (1975) for Switzerland and applied by Ebohon (2007) for Austria was followed, applying lower limits of elevation for the possible and for the probable distribution of permafrost. These limits are based on field evidence and depend on the topographic situation and the aspect. For Tajikistan, the original elevation limits were adapted according to the difference in mean annual air temperature (MAAT). Keller (1992) found out an elevation of 2,200 m a.s.l. for the 0°C isotherm in Switzerland. Müllebner (2010), using datasets provided by the Tajik Meteo Service, derived an elevation of 3,300 m a.s.l. for the 0°C isotherm in Tajikistan. Accordingly, the values from Haeberli (1975) and Ebohon (2007) were increased by 1,100 m for Tajikistan. Table 3 shows the original and the adapted scheme. The schemes were applied making use of the software GRASS GIS and the SRTM-4 Digital Elevation Model (Jarvis et al. 2008). The results for Tajikistan were corroborated with 65 rock glacier termini mapped in the Gunt and Shakhdara valleys in the southwestern Pamir. All active rock glaciers with a steep, geomorphologically active front and without vegetation cover were considered, disregarding features with an accumulation area of exposed ice. Only the lowermost termini of rock glacier systems were mapped.

Table 3. Potential lower permafrost limits for Austria / Tajikistan according to Haeberli (1975), Ebohon (2007) and Müllebner (2010).

	Lower boundary of sporadic permafrost (permafrost possible) (m)		Lower boundary of discontinuous permafrost (permafrost probable) (m)	
Aspect	exposed sites	protected sites	exposed sites	protected sites
N	2300 / 3400	1960 / 3060	2500 / 3600	2410 / 3510
NE	2450 / 3550	2100 / 3200	2600 / 3700	2500 / 3600
E	2575 / 3675	2220 / 3320	2720 / 3820	2520 / 3620
SE	2700 / 3800	2230 / 3330	2850 / 3950	2630 / 3730
S	2900 / 4000	2340 / 3440	2900 / 4000	2690 / 3790
SW	2650 / 3750	2230 / 3330	2850 / 3950	2630 / 3730
W	2600 / 3700	2160 / 3260	2700 / 3800	2510 / 3610
NW	2530 / 3630	2120 / 3220	2580 / 3680	2470 / 3570
flat	2590 / 3690	2640 / 3740	2710 / 3810	2900 / 4000

Scenarios of increasing MAAT (3.7 °C for Tajikistan and 3.5 °C for Austria until 2100; IPCC 2007) were taken as guideline for the projections of the potential future permafrost distribution.

Increases in MAAT of 1 °C, 2 °C, 3 °C and 4 °C were assumed in order to account for possible scenarios of permafrost retreat in the 21st century. The altitudinal lapse rate for Tajikistan was fixed to 0.062 °C/m using linear regression from the set of Tajik temperature data. A rate 0.054 °C/m was used for Austria, according to the value provided by Rolland (2003) for Tyrol. The elevation limits shown in Table 3 were then increased accordingly for each of the four scenarios. Only the lower limits of possible permafrost were used, not distinguishing between areas with possible and such with probable permafrost.

4 Results

4.1 The glacial environment

4.1.1 Distribution, extent and debris cover of glaciers in Tajikistan and Austria

Though both Tajikistan and Austria are rich in high-mountain landscapes, they differ substantially in their extent of glaciers. According to the WGI (NSIDC 1999–2009), 7,896 km² of Tajikistan (5.5% of the total area) are covered by glaciers, compared to 542 km² (0.6%) in Austria. The WGI lists 7126 glaciers for Tajikistan and 925 for Austria, so that the average surface area of single glaciers is 1.1 km² in Tajikistan and 0.6 km² in Austria. The largest single glacier in Tajikistan is the Fedchenko Glacier (156 km²), in Austria it is the Pasterze (20 km²). These figures show that the extent of glacierization is about one order of magnitude higher in Tajikistan than in Austria (Table 4).

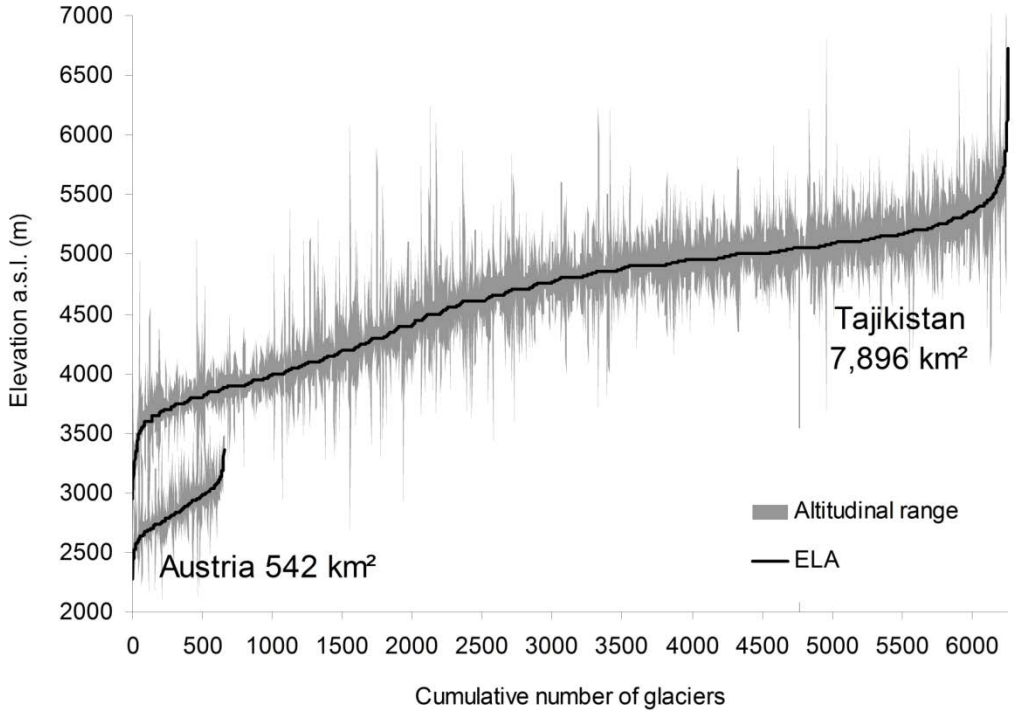

Fig. 2. Altitudinal range of equilibrium lines, upper and lower boundaries of glaciers and total glacier surface areas in Tajikistan and Austria as compiled from the WGI.

The WGI identifies 602 km² or 7.6% of the Tajik glacier surface as debris-covered. 1096 glaciers (15.4%) are at least partly covered by debris (see Table 4). The share of debris-covered glaciers

increases with glacier size. So does the ratio of debris-covered glacier surface, but to a much lesser extent. These patterns are also true for Austria, but the extent of debris cover is much smaller there. 85 Austrian glaciers (9.2%) are at least partly debris-covered, the debris cover accounts for 7.6 km² (1.4% of the total glacier surface). Comparing glaciers of the same size class, the percentage of glaciers with debris cover in the two countries is comparable, but the percentage of debris-covered glacier surface is still much higher in Tajikistan.

Table 4. Number and size of glaciers and percentage of debris cover in Tajikistan and Austria. Data source: WGI.

	Number		Surface area (km²)		Per cent of total		Debris cover	
Size class	glaciers total	debris-covered	glaciers total	debris-covered	number	surface area	per cent of number	per cent of surface area
Tajikistan								
≤0.5 km²	4385	202	1076.8	29.2	61.8	13.6	4.6	2.7
>0.5 – 1 km²	1152	221	877.1	48.4	16.2	11.1	19.2	5.5
>1 – 2 km²	768	250	1120.5	75.6	10.8	14.2	32.6	6.7
>2 – 5 km²	537	248	1630.9	132.0	7.6	20.7	46.2	8.1
>5 – 10 km²	153	99	1055.9	98.9	2.2	13.4	64.7	9.4
>10 – 20 km²	72	53	1043.7	90.8	1.0	13.2	73.6	8.7
>20 – 50 km²	25	20	750.1	82.2	0.4	9.5	80.0	11.0
>50 km²	4	3	341.1	39.1	0.1	4.3	75.0	11.5
Sum	7096	1096	7896.2	596.2	100.0	100.0	15.4	7.6
Austria								
≤0.5 km²	704	21	109.4	0.9	76.2	20.2	3.0	0.8
>0.5 – 1 km²	111	21	77.6	1.0	12.0	14.3	18.9	1.2
>1 – 2 km²	48	15	66.7	1.1	5.2	12.3	31.3	1.7
>2 – 5 km²	46	16	145.6	1.4	5.0	26.9	34.8	1.0
>5 – 10 km²	10	8	71.8	1.4	1.1	13.2	80.0	2.0
>10 km²	5	4	71.2	1.8	0.5	13.1	80.0	2.6
Sum	924	85	542.1	7.6	100.0	100.0	9.2	1.4

Due to the climatic and topographic conditions, glaciers occupy a higher altitudinal range in Tajikistan than in Austria (Fig. 2). According to the WGI (only considering those glaciers with assigned ELA, n = 6257 for Tajikistan, n = 655 for Austria), the average ELA, weighted by glacier surface, is 4896 m in Tajikistan and 2925 m in Austria.

4.1.2 Glacier development 1968–2009

Rates of glacier surface change vary substantially between different areas in Tajikistan, but also between different observation periods (Fig. 3). On average, the observed glaciers in the northern Pamir remained stable in the period 1968–2002, whilst most glaciers in the Rushan and Shugnan ranges of the southwestern Pamir were retreating at rates partly exceeding 1% per year, related to the 1968 surface. In the period 2002–2007, the glaciers of the northern Pamir were retreating at rates similar to those in the other study areas.

The results obtained suggest that the glaciers of the Pamir in general have shifted towards accelerated retreat in the period 2002–2007, compared to the period 1968–2002. More data and a finer resolution of the period 1968–2002 would be required to explore the reasons for the differentiated behaviour of the glaciers in different parts of the Pamir.

In the Alai mountains (northern Tajikistan), the retreat of the glaciers has continued since the 19th century. The dense meadows of the Zarafshan Valley allow the easy identification of the maximum glacial extent during the Little Ice Age in the 19th century and indicate a tremendous loss of thickness. According to data held by the Tajik Agency of Hydrometeorology, measurements at the Turo and Dihadang Glaciers have yielded annual rates of subsidence of about 1 m.

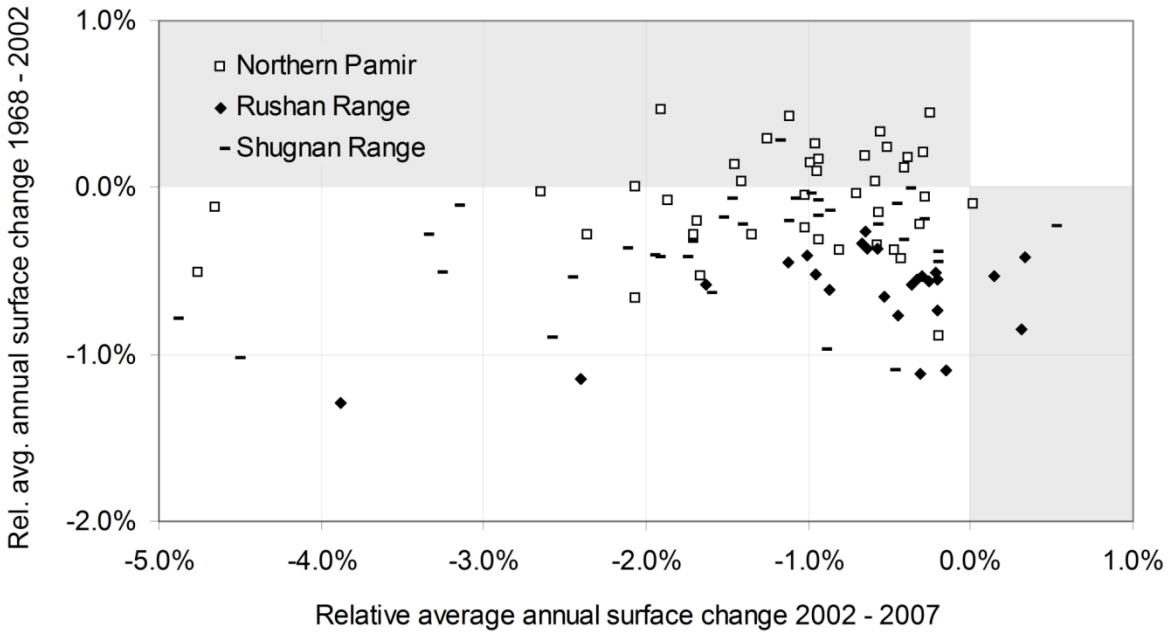

Fig. 3. Average annual change of surface area of glaciers in the Pamir for the periods 1968–2002 and 2002–2007.

During Soviet times, the length of the Zarafshan Glacier was measured at irregular time intervals using geodetic methods. A steady retreat accelerating towards the end of the 20th century was observed: 280 m from 1927–1961 (8 m/year), 980 m from 1961 to 1976 (65 m/year), further 1092 m from 1976 to 1991 (73 m/year) and 1650 m from 1991 to 2009 (92 m). In 2009, the snout of the Zarafshan Glacier was located approx. 5.5 km behind the most distal terminal moraine from the Little Ice Age. A similar behaviour was observed for other glaciers in the upper Zarafshan Valley (Fig. 4).

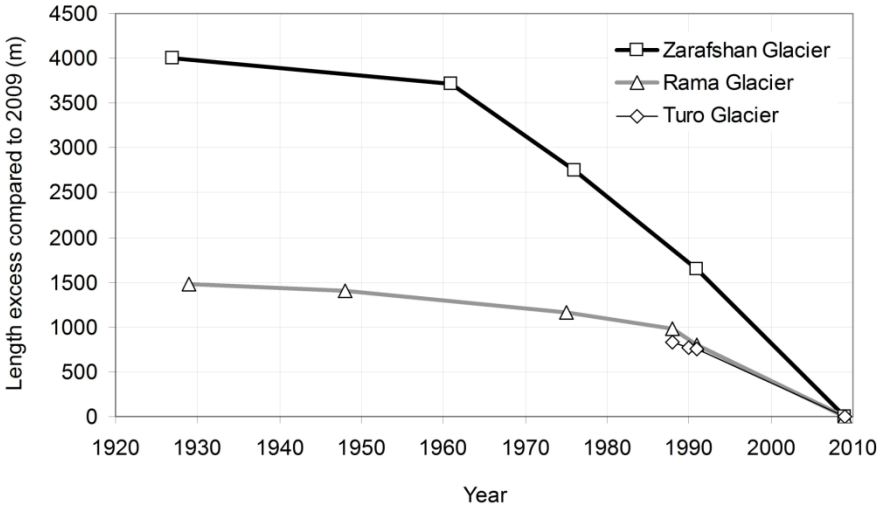

Fig. 4. Measured retreat of some of the major glaciers of the upper Zarafshan Valley 1927–2009.

In Austria, comparison of the glacier inventories of 1969 and 1998 yielded a loss of 17.1% of the glacier surface for the entire country, from 567 km² to 471 km² (Lambrecht and Kuhn 2007). Almost all glaciers were retreating in this period, with only a few exceptions. Whilst the loss in the heavily glacierized Ötztaler Alpen was close to average (17.6%), it was highly variable in the less glacierized mountain ranges, from a gain of 11.3% (Karnische Alpen) to a loss of 59.8% (Samnaungruppe). In general, the 1970s and early 1980s were characterized by largely positive mass balances and partial advances (Fig. 5), caused by an interplay of years with high winter accumulation and low summer temperature (Schöner et al. 2000; Lambrecht and Kuhn 2007). Related to the 1969 surface, the average annual loss until 1998 was 0.58%. This value is comparable to that one found for the Rushan Range (0.56%) and significantly higher than those for the other study areas in Tajikistan for a similar period: 0.40% for the Shugnan Range and 0.01% for the northern Pamir. However, the variation within each of the Tajik mountain ranges is considerable (Table 5).

Figure 5 shows the changes of glacier lengths between 1970 and 2009, compiled from the Glacier Reports of the Austrian Alpine Club (Österreichischer Alpenverein 1972–2010) and averaged by mountain range: the findings are in line with those from the glacier inventories, but they also illustrate the accelerated retreat in the first decade of the 21st century, with the extraordinarily hot summer of 2003. The Zillertaler Alpen experienced a pronounced glacial advance in the late 1970s and early 1980s (derived, however, from a small set of measured glaciers), a development not at all observed in the directly adjacent Venedigergruppe. The Obersulzbachkees in the latter area decreased by 1,008 m in length during the observation period, the Pasterze Glacier in the

Glocknergruppe retreated by 688 m. The annual decrease of glacier surface elevation measured for the Pasterze Glacier averaged between 4 and 5 m in the years 2006–2009.

Table 5. Glacier surface changes in selected areas of the Tajik Pamir 1968–2007.

Study area	n	Mean annual surface change (per cent)	Standard deviation (per cent)
North Pamir			
1969-2002	69	-0.01	0.39
2002-2007	71	-1.41	1.14
1969-2007	85	-0.17	0.32
Rushan			
1969-2002	58	-0.56	0.27
2002-2007	52	-0.75	0.81
1969-2007	42	-0.58	0.24
Shugnan			
1969-2002	60	-0.40	0.36
2002-2007	55	-1.52	1.28
1969-2007	50	-0.54	0.39

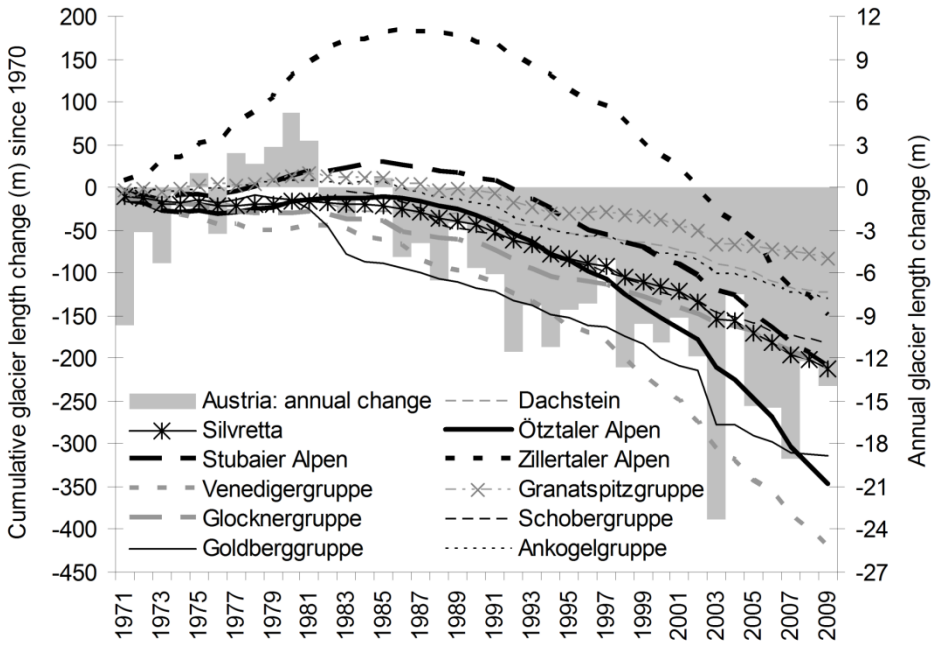

Fig. 5. Length changes 1970–2009 of selected Austrian glaciers, averaged by mountain range.

4.2 Evolving glacial lakes as potential hazards.

Figure 3 shows that the glaciers of the southwestern Pamir (Rushan Range, Shugnan Range) are at a more advanced stage of retreat than those of the northern Pamir. Retreating glaciers often leave behind a rim of lateral and terminal moraines comprised of buried ice overlain by till, an ideal terrain for glacial lakes to form. In 2007, 172 glacial lakes existed in the Gunt and Shakhdara Basins in the southwestern Pamir (Mergili and Schneider 2011). Most of them are located at 4,400–4,700 m a.s.l. and have formed – or at least gained much of their size – since 1968. Depending on topography, dam characteristics, ice content, seepage through the dam and the possibility of ice falls or landslides into the lakes, they are more or less susceptible to produce hazardous outburst floods (GLOFs; e.g. Costa and Schuster 1988; Huggel et al. 2002, 2003, 2004). Mergili and Schneider (2011) classified 6 of these lakes as very hazardous and 34 as hazardous. In contrast to the southwestern Pamir, few glacial lakes were detected in the northern Pamir. In the Zarafshan Valley, only some minor glacial lakes exist on the decaying glacier snouts, none of them are considered hazardous.

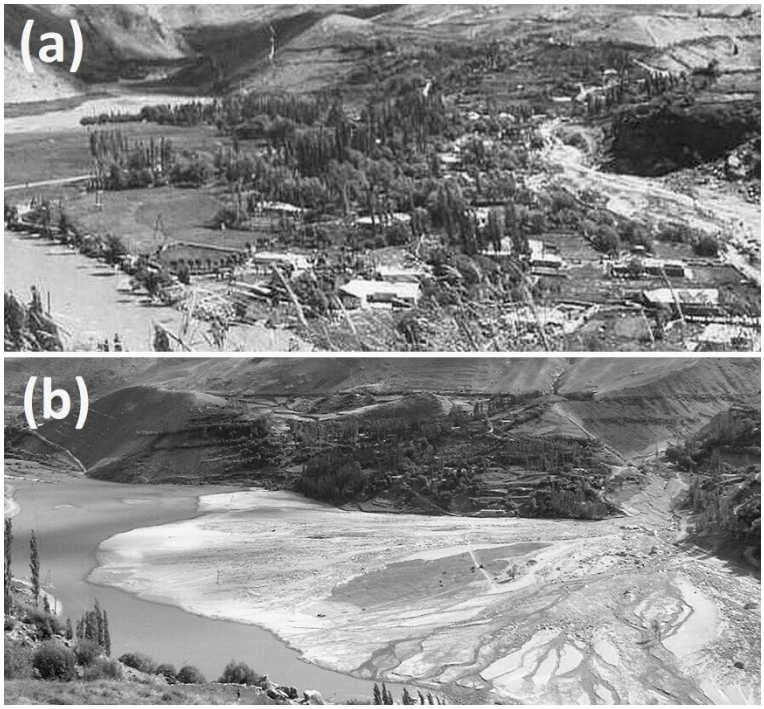

Fig. 6. The village of Dasht in the Shakhdara Valley (a) before (photo: FOCUS Humanitarian Assistance) and (b) after the GLOF of August 7, 2002.

History has shown that even small lakes may produce highly destructive GLOFs. On August 7, 2002, one of the numerous glacial lakes in the southwestern Pamir drained suddenly. The supraglacial lake had a surface area of 37,000 m² and an estimated volume of 320,000 m³. The magnitude of the event was multiplied due to entrainment and backwater effects, so that the resulting mud flow had an estimated volume of 1–1.5 Million m³ (Mergili and Schneider 2011). The village of Dasht 10.5 km downstream in the Shakhdara Valley (see Fig. 1) was largely destroyed and approx. 25 people lost their lives (Fig. 6). Field and remote sensing surveys have shown that the lake was very short-lived: it had formed less than two years before the event, in autumn 2000 or spring 2001. No lake of substantial size was detected in this place on older

images going back to 1968 or after the event up to 2009. The outburst occurred beneath the glacier surface, probably caused by weakening of a temporary blockage of the seepage channel having dammed the lake.

The most recent documented GLOFs on today's Austrian territory occurred in the 17th to 19th century, when the surging Vernagtferner repeatedly dammed lakes in the Ötz Valley in Tyrol (Hoinkes 1969; Braun 1995) producing a number of destructive GLOFs. Due to the lack of recent surges and the comparably small moraines, only few glacial lakes exist in the direct forefields of the retreating Austrian glaciers, and none of them are considered hazardous. In other parts of the Alps, however, such lakes exist and recent hazardous situations are evident (e.g. Werder et al. 2010).

4.3 Permafrost

Potential distribution of permafrost. 44.3 per cent of Tajikistan, but only 2.4% of Austria were identified as potential permafrost areas (Table 6). The high value for Tajikistan is primarily influenced by the extensive highlands of the eastern Pamir in the GBAO, which are almost entirely potential permafrost area (84.1% of GBAO was classified as potential permafrost area, 94% out of that area as permafrost probable). Except for Khatlon, also the remaining Tajik provinces display much larger shares of potential permafrost areas than most of the Austrian provinces. Only the value for Tyrol (11.7%) is comparable to that for the Tajik province of Sughd. However, Sughd includes extensive lowlands (Ferghana Basin), whilst Tyrol is entirely mountainous. More than 90% of the Tajik, but only 63% of the Austrian potential permafrost areas were classified as permafrost probable.

In terms of absolute values, almost 54,000 km² of potential permafrost area were identified in the GBAO, out of more than 63,000 km² for the entire territory of Tajikistan. In Austria, potential permafrost areas exceed 1,000 km² only in Tyrol, accounting for almost three thirds of the total for Austria (around 2,000 km²).

4.4 Field observations and model evaluation

The superficially most obvious permafrost features are rock glaciers. Such landforms of different sizes and states of activity are widespread all over the Pamir. Some of them retain lakes which are potentially prone to sudden drainage in the case of degradation of the rock glacier dam (Fig. 7).

The termini of the mapped rock glaciers were compared to the modelled lower limit of permafrost. 60 rock glaciers (92%) are located within designated permafrost areas (Fig. 8), 53 (82%) terminate in the zone with probable permafrost. More than half of the features (34 or 52%) end up more than 200 m above the lower limit of probable permafrost. These findings suggest that the scheme used provides a realistic estimate of the lower boundary of potential permafrost areas, but that rock glaciers alone are of limited use for permafrost delineation. In the study area, rock glaciers may terminate above their climatic limit for various reasons: (i) erosion of the rock glacier; (ii) very steep topographies where rock glaciers lose their coherence; (iii) rock glaciers are slow-moving features not necessarily in equilibrium with the climatic conditions. Furthermore, the location of the lower boundary of the active part is sometimes uncertain.

Table 6. Potential permafrost areas in Tajikistan and Austria (entire country and each province) in absolute and relative terms. PsPF = permafrost possible, PrPF = permafrost probable, rPrPF = ratio of areas with permafrost probable compared to the entire potential permafrost area. The total area was computed based on the raster maps used and differs slightly from the value given in Table 1 (see also Fig. 1).

	Area (km²)	PsPF (km²)	PsPF (per cent)	PrPF (km²)	PrPF (per cent)	rPrPF (per cent)
Tajikistan						
Tajikistan	142,485	63,072	44.3	58,168	40.8	92
Khatlon	24,293	16	0.1	8	0.0	52
GBAO	64,095	53,931	84.1	50,794	79.2	94
RRS	28,857	6,070	21.0	5,007	17.4	83
Sughd	25,241	3,056	12.1	2,358	9.3	77
Austria						
Austria	84,200	2,000	2.4	1,257	1.5	63
Tyrol	12,641	1,479	11.7	979	7.7	66
Vorarlberg	2,598	59	2.3	25	1.0	43
Upper Austria	12,017	9	0.1	3	0.0	31
Carinthia	9,558	182	1.9	100	1.0	55
Salzburg	7,170	264	3.7	150	2.1	57
Styria	16,487	8	0.0	1	0.0	9

Fig. 7. Khavrazdara (Bartang Valley): 1.9 km² Lake Khavraz retained by an active rock glacier.

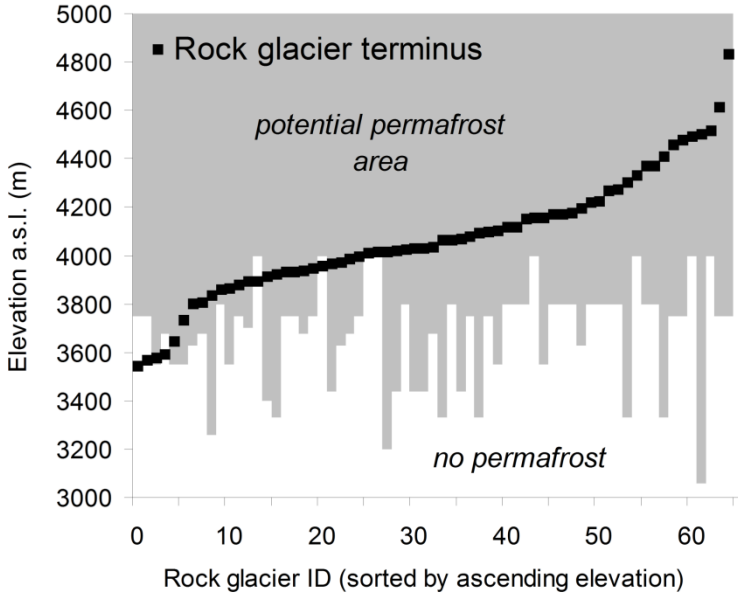

Fig. 8. Mapped rock glacier termini in the Pamir, related to the lower boundary of possible and probable permafrost.

4.5 Scenarios of permafrost retreat

Figure 9a illustrates the present potential permafrost areas in the two countries.

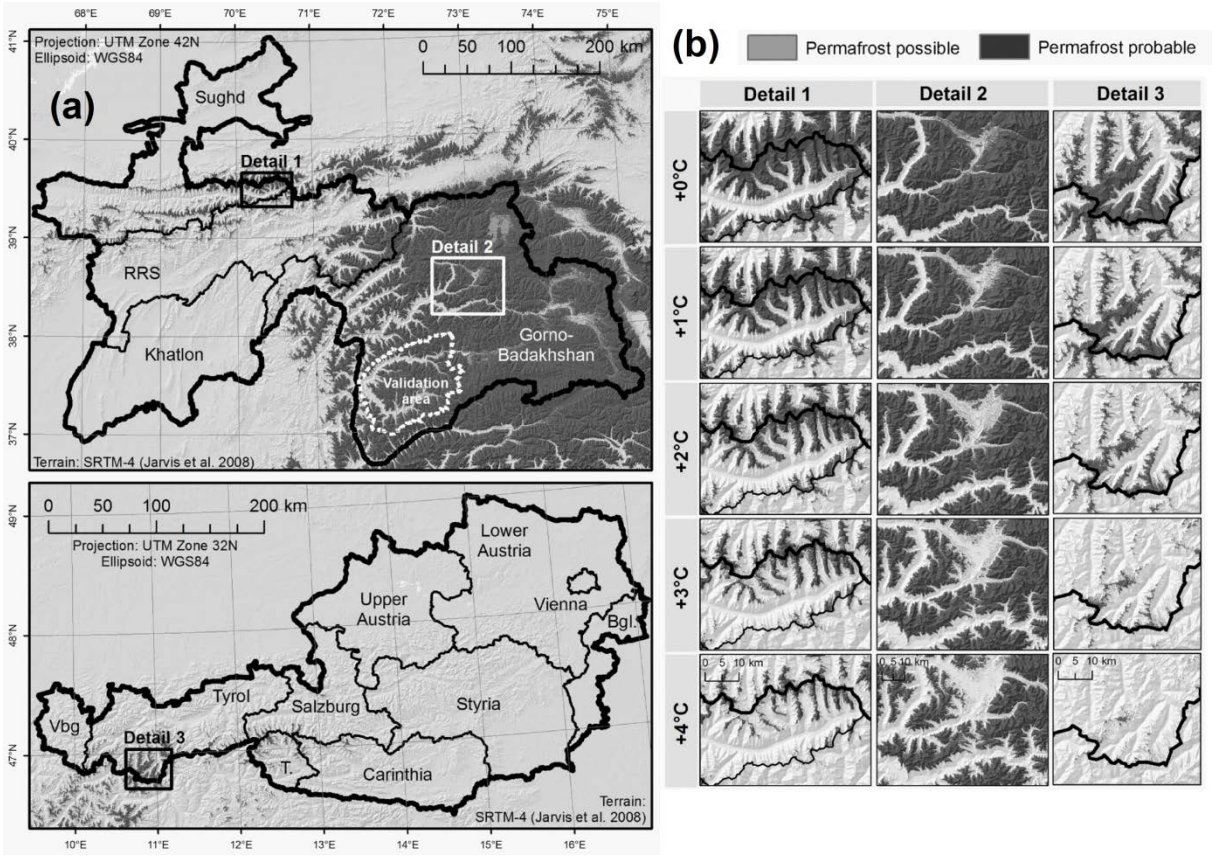

Fig. 9. (a) Potential distribution of permafrost in Tajikistan and Austria, (b) projections for different scenarios of increased MAAT for selected areas.

The projected patterns of permafrost retreat differ markedly between the two countries: in Tajikistan, due to the more extensive potential permafrost area in general, the predicted absolute changes are larger by approx. one order of magnitude than in Austria, whilst the predicted relative changes in Tajikistan are exceeded by those in Austria. However, the variability within each of the countries is also high (Fig. 9b and 10).

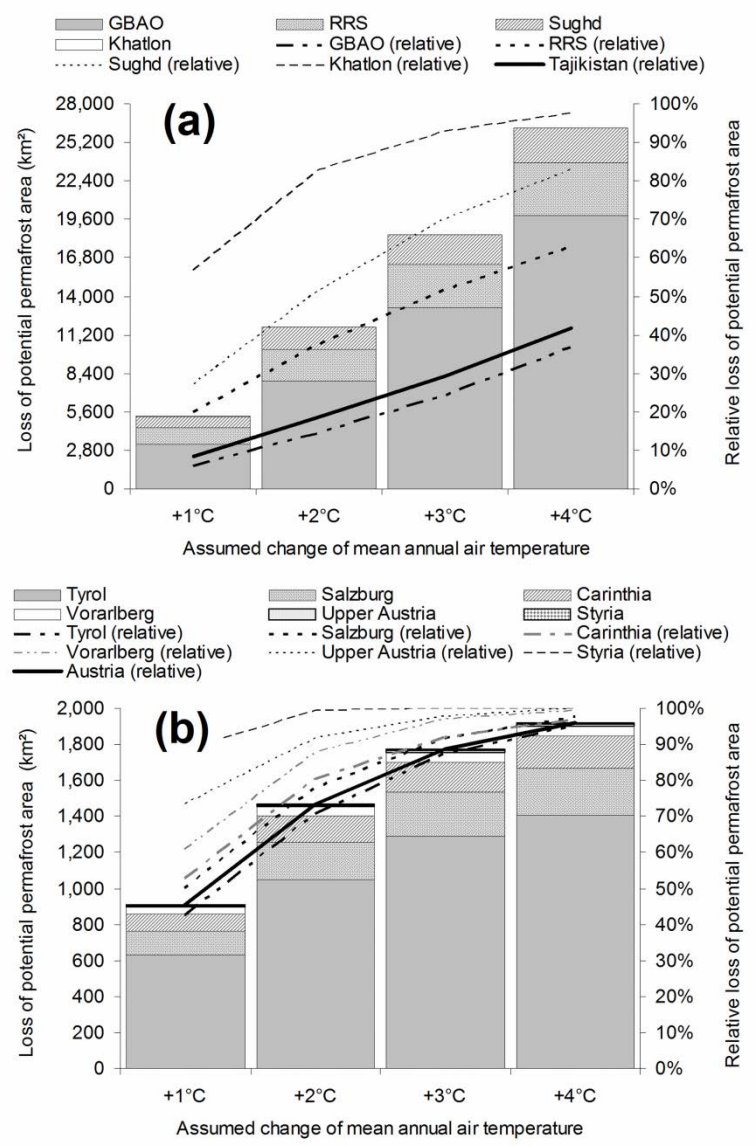

Fig. 10. Projected loss of potential permafrost areas in (a) Tajikistan and (b) Austria in absolute and relative terms.

The abundance of potential permafrost areas in the GBAO – particularly in the highlands of the eastern Pamir – leads to a tremendous potential loss in terms of absolute values, aggregating to roughly 20,000 km² in the case of a 4°C temperature increase. This value would, however, correspond to only 40% of the potential permafrost area of the GBAO. The remaining provinces of Tajikistan – with less extensive high-elevation area – would experience potential losses of up to a few thousands km², amounting to 63–96% of the potential permafrost areas. These values are comparable to those for Tyrol, the province of Austria with most permafrost in both absolute and relative terms. In each Austrian province, more than 90% of the potential permafrost areas

would disappear if the MAAT would increase by 4°C. In Upper Austria and Styria, with only marginal occurrences at present, there would be no more permafrost at all. Already with an increase of 2°C, each Austrian province would experience a loss between 70 and 99%. Due to the limited extent of potential permafrost areas in Austria in general, the absolute loss would – except for Tyrol – account for few hundred km² or less (see Fig. 10).

The characteristics presented above imply that in the GBAO, the rate of permafrost retreat remains largely constant with increasing temperature increase. In the other provinces of Tajikistan and particularly in Austria, the curves in Fig. 10 flatten out, indicating that the reservoir of permafrost becomes more and more depleted there.

5 Discussion

In the high-mountain areas of Tajikistan, one may distinguish three major zones of environmental change dynamics:

- In the northwest (Zarafshan Valley, Alai Mountains), the glaciers are in an advanced stage of retreat, and some small glaciers may disappear during the next few decades. It is likely that most of the permafrost will melt.
- In the southwestern Pamir, almost all glaciers are retreating and many glacial lakes are developing. At least one destructive outburst flood of such a lake (the Dasht event) has occurred there in the recent past, comparable events are possible in the near future. Permafrost may undergo substantial melting during the 21st century, but much of it will persist due to the high elevation of most areas.
- The highest portions of the northern and central Pamir are still highly glacierized. However, at least for the mapped area, a clear trend of glacier retreat during the past decade was observed. There are few glacial lakes, but more may develop over the next decades. Much of the permafrost is supposed to persist during the 21st century.

The situation of the Austrian glaciers and potential permafrost areas is partly comparable with the northwest of Tajikistan. More than 90% of the potential permafrost areas may disappear during the 21st century. Almost all glaciers are in an advanced stage of retreat, a trend which seems to have accelerated in the first decade of the 21st century. However, the rates of change in glacier length also for the largest Austrian glaciers are significantly lower than those measured in the Zarafshan Valley for a comparable period. Comparatively few glacial lakes exist in the direct forefields of Austrian and northern Tajik glaciers.

In different parts of the Pamir, a more comprehensive mapping campaign in combination with a higher temporal resolution of glacier observations and consistent meteorological data would be required to understand the differences of glacier development 1968–2002. Suggesting a relationship of the more positive development in the northern Pamir with the advances in Austria in the late 1970s and early 1980s would be highly speculative: in the case of Austria, the phenomenon is well correlated to the North Atlantic Oscillation (Schöner et al. 2000) which has limited influence on the Central Asian climate. Reliable high-elevation precipitation data in the area of the northern Pamir are available from the Gorbunov meteo station (4,169 m a.s.l) only for

the period 1970–1995. Increasing trends of both mean annual and winter precipitation were observed during this time.

A phenomenon worthy of attention is the much higher share of debris-cover on Tajik glaciers, compared to Austrian ones. To some extent, this phenomenon may be assigned to more active morphodynamics due to higher local relief, delivering more debris onto the glacier surface. More important, most of the Tajik mountain areas are arid, with less snow fall and therefore lower rates of accumulation than in Austria. This favours glaciers rich in debris which – particularly in a stage of retreat – may evolve into debris-covered glaciers or even rock glaciers (Ackert 1998). Many glaciers terminate as lobes intermediate between debris-covered glaciers, rock glaciers and ice-bearing moraine, so that the glacial and the periglacial domain are not always clearly distinguishable. From a methodological point of view, this phenomenon complicates mapping of glaciers and – in particular – of glacier fluctuations.

Many of those lobes are partially covered by glacial lakes. Though the recognition of potentially hazardous glacial lakes by means of GIS and remote sensing is comparatively easy (except for subglacial lakes), the prediction of outburst floods remains a challenge. Particular difficulties are connected to the estimation of travel distances and impact magnitudes, both at the local and the regional scale (Mergili and Schneider 2011; Mergili et al. 2011). The glacial lakes are usually far away from the area of impact and events occur at very long time intervals or as singularities, so that the population at risk is often not prepared for such events.

In Tajikistan, the population of the valleys strongly depends on meltwater from snow and glaciers for irrigation and therefore livelihood (Kassam 2009). However, the role of the glaciers for – and therefore also the impact of glacial retreat on – the water cycle, particularly runoff, is still disputed. Barnett et al. (2005) highlighted the shift of peak runoff from summer (the time of highest demand) to winter and spring. They mentioned Central Asia as one of the most-affected regions by such a shift, due to the natural settings and the limited water storage capacities. Kaser and Grosshauser (2010), however, showed that the contribution of meltwater quickly decreases with increasing distance from the glacierized areas. Unfortunately, quantitative local and regional data on the real contribution of meltwater from glaciers is sparse. It is clear, however, that the proportion of glacial meltwater in the runoff of Central Asian mountain rivers is much higher than in rivers of the humid Austrian Alps (Hagg and Braun 2005).

6 Conclusions

The research presented in this paper has illustrated that both in Tajikistan and in Austria, glaciers are in a stage of accelerated retreat. Indicators also exist for a retreat of permafrost which is, however, more difficult to quantify. The results of simple computer models suggest that much of the permafrost in both countries may disappear until the end of the 21st century. These changes in the high-mountain environment are connected to a changing hazard situation. Interactions of different types of hazardous phenomena involving both the glacial and the periglacial domains may lead to process chains possibly affecting communities tens of kilometres away from the source area (Haeberli et al. 2010a). For instance, melting of permafrost slopes heading into lakes

may result in mass movements triggering lake outburst floods. Detailed analyses of such scenarios and appropriate mitigation measures are required.

The extent of the glacial and periglacial environment is about one order of magnitude higher in Tajikistan than in Austria, both in absolute and in relative terms. The decision in which of the countries the changes discussed above pose the more severe problem largely depends on the viewpoint:

- if glaciers and permafrost are considered as environmental features worth of conservation, Austria is much more threatened because much of the glacier surface and most of the permafrost may disappear until the end of the 21st century;
- from a more practical point of view, larger problems are supposed to arise in Tajikistan. Potentially hazardous glacial lakes are evolving in the front of the retreating glaciers. Huge areas may become free of glaciers and permafrost, increasing the susceptibility of slopes to produce mass movements and, in the latter case, leading to ground subsidence. In Austria, the magnitude of this problem appears comparatively marginal, though the economic values concentrated at high elevation are higher and cases of damage on infrastructures possibly related to permafrost retreat were reported.

Furthermore, the dependence on meltwater from snow and glaciers for livelihood is higher in Tajikistan (with a much higher socio-economic vulnerability) than in the more humid Austrian Alps. Human-ecological studies of Kassam (2009) have shown that changes in the water – and also temperature – regime are already experienced by the local population in the Pamir, with both positive and negative impacts on their livelihood.

Acknowledgements

Much of the work presented in this paper was part of the project TajHaz (Remote Geohazards Assessment in Tajikistan) carried out in cooperation with FOCUS Humanitarian Assistance (an affiliate of the Aga Khan Development Network). The project was supported by the Swiss Agency for Development and Cooperation (SDC) and the UK Department for International Development (DFID). Special thanks go to Anvar Homidov, Alexander Pirov and Muzaffar Shodmonov from the Tajik Agency of Hydrometeorology for their contributions.

References

Ackert, R.P. Jr, 1998. A Rock Glacier/Debris-covered Glacier System at Galena Creek, Absaroka Mountains, Wyoming. Geografiska Annaler, 80A(3–4), 267–276. doi:10.1111/j.0435-3676.1998.00042.x

Aniya, M., Sato, H., Naruse, R., Skvarca, P. and Casassa, G., 1997. Recent Glacier Variations in the Southern Patagonia Icefield, South America. Arctic and Alpine Research, 29(1), 1–12.

Armstrong, R., Raup, B., Khalsa, S.J.S., Barry, R., Kargel, J., Helm, C. and Kieffer, H., 2005. GLIMS glacier database. National Snow and Ice Data Center, Boulder. Digital media.

Bajracharya, S.R., Mool, P.K. and Shrestha, B.R., 2007. Impact of climate change on Himalayan glaciers and glacial lakes: Case studies on GLOF and associated hazards in Nepal and Bhutan. ICIMOD, Kathmandu.

Barnett, T.P., Adam, J.C. and Lettenmaier, D.P., 2005. Potential impacts of a warming climate on water availability in snow-dominated regions. Nature, 438, 303–309. doi:10.1038/nature04141

Beniston, M., 2003. Climatic Change in Mountain Regions: A Review of Possible Impacts. Climatic Change, 59(1–2), 5–31. doi:10.1023/A:1024458411589

Bolch, T., Buchroithner, M.F., Kunert, A., Kamp, U., 2008. Automated delineation of debris-covered glaciers at Mt. Everest based on ASTER imagery. Grazer Schriften der Geographie und Raumforschung, 43, 13–24.

Braun, L.N., 1995. The main results of 100 years of research at the Vergtferner, Oetztal, Austria. Houille Blanche, 5–6, 109–110.

Chinn, T., Winkler, S., Salinger, M.J. and Haakensen, N., 2005. Recent glacier advances in Norway and New Zealand: a comparison of their glaciological and meteorological causes. Geografiska Annaler: Series A, Physical Geography, 87(1), 141–157.

Cook, A.J., Fox, A.J., Vaughan, D.G. and Ferrigno, J.G, 2005. Retreating Glacier Fronts on the Antarctic Peninsula over the Past Half-Century. Science, 308(5721), 541–544. doi:10.1126/science.1104235

Costa, J.E. and Schuster, R.L., 1988. The formation and failure of natural dams. Geological Society of America Bulletin, 100, 1054–1068. doi:10.1130/0016-7606(1988)100<1054:TFAFON>2.3.CO;2

Dolgoushin, L.D. and Osipova, G.B., 1975. Glacier surges and the problem of their forecasting. IAHS Publication, 104, 292–304.

Ebohon, B., 2007. Modellierung der Permafrostverbreitung in Österreich. Diploma thesis, University of Vienna.

Gspurning, J., Tintor, W., Tribuser, M. and Wakonigg, H., 2004. Volumen- und Flächenveränderungen an der Pasterze von1981 bis 2000. Carinthia II, 194, 463–472.

Haeberli, W., 1975. Untersuchungen zur Verbreitung von Permafrost zwischen Flüelapass und Piz Grialetsch (Graubünden). Dissertation, University of Basel.

Haeberli, W.,1992. Construction, environmental problems and natural hazards in periglacial mountain belts. Permafrost and Periglacial Processes, 3(2), 111–124. doi:10.1002/ppp.3430030208

Haeberli, W., Clague, J.J., Huggel, C., and Kääb, A., 2010a. Hazards from lakes in high-mountain glacier and permafrost regions: Climate change effects and process interactions. Avances de la Geomorphología en España, 2008-2010, XI Reunión Nacional de Geomorphología, Solsona, 439–446.

Haeberli, W., Portocarrero, C., and Evans, S., 2010b. Nevado Hualcán, Laguna 513 y Carhuaz 2010 – Observaciones, evaluación y recomendaciones (un corto informe técnico luego de las

reuniones y visita de campo en Julio 2010). Unpublished report on behalf of the Communidad Provincial de Carhuaz.

Haeberli, W., Wegmann, M. and Von der Muehll, D., 1997. Slope stability problems related to glacier shrinkage and permafrost degradation in the Alps. Eclogae Geologicae Helveticae, 90, 407–414.

Hagg, W. and Braun, L., 2005. The influence of glacier retreat on water yield from high mountain areas: Comparison of Alps and Central Asia, In: De Jong, C., Ranzi, R., Collins, D., (eds.), Climate and Hydrology in Mountain Areas, Wiley, Chichester. 263–275.

Hall, D.K., Bayr, K.J., Schöner, W., Bindschadler, R.A. and Chien, J.Y.L., 2003. Consideration of the errors inherent in mapping historical glacier positions in Austria from the ground and space (1893–2001). Remote Sensing of Environment, 86(4), 566–577. doi:10.1016/S0034-4257(03)00134-2

Hall, D.K., Bayr, K.J., Bindschadler, R.A. and Schöner, W., 2001. Changes in the Pasterze Glacier, Austria, as Measured from the Ground and Space. Proceedings of the 58th Eastern Snow Conference, Ottawa.

Harris, C., Arenson, L. U., Christiansen, H. H., Etzelmüller, B., Frauenfelder, R., Gruber, S., Haeberli, W., Hauck, C., Hölzle, M., Humlum, O., Isaksen, K., Kääb, A., Kern-Lütschg, M.A., Lehning, M., Matsuoka, N., Murton, J.B., Nötzli, J., Phillips, M., Ross, N., Seppälä, M., Springman, S.M. and Vonder Mühll, D. (2009). Permafrost and climate in Europe: Monitoring and modelling thermal, geomorphological and geotechnical responses. [Review]. Earth-Science Reviews, 92(3–4), 117–171. doi:10.1016/j.earscirev.2008.12.002

Harrison, S., Glasser, N., Winchester, V., Haresign, E., Warren, C., and Jansson, K., 2006. A glacial lake outburst flood associated with recent mountain glacier retreat, Patagonian Andes. Holocene, 16, 611–620. doi:10.1191/0959683606hl957rr

HISTALP, 2009. Historical Instrumental Climatological Surface Time Series of the Greater Alpine Region. Digital media.

Hoinkes, H.C., 1969. Surges of the Vernagtferner in the Otztal Alps since 1599. Canadian Journal of Earth Sciences, 6, 853–861. doi: 10.1139/e69-086

Hooker, B.L. and Fitzharris, B.B., 1999. The correlation between climatic parameters and the retreat and advance of Franz Josef Glacier, New Zealand. Global and Planetary Change, 22(1-4), 39–48. doi:10.1016/S0921-8181(99)00023-5

Huber, U., Bugmann, H. and Reasoner, M., 2005. Global Change and Mountain Regions. An overview of current knowledge. Advances in Global Change Research. Springer, Dordrecht.

Huggel, C., Haeberli, W., Kääb, A., Bieri, D. and Richardson, S., 2004. An assessment procedure for glacial hazards in the Swiss Alps. Canadian Geotechnical Journal, 41(6), 1068–1083. doi:10.1139/t04-053

Huggel, C., Kääb, A., Haeberli, W. and Krummenacher, B., 2003. Regional-scale GIS-models for assessment of hazards from glacier lake outbursts: evaluation and application in the Swiss Alps. Natural Hazards and Earth System Sciences, 3, 647–662.

Huggel, C., Kääb, A., Haeberli, W., Teysseire, P. and Paul, F., 2002. Remote sensing based assessment of hazards from glacier lake outbursts: a case study in the Swiss Alps. Canadian Geotechnical Journal, 39, 316–330. doi:10.1139/t01-099

IPCC, 2007. Climate Change 2007: The Physical Science Basis. Contribution of Working Group I to the Fourth Assessment Report of the Intergovernmental Panel on Climate Change [Solomon, S., Qin, D., Manning, M., Chen, Z., Marquis, M., Averyt, K.B., Tignor, M. and Miller, H.L., (eds.)]. Cambridge University Press, Cambridge.

Iturrizaga, L., 2005. New observations on present and prehistorical glacier-dammed lakes in the Shimshal valley (Karakoram Mountains). Journal of Asian Earth Sciences, 25(4), 545–555. doi:10.1016/j.jseaes.2004.04.011

Jarvis, A., Reuter, H.I., Nelson, A. and Guevara, E., 2008. Hole-filled seamless SRTM data V4. International Centre for Tropical Agriculture (CIAT), available from http://srtm.csi.cgiar.org.

Kaser, G., 1999. A review of the modern fluctuations of tropical glaciers. Global and Planetary Change, 22, 93–103. doi:10.1016/S0921-8181(99)00028-4

Kaser, G. and Grosshauser, M., 2010. The contribution potential of glaciers to Himalaya river runoff. Geophysical Research Abstracts, 12, EGU2010-10962.

Kassam, K.A., 2009. Viewing Change Through the Prism of Indigenous Human Ecology: Findings from the Afghan and Tajik Pamir. Human Ecology, 37, 677–690. doi:10.1007/s10745-009-9284-8

Keller, F., 1992. Automated mapping of mountain permafrost using the program PERMAKART within the geographical information system ARC/INFO. Permafrost and Periglacial Processes, 3, 133–138. doi: 10.1002/ppp.3430030210

Kneisel, C., Rothenbühler, C., Keller, F. and Haeberli, W., 2007. Hazard assessment of potential periglacial debris flows based on GIS-based spatial modelling and geophysical field surveys: a case study in the Swiss Alps. Permafrost and Periglacial Processes, 18, 259–268. doi:10.1002/ppp.593

Kotlyakov, V.M., 1980. Problems and results of studies of mountain glaciers in the Soviet Union. IAHS Publication, 126, 129–136.

Kotlyakov, V.M., Osipova, G.B. and Tsvetkov, D.G., 2008. Monitoring surging glaciers of the Pamirs, Central Asia, from space. Annals of Glaciology, 48, 125–134. doi:10.3189/172756408784700608

Krainer, K., 2007. Permafrost und Naturgefahren in Österreich. Online-Fachzeitschrift des Bundesministeriums für Land- und Forstwirtschaft, Umwelt und Wasserwirtschaft , 2007. www.laendlicher-raum.at/filemanager/download/19380/ [accessed on November 2, 2011]

Krummenacher, B., Affentranger, R., Kienholz, H., Eisenring, S. and Haeberli, W., 2003. Use of the solar compass to estimate the presence of permafrost. ICOP 2003 Permafrost: Proceedings of the Eighth International Conference on Permafrost, Zurich, Switzerland, 1, 611–615.

Kuhn, M., Dreiseitl, E., Hofinger, S., Markl, G., Span, N., and Kaser, G., 1999. Measurements and models of the mass balance of Hintereisferner. Geografiska Annaler, 81A, 659 – 670. doi:10.1111/j.0435-3676.1999.00094.x

Lambrecht, A. and Kuhn, M., 2007. Glacier changes in the Austrian Alps during the last three decades, derived from the new Austrian glacier inventory. Annals of Glaciology, 46(1), 177–184. doi:10.3189/172756407782871341

Lieb, G.K., 1998. High-mountain permafrost in the Austrian Alps. Proceedings of the 7th International Conference on Permafrost, Yellowknife, Canada, 663–668.

Marchenko, S.S., Gorbunov, A.P. and Romanovsky, V.E., 2007. Permafrost warming in the Tien Shan Mountains, Central Asia. Global and Planetary Change, 56, 311–327. doi:10.1016/j.gloplacha.2006.07.023

Mergili, M. and Schneider, J.F., 2011. Regional-scale analysis of lake outburst hazards in the southwestern Pamir, Tajikistan, based on remote sensing and GIS. Natural Hazards and Earth System Sciences 11, 1447–1462. doi:10.5194/nhess-11-1447-2011

Mergili, M., Schneider, D., Worni, R., and Schneider, J.F., 2011. Glacial Lake Outburst Floods (GLOFs): challenges in prediction and modelling. In: Genevois, R., Hamilton, D.L. and Prestininzi, A., (eds.), Proceedings of the 5th International Conference on Debris-Flow Hazards Mitigation: Mechanics, Prediction and Assessment, Padua, Italy, June 14–17, 2011. Italian Journal of Engineering Geology and Environment – Book, 973–982.

Middleton, R. and Thomas, H., 2008. Tajikistan and the High Pamirs. A Companion and Guide. Odyssey, Hong Kong.

Müllebner, B., 2010. Modelling of potential permafrost areas in the Pamir and Alai mountains (Tajikistan) using Remote Sensing and GIS techniques. Master thesis, BOKU University, Vienna.

Narama, C., Duishonakunov, M. , Kääb, A., Daiyrov M., and Abdrakhmatov, K., 2010. The 24 July 2008 outburst flood at the western Zyndan glacier lake and recent regional changes in glacier lakes of the Teskey Ala-Too range, Tien Shan, Kyrgyzstan. Natural Hazards and Earth System Sciences, 10, 647–659.

Nekrasov, I.A. and Klimovsky I.V., 1978. Permafrost of BAM zone. Nauka, Novosibirsk.

Nicolussi, K., 1990. Bilddokumente zur Geschichte des Vernagtferners im 17. Jahrhundert = Documentation of the history of Vernagtferner in the 17th century by paintings and drawings. Zeitschrift für Gletscherkunde und Glazialgeologie, 26(2), 97–119.

NSIDC, 1999–2009. World glacier inventory. World Glacier Monitoring Service and National Snow and Ice Data Center/World Data Center for Glaciology. Boulder, CO. Digital media.

Österreichischer Alpenverein, 1972–2010. Gletscherberichte. Sammelberichte über die Gletschermessungen des Österreichischen Alpenvereins in den Jahren 1971 bis 2009. Compiled

by H. Kinzl, G. Patzelt and A. Fischer. Mitteilungen des Österreichischen Alpenvereins/Bergauf, volumes 27–65.

Patzelt, G., 1980. The Austrian glacier inventory: status and first results. IAHS Publication, 126, 181–183.

Paul, F., Huggel, C. and Kääb, A., 2004. Combining satellite multispectral image data and a digital elevation model for mapping debris-covered glaciers. Remote Sensing of Environment, 89, 510–518. doi:10.1016/j.rse.2003.11.007

Richardson, S.D. and Reynolds, J.M., 2000. An overview of glacial hazards in the Himalayas. Quaternary International, 65/66, 31–47. doi:10.1016/S1040-6182(99)00035-X

Rolland, C., 2003. Spatial and Seasonal Variations of Air Temperature Lapse Rates in Alpine Regions. Journal of Climate, 16, 1032–1046. doi:10.1175/1520-0442(2003)016<1032:SASVOA>2.0.CO;2

Schöner, W., Auer, I. and Böhm, R., 2000. Climate variability and glacier reaction in the Austrian eastern Alps. Annals of Glaciology, 31, 31–38. doi:10.3189/172756400781819806

Tinti, S., Maramai, A. and Cerutti, A.V., 1999. The Miage Glacier in the Valley of Aosta (Western Alps, Italy) and the extraordinary detachment which occurred on August 9, 1996. Physics and Chemistry of the Earth (A), 24(2), 157–161. doi:10.1016/S1464-1895(99)00012-5

Tweed, F.S. and Russell, A.J., 1999. Controls on the formation and sudden drainage of glacier-impounded lakes: implications for jökulhlaup characteristics. Progress in Physical Geography, 23(1), 79–110. doi:10.1177/030913339902300104

Wang, D., Liu, J.,Hu, L. and Zhang, M., 2009. Monitoring and Analyzing the Glacier Lake Outburst Floods and Glacier Variation in the Upper Yarkant River, Karakoram. Journal of Glaciology and Geocryology, 2009-05. doi:CNKI:SUN:BCDT.0.2009-05-005.

Werder, M.A., Bauder, A., Funk, M. and Keusen, H.-R., 2010. Hazard assessment investigations in connection with the formation of a lake on the tongue of Unterer Grindelwaldgletscher, Bernese Alps, Switzerland. Natural Hazards and Earth System Sciences, 10, 227–237.

Appendix 5

Spatio-temporal development of high-mountain lakes in the headwaters of the Amu Darya River (Central Asia)

Research article in press

Mergili, M., Müller, J.P., Schneider, J.F. (2013): Spatio-temporal development of high-mountain lakes in the headwaters of the Amu Darya River (Central Asia). Global and Planetary Change, DOI: 10.1016/j.gloplacha.2013.04.001.

Original article:
http://www.sciencedirect.com/science/article/pii/S092181811300091X

Abstract

The sources of the Amu Darya, one of the major Central Asian rivers draining to the Aral Sea, are located in the glacierized high-mountain areas of Tajikistan, Kyrgyzstan and Afghanistan. There, climate change and the resulting retreat of glaciers have led to the formation of numerous new glacial lakes. Other lakes in the area are embedded in older glacial landscapes (erosion lakes) or retained by block or debris dams (e.g., Lake Sarez). A multi-temporal lake inventory is prepared and analysed, based on remotely sensed data. Corona images from 1968 are used as well as more up-to-date ASTER and Landsat 7 scenes. 1642 lakes are mapped in total, 652 out of them are glacial lakes. 73% of all lakes are located above 4000 m a.s.l. Glacial lakes, abundant in those areas where glacier tongues retreat over flat or moderately steep terrain, have experienced a significant growth, even though changes are often superimposed by short-term fluctuations. The analysis results also indicate a shifting of the growth of glacial lakes from the south western Pamir to the central and northern Pamir during the observation period. This trend is most likely associated with more elevated contribution areas in the central and northern Pamir. The lakes of the other types have remained constant in size in general. The lake development reflects changes in the state of the water resources in the study area on the one hand and determines the level of lake outburst hazards on the other hand.

Keywords

Central Asia, Glacial lakes, High-mountain environmental change, Pamir, Remote sensing

1 Introduction

The Amu Darya is one of the most important rivers in the lowlands of Central Asia. Its sources are located in the glacierized high-mountain areas of Tajikistan, Kyrgyzstan and Afghanistan (Pamir, Alai and Hindukush mountains). They include the upper catchments of the Surkhob River, the Khingob River and the Panj River (Fig. 1). The Surkhob and Khingob Rivers, after their confluence, continue as Vakhsh River, a tributary to the Panj River forming the Tajik–Afghan border. After the confluence of Panj and Vakhsh, the river continues as Amu Darya all the way to the Aral Sea. Controlling of the water flow of the Vakhsh River in Tajikistan for hydropower generation has led to political tensions with Uzbekistan and Turkmenistan where the water is extensively used for irrigation, and inappropriate water management practices have led to the shrinkage of the Aral Sea (e.g., Micklin, 1988; Micklin and Aladin, 2008). The runoff regime of the Amu Darya and other Central Asian river systems, and the contribution of glacial melt water, have been the subject of comprehensive research (e.g., Agaltseva et al., 1997; Aizen and Aizen, 1997; Aizen et al., 2007a). Particularly in the valleys of those arid mountain areas, melt water is highly important for the livelihood of the people (e.g., irrigation, hydropower generation), whilst its importance diminishes in humid areas and with increasing distance from the glaciers (Hagg and Braun, 2005; Kaser and Grosshauser, 2010).

High-mountain environments are highly dynamic and sensitive systems. Therefore they serve as early indicators for climate fluctuations, including snow, glaciers, permafrost, ecosystems and the water cycle (e.g., Beniston, 2003; Huber et al., 2005; Harris et al., 2009). There is overwhelming evidence for a worldwide accelerated retreat of glaciers over the last few decades (WGMS, 2008), involving the tropics (e.g., Kaser, 1999), arid and humid mid-latitudes (e.g., Aizen et al., 2007b; Lambrecht and Kuhn, 2007) and the polar regions (e.g., Cook et al., 2005). Much of this retreat has been attributed to the evident atmospheric temperature rise (IPCC, 2007). However, glacial retreat is not occurring at the same rates and with the same characteristics worldwide.

Locally, the dynamics of the glacial and periglacial environment disturb the equilibrium of the system and therefore lead to an increased level of hazard (Evans and Clague, 1994; Huggel et al., 2004a,b; Kääb et al., 2005; IPCC, 2007; Quincey et al., 2007; Harris et al., 2009; Dussaillant et al., 2010; Haeberli et al., 2010a). One particular aspect is the formation of glacial lakes, dammed by moraines or by the glaciers themselves. Such lakes often occur in areas influenced by permafrost. Tweed and Russell (1999) distinguished nine types of ice-dammed lakes. On the one hand, glacial lakes mirror the state of the glaciers as source of fresh water. On the other hand some lakes are prone to sudden outbursts (Glacial Lake Outburst Floods or GLOFs) and pose a potential threat to the downstream communities. Most studies published on glacial lakes are related to GLOF events or GLOF hazard. Studies cover most glacierized mountain areas in the world, e.g., in the Himalayas of Nepal and Bhutan (Watanabe and Rothacher, 1996; Richardson and Reynolds, 2000; Bajracharya et al. 2007; ICIMOD, 2011), the Karakorum (Hewitt, 1982; Hewitt and Liu, 2010), the Pamir (Mergili and Schneider, 2011), the Tien Shan (Narama et al., 2010; Bolch et al., 2011), the Andes (Vilímek et al., 2005; Harrison et al., 2006; Haeberli et al., 2010b), the North American mountains (Clarke, 1982), the Norwegian mountains (Breien et al., 2008) and the western Alps (Haeberli, 1983; Tinti et al., 1999; Huggel et al., 2002, 2003). The anticipation of possible glacial lake development is seen as a first important step of hazard assessment

(Frey et al., 2010). GLOFs can evolve in different ways, for example by rock/ice avalanches or ice fronts calving into lakes, rising lake levels leading to overflow, progressive incision, mechanical rupture or retrogressive erosion of a dam, hydrostatic failure or degradation of glacier dams or ice-cores in moraine dams (Walder and Costa, 1996; Richardson and Reynolds, 2000). Peak discharges are often some magnitudes higher than in the case of "normal" floods (Cenderelli and Wohl, 2001). Entrainment may considerably increase the event magnitude and convert the flood into a destructive debris flow.

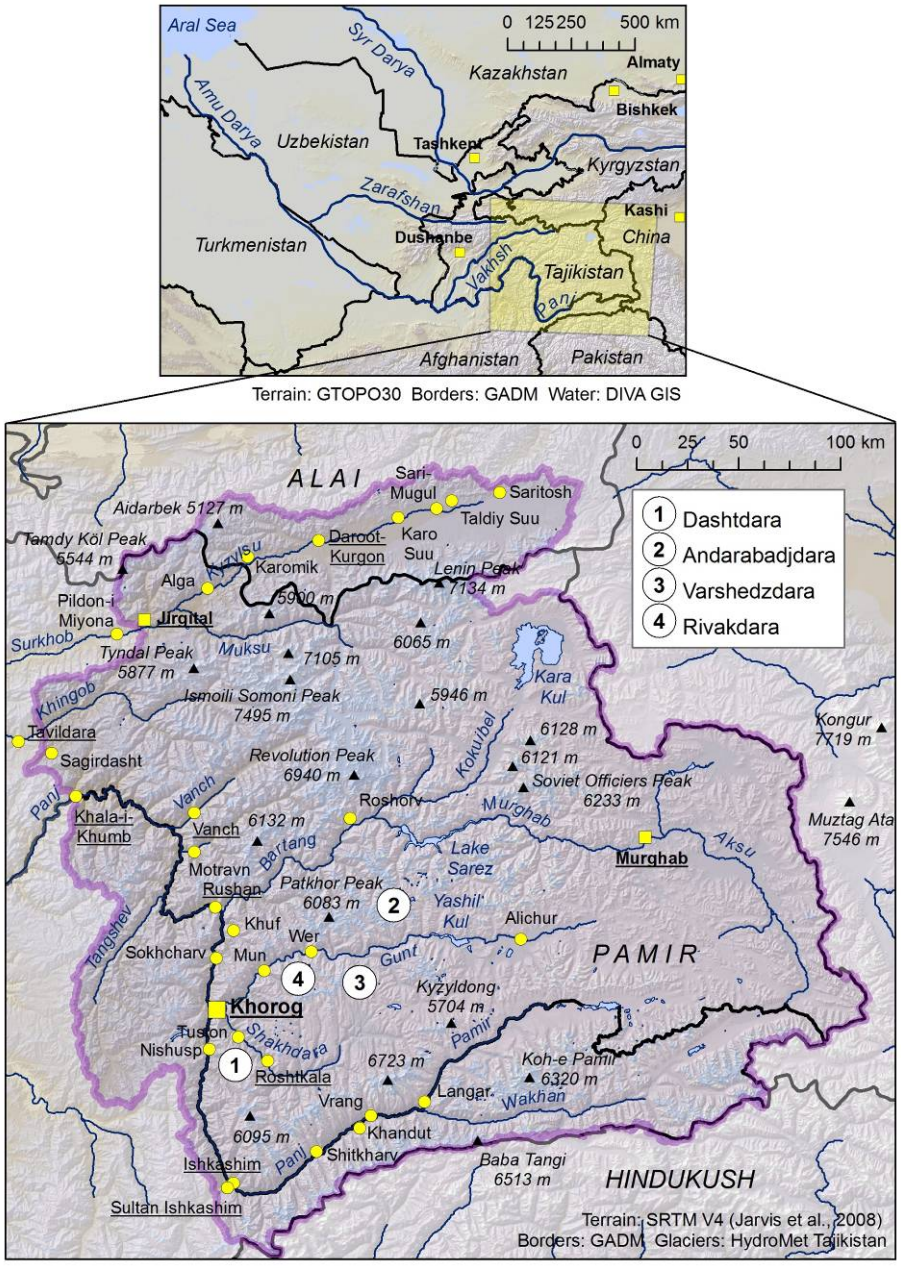

Fig. 1 Study area, including the headwaters of the Amu Darya in the Pamir, Alai and Hindukush (Tajikistan, Kyrgyzstan and Afghanistan).

Also other types of lakes are relevant from a hazard perspective (Evans, 1986; Costa and Schuster, 1988; Walder and O'Connor, 1997). Landslide dams are of particular interest as most of them fail within the first year after their formation (Costa and Schuster, 1988). In the seismically

active Central Asian mountains, recent and former landslide-dammed lakes are common. There is still controversy about the safety of Usoi Dam, the highest landslide dam worldwide, impounding Lake Sarez since its formation during a major earthquake in 1911 (e.g., Schuster and Alford, 2004; Risley et al., 2006). On the other hand, there are discussions on the use of Lake Sarez – and other lakes – for hydropower generation. In general, the use of high-mountain lakes for hydropower generation is a subject of increasing interest (Terrier et al., 2011).

The aspects outlined above highlight the importance of up-to-date-knowledge on high-mountain lakes. Whilst the level of information is considerable in some mountain areas of the world, the knowledge about the spatial distribution, and even more the temporal development, of high-mountain lakes in the Pamir is still limited.

The present article attempts to fill this gap by focusing on the analysis of the distribution and the temporal development of lakes in the headwaters of the Amu Darya catchment. For this purpose, a multi-temporal lake inventory is prepared and the spatial distribution of the lake characteristics is analysed as well as the patterns of lake development. It is attempted to link the findings to observed glacier dynamics. The results shall serve as a baseline for the assessment of lake outburst hazards and for studies on the potential of the lakes for hydropower generation.

Next, the study area is introduced (Chapter 2). Then, the methods applied to explore the spatial distribution and the temporal development of high-mountain lakes in the study area are outlined (Chapter 3). The presentation of the results (Chapter 4) is followed by a discussion (Chapter 5) and the conclusions (Chapter 6).

2 Study area

Here, a 98,300 km² study area is considered, extending from 1670 m a.s.l. near Khala-i-Khumb to 7495 m at the top of Ismoili Somoni Peak (see Fig. 1). The northern and southern limits of the study area are the Alai and Hindukush ranges in Kyrgyzstan and Afghanistan, respectively. They largely extend in east-west direction. In between, the Pamir in the Gorno-Badakhshan Autonomous Oblast of Tajikistan represents the largest share of the study area. The western Pamir is characterized by glacierized mountain ranges exceeding 6000 m a.s.l. and deeply incised, fairly densely populated valleys. The eastern Pamir represents an arid highland above 3500 m a.s.l. with glaciers covering only the highest peaks. The northern Pamir with the Academy of Sciences and Transalai ranges carries three peaks exceeding 7000 m a.s.l. and is extensively glacierized. The Fedchenko Glacier extends over a length of >75 km and covers a surface area >700 km². Many glacier tongues in the study area are covered by debris, making it hard to delineate their extent from satellite imagery or superficial field surveys. Even though a general retreat of the areas of exposed ice was identified for several mountain ranges within the study area (e.g., Khromova et al., 2006; Haritashya et al., 2009; Mergili et al, 2012), melting of ice within decaying debris-covered glacier tongues may contribute a significant share of the total loss of ice volume on the one hand and favours the development of lakes in the subsiding areas on the other hand.

The climate in the study area is temperate semi-arid to arid and continental with hot summers and cold winters. Most meteorological stations in the study area have recorded a positive trend of the mean annual air temperature (MAAT) for the period 1940–2000 (Makhmadaliev et al., 2008).

The increase of the MAAT did not exceed +1°C for any of the station. One station even displayed a negative trend. However, the most recent data available are from the valleys, which deviate considerably from the conditions in the high-mountain areas. The state of information suffers from a lack of up-to-date high-altitude meteorological data. The Fedchenko station does not provide reliable data since 1995. According to the 4th IPCC report (IPCC, 2007), the median of the projected increase of the MAAT from 1980–1999 to 2080–2099 for Tajikistan is 3.7 °C.

The changing temperature regime impacts the livelihood of the local communities in both a positive and a negative way (Kassam, 2009). Much of these impacts concern water resources related to the numerous glaciers and lakes in the headwaters of the valleys.

3 Materials and methods

3.1 Lake identification and classification

The study presented relies primarily on the analysis of medium-resolution satellite imagery. In order to obtain the most recent state of the lakes in the study area in a consistent way, ASTER images of 2009 are used as the primary source of information (raster cell size: 15 m). However, since it is not possible to cover the entire area with cloud- and snow-free scenes from one single year, let alone day, also ASTER images and pan-sharpened Landsat 7 scenes from 2007, 2008 and 2010 are used. Verification and the collection of additional information for each lake are supported by high-resolution Google Earth scenes.

Table 1 Lake types as distinguished in the mapping and analysis.

Lake type	Criterion
1 Erosion lake	Impounded by pronounced rock barriers or embedded in undulating landscapes most likely formed during the Pleistocene, at some distance from the recent glaciers, but often still above 4000 m a.s.l. The term erosion lake follows ICIMOD (2011).
2 Block or debris-dammed lake	Impounded by dams dominated by coarse blocks, debris, or a combination of both, most commonly representing Pleistocene terminal moraines, landslide deposits, or talus or debris cones.
3 Glacial lake	Either directly embedded in the exposed ice or retained by debris-covered glacier tongues, rock glaciers, or fresh moraines.

The manual delineation of the boundaries of each single lake in the study area is preferred to an automatic procedure. Even though automatic lake identification procedures from optical or radar satellite imagery are well introduced (e.g., Huggel et al., 2002; Kääb et al., 2005; Strozzi et al., 2012) it turned out that, in this specific case, the amount of manual post- processing required would most likely more than offset the advantages of an automated lake detection.

Three lake types are distinguished. The classification scheme chosen is kept as simple as possible, constrained to criteria identifiable from the remotely sensed data used (Table 1 and Fig. 2). The approach can be considered reproducible as the visual image interpretation is based on clear,

largely objective criteria. A more detailed lake classification could only be done at the cost of higher uncertainties and poor reproducibility. Particularly in the case of glacial lakes (Type 3), no further distinction into pro-glacial, supra-glacial etc. (e.g., Tweed and Russell, 1999; ICIMOD, 2011) lakes is applied. The transition between the various types of glacial lakes is rather gradual than sharp and their identification requires at least high-resolution imagery (Kääb et al., 2005) or even geophysical methods not applicable at the regional scale.

The elevation a.s.l. of each lake is extracted from the SRTM V4 digital elevation model (Jarvis et al., 2008; approx. 90 m raster cell size) using the location of the lake centroid as reference. The lake area A (m²) is computed from the mapped polygons. All lakes with $A < 2500$ m² are disregarded.

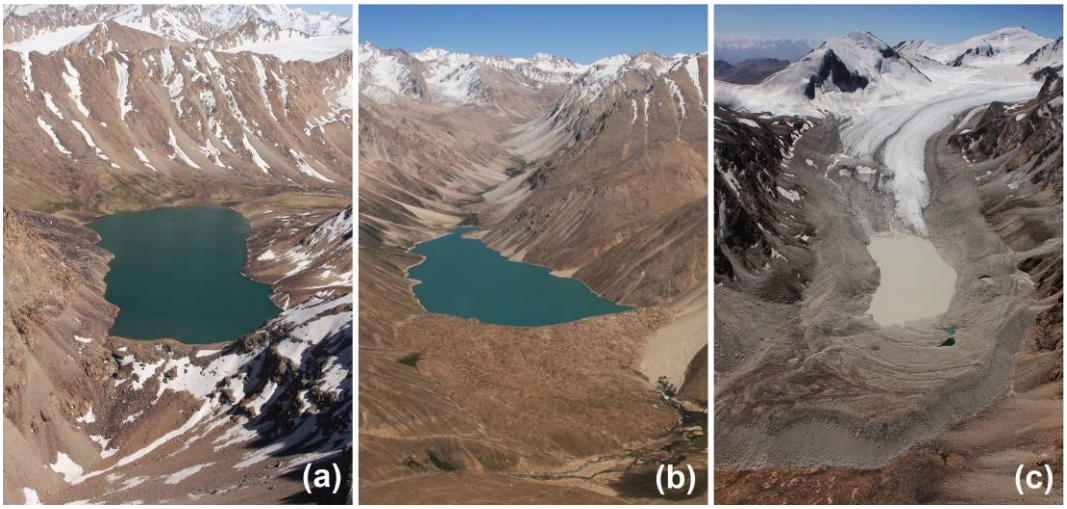

Fig. 2 Examples for lakes of the various types – a Erosion lake (Type 1) b Lake impounded by block or debris dam (Type 2) c Glacial lake (Type 3).

3.2 Lake area development

The lake evolution or lake area development is expressed as the change of lake surface area during the observation period both in absolute and relative terms,

$$D_A = A_2 - A_1,\ r_A = \frac{A_2}{A_1}, \qquad (1)$$

where D_A is the absolute lake area development (m²), r_A is the relative lake area development (ratio) and A_1 and A_2 are the lake areas (m²) at the beginning and at the end of the observation period. In addition to the entire period from 1968 – 2009, two sub-periods are considered: Period 1 from 1968 – 2002 and Period 2 from 2002 – 2009. Scanned and georectified declassified Corona images (raster cell size <5 m) are used for 1968, ASTER and pan-sharpened Landsat 7 images for 2001 and – as already explained above – for 2009. Since appropriate ASTER and Landsat scenes are not available for the entire area from one single year, scenes are also taken from up to two years earlier or later. Only lakes with a surface area $A \geq 2500$ m² in 2009 are considered in the analysis.

The accuracy of lake polygons mapped from medium-resolution satellite imagery suffers from uncertainties related to the subjectivity of polygon construction and to the geometric distortion

of the imagery, which cannot always be completely removed with reasonable effort. Since lakes are always flat, the problem of distortion is supposed to be less significant than for mapping efforts on inclined slopes. However, the distortion uncertainty u_c still exists and is tested using Landsat scenes as reference. u_c quantifies the absolute value of the relative difference between the lake area mapped from the Landsat scene and the lake area mapped from the ASTER or Corona scene. For Corona scenes, $u_c \leq 14\%$ with 75% confidence, $u_c \leq 20\%$ with 90% confidence and $u_c \leq 27\%$ with 95% confidence. For the ASTER scenes, the uncertainty of the mapped area $u_c \leq 4\%$ with 75% confidence, $u_c \leq 6\%$ with 90% confidence and $u_c \leq 13\%$ with 95% confidence. Also the effects of mapping uncertainty are supposed to be significant at the image resolution used and are therefore analysed. Empirical tests show that the manual definition of lake boundaries on ASTER images, based on subjective interpretation, is subject to a mapping uncertainty in the order of one raster cell (i.e., 15 m). Corona scenes have a higher resolution, but are only available as greyscale images, making mapping more difficult and uncertain. The mapping uncertainty is set to $u_m = 5$ m for Corona imagery. The degree of the effects of distortions and uncertain polygon boundaries on the derived lake area depends on the lake area itself. Assuming a circular lake,

$$A_{\max} = (1+u_c)\cdot\left(\sqrt{\frac{A_m}{\pi}}+u_m\right)^2\pi,\ A_{\min} = (1-u_c)\cdot\left(\sqrt{\frac{A_m}{\pi}}-u_m\right)^2\pi, \quad (2)$$

where A_{max} and A_{min} are the maximum and minimum possible lake areas (m²), A_m is the mapped lake area (m²) and u_m is the mapping uncertainty (m). Growing and shrinking lakes are therefore defined as

$$D_{A,g} = A_{2,\min} - A_{1,\max},\ D_{A,g} > 0,\ r_{A,g} = \frac{A_{2,\min}}{A_{1,\max}},\ r_{A,g} > 1, \quad (3)$$

$$D_{A,s} = A_{2,\max} - A_{1,\min},\ D_{A,s} < 0,\ r_{A,s} = \frac{A_{2,\max}}{A_{1,\min}},\ r_{A,s} < 1, \quad (4)$$

where the subscripts s and g stand for shrinkage and growth. This procedure gives a minimum number of growing and shrinking lakes, only considering those where the trend of evolution can be determined with a certain degree of confidence. The real number of growing or shrinking lakes and the absolute values of D_A and r_A may be higher.

4 Results

4.1 Spatial distribution of lakes

1642 lakes are identified in the study area: 885 erosion lakes (Type 1 in Table 1; see Fig. 2), 105 lakes impounded by block or debris dams (Type 2) and 652 glacial lakes (Type 3). Table 2 summarizes some statistical key features of the lakes of the various types.

The distribution of lakes of different types and size classes is shown in Fig. 3. The southern Pamir is a hot spot for erosion lakes, whilst the glacial lakes obviously group together very close to glacierized areas (Fig. 4). However, whilst the density of glacial lakes is comparatively high in

the ranges of the south western Pamir and also in the extensively glacierized central Pamir, almost no glacial lakes exist in some parts of the western Pamir. These patterns are a consequence of the topographic characteristics of the various mountain ranges as illustrated by Fig. 5: the ROC (Receiver Operating Characteristic) curves indicate the degree to which the distribution of a binary target variable (in this case, raster cells with a density of glacial lakes ≥20 are set to 1, all other raster cells are set to 0) is explained by a predictor variable (density of glaciers and density of areas with moderate topography, respectively). The true positive rate (fraction of true positive predictions out of all positive observations) is plotted against the false positive rate (fraction of false positive predictions out of the negative observations) at certain threshold levels, i.e., a straight diagonal line would represent a random distribution. Here, all raster cells with a slope <10° are considered as areas with moderate topography, the density of such areas as well as of glaciers is computed with a search radius of 10 km, analogous to the lake density. Not surprisingly, there is a strong positive correlation between glacial lake density and glaciers (area under curve AUC = 0.833, 0.5 would represent a random distribution). Using the product of glacier density and the density of areas with moderate topography, the AUC rises only slightly to 0.852, illustrating the dominance of glacier density as a predictor (see Fig. 5a). When removing all areas with a distance >10 km to the next glacier from the analysis, the clear preference of the occurrence of glacial lakes in areas with moderate topography becomes more obvious (AUC = 0.659; see Fig. 5b).

Table 2 Lake statistics, organized by lake type. n = number of lakes, A_{med} and A_{max} = median and maximum lake area, z_{med}, z_{max} and z_{min} = median, maximum and minimum elevation a.s.l.

Lake type	n	A_{med} (km²)	A_{max} (km²)	z_{med} (m)	z_{max} (m)	z_{min} (m)
1 Erosion lake	885	0.015	404.55	4294	5131	1716
2 Block or debris dam	105	0.018	88.51	4265	4956	2314
3 Glacial lake	652	0.007	1.89	4505	5109	3057
Total	1642	0.010	404.55	4395	5131	1716

Fig. 6 plots the distribution of the dam types and the lake areas vs. elevation. Only 26.7% of all lakes, but 80.6% of the lake area are below 4000 m a.s.l. Out of the total lake area of 727 km², the Kara Kul – located at approx. 3900 m a.s.l. – accounts for 405 km² or 55.7%. Also most of the other large lakes in the area occupy areas between 3000 and 4000 m a.s.l., many of them are retained by block dams at the bottom of large valleys (Type 2; e.g., Lake Sarez and Yashil Kul). Above the steep valley flanks Pleistocene glaciers have shaped undulating plains. This environment favours the occurrence of Type 1 lakes (Fig. 7). Above 4500 m a.s.l., in the zone of recent glaciers and fresh moraines, lakes of Type 3 become more abundant. The highest lakes are identified above 5100 m a.s.l. Most of the lakes below 4000 m a.s.l. are in the northern part of the study area whilst less than 10% of all lakes in the south western Pamir are located below this threshold.

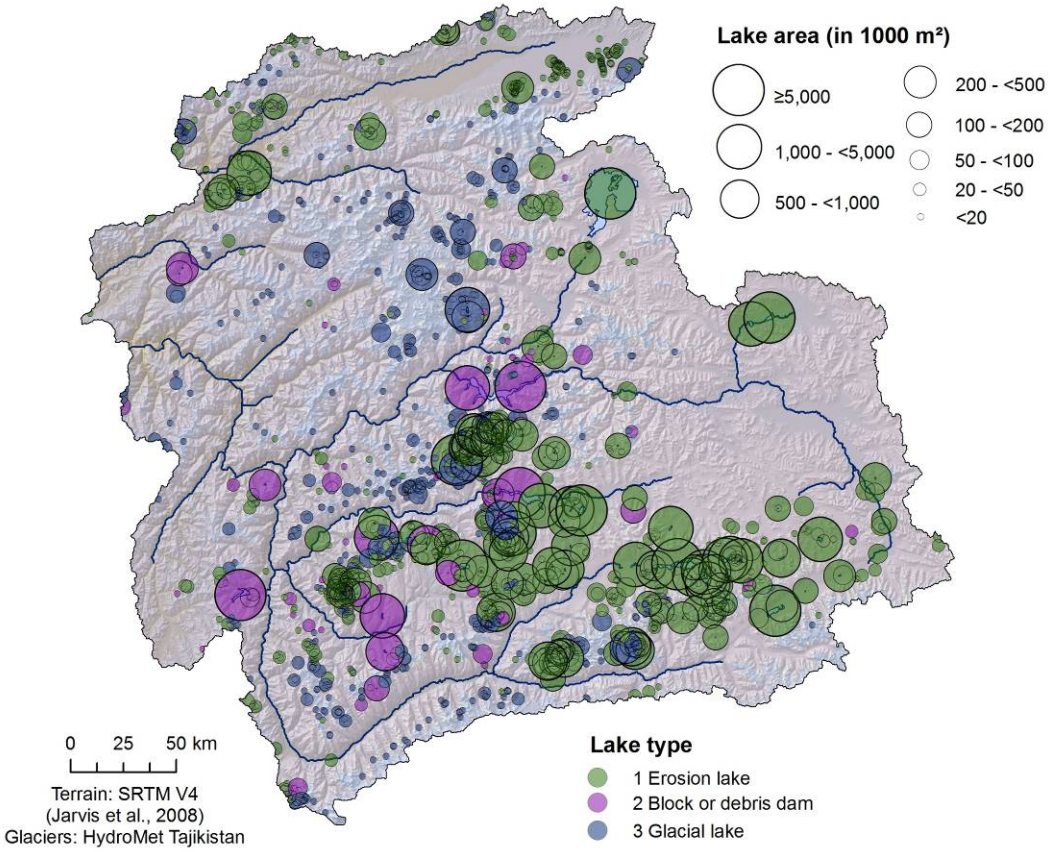

Fig. 3 Distribution of lakes in the study area according to types and size classes.

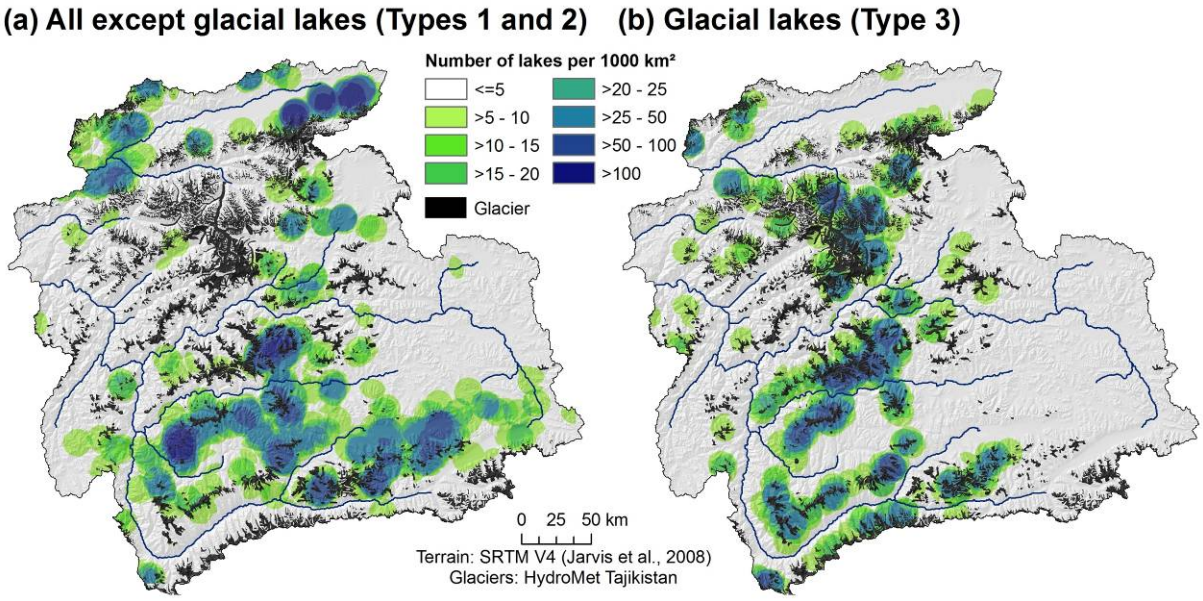

Fig. 4 Density of a all except glacial lakes and b glacial lakes, circle radius = 10 km.

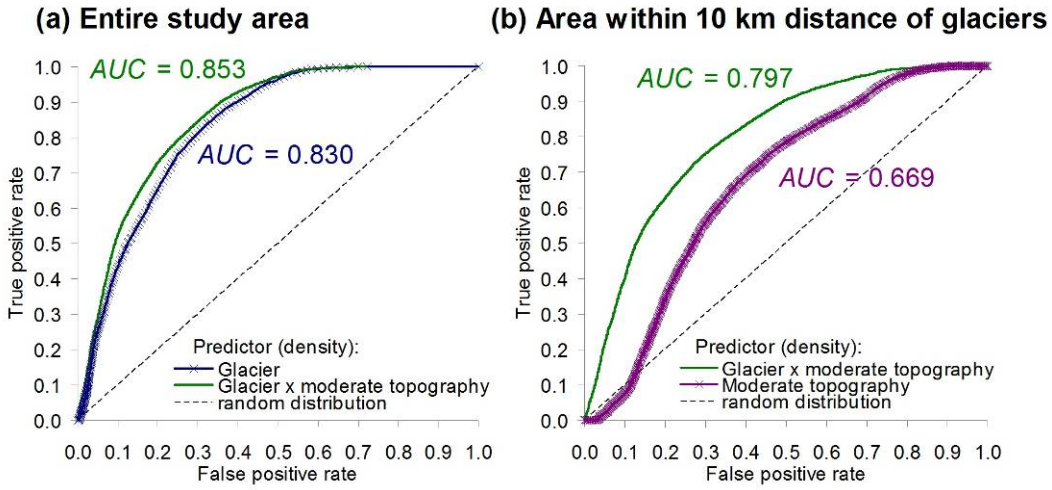

Fig. 5 ROC plots of the prediction rate of the location of the glacial lakes depending on the location of the glaciers and areas with moderate topography – densities within a radius of 10 km are used for all variables (see Fig. 4) a for the entire study area b constrained to areas within a 10 km distance from the next glacier – *AUC* = area under curve.

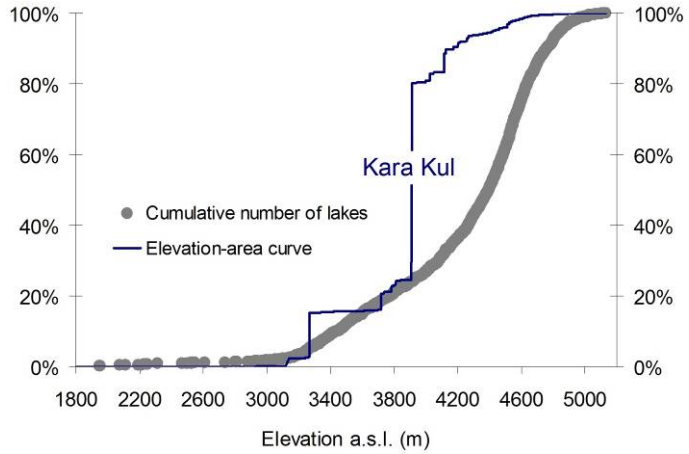

Fig. 6 Cumulative hypsographic curves of lake number and area.

The high elevation of many lakes leads to the assumption of a certain influence of permafrost, possibly affecting the stability of the dams themselves as well as the stability of adjacent slopes and rock walls (Haeberli et al., 2010a). No detailed and up-to-date permafrost investigations are available for the study area, but national or even global datasets of the potential permafrost distribution become increasingly available (e.g., Gruber, 2012). Here, a map of the potential present and future distribution of discontinuous and sporadic permafrost in Tajikistan (Mergili et al., 2012) is used. It was derived by adapting the scheme developed by Haeberli (1975) for Switzerland to the conditions in Tajikistan. Four scenarios of atmospheric temperature increase were assumed, using the IPCC scenarios until the year 2100 (IPCC, 2007) as reference.

Table 3 illustrates that 95.6% of all glacial lakes are located in areas with at least sporadic permafrost, and more than 92.2% are found in areas with discontinuous permafrost. Since the lakes of the other types are, in average, found at a lower elevation, 90.6% of all lakes are located in areas with at least sporadic permafrost, whilst 81.5% are found in areas with discontinuous permafrost.

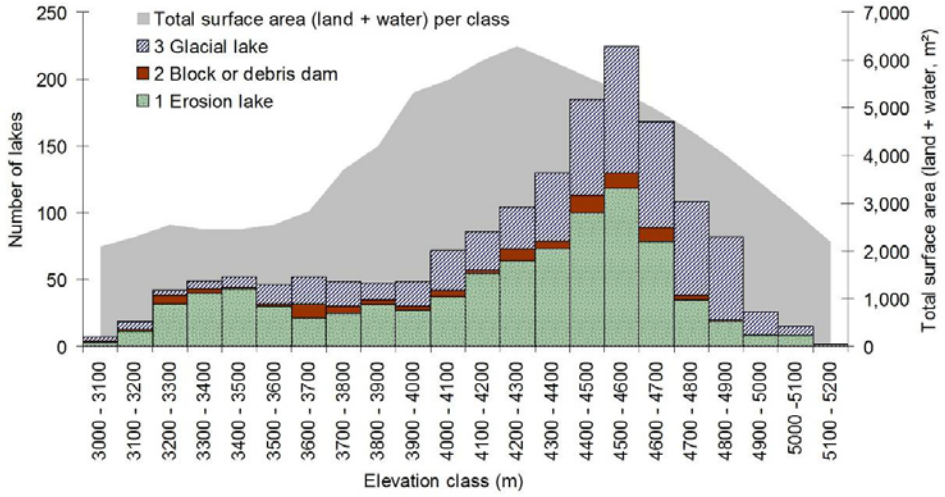

Fig. 7 Distribution of lakes of the various types according to the elevation – only those lakes above 3000 m a.s.l. are shown, the total surface area for each elevation class (land + water) is shown as reference.

Table 3 Number and percentage of lakes located in areas with a potential for discontinuous and sporadic permafrost for various assumptions of increasing air temperature.

Lake type	*n*	+0°C	+1°C	+2°C	+3°C	+4°C
Discontinuous permafrost						
1 Erosion lake	885	660 (74.6%)	604 (68.2%)	541 (61.1%)	476 (53.8%)	382 (43.2%)
2 Block or debris dam	105	77 (73.3%)	67 (63.8%)	60 (57.1%)	52 (49.5%)	43 (41.0%)
3 Glacial lake	652	601 (92.2%)	575 (88.2%)	538 (82.5%)	494 (75.8%)	433 (66.4%)
Total	1642	1338 (81.5%)	1246 (75.9%)	1139 (69.4%)	1022 (62.2%)	858 (52.3%)
Sporadic permafrost						
1 Erosion lake	885	779 (88.0%)	730 (82.5%)	641 (72.4%)	571 (64.5%)	514 (58.1%)
2 Block or debris dam	105	86 (81.9%)	81 (77.1%)	72 (68.6%)	66 (62.9%)	58 (55.2%)
3 Glacial lake	652	623 (95.6%)	612 (93.9%)	595 (91.3%)	557 (85.4%)	520 (79.8%)
Total	1642	1488 (90.6%)	1423 (86.7%)	1308 (79.7%)	1194 (72.7%)	1092 (66.5%)

Increasing atmospheric temperatures, leading to permafrost retreat, could substantially change this situation and therefore alter the stability of the dams (see Table 3). With +4°C, 79.8% of all glacial lakes would be found in areas of at least sporadic permafrost and only 66.4% would be located in discontinuous permafrost areas. For all lakes, the percentages would assume 66.5% and 52.3%, respectively.

4.2 Lake evolution 1968–2009

The minimum number and percentage of growing and shrinking lakes are summarized in Table 4, with the results yielded with the 90% confidence taken as reference and the results yielded with the 75% and 95% confidence values given in brackets. Fig. 8 illustrates the absolute and relative patterns of lake evolution.

A highly significant growth of glacial lakes in the observation period can be confirmed, whilst lakes of the other types do not display such clear signals and have obviously remained largely constant in size in average. The tendency of glacial lakes to grow is much more pronounced in relative than in absolute terms since the lakes are in average smaller than those of the other types (see Table 2). 40.8% of all glacial lakes in the study area are confirmed as growing during the observation period with a 90% confidence. In contrast, a shrinking trend can be confirmed for very few glacial lakes only (see Table 4).

Out of the 266 growing glacial lakes, 214 (80.5%) were smaller than 2,500 m² in 1968 or did not exist at all. It has to be considered that lakes <2,500 m² are not regarded in the 2009 dataset, resulting in the neglect of disappearing lakes. Even so, a clear trend of growth can be confirmed since the remaining number of 52 lakes clearly exceeds the number of 12 shrinking lakes.

Erosion lakes show moderate trends in both directions. Only 6.6% of the lakes of Type 1 are confirmed as growing, 4.6% as shrinking. Given the confidence of 90%, at least part of these changes may be interpreted as noise. Furthermore, short-term fluctuations of the lake level are most likely involved. Also the magnitude of growth of these lakes is much smaller than that of glacial lakes, both in absolute and in relative terms (see Fig. 8). The trends observed for lakes impounded by block or debris dams (Type 2; 5.7% growing, 2.9% shrinking with 90% confidence) are not considered significant due to the small number of lakes of this type in general.

A significant growth over both of the observation periods 1 and 2 (continuity) can be confirmed for very few lakes only (see Table 4 and Fig. 8b and f). Most of them are glacial lakes (12 out of 13). This initially surprising finding may be related to less significant trends being covered by the mapping uncertainty (the confidence interval is relatively broad) and to short-term fluctuations blurring the long-term trends. However, it also reflects the dynamics of high-mountain geosystems, where changes on various time scales are superimposed. Some glacial lakes appear and grow within a short time window (sometimes less than one year), whilst others grow ±continuously over years and decades.

One of the most striking examples of a rapidly developing lake is located in the headwaters of the Dashtdara Valley (see Fig. 1; referred to as Lake Dasht). Lake Dasht developed probably in spring or early summer 2001 on the tongue of a debris-covered glacier. None of the older satellite

images indicated the existence of a lake in that place. The lake only slightly increased in area until it drained suddenly on August 7, 2002 (Fig. 9). The resulting GLOF caused major damage and dozens of fatalities in the village of Dasht 11 km downstream (Mergili and Schneider, 2011; Mergili et al., 2012). Only a small pond remained in the former lake bed which did not fill up again. Since the drainage occurred beneath the glacier surface, the most likely interpretation of the observations is that a drainage channel within the glacier was suddenly blocked at the end of 2000 or in the beginning of 2001, allowing the development of the lake. With increasing lake size and therefore pressure, the blockage failed and the lake drained suddenly.

Table 4 Confirmed (90% confidence) number of growing and shrinking lakes in absolute terms and as percentage of the total number of lakes of each type – the numbers in brackets represent the results yielded with 95% and 75% confidence (see text for details).

Lake type	Growing lakes	Percentage of growing lakes	Shrinking lakes	Percentage of shrinking lakes
Entire period				
1 Erosion lake	58 (55-64)	6.6 (6.2-7.2%)	41 (22-54)	4.6 (2.5-6.1%)
2 Block/debris dam	6 (5-6)	5.7 (4.8-5.7%)	3 (3-5)	2.9 (2.9-4.8%)
3 Glacial lake	266 (251-278)	40.8 (38.5-42.6%)	12 (6-16)	1.8 (0.9-2.5%)
Total	330 (311-348)	20.1 (18.9-21.2%)	56 (31-75)	3.4 (1.9-4.6%)
Entire period (continuity)				
1 Erosion lake	1 (1-2)	0.1 (0.1-0.2%)	0 (0-0)	0.0 (0.0-0.0%)
2 Block/debris dam	0 (0-0)	0.0 (0.0-0.0%)	0 (0-0)	0.0 (0.0-0.0%)
3 Glacial lake	12 (7-16)	1.8 (1.1-2.5%)	1 (0-1)	0.2 (0.0-0.2%)
Total	13 (8-18)	0.8 (0.5-1.1%)	1 (0-1)	0.1 (0.0-0.1%)
Period 1				
1 Erosion lake	46 (42-50)	5.2 (4.7-5.6%)	58 (39-79)	6.6 (4.4-8.9%)
2 Block/debris dam	6 (5-7)	5.7 (4.8-6.7%)	6 (0-6)	5.7 (0.0-5.7%)
3 Glacial lake	185 (178-188)	28.4 (27.3-28.8%)	34 (26-41)	5.2 (4-6.3.0%)
Total	237 (225-245)	14.4 (13.7-14.9%)	98 (65-126)	6.0 (4-7.7.0%)
Period 2				
1 Erosion lake	23 (19-27)	2.6 (2.1-3.1%)	4 (3-5)	0.5 (0.3-0.6%)
2 Block/debris dam	2 (0-3)	1.9 (0.0-2.9%)	0 (0-0)	0.0 (0.0-0.0%)
3 Glacial lake	86 (78-91)	13.2 (12.0-14.0%)	12 (9-13)	1.8 (1.4-2.0%)
Total	111 (97-121)	6.8 (5.9-7.4%)	16 (12-18)	1.0 (0.7-1.1%)

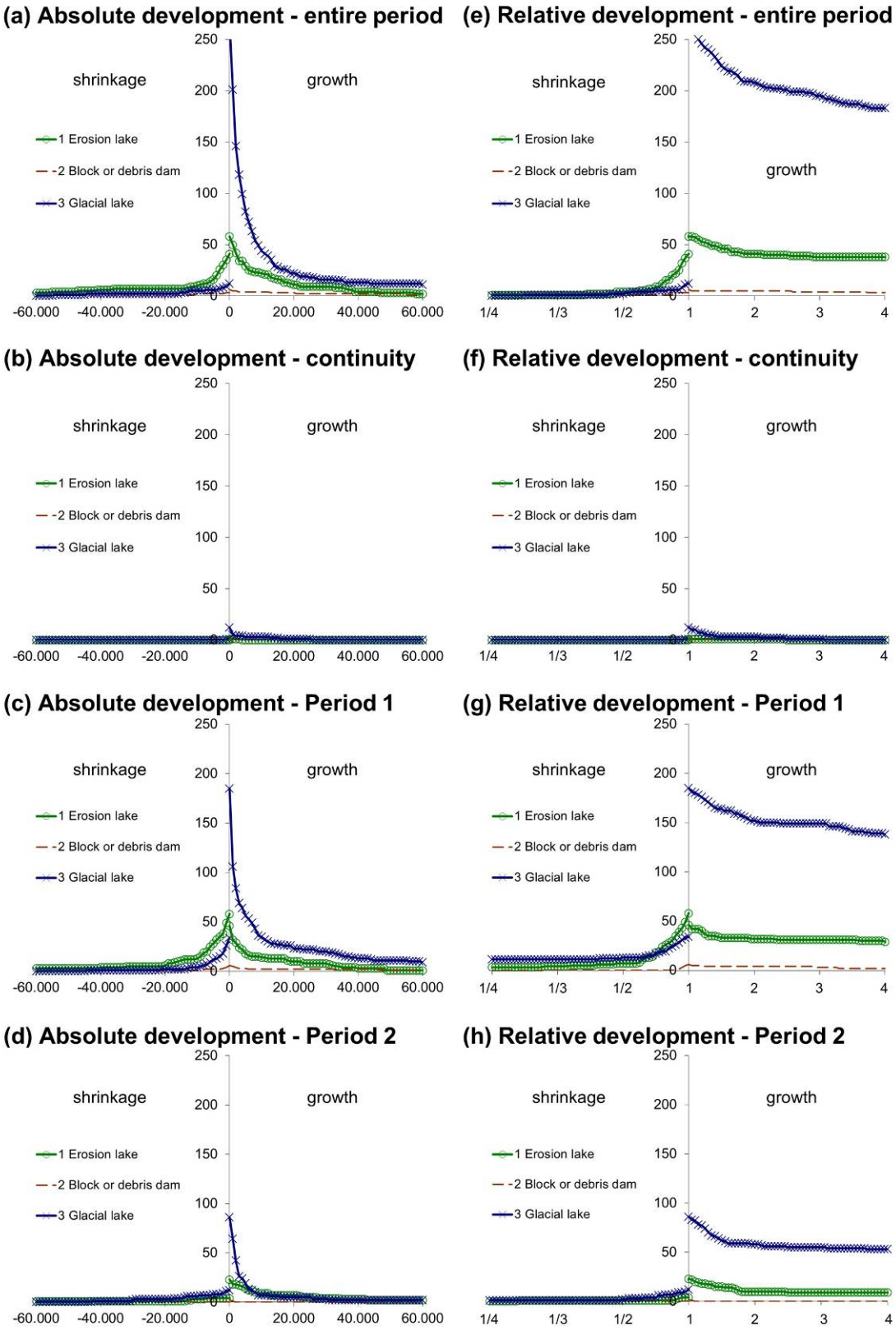

Fig. 8 Lake evolution for the entire investigation period as well as for the periods 1 and 2 a–d in absolute terms (x axis: m² growth or shrinkage; y axis: number of lakes beyond the x value) and e–f in relative terms (x axis: factor of growth or shrinkage), b and f (continuity) include all lakes displaying the same tendency (either growth or shrinkage) in both periods.

Lake Dasht is not included in the analysis presented here as it did not exist in 2009. However, in general it is likely that very few lakes have disappeared during the observation period. The Dasht event was the only major GLOF recorded, and the disappearance of lakes due to sedimentation usually extends over longer periods.

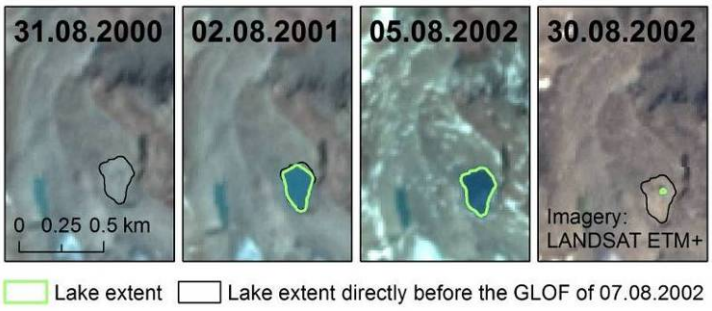

Fig. 9 Temporal development and sudden drainage of Lake Dasht.

One of the dominant lake evolution processes in the study area is the ±continuous growth of lakes in the forefield of retreating glaciers. Two unnamed lakes in the headwaters of the Andarabadjdara Valley (see Fig. 1; referred to as Lake Andarabadj) and the Varshedzdara Valley (see Fig. 1; referred to as Lake Varshedz) are among the largest glacial lakes of this type in the study area. Both drain to the Gunt Valley (see Fig. 1) and were much smaller in summer 1968 than in 2008 and 2007, respectively (Fig. 10). Table 5 quantifies the absolute and relative evolution of the size of the two lakes. Whilst there is no indication for a stabilization of the size of Lake Andarabadj, it seems that the growth rate of Lake Varshedz has reached its maximum earlier and slowed down considerably at least since the beginning of the 21st century. This is confirmed by helicopter surveys in 2009 and 2011, indicating a stable lake size comparable to that of 2007. The glacial lakes in the Rivakdara Valley (see Fig. 1), another tributary of the Gunt valley, show a similar behaviour as shown for Lake Varshedz.

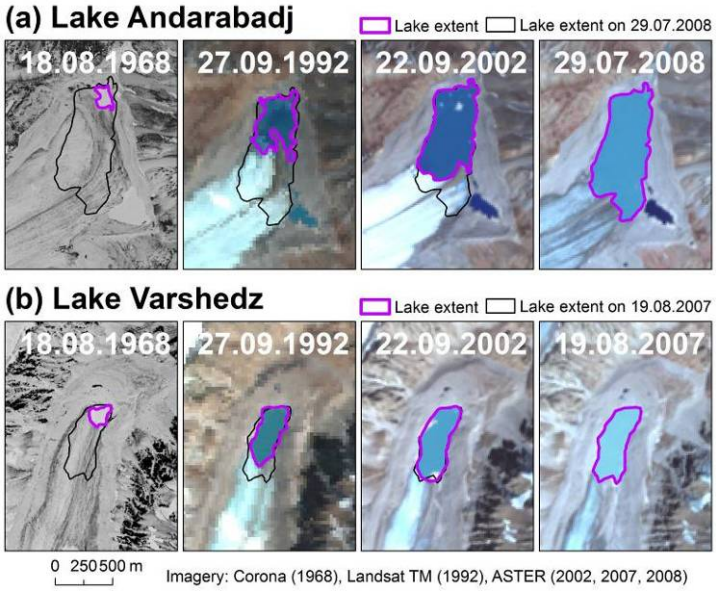

Fig. 10 a Lake Andarabadj and b Lake Varshedz – both lakes have shown a continuous increase in surface since 1968.

Table 5 Development of the surface areas of Lake Andarabadj and Lake Varshedz in absolute and relative terms, the percentages relate to the lake area in 2008 (Lake Andarabadj) and 2007 (Lake Varshedz), respectively.

	1968	1992	2002	2007/2008
Lake Andarabadj	20,636 m²	136,492 m²	296,477 m²	407,872 m²
	5.1%	33.5%	72.7%	100.0%
Lake Varshedz	23,327 m²	98,869 m²	147,048 m²	152,413 m²
	15.3%	64.9%	96.5%	100.0%

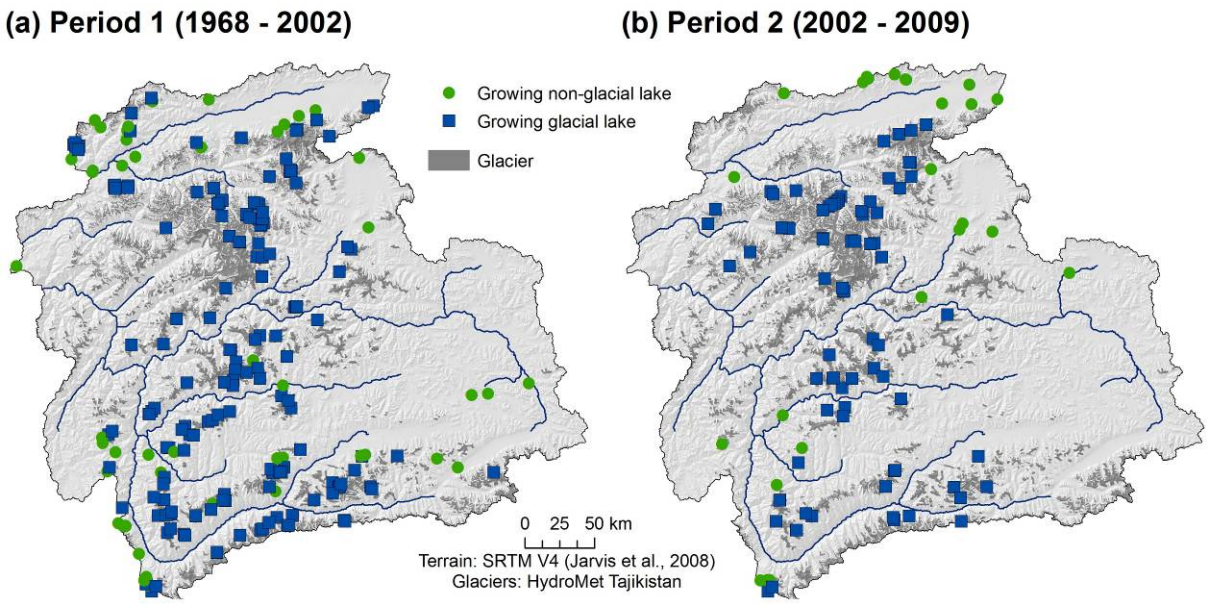

Fig. 11 Location of non-glacial lakes (Types 1 and 2) and glacial lakes (Type 3) growing a in Period 1 and b in Period 2.

Despite the low number of lakes with confirmed growth in both of the periods, the trends shown for Lake Varshedz and Lake Andarabadj reflect the situation in the study area: in average, glacial lakes have increased in size in both observation periods, a trend that is confirmed for 28.4% of them in Period 1 and for 13.2% in Period 2 (see Table 4). The more prominent trend in Period 1 can partly be explained by the longer duration. On the other hand it confirms the general deceleration of lake development in the south western Pamir – with many glacial lakes, including Lake Varshedz and the lakes in the upper Rivakdara mentioned above – during the first decade of the 21st century. Fig. 11 shows a comparison of growing non-glacial and glacial lakes for the two investigation periods. In Period 1, an increase in size is confirmed for 60 (22.0%) out of the 273 glacial lakes in the south western Pamir, whilst this number has decreased to 25 (9.2%) in Period 2. In the central and northern Pamir, 52 (34.0%) out of 153 glacial lakes are confirmed growing in Period 1, 45 (29.4%) in Period 2. Whilst the decrease of the rate of growing glacial lakes in the south western Pamir is in line with the trend observed for the entire study area, the minor negative trend in the central and northern Pamir is most likely a consequence of the shorter observation period only. The higher ratio of growing glacial lakes in the central and

northern Pamir in general reflects the more dynamic high-mountain environment there. 47.1% of all lakes observed in 2009 did not exist in 1968 (south western Pamir: 10.3%).

Since the peaks in the central and northern Pamir are in general higher than those in the south western Pamir, the northward shift of glacial lake growth is reflected in – or is a consequence of – the elevation patterns. Among those glacial lakes with a vertical extent of their catchment >200 m, lakes growing in Period 2 are in average found at a lower elevation (4225 m a.s.l.) than those growing during Period 1 (4470 m a.s.l.). In contrast, the catchments of the lakes growing in Period 2 peak higher up (average maximum elevation for Period 1: 5196 m; for Period 2: 5433 m). With more elevated accumulation areas of the glaciers and therefore larger ice reservoirs, the termini of the tongues – and consequently also most of the glacial lakes – are found at a lower elevation, compared to those glaciers with a more limited accumulation area.

The number of growing lakes of the remaining types is too small to allow for the derivation of robust spatial trends. In contrast to the glacial lakes, several erosion lakes were slightly shrinking in Period 1, a trend that was not observed in Period 2 (see Table 4 and Fig. 8). This phenomenon is interesting insofar as it counters the trend of the glacial lakes, displaying a more pronounced growth in Period 1 than in Period 2. It is most likely a consequence of intra- or short-term inter-annual variations of the lake level as well as of the neglect of lakes <2,500 m² in the 2009 dataset.

5 Discussion

The study illustrates the existence and characteristics of high-mountain lakes in the headwaters of the Amu Darya River, Central Asia. The evolution of each lake in the period 1968 – 2009 is quantified. Despite the uncertainties connected to the multi-temporal mapping from medium-resolution satellite imagery and to short-term fluctuations of the lake level, it can be confirmed that glacial lakes are the most dynamic type, with a strong trend of growth. Even though the existence of a relationship between glacier retreat and the formation or growth of glacial lakes seems obvious (see Fig. 10), the quantification of this relationship is hampered by the complexity of the issue as well as by the relative scarcity of detailed information on the recent glacier development in the study area. Numerous measurements were discontinued in the early 1990 as a consequence of the political and economic transformations in Central Asia (IAHS/UNEP/UNESCO, 1998). Compared to the Tien Shan (e.g., Khromova et al., 2003; Aizen et al., 2006, 2007b; Surazakov and Aizen, 2006), less detailed recent data are available for the Pamir. Haritashya et al. (2009) analysed the development of 30 glacier tongues in the Wakhan Pamir (Afghanistan) in the period 1976 – 2003, 28 of which were retreating (maximum rate: 36 m per year). They highlighted the relationship of this retreat to the formation of a number of glacial lakes. Khromova et al. (2006), for the eastern Pamir, found a decrease of the glacier area by 11.6% (corresponding to 1.05% per year) for the period 1990–2001, compared to a 7.8% decrease (0.65% per year) for the period 1978–1990. Mergili et al. (2012) investigated a set of 118 glaciers in the south western Pamir which, in the period 2002–2007, decreased in area by 1.15% per year in average (1969–2002: 0.48%). The quantification of the retreat of debris-covered glaciers requires detailed investigations at the local scale. Furthermore, the evolution of lakes as documented in Fig. 8 and Table 4 and shown in Fig. 10 is not only related to changes of glacier length or area, but also to the subsidence of the glacier surface and the specific topographic

conditions. Clusters of glacial lakes can only develop on comparatively flat terrain at the elevation of the retreating glacier tongues. An extremely simple but efficient way of a first-order assessment is to define all areas with a low surface slope. Frey et al. (2010) used an upper threshold of 5°, a threshold of 10° is applied here. Such conditions were given over large areas of the south western Pamir during the observation period. The deceleration of lake development observed there during the last decade may be connected to changing patterns of glacier dynamics, but also to the retreat of the glacier tongues over steeper terrain. More detailed research on the conditioning of the basal topography beneath the glaciers will be required in order to predict the future trends for the various parts of the study area (e.g., Linsbauer et al., 2012; Paul and Linsbauer, 2012).

The moving centre of the growth of glacial lakes from the south western Pamir to the central and northern Pamir may reflect the trends of glacier dynamics. It is hypothesized that the process of glacier retreat has started later there than in the south western Pamir. Mergili et al. (2012) have found indicators for such a trend, but more definitive up-to-date information is still needed. The climate in the high-elevation areas of the central and northern Pamir is comparably humid, possibly leading to more favourable accumulation patterns than in other parts of the study area and consequently to a delayed response to the increase in atmospheric temperature. Given the uncertainties and the comparatively short duration of Period 2, the significance of the derived trends has to be re-evaluated in one or two decades.

The hazard connected to the formation and existence of lakes strongly depends on the dam type. The dams of glacial lakes (Type 3) commonly contain ice (glacier, ice-cored moraine, rock glacier) and melting of this ice may drastically change the static equilibrium of the dam. Even though many glacial lakes are located on or in front of retreating glacier tongues and display a ±continuous growth, also those lakes quickly appearing or disappearing are highly relevant from a hazard perspective (2002 Dasht event). There is a potential for the formation of such lakes due to the presence of numerous surging glaciers which may temporarily block valley outlets (Kotlyakov et al., 2008). Landslide-dammed lakes of Type 2, in contrast to glacial lakes, are commonly short-lived and often drain within a few days or weeks after their formation (Costa and Schuster, 1988). However, they may also remain constant in size for decades and centuries. The findings presented shall be used as input for analysing the susceptibility of mountain communities and infrastructures to lake outburst floods in the study area, based on the work of Mergili and Schneider (2011) and Mergili et al. (2011). The regional-scale analysis scheme developed and applied to the south western Pamir by Mergili and Schneider (2011) shall be further improved and extended, and applied to the entire headwater region of the Amu Darya River.

6 Conclusions

A multi-temporal lake inventory was prepared for the study area. Altogether, 1642 lakes >2500 m² were detected from remotely sensed data. A clear growing trend was observed among the 652 glacial lakes, which does not apply to lakes of other types (erosion lakes and such lakes retained by block or debris dams). The long-term lake development is most likely blurred by intra- and short term inter-annual variations of the lake area. Glacial lake growth is related to

glacier retreat or decay in rather flat areas. A shift of glacial lake growth towards more elevated catchments is observed. However, more data and a longer observation period will be required to confirm this trend. The lake inventory will be an essential input for analysing the hazards related to possible lake outburst floods. More data on the glacier development are needed to better analyse the relationship between glacier retreat and lake evolution.

Acknowledgements

The work presented is part of the project PAMIR supported by the European Commission (EC) and the Austrian Development Agency (ADA), as well as of the project TajHaz supported by FOCUS Humanitarian Assistance (an affiliate of the Aga Khan Development Network), the Swiss Agency for Development and Cooperation (SDC) and the UK Department for International Development (DFID). The Tajik Agency of Hydrometeorology has provided meteorological and glaciological data. Special thanks for their support go to Fabian Gruber, Stefan Koch, Fabian Znojemsky and Christoph Waldhör, BOKU University, Vienna. Furthermore, the valuable suggestions provided by Wilfried Haeberli and another anonymous reviewer are acknowledged.

References

Agaltseva, N.A., Borovikova, L.N., Konovalov, V.G., 1997. Automated system of runoff forecasting for the Amudarya River basin. Destructive Water: Water-Caused Natural Disasters, their Abatement and Control (Proceedings of the Conference held at Anaheim, California, June 1996), IAHS Publication 239, 193–201.

Aizen, V.B., Kuzmichenok, V.A., Surazakov, A.B., Aizen, E.M., 2006. Glacier changes in the central and northern Tien Shan during the last 140 years based on surface and remote-sensing data. Annals of Glaciology, 43, 202–213.

Aizen, V.B., Aizen, E.M., 1997. Hydrological cycles on the north and south peripheries of mountain–glacial basins of Central Asia. Hydrological Processes, 11, 451–469.

Aizen, V.B., Aizen, E.M., Kuzmichenok, V.A., 2007a. Glaciers and hydrological changes in the Tien Shan: simulation and prediction. Environmental Research Letters, 2, 045019. doi:10.1088/1748-9326/2/4/045019

Aizen, V.B., Kuzmichenok, V.A., Surazakov, A.B., Aizen, E.M., 2007b. Glacier changes in the Tien Shan as determined from topographic and remotely sensed data. Global and Planetary Change, 56, 328–340.

Bajracharya, S.R., Mool, P.K. and Shrestha, B.R., 2007. Impact of climate change on Himalayan glaciers and glacial lakes: Case studies on GLOF and associated hazards in Nepal and Bhutan. ICIMOD, Kathmandu.

Beniston, M., 2003. Climatic Change in Mountain Regions: A Review of Possible Impacts. Climatic Change, 59(1–2), 5–31.

Bolch, T., Peters, J., Yegorov, A., Prafhan, B., Buchroithner, M., Blagoveshchensky, V., 2011. Identification of potentially dangerous glacial lakes in the northern Tien Shan. Natural Hazards, 59, 1691–1714.

Breien H., De Blasio F. V., Elverhoi A., and Hoeg K., 2008. Erosion and morphology of a debris flow caused by a glacial lake outburst flood, Western Norway. Landslides, 5(3), 271–280.

Cenderelli D.A., Wohl E.E., 2001. Peak discharge estimates of glacial lake outburst floods and "normal" climatic floods in Mount Everest region, Nepal. Geomorphology, 40, 57–90.

Cook, A.J., Fox, A.J., Vaughan, D.G., Ferrigno, J.G, 2005. Retreating Glacier Fronts on the Antarctic Peninsula over the Past Half-Century. Science, 308(5721), 541–544.

Clarke, G.K.C., 1982. Glacier outburst floods from 'Hazard Lake', Yukon Territory, and the problem of flood magnitude prediction. Journal of Glaciology, 28(98), 3–21.

Costa, J. E., Schuster, R.L., 1988. The formation and failure of natural dams. Geological Society of America Bulletin, 100, 1054–1068.

Dussaillant A., Benito G., Buytaert W., Carling P., Meier C., Espinoza F., 2010. Repeated glacial-lake outburst floods in Patagonia: an increasing hazard? Natural Hazards, 54(2), 469–481.

Evans S.G., Clague J.J., 1994. Recent climatic change and catastrophic geomorphic processes in mountain environments. Geomorphology, 10(1-4), 107–128.

Evans S.G., 1986. The maximum discharge of outburst floods caused by the breaching of man-made and natural dams. Canadian Geotechnical Journal, 23, 385–387.

Frey, H., Haeberli, W., Linsbauer, A., Huggel, C. and Paul, F., 2010. A multi level strategy for anticipating future glacier lake formation and associated hazard potentials. Natural Hazards and Earth System Sciences, 10, 339–352.

Gruber, S., 2012. Derivation and analysis of a high-resolution estimate of global permafrost zonation. The Cryosphere, 6, 221–233.

Haeberli, W., 1975. Untersuchungen zur Verbreitung von Permafrost zwischen Flüelapass und Piz Grialetsch (Graubünden). Dissertation, University of Basel.

Haeberli, W., 1983. Frequency and characteristics of glacier floods in the Swiss Alps. Annals of Glaciology, 4, 85–90.

Haeberli, W., Clague, J. J., Huggel, C., Kääb, A., 2010a. Hazards from lakes in high-mountain glacier and permafrost regions: Climate change effects and process interactions. Avances de la Geomorphología en España, 2008-2010, XI Reunión Nacional de Geomorphología, Solsona, 439–446.

Haeberli, W., Portocarrero, C., Evans, S., 2010b. Nevado Hualcán, Laguna 513 y Carhuaz 2010 – Observaciones, evaluación y recomendaciones (un corto informe técnico luego de las reuniones y visita de campo en Julio 2010). Unpublished report on behalf of the Comunidad Provincial de Carhuaz.

Hagg, W., Braun, L., 2005. The influence of glacier retreat on water yield from high mountain areas: Comparison of Alps and Central Asia, In: De Jong, C., Ranzi, R., Collins, D., (eds.), Climate and Hydrology in Mountain Areas, Wiley, Chichester. 263–275.

Haritashya, U.K., Bishop, M.P., Shroder, J.F., Bush, A.B.G., Bulley, H.N.N., 2009. Space-based assessment of glacier fluctuations in the Wakhan Pamir, Afghanistan. Climatic Change, 94, 5–18.

Harris, C., Arenson, L.U., Christiansen, H.H., Etzelmüller, B., Frauenfelder, R., Gruber, S., Haeberli, W., Hauck, C., Hölzle, M., Humlum, O., Isaksen, K., Kääb, A., Kern-Lütschg, M.A., Lehning, M., Matsuoka, N., Murton, J.B., Nötzli, J., Phillips, M., Ross, N., Seppälä, M., Springman, S.M., Vonder Mühll, D., 2009. Permafrost and climate in Europe: Monitoring and modelling thermal, geomorphological and geotechnical responses. Earth-Science Reviews, 92(3–4), 117–171.

Harrison, S., Glasser, N., Winchester, V., Haresign, E., Warren, C., Jansson, K., 2006.. A glacial lake outburst flood associated with recent mountain glacier retreat, Patagonian Andes. Holocene, 16, 611–620.

Hewitt, K., 1982. Natural dams and outburst floods in the Karakorum Himalaya. In: Glen J.W., (ed.): Hydrological aspects of alpine and high-mountain areas. IAHS Publication 138, 259–269.

Hewitt, K., Liu, J., 2010. Ice-dammed lakes and outburst floods, Karakoram Himalaya: historical perspectives on emerging threats. Physical Geography, 31(6), 528–551.

Huber, U., Bugmann, H., Reasoner, M., 2005. Global Change and Mountain Regions. An overview of current knowledge. Advances in Global Change Research. Springer, Dordrecht.

Huggel, C., Kääb, A., Haeberli, W., Teysseire, P., Paul, F., 2002. Remote sensing based assessment of hazards from glacier lake outbursts: a case study in the Swiss Alps. Canadian Geotechnical Journal, 39, 316–330.

Huggel, C., Kääb, A., Haeberli, W., Krummenacher, B., 2003. Regional-scale GIS-models for assessment of hazards from glacier lake outbursts: evaluation and application in the Swiss Alps. Natural Hazards and Earth System Sciences, 3, 647–662.

Huggel, C., Haeberli, W., Kääb, A., Bieri, D., Richardson, S., 2004a. Assessment procedures for glacial hazards in the Swiss Alps. Canadian Geotechnical Journal, 41(6), 1068–1083.

Huggel, C., Kääb, A., Salzmann, N., 2004b. GIS-based modeling of glacial hazards and their interactions using Landsat-TM and IKONOS imagery. Norwegian Journal of Geography, 58, 761–773.

IAHS/UNEP/UNESCO, 1998. Fluctuations of glaciers 1990–1995, vol. 7. Haeberli, W., Hoelzle, M., Suter, S., & Frauenfelder, R. (compilers) for World Glacier Monitoring Service, Zurich. International Association of Hydrologic Sciences, Wallingford, U.K.

ICIMOD, 2011. Glacial lakes and glacial lake outburst floods in Nepal. ICIMOD, Kathmandu.

IPCC, 2007. Climate Change 2007: The Physical Science Basis. Contribution of Working Group I to the Fourth Assessment Report of the Intergovernmental Panel on Climate Change [Solomon, S., Qin, D., Manning, M., Chen, Z., Marquis, M., Averyt, K. B., Tignor, M., and Miller, H.L. (eds.)]. Cambridge University Press, Cambridge, United Kingdom and New York, NY, USA.

Jarvis, A., Reuter, H.I., Nelson, A., Guevara, E., 2008. Hole-filled seamless SRTM data V4. International Centre for Tropical Agriculture (CIAT), available from http://srtm.csi.cgiar.org.

Kääb, A., Huggel, C., Fischer, L., Guex, S., Paul, F., Roer, I., Salzmann, N., Schlaefli, S., Schmutz, K., Schneider, D., Strozzi, T., and Weidmann, Y., 2005. Remote sensing of glacier- and permafrost-related hazards in high mountains: an overview. Natural Hazards and Earth System Sciences, 5, 527–554.

Kaser, G., 1999. A review of the modern fluctuations of tropical glaciers. Global and Planetary Change, 22, 93–103.

Kaser, G., Grosshauser, M., 2010. The contribution potential of glaciers to Himalaya river runoff. Geophysical Research Abstracts, 12, EGU2010-10962.

Kassam, K.A., 2009. Viewing Change Through the Prism of Indigenous Human Ecology: Findings from the Afghan and Tajik Pamir. Human Ecology, 37, 677–690.

Khromova, T.E., Dyurgerov, M.B., & Barry, R.G., 2003. Late-twentieth century changes in glacier extent in the Ak-shirak Range, Central Asia, determined from historical data and ASTER imagery. Geophysical Research Letters, 30(16), 1863.

Khromova, T.E., Osipova, G.B., Tsvetkov, D.G., Dyurgerov, M.B., Barry, R.G., 2006. Changes in glacier extent in the eastern Pamir, Central Asia, determined from historical data and ASTER imagery. Remote Sensing of Environment, 102, 24–32.

Kotlyakov, V.M., Osipova, G.B., Tsvetkov, D.G., 2008. Monitoring surging glaciers of the Pamirs, Central Asia, from space. Annals of Glaciology, 48, 125–134.

Lambrecht, A., Kuhn, M., 2007. Glacier changes in the Austrian Alps during the last three decades, derived from the new Austrian glacier inventory. Annals of Glaciology, 46(1), 177–184.

Linsbauer, A., Paul, F., Haeberli, W., 2012. Modeling glacier thickness distribution and bed topography over entire mountain ranges with GlabTop: Application of a fast and robust approach. Journal of Geophysical Research, 117, F03007, doi:10.1029/2011JF002313.

Makhmadaliev, B., Kayumov, A., Novikov, V., Mustaeva, N., Rajabov, I. (eds.), 2008. The Second National Communication of the Republic of Tajikistan under the United Nations Framework Convention on Climate Change. State Agency for Hydrometeorology, Dushanbe, Tajikistan.

Mergili, M., Schneider, J.F., 2011. Regional-scale analysis of lake outburst hazard in the southwestern Pamir, Tajikistan, based on remote sensing and GIS. Natural Hazards and Earth System Sciences, 11, 1447–1462.

Mergili, M., Kopf, C., Müllebner, B., Schneider, J.F., 2012. Changes of the cryosphere in the high-mountain areas of Tajikistan and Austria: a comparison. Geografiska Annaler, Series A, 94(1), 79–96.

Mergili, M., Schneider, D., Worni, R., Schneider, J.F., 2011. Glacial Lake Outburst Floods (GLOFs): challenges in prediction and modelling. In: Genevois R., Hamilton D.L., Prestininzi A., (eds.):Proceedings of the 5th International Conference on Debris-Flow Hazards Mitigation: Mechanics, Prediction and Assessment, Padova, June 14–17, 2011. Italian Journal of Engineering Geology and Environment – Book, 973–982.

Micklin, P.P., 1988. Desiccation of the Aral Sea: A Water Management Disaster in the Soviet Union. Science, 241(4870), 1170–1176.

Micklin, P.P., Aladin, N.V., 2008. Reclaiming the Aral Sea. Scientific American, 298, 64–71.

Narama, C., Duishonakunov, M. , Kääb, A., Daiyrov, M., Abdrakhmatov, K., 2010. The 24 July 2008 outburst flood at the western Zyndan glacier lake and recent regional changes in glacier lakes of the Teskey Ala-Too range, Tien Shan, Kyrgyzstan. Natural Hazards and Earth System Sciences, 10, 647–659, 2010.

Paul, F., Linsbauer, A., 2012. Modeling of glacier bed topography from glacier outlines, central branch lines, and a DEM. International Journal of Geographic Information Science, doi:10.1080/13658816.2011.627859

Quincey D.J., Richardson S.D., Luckman A., Lucas R.M., Reynolds J.M., Hambrey M.J., Glasser N.F., 2007. Early recognition of glacial lake hazards in the Himalaya using remote sensing datasets. Global and Planetary Change, 56(1-2), 137–152.

Richardson, S.D. and Reynolds, J.M., 2000. An overview of glacial hazards in the Himalayas. Quaternary International, 65/66, 31–47.

Risley, J.C., Walder, J.S., Denlinger, R., 2006. Usoi dam wave overtopping and flood routing in the Bartang and Panj rivers, Tajikistan. Natural Hazards, 38(3), 375–390.

Schuster, R.L., Alford, D., 2004. Usoi Landslide Dam and Lake Sarez, Pamir Mountains, Tajikistan. Environmental & Engineering Geoscience, 10(2), 151–168.

Strozzi, T., Wiesmann, A., Kääb, A., Joshi, S., Mool, P., 2012. Glacial lake mapping with very high resolution satellite SAR data. Natural Hazards and Earth System Sciences, 12, 2487–2498.

Surazakov, A.B., Aizen, V.B., 2006. Estimating Volume Change of Mountain Glaciers Using SRTM and Map-Based Topographic Data. IEEE Transactions on Geoscience and Remote Sensing, 44, 2991–2995.

Terrier, S., Jordan, F., Schleiss, A.J., Haeberli, W., Huggel, C., Künzler, M., 2011. Optimized and adapted hydropower management considering glacier shrinkage scenarios in the Swiss Alps. Proceedings of the International Symposium on Dams and Reservoirs under Changing Challenges - 79th Annual Meeting of ICOLD, Swiss Committee on Dams, Lucerne, Switzerland (Schleiss, A., Boes, R.M., eds), Taylor & Francis Group, London, 497–508.

Tinti, S., Maramai, A., Cerutti, A.V., 1999. The Miage Glacier in the Valley of Aosta (Western Alps, Italy) and the Extraordinary Detachment which Occurred on August 9, 1996. Physics and Chemistry of the Earth (A), 24(2), 157–161.

Tweed, F.S., Russell, A.J., 1999. Controls on the formation and sudden drainage of glacier-impounded lakes: implications for jökulhlaup characteristics. Progress in Physical Geography, 23(1), 79–110.

Vilímek, V., Zapata, M. L., Klimes, J., Patzelt, Z., Santillán N., 2005. Influence of glacial retreat on natural hazards of the Palcacocha Lake area, Peru. Landslides, 2(2), 107–115.

Walder J.S., Costa J.E., 1996. Outburst floods from glacier-dammed lakes: the effect of mode of lake drainage on flood magnitude. Earth Surface Processes and Landforms, 21, 701–723.

Walder, J.S., O'Connor, J.E., 1997. Methods for Predicting Peak Discharge of Floods Caused by Failure of Natural and Constructed Earth Dams. Water Resources Research, 33(10), 2337–2348.

Watanabe, T., Rothacher, D., 1996. The 1994 Lugge Tsho glacial lake outburst flood, Bhutan Himalaya. Mountain Research and Development, 16, 77–81.

WGMS, 2008. Global Glacier Changes: Facts and Figures (Zemp, M., Roer, I., Kääb, A., Hoelzle, M., Paul, F., Haeberli, W., eds.), UNEP, World Glacier Monitoring Service, University of Zurich, Switzerland. Free download from WGMS and UNEP websites.

Appendix 6

Regional-scale analysis of high-mountain multi-hazard and risk in the Pamir (Tajikistan) with GRASS GIS

Discussion paper

Gruber, F.E., Mergili, M. (2013): Regional-scale analysis of high-mountain multi-hazard and risk in the Pamir (Tajikistan) with GRASS GIS. Natural Hazards and Earth System Sciences Discussions, 1, 1689–1747.

Original article: http://www.nat-hazards-earth-syst-sci-discuss.net/1/1689/2013/nhessd-1-1689-2013.html

Abstract

We present a model framework for the regional-scale analysis of high-mountain multi-hazard and -risk, implemented with the Open Source software package GRASS GIS. This framework is applied to a 98,300 km² study area centred in the Pamir (Tajikistan). It includes (i) rock slides, (ii) ice avalanches, (iii) periglacial debris flows and (iv) lake outburst floods. First, a hazard indication score is assigned to each relevant object (steep rock face, glacier or periglacial slope, lake). This score depends on the susceptibility and on the expected event magnitude. Second, the possible travel distances, impact areas and, consequently, impact hazard indication scores for all types of processes are computed using empirical relationships. These scores are finally superimposed with an exposure score derived from the type of land use, resulting in a raster map of risk indication scores finally discretized at the community level. The analysis results are presented and discussed at different spatial scales. The major outcome of the study, a set of comprehensive regional-scale hazard and risk indication maps, shall represent an objective basis for the prioritization of target communities for further research and risk mitigation measures.

Keywords

Central Asia, GRASS GIS, Mass movements, Multi-hazard, Regional scale, Risk indication map

1 Introduction

High-mountain areas are commonly experiencing pronounced environmental changes such as permafrost melting and the retreat of glaciers, caused by atmospheric temperature increase (Beniston, 2003; Huber et al., 2005; IPCC, 2007; WGMS, 2008; Harris et al., 2009). Together with earthquakes or volcanic eruptions, they disturb the dynamic equilibrium of the fragile high-mountain geomorphic systems, leading to an increased occurrence of rapid mass movements (Evans and Clague, 1994; Huggel et al., 2004a,b; Kääb et al., 2005; IPCC, 2007; Quincey et al., 2007; Harris et al., 2009; Dussaillant et al., 2010; Haeberli et al., 2010a).

Whilst such mass movements often occur in remote areas and remain unrecognized, they may also evolve into long-distance flows affecting the communities in the valleys. Such processes are referred to as remote geohazards. They are commonly related to the massive entrainment of loose material or the interaction of two or more process types (process chain). Several cases are evident where slope failures including rock and/or ice have converted into long-distance avalanches and consecutive processes. A striking example is the 1970 Huascarán event (Cordillera Blanca, Peru) where several 1000 people lost their lives in the town of Yungay (Evans et al., 2009a). On September 20, 2002, a rock-ice avalanche in the Russian Caucasus entrained a glacier. The resulting flow continued for 20 km as an avalanche of ice, rock and debris and for further 15 km as mud flow, resulting in approx. 140 fatalities (Kolka/Karmadon event; Huggel et al., 2005). On April 11, 2010, an ice avalanche from far upslope rushed into Laguna (Lake) 513 in the Cordillera Blanca, causing a destructive outburst flood (Haeberli et al., 2010b).

Lakes are commonly involved in remote geohazard processes (Costa, 1985; Evans, 1986; Costa and Schuster, 1988; Walder and Costa, 1996; Walder and O'Connor, 1997). Landslide-dammed lakes are of particular interest as most of them drain within the first year after their formation (Costa and Schuster, 1988) whilst others persist for centuries. Glacial lakes, impounded by ice (Tweed and Russell, 1999) or (often ice-cored) moraines, are commonly coupled to retreating or surging glaciers and therefore highly dynamic. Such lakes often occur in areas influenced by permafrost. Some lakes are prone to sudden drainage (Glacial Lake Outburst Floods or GLOFs). Studies of this phenomenon cover most glacierized mountain areas in the world such as the Himalayas (Watanabe and Rothacher, 1996; Richardson and Reynolds, 2000; ICIMOD, 2011), the Karakorum (Hewitt, 1982; Hewitt and Liu, 2010), the Pamir (Mergili and Schneider, 2011), the Tien Shan (Narama et al., 2010; Bolch et al., 2011), the Andes (Vilímek et al., 2005; Harrison et al., 2006; Haeberli et al., 2010b), the North American mountains (Clarke, 1982), the Norwegian mountains (Breien et al., 2008) and the western Alps (Haeberli, 1983; Tinti et al., 1999; Huggel et al., 2002, 2003). GLOFs can evolve in different ways, for example by mass movements into lakes, rising lake levels leading to overflow, progressive incision, mechanical rupture or retrogressive erosion of a dam, hydrostatic failure or degradation of glacier dams or ice-cores in moraine dams (Walder and Costa, 1996; Richardson and Reynolds, 2000). Peak discharges are often some magnitudes higher than in the case of ordinary floods (Cenderelli and Wohl, 2001). Entrainment may considerably increase the event magnitude and convert the flood into a destructive debris flow.

A common feature of long-distance rock mass movements, ice avalanches, debris flows, lake outburst floods and related process chains is their occurrence as rare (low frequency) or singular events. The location, timing, magnitude and impact area of remote geohazard events are often hard or even impossible to predict, even though the governing processes are fairly well understood and specific events were successfully back-calculated with deterministic computer models (Evans et al., 2009a, b). This is particularly true where multiple hazards are evident over a large area and/or where the resources for a broad-scale continuous monitoring of potentially hazardous situations are lacking, i.e. in developing countries. Here it is essential to identify possible source and – particularly – impact areas of remote geohazard processes at the broad (regional) scale in order to prioritize target areas for risk mitigation measures. Huggel et al. (2003, 2004a, b) and Mergili and Schneider (2011) have presented computer models suitable for the regional-scale analysis of high-mountain hazards such as GLOFs, periglacial debris flows or ice avalanches. Some of these models include process interactions. However, they neither attempt to account for the risk nor are they applied to very large areas. These gaps hamper a more focused and comprehensive identification of possible target areas for risk mitigation.

Here we demonstrate a novel model framework for the regional-scale analysis of high-mountain hazards and risks, including (i) rock slides, commonly converting into rock avalanches or, in glacierized areas, into rock-ice avalanches, (ii) ice-avalanches, (iii) periglacial debris flows and (iv) lake outburst floods, often evolving into flows of debris or mud. Examples of these results of processes, or of situations possibly leading to their occurrence, are illustrated in Fig. 2. Process chains including more than one of the above process types are also considered. The study area in the Pamir (Tajikistan, Central Asia) is introduced in Section 2. The data used for the study is presented in Section 3 and the model framework is explained in detail in Section 4. Section 5 gives an overview of the model results which are discussed in Section 6. Section 7 summarizes the essence of the study.

2 Study area

A 98,300 km² study area in Central Asia is considered, extending from 1670 m a.s.l. near Khala-i-Khumb to 7495 m at the top of Ismoili Somoni Peak and largely corresponding to the headwaters of the Amu Darya River (Fig. 1). The northern and southern boundaries of the area are formed by the Alai and Hindukush ranges in Kyrgyzstan and Afghanistan. In between, the Pamir in the Gorno-Badakhshan Autonomous Oblast of Tajikistan represents the largest share of the study area.

The western Pamir is characterized by glacierized mountain ranges exceeding 6000 m a.s.l. and deeply incised valleys. The eastern Pamir represents an arid highland above 3500 m a.s.l. with glaciers covering only the highest peaks. The more humid northern Pamir with the Academy of Sciences and Transalai ranges peaks above 7000 m a.s.l. and is extensively glacierized. The Fedchenko Glacier extends over a length of >75 km and covers a surface area >700 km².

Intense tectonic uplift in combination with glacial and fluviatile erosion (Mahmood et al., 2008) has resulted in a particularly pronounced relief. Consequently the geomorphic activity is high, including a large variety of mass wasting processes. They are commonly triggered by earthquakes

as the seismic activity and, therefore, the seismic hazard are significant (Giardini et al., 1999). Few large historic events such as the 1911 Sarez rock slide (Schuster and Alford, 2004; Risley et al., 2006; see Fig. 2a) or the 1949 Khait rock avalanche (Evans et al., 2009b) are well documented. The deposit of the 2 km² Sarez rock slide forms the 600 m high Usoi Dam, the highest dam worldwide. It retains the 60 km long Lake Sarez, the safety of which is still disputed (e.g., Risley et al., 2006).

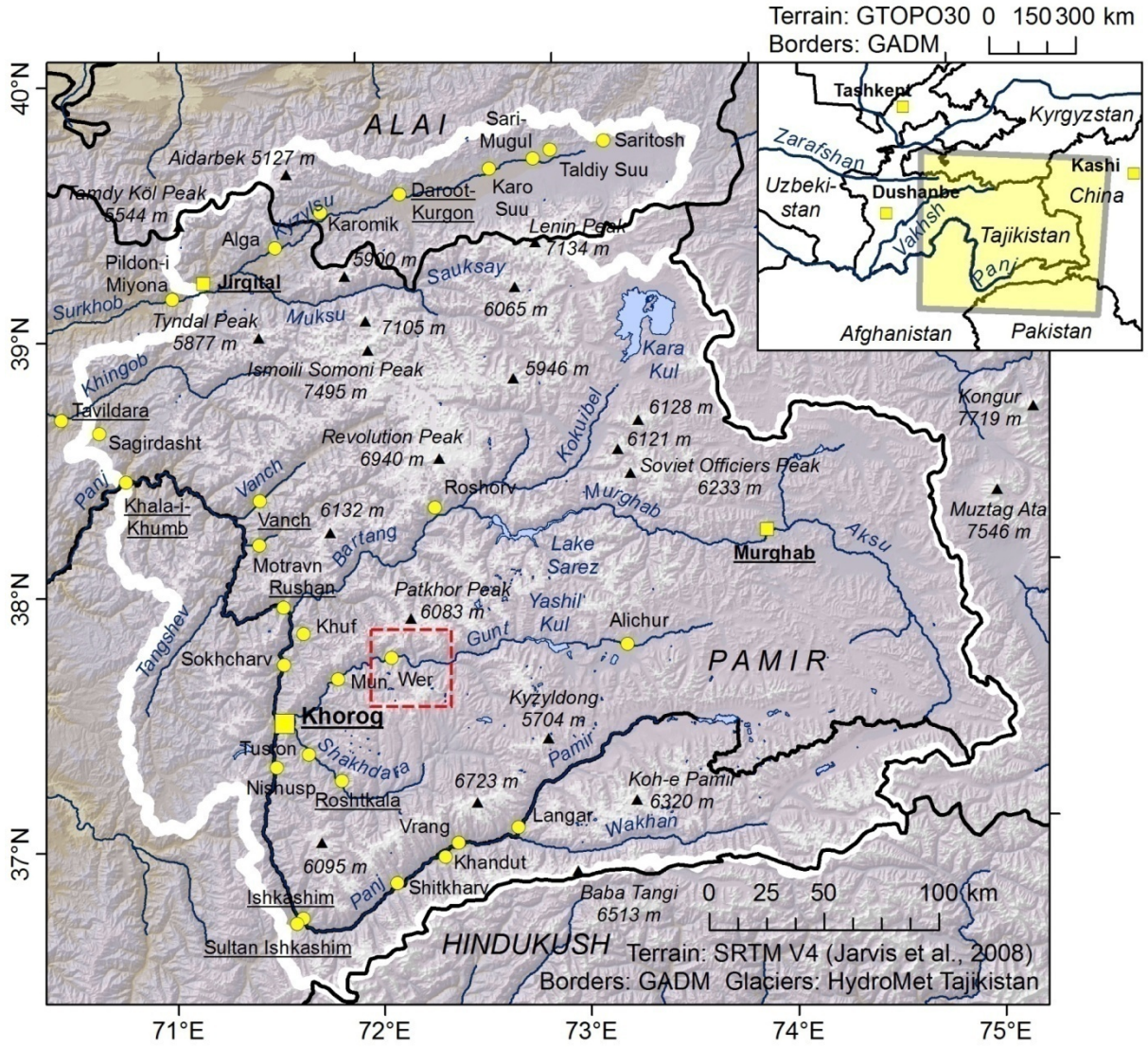

Fig. 1 Study area. The dashed red rectangle delimits the area shown in Fig. 14.

The climate in the study area is temperate semi-arid to arid and continental with hot summers and cold winters. Most meteorological stations in the study area have recorded a positive trend of the mean annual air temperature (MAAT) in the period 1940–2000 (Makhmadaliev et al., 2008). The state of information suffers from a lack of up-to-date high-altitude meteorological data. According to the 4th IPCC report (IPCC, 2007), the median of the projected increase of the MAAT from 1980–1999 to 2080–2099 for Tajikistan is 3.7 °C.

Consequently, many glaciers are retreating (e.g. Khromova et al., 2006; Haritashiya et al., 2009; Mergili et al, 2012a), favouring the development of lakes in the glacier forefields or in subsiding

areas on the glaciers. Mergili et al. (2013) detected a total number of 652 glacial lakes in the study area. A GLOF in 2002 caused dozens of fatalities, several more lakes are susceptible to sudden drainage (Mergili and Schneider, 2011; see Fig. 2d). Further, the retreat of glaciers over steep rock cliffs (see Fig. 2b) may lead to the increased occurrence of ice avalanches. The shift of the permafrost boundary to higher areas results in the possible destabilization of rock and debris. Periglacial debris flows observed in the study area are most commonly associated with the termini of rock glaciers (see Fig. 2c).

The valleys in the study area are fairly densely populated, with Khorog as the only urban centre (see Fig. 1). The local communities strongly depend on the natural resources and are therefore affected by the consequences of the changing temperature regime in both positive and negative ways (Kassam, 2009).

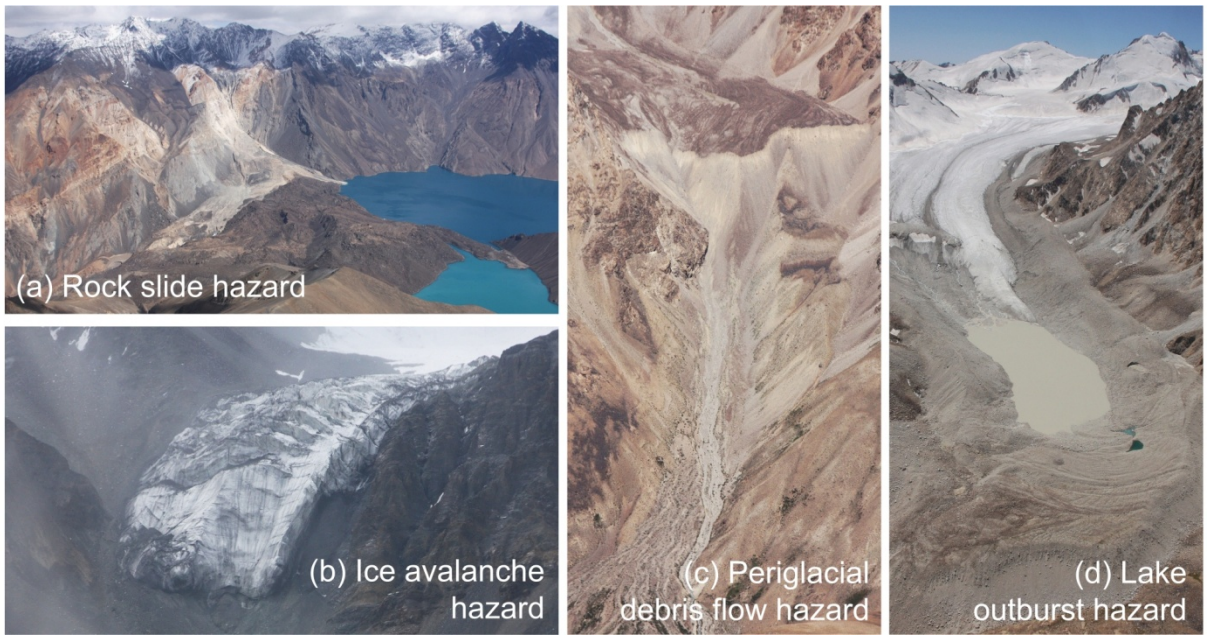

Fig. 2 Processes covered by the high-mountain multi-hazard and -risk indication model. (a) The 2 km² rock slide deposit impounding lake Sarez, triggered by an earthquake in 2011, (b) hanging glacier in the Sauksay Valley prone to produce ice avalanches, (c) periglacial debris flow starting from a rock glacier terminus in the upper Gunt Valley, (d) Lake Varshedz in a southern tributary of the Gunt Valley, one of many glacial lakes possibly susceptible to sudden drainage. All photos taken by M. Mergili.

3 Data

The data the high-mountain multi-risk analysis builds on are summarized in Table 1. The ASTER GDEM V2, a product of METI and NASA, is used as input digital elevation model (DEM). It is provided at a cell size of approx. 30 x 30 m. Here a version resampled to 60 x 60 m is applied. Secondary data sets such as elevation with filled sinks, slope and flow direction are generated from the DEM which is further used to generate a gridded data set of the MAAT, making use of temperature data recorded at the stations of the Tajik HydroMet Agency and a vertical temperature gradient of 0.0062°C m^{-1} (Müllebner, 2010; Fig. 3a).

The identification of areas with melting permafrost builds on the permafrost indication map for Tajikistan presented by Mergili et al. (2012a): a set of rules-of-thumb for the lower boundaries of sporadic and discontinuous permafrost in Switzerland (Haeberli, 1975) is adapted to the conditions in Tajikistan. This set of rules is then combined with the DEM in order to produce a gridded dataset indicating the possibility of permafrost occurrence for each raster cell. Applying the temperature gradient of Müllebner (2010), the effects of atmospheric temperature increase on permafrost distribution are explored. Areas where the model predicts either sporadic or discontinuous permafrost for the current state, but no permafrost of either of the two types for a temperature increase of +2°C or +4°C, represent separate classes. Such areas are of particular interest for the permafrost susceptibility score S_p (Fig. 3b; see Section 4).

Table 1 Input data, rm = raster map, tc = table column.

Parameter	Data type	Source
Elevation	rm, m a.s.l.	ASTER GDEM V2, a product of METI and NASA
Glaciers	rm, boolean	Semi-automated classification of Landsat 7 imagery
Lake ID	rm, nominal	Manual mapping from ASTER and Landsat imagery (Mergili et al., 2013)
For each lake:		
Lake type	tc, nominal	Qualitative interpretation of ASTER, Landsat and Google Earth® imagery (Mergili et al., 2013)
Lake drainage	tc, boolean	
Calving of ice	tc, boolean	
Lake area A_l	tc, m²	Derived from mapped lakes
Lake evolution	tc, boolean	Mapped, 75% confidence of growing trend in at least one of the periods 1968–2002 and 2002–2009 (Mergili et al., 2013)
Mean Annual Air Temperature MAAT	rm, °C	Temperature map of Müllebner (2010) based on regression of data recorded by the Tajik HydroMet Agency with elevation
Permafrost susceptibility S_p	rm, nominal	Permafrost indication map of Mergili et al. (2012a) for Tajikistan, based on the adaptation of the rules-of-thumb of Haeberli (1975)
Seismic susceptibility S_s	rm, g	GSHAP Global Seismic Hazard Map (Giardini et al., 1999): peak ground acceleration PGA with 10% chance of exceedance in 50 years
Exposure E	rm, nominal	Manual mapping of land use from ASTER, Landsat and Google Earth® imagery
Community ID	rm, nominal	

The seismic susceptibility of the area S_s is defined according to the peak ground acceleration with 10% chance of exceedance in 50 years (PGA), expressed in relation to gravity g. The Global Seismic Hazard Map (Giardini et al., 1999), an outcome of the Global Seismic Hazard Assessment Program (GSHAP), is employed (see Fig. 3c).

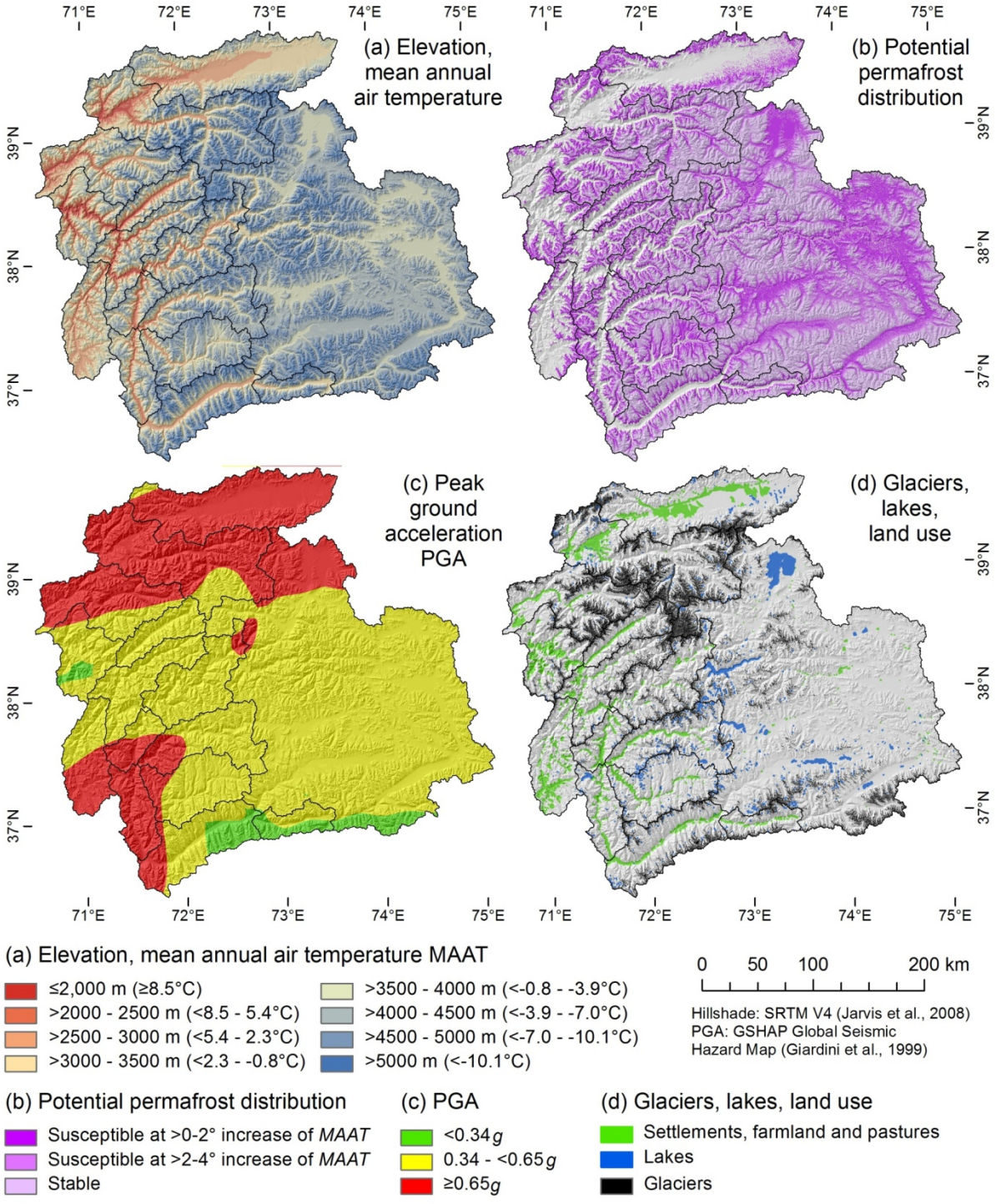

Fig. 3 Input data: (a) Elevation and mean annual air temperature, (b) potential permafrost distribution, (c) peak ground acceleration, (d) mapped glaciers, lakes and land use.

A raster map representing the glaciers in the study area is generated by a semi-automated classification of Landsat 7 satellite imagery of 2001. Three classes are distinguished: debris-

covered glacier, glacier with exposed ice and no glacier (see Fig. 3c). The lakes in the study area are covered by the comprehensive lake inventory presented by Mergili et al. (2013), providing detailed information on 1640 lakes (see Table 1; see Fig. 3c). Besides the tabular information, a raster map with the unique ID of each lake is used.

The exposure of the communities in the study areas to high-mountain hazards (see Fig. 3d) is generated from a raster map depicting the land use associated with each cell derived by the qualitative interpretation of ASTER, Landsat and Google Earth® imagery. Table 2 shows the key used for deriving the exposure score E from the land use map, taking values in the range 0–4. Linear structures such as roads or power lines are not considered. Each raster cell with $E > 0$ is associated to one of the 628 communities identified in the study area. The communities largely correspond to the villages depicted in the Soviet Topographic Maps 1:50,000 and 1:100,000. However, two or more villages are grouped to one community in cases where cells with $E > 0$ cannot clearly be assigned to one specific village.

Table 2 Risk indication score R: combination of IH and E with scoring scheme for the exposure E as a function of land use.

E↓IH→	Land use	6	5	4	3	2	1	0
4 (Higher)	Built-up areas, often mixed with farmland or pastures	6	5	4	3	2	1	0
3	Farmland or pastures with some buildings	5	4	3	2	1	1	0
2	Farmland, pastures or forest with no or few buildings	4	3	2	1	1	1	0
1	Extensively used or temporarily unused land	3	2	1	1	1	1	0
0 (Lower)	No identifiable land use	0	0	0	0	0	0	0

4 Model

4.1 Concept of the multi-hazard and risk analysis

The high-mountain multi-hazard and -risk indication computer model is implemented with the Open Source software package GRASS GIS (Neteler and Mitasova, 2007; GRASS Development Team, 2013). This software builds on a flexible modular design. Simple bash scripting can be used to facilitate work flows by combining existing modules. Furthermore, new modules can be added by individual developers, so that the standard GIS functions are complemented by a large array of more specialized applications. Such applications can be used individually or made publicly available. Examples of mountain hazard models implemented with GRASS GIS include r.debrisflow (Mergili et al., 2012b), r.avalanche (Mergili et al., 2012c) and r.rotstab (Mergili et al., submitted). The model presented here builds on a combination of newly developed or upgraded modules and bash scripts. The logical framework of the model is illustrated in Fig. 4, the modules dealing with the specific process types are detailed in Section 4.2 to Section 4.5. The model is executed at a raster cell size of 60 x 60 m.

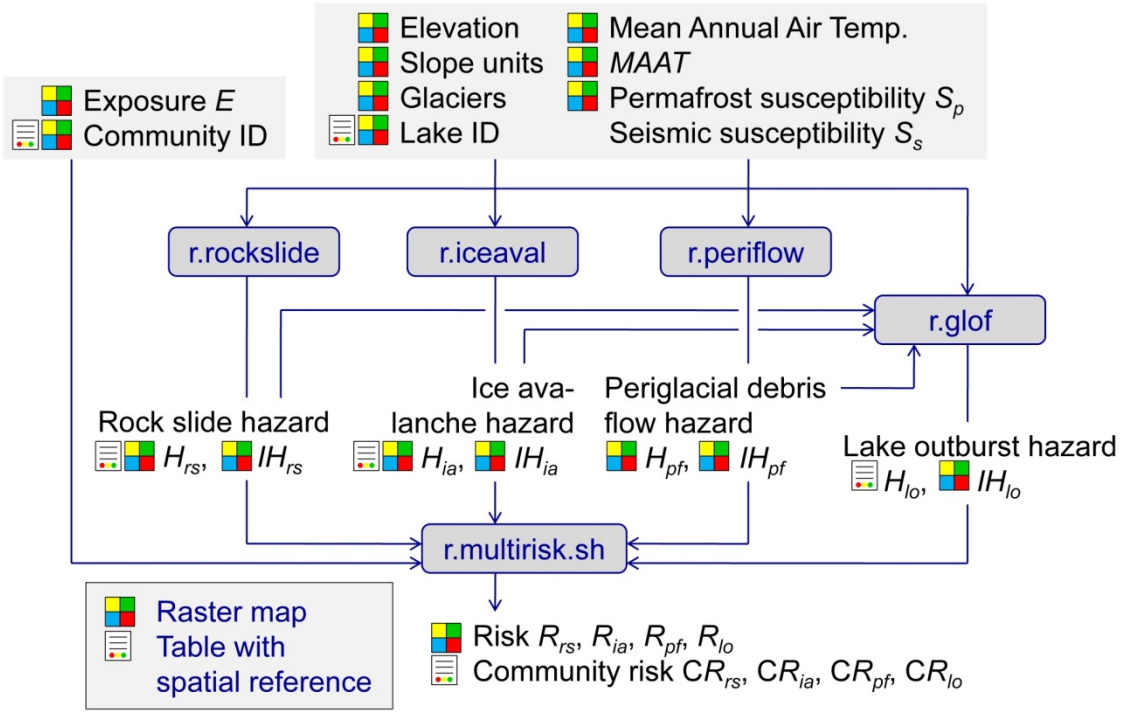

Fig. 4 Logical framework of the high-mountain multi-hazard and -risk indication model.

The high-mountain hazard analysis procedure applied at the regional scale aims at the identification of possible (i) source areas and (ii) impact areas of hazardous processes. The risk analysis combines the hazard in the impact areas, the impact hazard *IH*, with the exposure *E* there in order to derive a risk indication score *R* in the range 0–6. Table 2 shows the matrix employed for the combination of *IH* and *E*.

The following types of processes are considered: (i) rock slides, (ii) ice avalanches, (iii) periglacial debris flows and (iv) lake outburst floods. All of them show a potential for long travel distances and therefore represent a significant threat for the populated areas in the valleys. Even though each process type is considered separately, interactions are included in the model, such as triggering of a lake outburst flood by the impact of an upslope mass movement (see Fig. 4).

Table 3 Hazard indication score *H*: combination of *S* and *M*, with thresholds of (a) rock slide volume V_{rs} (106 m^3), (b) area of hanging glacier A_a (103 m^2) and (c) lake area A_l(103 m^2).

M↓S→	(a)	(b)	(c)	6	5	4	3	2	1	0
6 (Higher)	≥24.3	>200.0	>200.0	6	6	5	5	4	3	0
5	8.1 – <24.3	100.0 – <200.0	100.0 – <200.0	6	5	5	4	3	2	0
4	2.7 – <8.1	50.0 – <100.0	50.0 – <100.0	5	5	4	4	3	2	0
3	0.9 – <2.7	25.0 – <50.0	25.0 – <50.0	5	4	4	3	3	2	0
2	0.3 – <0.9	12.5 – <25.0	12.5 – <25.0	4	3	3	3	2	2	0
1	0.1 – <0.3	5.0 – <12.5	5.0 – <12.5	3	2	2	2	2	1	0
0 (Lower)	<0.1	<5.0	<5.0	0	0	0	0	0	0	0

Table 4 Impact hazard indication score *IH*: combination of *H* and *I*, r_ω is computed according to Eq. 1.

I↓H→	r_ω	6	5	4	3	2	1	0
6 (Higher)	≥2.000	6	6	5	5	4	3	0
5	1.500 – <2.000	6	5	5	4	3	2	0
4	1.000 – <1.500	5	5	4	4	3	2	0
3	0.667 – <1.000	5	4	4	3	3	2	0
2	0.333 – <0.667	4	3	3	3	2	2	0
1	0.000 – <0.333	3	2	2	2	2	1	0
0 (Lower)	<0.000	0	0	0	0	0	0	0

The scoring scheme employed for the hazard analysis follows the same basic principle for all types of processes. It builds on susceptibility, hazard and risk indication scores to be understood as ordinal numbers, not allowing for the use of arithmetic operations. Two-dimensional matrices are therefore used, all scores can take values in the range 0–6 (Table 3 and Table 4).

The hazard indication score for the onset of a process *H* is computed by combining the score for the susceptibility *S* with the score for the expected magnitude *M*. The susceptibility is understood as the tendency of a lake, part of a glacier or slope to produce an event and acts as a surrogate for the frequency. The expected process magnitude is based on the possible onset volume (rock slides) or on the possible onset area (ice avalanches, lake outburst floods; see Table 3).

The impact susceptibility represents the tendency of a GIS raster cell to be affected by one of the considered processes. It is derived by routing the mass movement from the onset area down through the DEM. At the regional scale, empirical relationships are suitable for relating the travel distance *L* or the angle of reach ω_r of a flow to the involved volume *V* or the peak discharge Q_p, or for defining a global value of ω_r. The appropriate values or relationships are employed for each process type, applying the lower envelope ($\omega_{r,E}$, maximum travel distance) and the average $\omega_{r,A}$ usually observed for the considered process (see Section 4.2 – Section 4.5). A random walk procedure weighted for local slope and maintenance of flow direction is applied for routing. This, by applying a sufficiently large number of random walks, ensures a certain degree of lateral spreading. Furthermore, the linear distance from the starting point has to increase with each step of the routing procedure. For each passed cell, the average slope angle from the starting point, ω, is updated. Each random walk terminates as soon as $\omega \leq \omega_{r,E}$. The impact susceptibility score *I* of each cell builds on the maximum of the ratio

$$r_\omega = 1 - \frac{\tan \omega_{r,A} - \tan \omega}{\tan \omega_{r,A} - \tan \omega_{r,E}} \qquad \text{Eq. 1}$$

over all random walks. $r_\omega = 1$ at the average angle of reach and $r_\omega = 0$ at the lower envelope (see Table 4). *I* is determined separately for each hypothetic event. The impact hazard indication score *IH* map, discretized on the basis of GIS raster cells, is derived by combining *H* and *I*.

As the final step of the hazard analysis, the impact hazard indication scores IH_i for all hypothetic events i are combined in order to derive a raster map of the global hazard indication score IH. The maximum score is used for each raster cell:

$$IH = max(IH_1, IH_2, \dots, IH_n), \qquad \text{Eq. 2}$$

where the indices 1, 2, ... , n represent the hypothetic event IH_i is associated with, n is the total number of possible onset areas for the considered process type.

Whilst the general concept outlined is applied to all types of hazards, the specific procedures for each process type are detailed in Section 4.2 – Section 4.5. Below, the subscript rs stands for rock slides, ia for ice avalanches, pf for periglacial debris flows and lo for lake outburst floods. Maps of IH and R are determined separately for each process.

Given the uncertainties inherent to the regional-scale hazard and risk analysis, the discretization of the results at a raster cell size of 60 x 60 m may pretend a level of detail not supported by the methodology used. According to the purpose of the study, the prioritization of target communities for risk mitigation measure, community-based risk indication scores for each process type (CR_{rs}, CR_{ia}, CR_{pf}, CR_{lo}) are derived. The maxima of the raster cell-based risk indication scores over all cells representing the considered village are applied. However, if the highest risk indication score R assigned to a community applies to an area <10,000 m², CR is reduced by 1. In such cases a lower score of R, if it applies to a larger area, may determine the score of CR for the community.

4.2 Rock slide hazard

The GRASS raster module employed for the rock slide hazard analysis is named r.rockslide and, to some extent, builds on the approach of Hergarten (2012). The logical framework of r.rockslide is illustrated in Fig. 5.

Loops over all raster cells within the study area are performed separately for four assumptions of sliding plane inclination $\beta_{s,i}$ (Table 5). If the local slope $\beta > \beta_{s,i}$ for a tested cell, the cell is considered as seed cell for a possible rock slide. In order to simulate a progressive failure, an inverse cone with a vertical axis and an inclination of $\beta_{s,i}$ is introduced. The apex of this cone coincides with the seed cell (see Fig. 5). All material above the cone surface (terrain elevation > cone elevation) is considered as potential rock slide material, imitating a rock slide involving all over-steepened terrain with respect to the base cell. For each seed cell, the volume V_{rs} removed by the associated rock slide is recorded.

The susceptibility score S_{rs} for each cell with terrain elevation > cone elevation is determined according to Table 5, including the sliding plane inclination $\beta_{s,i}$ and the permafrost susceptibility S_p as conditioning factors, and the seismic susceptibility S_s as possible triggering factor. S_{rs} can take values in the range 0–6. The rock slide hazard indication score H_{rs} is computed according to Table 3, with the possible event magnitude represented by the rock slide volume V_{rs}. Each cell may possibly be affected by rock slides from more than one seed cell. The final hazard indication score for each raster cell is defined as the maximum of $H_{rs,i}$ out of all relevant possible rock slides i:

$$H_{rs} = max\left(H_{rs,1}, H_{rs,2}, \ldots, H_{rs,n}\right), \quad \text{Eq. 3}$$

where the indices 1, 2, ... *n* denote the id of the considered possible rock slide, *n* is the number of possible rock slides.

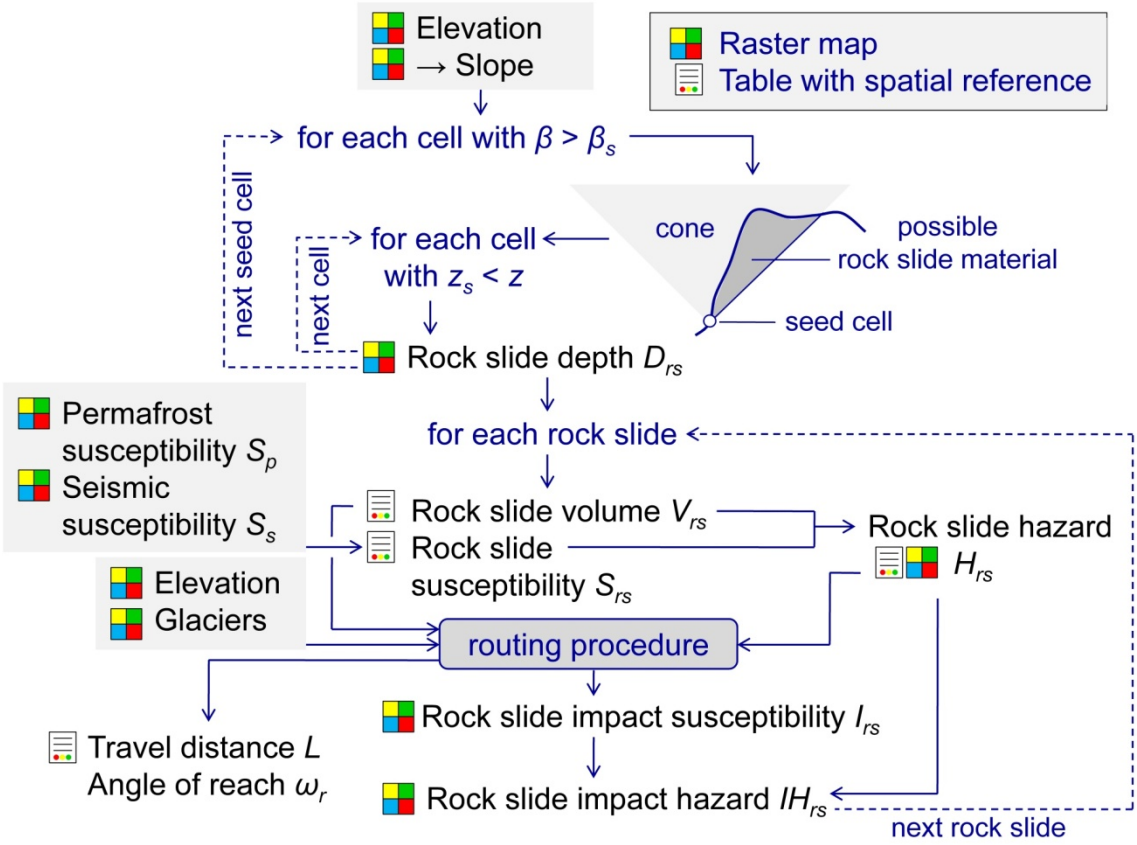

Fig. 5 Logical framework of the rock slide model (r.rockslide).

The expected travel distance is estimated separately for each single possible slide (see Fig. 5), using a relationship of the type

$$\log_{10} \tan \omega_r = a \log_{10} V_r + b, \quad \text{Eq. 4}$$

where ω_r is the angle of reach and V_{rs} is the rock slide volume. The curve has to be cut off at $\tan \omega = \tan \varphi$, where φ is the angle of repose. Eq. 4 is only valid as long as the slide starts from rest. *a* and *b* depend on the process type, *b* can also be varied in order to account for uncertainties of the relationship used. Two relationships are applied:

4. For rock slides in non-glacierized areas, the prediction curve suggested by Scheidegger (1973) is used. It was derived from a set of 33 historic and prehistoric events. The correlation coefficient is 0.82, the standard deviation is 0.14298. a = -0.15666, b = 0.62419 for the average and 0.36418 for the envelope.
5. It is well established that rock slides in glacierized areas often convert into rock-ice avalanches with longer travel distances (Evans and Clague, 1988; Bottino et al., 2002). If the rock slide starts in a glacierized area, or as soon as it moves over a glacier, the relationship suggested by Noetzli et al. (2006) is applied: a = -0.103, b = 0.165 for the average and -0.040 for the envelope.

Table 5 Rock slide susceptibility score S_{rs}. The initial values of S_{rs} are determined from the sliding plane inclination $\beta_{s,i}$, these values are then increased according to permafrost susceptibility and seismic susceptibility, g is gravity (m s^{-2}).

Criterion	Remarks	S_{rs}
Sliding plane inclination $\beta_{s,i}$	tan ($\beta_{s,i}$) ≥ 1.000 – < 1.333	1
	tan ($\beta_{s,i}$) ≥ 1.333 – < 1.667	2
	tan ($\beta_{s,i}$) ≥ 1.667 – < 2.000	3
	tan ($\beta_{s,i}$) ≥ 2.000	4
Permafrost susceptibility	No permafrost or stable permafrost	±0
	Susceptible to melting at ΔMAAT >0 – 4°	+1
Seismic susceptibility	PGA < 0.34 g	±0
	PGA ≥0.34 – <0.65 g	+1
	PGA ≥ 0.65 g	+2

The steeper regression line for non-glacierized areas results in the prediction of longer travel distances by the Scheidegger (1973) model for very large volumes (V_r > 361 10^6 m³ for the regression, V_r > 34 10^6 m³ for the envelope). This phenomenon has no physical basis but can most likely be attributed to a lack of very large events in the data set used by Noetzli et al. (2006). In the r.rockslide model, the relationship yielding the longer travel distance is used for rock slides in glacierized areas. Further, the runup height R at the opposite slope is limited by the envelope of the regression derived from the dataset presented by Hewitt et al. (2008):

$$\log_{10} R \leq 0.375 \cdot \log_{10} V_r - 0.62077 \,. \quad \text{Eq. 5}$$

100 random walks are performed for each rock slide or rock-ice avalanche, each of them starting at the highest raster cell of the hypothetic failure plane. The impact susceptibility score I_{rs} and the impact hazard indication score IH_{rs} are finally derived according to Eq. 1, Eq. 2 and Table 4. Eq. 1 is here applied with the logarithms of tan ω, tan $\omega_{r,E}$ and tan $\omega_{r,A}$.

4.3 Ice avalanche hazard

The logical framework of the ice avalanche hazard model r.iceaval is illustrated in Fig. 6. The slope beyond which glaciers or portions of glaciers are susceptible to produce ice avalanches depends on the properties of the ice which are strongly determined by the ice temperature. As data on ice temperature is not commonly available, mean annual air temperature is often used as a surrogate. Huggel et al. (2004a) state that temperate glaciers produce ice avalanches at slopes above 25°, cold glaciers at slopes above 45°. Here, a set of 11 cases (Alean, 1985; Huggel et al., 2004a) is taken as the basis for devising a scheme for ice avalanche susceptibility S_{ia} (Fig. 7). A quadratic regression is fitted for this purpose, with

$$\tan\beta = 3.2 \cdot 10^{-3} MAAT^2 - 2.03 \cdot 10^{-2} MAAT + \eta \,, \quad \text{Eq. 6}$$

where β is the slope and $MAAT$ is the mean annual air temperature (°C). The intercept $\eta = 0.5555$ for the regression and 0.357672 for the envelope. The thresholds applied to the ice avalanche susceptibility classes $S_{ia} = 0–4$ are determined from Eq. 1 with η set in the way to split the data set into quartiles (see Fig. 7). S_{ia} is increased according to the seismic susceptibility (see Table 1) so that the possible score values cover a range from 0–6.

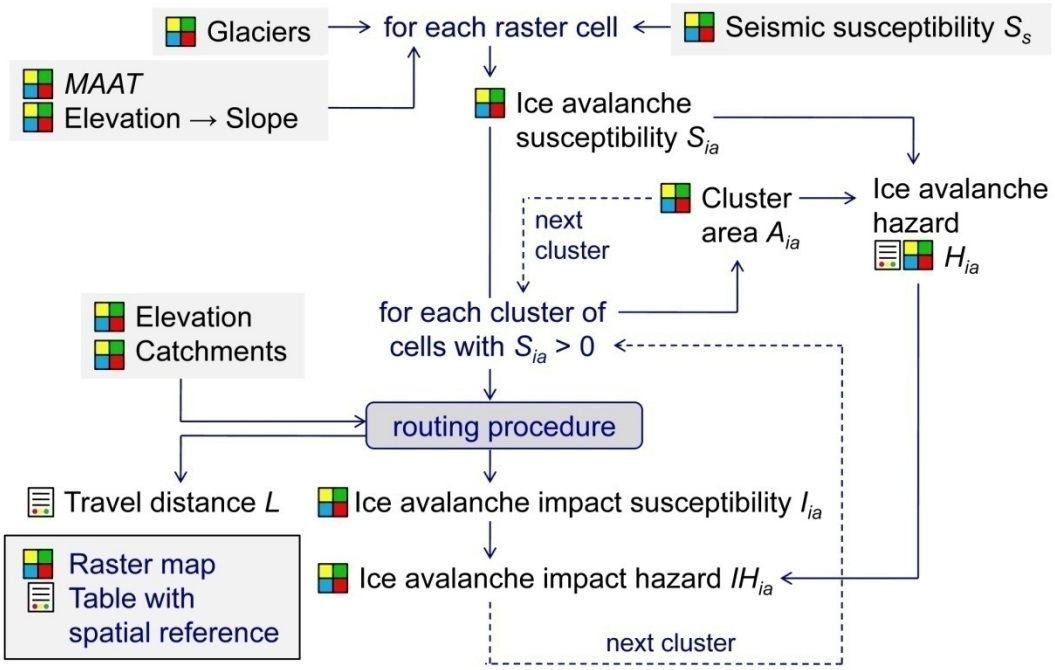

Fig. 6 Logical framework of the ice avalanche model (r.iceaval).

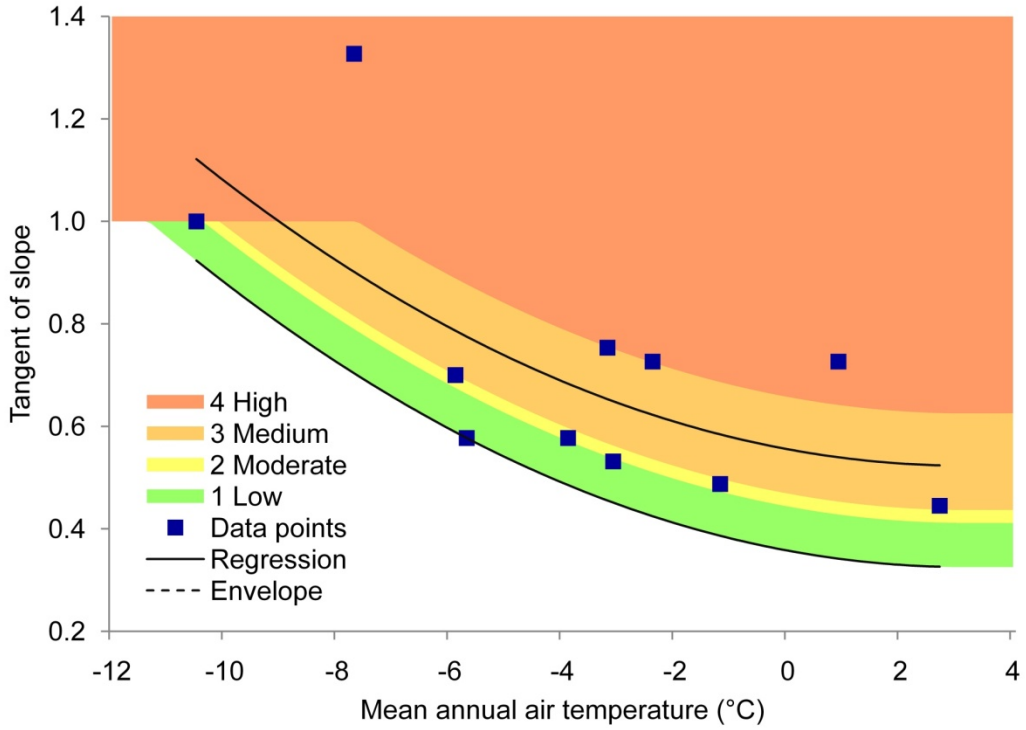

Fig. 7 Scoring scheme applied for ice avalanche susceptibility according to data presented by Alean (1985) and Huggel et al. (2004a).

Next, clusters of cells with $S_{ia}>0$ are identified. S_{ia} is increased by 1 for all clusters at glacier termini (no abutment). The ice avalanche hazard indication score H_{ia} is derived according to Table 3, combining S_{ia} and the area of each cluster.

For each cluster, 100 random walks are applied for routing the possible ice avalanche down, starting at the highest point of the cluster. According to Huggel et al. (2004a), the travel path of ice avalanches is constrained by an average slope of 17°, except for very large events (>5 10^6 m³). However, such events are most commonly rock-ice avalanches or complex process chains (e.g., 1962 and 1970 Huascarán events, 2002 Kolka/Karmadon event), which are covered separately here, or related to volcanic processes (1980 Iliamna event, Alaska). Therefore, and since the ice avalanche volume cannot be derived with the method applied, we constrain the impact area with an average slope of 17° (tan $\omega_{r,E} = 0.31$). In the dataset used by Huggel et al. (2004a), the minimum value of the average slope is tan $\omega = 0.44$, tan $\omega_{r,E}$ is set to the average 0.375 and I_{ia} is computed according to Eq. 1. Eq. 2 and Table 4 are applied in order to derive the ice avalanche impact hazard indication score IH_{ia}.

4.4 Periglacial debris flow hazard

Melting permafrost on steep slopes leaves behind a certain amount of loose debris susceptible to mobilization as debris flows. Such processes may occur in the active layer, but even more where permafrost is retreating. Here, we only consider areas where retreating permafrost is assumed (see Table 1; Mergili et al., 2012a). Fig. 8 shows the logical frame work of the periglacial debris flow model r.periflow. Huggel et al. (2004b) noted that, in contrast to ordinary debris flows, parameters such as slope curvature or the proximity to the stream network are hardly significant for the onset of such processes. Further, they commonly occur at slope angles from 27–38°. Table 6 shows the scheme applied here for deriving the susceptibility of each raster cell to periglacial debris flows S_{pf} in the range from 0–6. We follow the findings of Huggel et al. (2004b) with regard to slope. Unfortunately, no means for the reliable distinction of bedrock and debris at the relevant scale are known to the authors. Besides slope and the state of the permafrost, the seismic susceptibility is considered for deriving S_{pf} (see Table 1 and Table 6).

In contrast to the other processes considered in the present study, there are no means to approximate the onset volume and therefore the process magnitude. Clusters of susceptible cells are often large whilst the onset of debris flow processes is most commonly a rather localized process. We therefore use the approximation $H_{pf} = S_{pf}$ (see Fig. 8).

Consequently, the routing procedure (i) has to be started separately from each raster cell with $S_{pf} > 0$, and (ii) the average slope determining the impact area has to be independent from volume. Due to the commonly large clusters of starting cells, only 10 random walks are started from each cell. Huggel et al. (2004b) give an envelope average slope of the travel path of 11° (tan $\omega_{r,E} = 0.194$) which is also applied here. The maximum average slope is taken from Corominas et al. (2003) who provide a value of 26° (tan $\omega = 0.488$) for debris flows <800 m³ propagating on undisturbed flow paths assumed for the study area. The average of the two values, 0.341, is taken as tan $\omega_{r,A}$. I_{pf} is computed according to Eq. 1. For $I_{pf} < 4$, the runup on the opposite slope is restricted. Eq. 2 and Table 4 are applied to derive the periglacial debris flow impact hazard indication score IH_{pf}.

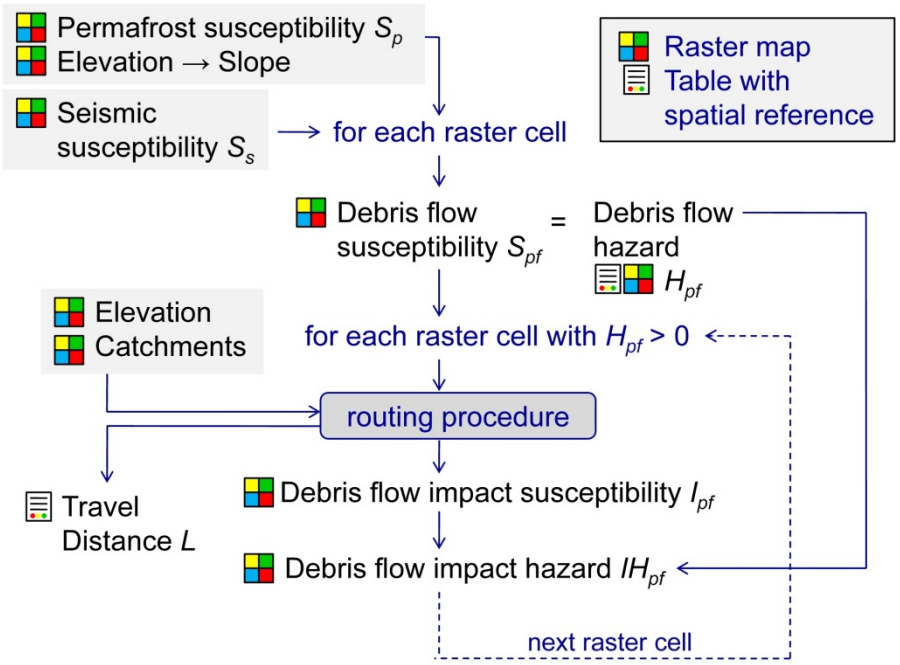

Fig. 8 Logical framework of the periglacial debris flow model (r.periflow).

Table 6 Scoring scheme for periglacial debris flow susceptibility S_{pf}.

Criterion	Remarks	$S_{lo,i}$
Slope β	$\tan\beta < 0.5$	0
	$\tan\beta = 0.5 - <0.6$	1
	$\tan\beta = 0.6 - <0.7$	2
	$\tan\beta = 0.7 - 0.8$	3
	$\tan\beta > 0.8$	0
Permafrost susceptibility	No permafrost or stable permafrost	0
	Susceptible to melting at ΔMAAT >2 – 4°	±0
	Susceptible to melting at ΔMAAT >0 – 2°	+2
Seismic susceptibility	PGA< 0.65 g	±0
	PGA≥ 0.65 g	+1

4.5 Lake outburst hazard

An improved version of the GRASS GIS raster module r.glof (Mergili and Schneider, 2011) is used for the lake outburst hazard analysis. The logical framework of r.glof is illustrated in Fig. 9.

First, the susceptibility scores for (i) lake outburst caused by internal factors (dam failure) $S_{lo,i}$ and (ii) lake outburst triggered by external factors (impact of mass movements) $S_{lo,e}$ are considered separately (see Fig. 9). $S_{lo,i}$ and $S_{lo,e}$ can take values in the range 0–6, negative values are set to 0.

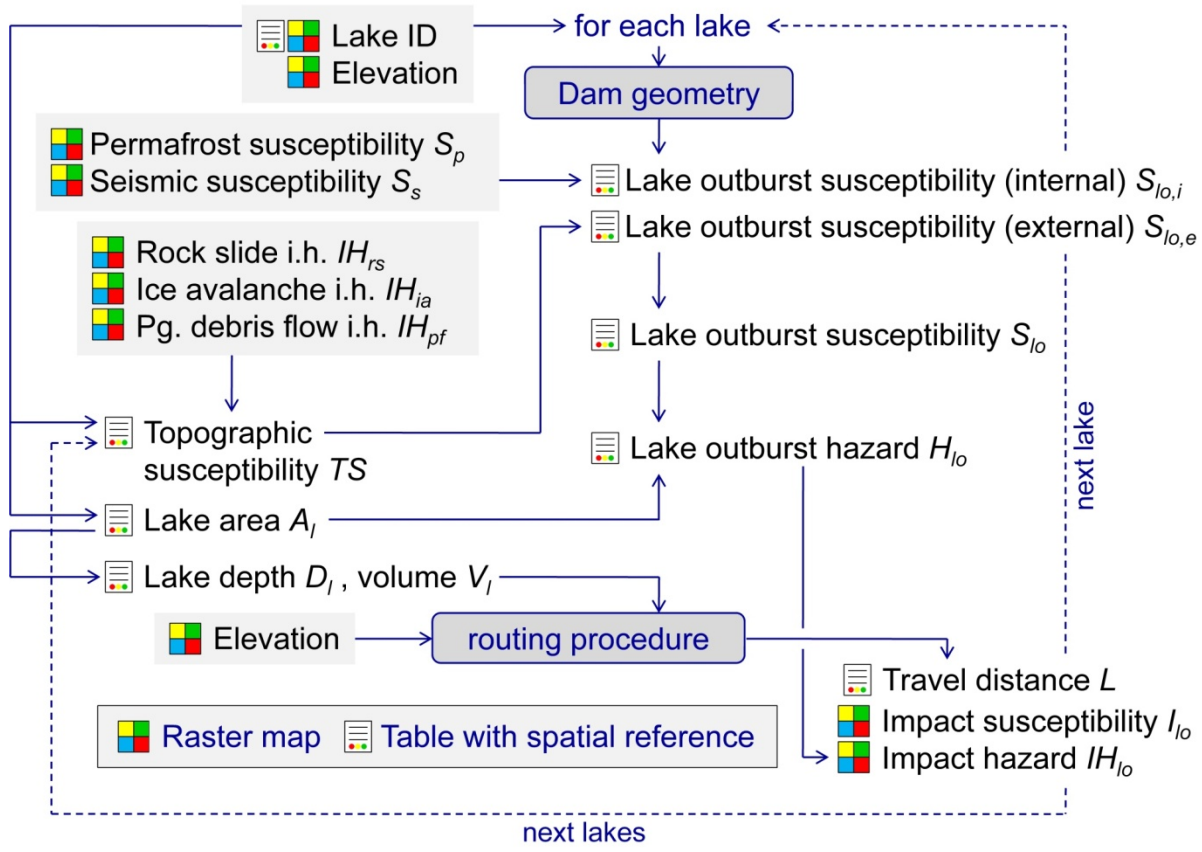

Fig. 9 Logical framework of the lake outburst model (r.glof).

The derivation of $S_{lo,i}$ builds on the following key parameters: (i) lake type, indicating the dam material; (ii) mode of lake drainage; (iii) lake evolution; (iv) dam geometry; (v) permafrost susceptibility; (vi) seismic susceptibility (see Table 1). Table 7 shows the scoring scheme applied. The lake type (Mergili et al., 2013) is taken as basis, with glacial lakes receiving the highest score. Dams with seepage are considered more susceptible to failure than dams with surface runoff, and growing lakes are considered more susceptible than stable or shrinking ones. The dam geometry is expressed as an idealized average downstream slope of the dam: the dam width W is defined as the Euclidean distance between the lake outlet and the closest raster cell along the downstream flow path with a lower elevation than the average lake bottom, using the average lake depth D_l according to Huggel et al. (2002):

$$D_l = 1.04 \cdot 10^{-1} A_l^{0.42}, \text{ Eq. 7}$$

where A_l is the lake area (m²), D_l is given in m. The tangent of the average slope of the dam in outflow direction, $\tan \beta_d$, is derived as D_l/W. For very gentle downstream average slopes $\tan \beta_d < 0.02$, $S_{lo,i}$ is decreased by 1 (see Table 7).

The event at Laguna 513 in the Cordillera Blanca (Haeberli et al., 2010b) has shown the need to include the entire catchment when analyzing lake outburst susceptibility. The topographic susceptibility TS is introduced in order to account for this need, employing the impact hazard indication scores for rock slides IH_{rs}, for ice avalanches IH_{ia}, for periglacial debris flows IH_{pf}, and for outburst floods of lakes in the upper catchment IH_{lo}. The overall maximum score over the

raster cells representing the considered lake ($IH_{ia,max}$, $IH_{rs,max}$, $IH_{pf,max}$ and $IH_{lo,max}$) applies, but the impact of periglacial debris flows and upstream lake outburst floods is down-weighted:

$$TS = max(IH_{rs,max}, IH_{ia,max}, IH_{pf,max} - 3, IH_{lo,max} - 3). \quad \text{Eq. 8}$$

The topographic susceptibility is taken as the basis for the rating of the susceptibility to lake outburst triggered by external factors $S_{lo,e}$. If direct calving of ice into the lake is possible, the score for $S_{lo,e}$ is set to a minimum of 3.

The maximum of $S_{lo,i}$ and $S_{lo,e}$ is used as lake outburst susceptibility S_{lo}. S_{lo} is reduced for lakes with a high freeboard F (defined as the difference between the DEM with filled sinks and the original DEM for the lake centre): for lakes with $F > 50$ m the score is decreased by 3. For lakes with $F > 25$ m it is decreased by 2, and for lakes with $F > 10$ m, the score is decreased by 1 in order to derive the final value of S_{lo}.

The lake area is most likely the best surrogate for M_{lo} since the lake volume is uncertain. Table 7 shows the matrix for the lake outburst hazard indication score H_{lo} which is discretized on the basis of lakes.

Table 7 Scoring scheme for susceptibility to lake outburst triggered by internal factors S_{lo}. The initial values of S_{lo} are determined from the dam material, these values are then increased or decreased according to lake drainage, lake evolution, downstream slope of dam, permafrost susceptibility and seismic susceptibility.

Criterion	Remarks	$S_{lo,i}$
Lake type (dam material)	Erosion lake	0
	Block- or debris-dammed lake	1
	Glacial lake	3
Lake drainage	Permanent or temporary superficial drainage	-1
	No recognizable superficial drainage	±0
Lake evolution	Stable or shrinking	±0
	Growing trend in either the period 1968–2002 or 2002–2009	+1
Downstream slope of dam β_d	$\tan \beta_d < 0.02$	-1
	$\tan \beta_d \geq 0.02$	±0
Permafrost susceptibility	No permafrost or stable permafrost	±0
	Susceptible to melting at ΔMAAT >0 – 4°	+1
Seismic susceptibility	PGA< 0.65 g	±0
	PGA≥ 0.65 g	+1

Possible outburst floods are routed downwards through the DEM separately for each lake, the travel distance is determined according to the relationships listed in Table 8. After the deposition

of the debris or mud, or if not much sediment is entrained at all, the flood may propagate much farther: Haeberli (1983) suggests an average angle of reach of 2–3°, but also travel distances exceeding 200 km are reported (e.g., Hewitt, 1982).

In order to achieve a robust estimate of the travel distance, the impact area of possible lake outburst floods and, consequently, the impact susceptibility I_{lo}, the approaches T1 – T4 shown in Table 8 are combined (Eq. 1 is not applied for lake outburst floods). The lake outburst flood is routed down starting from the outlet of the considered lake. 800 random walks are performed for each lake. A random walk is forced to terminate if it impacts a larger lake.

Table 8 Empirical relationships used for estimating the travel distance of lake outburst floods. GLOF = glacial lake outburst flood, L = travel distance, V_d = debris flow volume, ΔZ = loss of elevation, ω_r = average slope of reach, Q_p = peak discharge.

	Relationship	References	Remarks
T1	$L = 1.9 V_d^{0.16} \Delta Z^{0.83}$	Rickenmann (1999)	for debris flows in general
T2	$\omega_r = 11°$	Haeberli (1983), Huggel et al. (2003), Huggel et al. (2004a)	for debris flows from GLOFs, applied with $\omega_r = 8°$ in the present study (Mergili and Schneider, 2011)
T3	$\omega_r = 18 Q_p^{-0.07}$	Huggel (2004)	worst case for debris flows from GLOFs
T4	$\omega_r \geq 2°$	Haeberli (1983), Huggel et al. (2004a)	for floods from GLOFs

Table 9 Empirical regression equations relating peak discharge Q_p of glacial lakes to outburst volume V_l and lake depth (dam height) D_l. ϱ_w = density of water (kg/m²), g = gravity (m/s²), *envelope (worst case).

Reference		Q_p (m³/s) of glacial lakes
Costa (1985)	Q1	$113 (10^{-6} V_l)^{0.61}$
	Q2	$3.8 (10^{-6} V_l D_l)^{0.61}$
Costa and Schuster (1988)	Q3	$1.3 \cdot 10^{-4} (\rho_W \cdot g \cdot V_l \cdot D_l)^{0.60}$
	Q4	$5.5 \cdot 10^{-6} (\rho_W \cdot g \cdot V_l \cdot D_l)^{0.59}$
Walder and O'Connor (1997)	Q5*	$2.2 \cdot 10^{-1} V_l^{0,66}$
	Q6*	$1.1 (V_l D_l)^{0,47}$

For T1, the debris flow volume V_d is set to five times the outburst volume (maximum sediment concentration in steep flow channels ~80% according to Iverson, 1997) in order to account for sediment bulking. The outburst volume is set to the entire lake volume, lake area A_l multiplied with lake depth D_l). For T2, we use an angle of reach $\omega_r = 8°$ which is most likely more suitable for the study area (Mergili and Schneider, 2011) than $\omega_r = 11°$ as suggested by Haeberli (1983). Several authors have introduced empirical relationships for relating the peak discharge Q_p (m³/s) – required as input for the relationship T3 in Table 8 – to the outburst volume and the dam height (Costa, 1985; Costa and Schuster, 1988; Walder and O'Connor, 1997; Table 9). Q_p is determined from the maximum of the results computed with the relationships Q1 to Q6 shown in Table 9. T1 and T3 are only applied to glacial lakes as there is no basis available for calculating the depth or volume of lakes assigned to the other types. Instead, the angle of reach is set to $\omega_r = 11°$ (the value suggested by Haeberli, 1983) for T1 and to $\omega_r = 14°$ for T3.

The number of relationships T1 – T4 (see Table 8) predicting an impact on a given raster cell determines the impact susceptibility: if all four relationships predict an impact, $I_{lo} = 6$, three relationships results in $I_{lo} = 5$ and so forth. For $I_{lo} < 6$, the runup on the opposite slope is restricted. If only an impact as flood is predicted, (T4; $I_{lo} \leq 3$), the impact susceptibility is further differentiated according to ω: for $\omega \geq 6$, $I_{lo} = 3$, for $\omega \geq 4$, $I_{lo} = 2$ and for $\omega \geq 2$, $I_{lo} = 1$. T4 is only applied to lakes ≥50,000 m². Furthermore, the criterion that the distance from the source has to increase with each computing step is disabled for floods.

In an analogous way to the scores for the rock slides, ice avalanches and periglacial debris flows (see Section 4.2 to Section 4.4), the impact hazard indication score is then derived by combining I_{lo} with H_{lo} of the corresponding lake (see Table 4). The global impact hazard indication score IH_{lo} of a given raster cell is defined as the maximum of all lake-specific scores (see Eq. 2).

5 Results

The total area with significant periglacial debris flow (PF) susceptibility/hazard is much larger than those for the other hazard types: 9.9% of the entire study area are designated as possible PF source areas, based on the criteria defined in Table 6. 42.7% out of this area are assigned the three higher susceptibility scores 4–6 (Fig. 10a). This pattern indicates the ubiquity of hazardous areas on the one hand, but also the limited means of a sharper delineation on the other hand. In contrast, the ice avalanche (IA) susceptibility and the lake outburst (LO) susceptibility, due to their confinement to glaciers and lakes, respectively, are constrained in a much sharper way. 1.6% of the total study area are identified as susceptible to IA, 64.5% out of this area are assigned the susceptibility scores 4–6 (see Fig. 10a). The LO susceptibility is discretized on the basis of lakes. 70.9% of all lakes are assigned susceptibility scores >0, 50.0% of these lakes the susceptibility scores 4–6 (see Fig. 10a). The rock slide (RS) susceptibility displays intermediate patterns in terms of the total area identified as susceptible (4.7% of the total study area). However, only 16.2% of this area – a much lower value than those associated with the other process types – are assigned the susceptibility scores 4–6 (see Fig. 10a). The reason for this phenomenon is the limited area occupied by very steep slopes (see Table 5).

The distribution of the raster cells or lakes identified as susceptible among the six hazard indication score classes is illustrated in Fig. 10b, depending on the susceptibility and the possible process magnitude (see Table 3). 38.1% of the RS and 68.4% of the IA are assigned the hazard indication scores 4–6. In the case of PF, hazard and susceptibility are identical due to lacking means for an estimation of the magnitude (see Section 4.4). Comparatively few lakes (23.9%) are assigned the LO hazard indication scores 4–6. This phenomenon is explained by the large number of rather small but highly susceptible lakes.

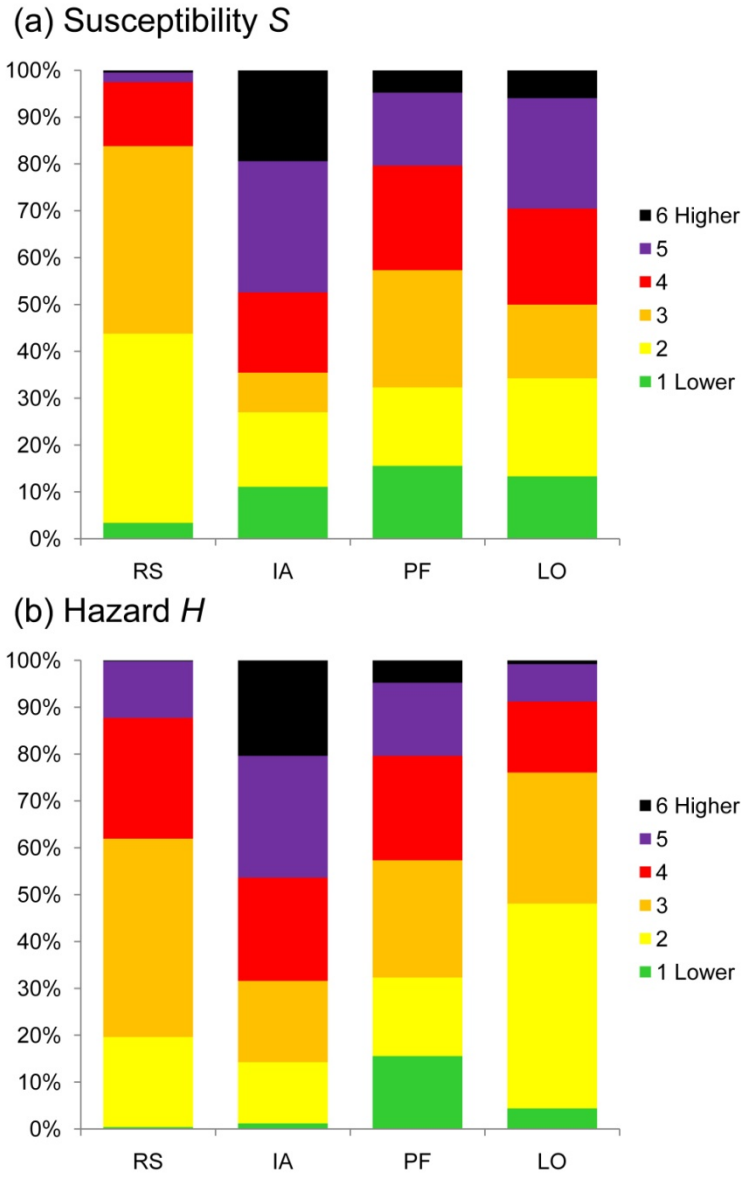

Fig. 10 Relative abundance of (a) the susceptibility and (b) the hazard indication score values for the four considered processes. The values for rock slides (RS), ice avalanches (IA) and periglacial debris flows (PF) relate to raster cells, the values for lake outburst floods (LO) to lakes. Only those raster cells or lakes with a score of at least 1 are considered.

Fig. 11 represents the hazard indication scores for each process type broken down to the level of small catchments identical to the output parameter basin of the GRASS GIS raster module r.watershed (GRASS Development Team, 2013) with a threshold parameter of 5000. The

maximum out of all raster cell-based hazard indication scores is shown for each catchment, except for the LO hazard where the value assigned to each lake is illustrated.

As expected, the RS hazard (see Fig. 11a) is highest in areas with a particularly steep topography in the northern and central Pamir. More localized high-hazard areas are distributed throughout the study area. The IA hazard (see Fig. 11b) is high in most glacierized areas (see Fig. 3d), particularly in parts of the northern Pamir where large portions of steep glaciers are extremely abundant. Within these zones the inter-catchment differentiation of hazardous areas is rather poor.

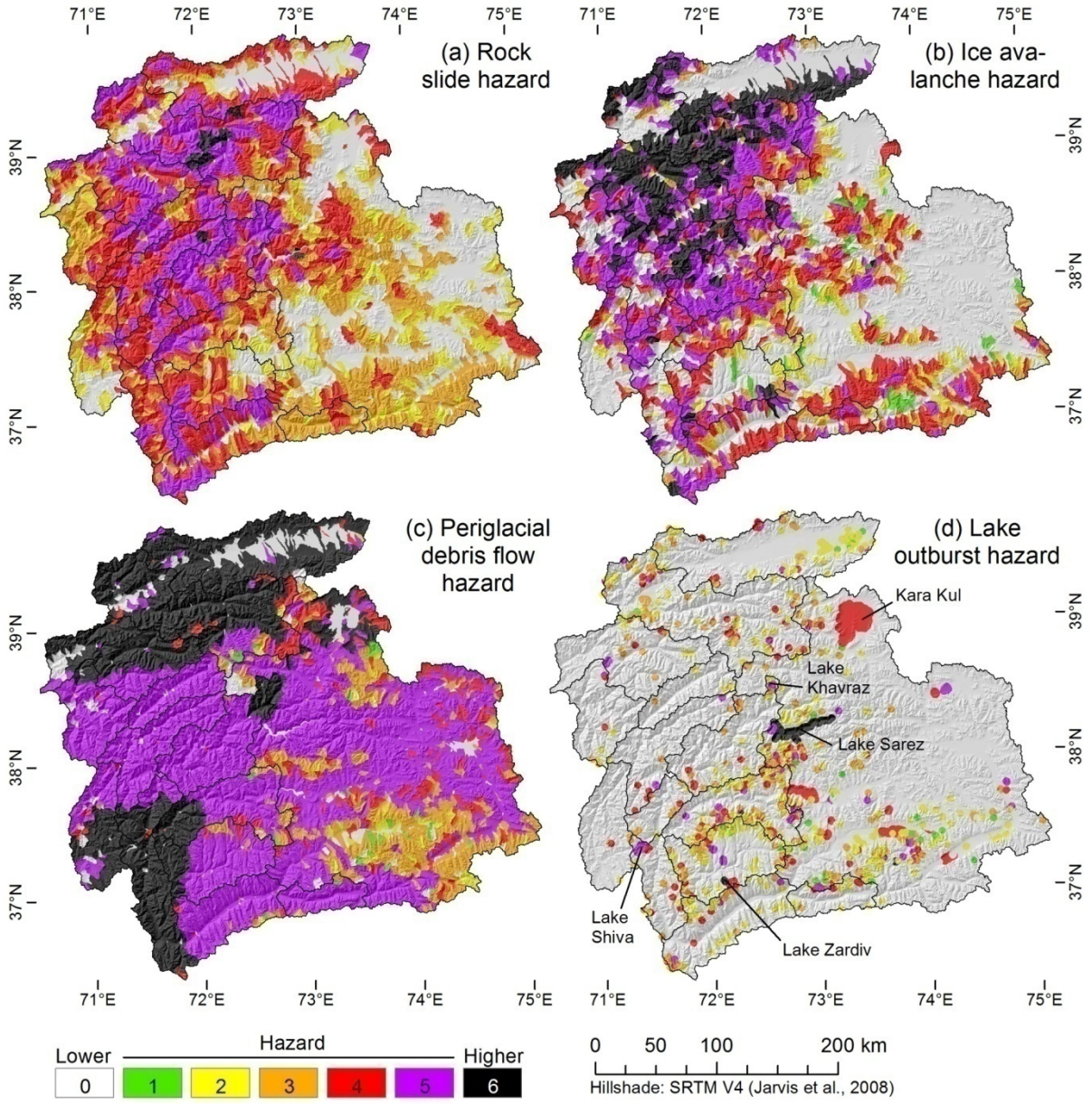

Fig. 11 Distribution of (a) rock slide, (b) ice avalanche, (c) periglacial debris flow and (d) lake outburst hazard over the entire study area. The maximum score is shown for each catchment.

The PF hazard is poorly differentiated at the catchment scale: steep slopes near the permafrost boundary are almost ubiquitous in the study area (see Fig. 3b), except for the elevated and comparatively gently inclined south eastern portion. The most notable regional pattern is

therefore attributed to the seismic susceptibility. The patterns observed in Fig. 11c are further a consequence of the limited input information that can be reasonably applied at the regional scale (see Table 6). A detailed inventory of rock glaciers (comparable to the inventories prepared for glaciers and lakes, see Fig. 3d) could help to sharpen the distinction between more and less hazardous areas. However, as rock glaciers are extremely common throughout the study area, the patterns at the inter-catchment level would most likely remain unchanged.

As the LO hazard is directly related to the well-known lake distribution it can be discretized at a high level of detail (see Fig. 11d). Nine lakes are assigned the highest LO hazard indication score $H_{lo} = 6$, the largest of them is Lake Sarez. Even though – or because – the safety of Lake Sarez is highly disputed (e.g., Risley et al., 2006), this classification seems reasonable. The LO susceptibility score $S_{lo} = 5$ is a consequence of the high topographic susceptibility. The same is true for Lake Zardiv, with 0.7 km² the second largest lakes with $H_{lo} = 6$ (see Fig. 11d).

Table 10 Percentage of lakes assigned each class of lake outburst (LO) susceptibility (internal and external factors) and hazard indication scores according to lake type.

Lake type	LO susceptibility score (internal factors)							
	0	1	2	3	4	5	6	Sum
Erosion lakes	33.1%	40.8%	24.7%	1.5%	0.0%	0.0%	0.0%	883
Block- or debris-dammed lakes	12.4%	17.1%	44.8%	24.8%	1.0%	0.0%	0.0%	105
Glacial lakes	38.2%	0.0%	0.0%	4.4%	31.1%	24.5%	1.7%	652
	LO susceptibility score (external factors)							
	0	1	2	3	4	5	6	Sum
Erosion lakes	42.1%	5.3%	18.9%	16.5%	7.5%	7.7%	1.9%	883
Block- or debris-dammed lakes	18.1%	1.0%	10.5%	14.3%	18.1%	32.4%	5.7%	105
Glacial lakes	40.8%	0.2%	3.5%	11.3%	15.5%	21.3%	7.4%	652
	LO hazard indication score							
	0	1	2	3	4	5	6	Sum
Erosion lakes	24.5%	5.8%	34.2%	19.0%	10.6%	5.3%	0.6%	883
Block- or debris-dammed lakes	12.4%	0.0%	31.4%	23.8%	13.3%	16.2%	2.9%	105
Glacial lakes	38.2%	0.0%	26.5%	20.2%	10.4%	4.4%	0.2%	652

Further lakes of interest are, e.g., Lake Khavraz and Lake Shiva. Lake Khavraz is an 1.9 km² lake impounded behind a rock glacier at an elevation of 4000 m a.s.l., in the zone of possibly melting

permafrost. Here both the topographic susceptibility ($S_{lo,e}$ = 5) and the LO susceptibility due to internal factors ($S_{lo,i}$ = 5) are at high levels. Lake Shiva is assigned a susceptibility in the medium range of the scale (S_{lo} = 3) and a sudden drainage is not likely but, due to the large size of 15.2 km², H_{lo} = 5. The lake is located close to several communities in the Panj Valley which could be affected in the case of such an event. The largest lake in the study area, Kara Kul, is assigned a hazard indication score of 4 (see Fig. 11d). The LO susceptibility of Kara Kul is rated with a score of S_{lo} = 2, only the very large lake area (405 km²) leads to the relatively high hazard indication score. The fact that a closer look reveals no significant outburst hazard of Kara Kul suggests that the approach used tends to overestimate the hazard for large lakes. One reason for this phenomenon is the topographic susceptibility: large lakes have the ability to alleviate the impact of mass movements rather than small lakes. However, an objective basis to include the dependence of the topographic susceptibility on lake size is missing. Table 10 summarizes the LO susceptibility and hazard by lake type. Whilst – as prescribed by the scheme shown in Table 7 – glacial lakes clearly display the higher scores of the LO susceptibility due to internal factors, this tendency is less pronounced – but still visible – for the LO susceptibility due to external factors.

The median and maximum travel distances computed for each process type are summarized in Table 11. The RS model commonly predicts travel distances of 3.0 km (average) – 5.6 km (envelope), but for very large events (>800 10^6 m³) extending over vertical distances >4000 m the model, when applied with the envelope, predicts a travel distance of almost 50 km (see Eq. 4). The IA model ($\omega_{r,E}$ = 17°) and the PF model ($\omega_{r,E}$ = 11°) predict shorter travel distances. Note that, in both cases, the difference between the median and the maximum is only caused by topography and not by the assumed process magnitude. The LO model predicts the possibility of a significant debris flow for less than half of all lakes (no meaningful median value can therefore be given in Table 11). The reason for this phenomenon is mainly the gentle slope observed downstream from many lakes. However, lakes with steeper downstream slopes can produce debris flows with travel distances >15 km and floods >80 km, according to the model.

Fig. 12 shows the distribution of the impact hazard. For clarity, only the raster cell values along the main flow channels are shown. It is clear that the general patterns of the impact hazard at the broad scale resemble those of the hazard shown in Fig. 11: whilst a possible impact of rock slides and periglacial debris flows is shown for most valleys particularly in the western part of the study area (Fig. 12a and Fig. 12c), a more localized impact of ice avalanches and lake outburst floods is suggested by the model (Fig. 12b and Fig. 12d).

Table 11 Maximum and median travel distances L (m) computed for each process. RS = rock slides, IA = ice avalanches, PF = periglacial debris flows, LO = lake outburst floods, A = average, E = envelope, dfl = debris flow, fld = flood.

	RS (A)	RS (E)	IA (E)	PF (E)	LO (dfl)	LO (fld)
Maximum	23,867	49,516	10,735	15,906	15,597	81,946
Median	2,964	5,628	2,013	2,618	–	12,589

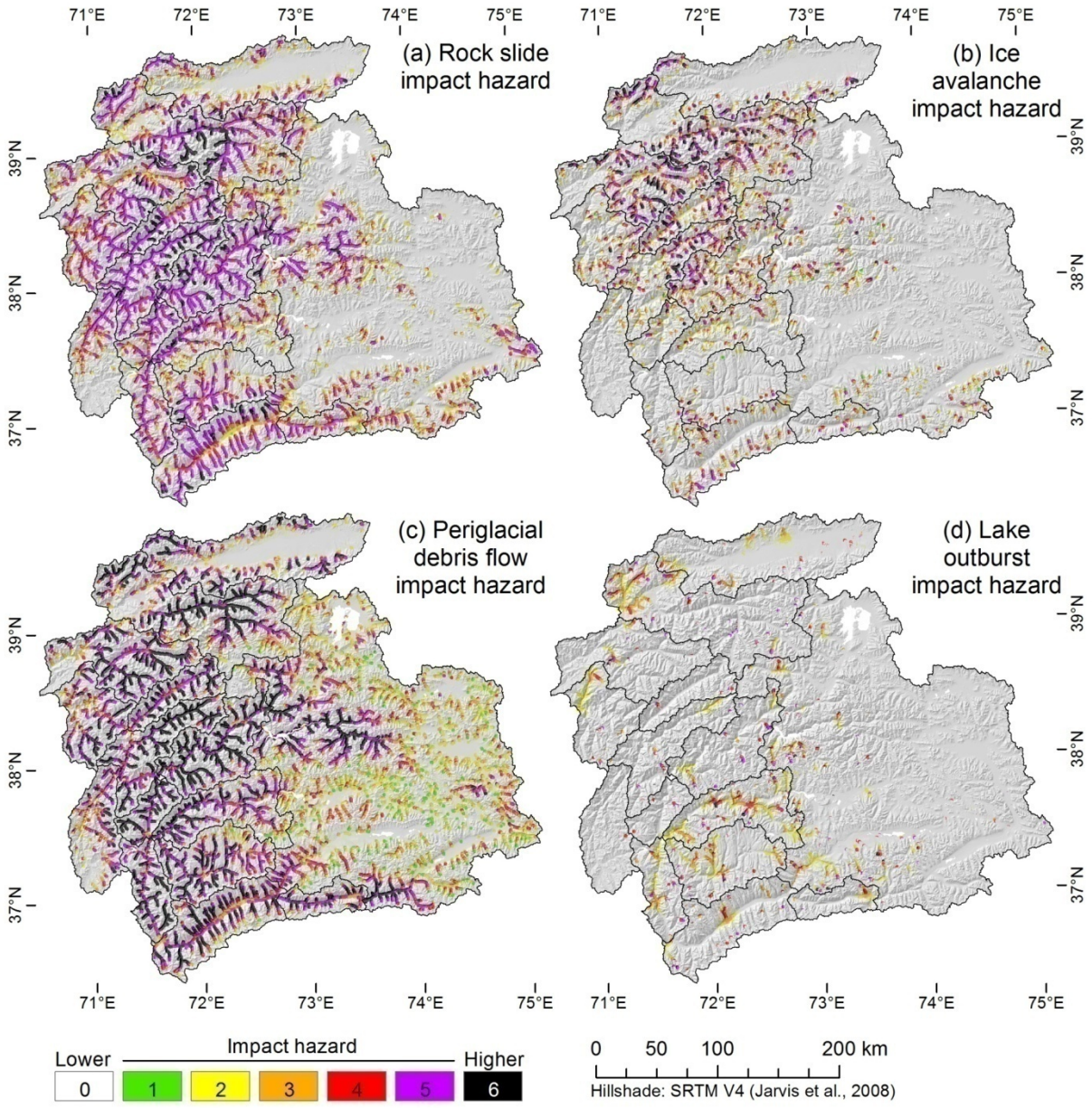

Fig. 12 Impact hazard for each process, (a) rock slides, (b) ice avalanches, (c) periglacial debris flows, (d) lake outburst floods. For clarity, only the scores along the main flow lines are shown.

The distribution of community risk over the study area reflects the patterns shown in Fig. 11 and Fig. 12 on the one hand, and the distribution of the exposed communities on the other hand. Fig. 13 illustrates the relative frequency of the community risk indication score classes for 15 regions within the study area, each of them representing a catchment or section of a catchment. The eastern Pamir is considered as one single region due to the low number of communities there. Except for the very western part of the study area, the eastern Pamir and the Kyrgyz part of the study area (Chan-Alai Valley) in the north, all regions are dominated by communities with a significant rock slide risk, the highest scores are observed for the villages in the rugged Bartang and middle Panj valleys as well as in the Gunt Valley (see Fig. 13a). The hot spots of ice avalanche risk are identified in the Vanch and Bartang valleys, both deeply incised into glacierized mountain ranges (see Fig. 13b). This type of risk plays a less prominent role in the other regions.

Also the risk of periglacial debris flows is highest in the deep gorges of the western Pamir, decreasing towards north where permafrost is less abundant (see Fig. 13c). However, the model predicts a significant PF risk for most communities throughout the study area. This is not the case for the risk caused by lake outburst floods, which is significant mainly in the south western Pamir and in part of the northern Pamir (see Fig. 13d). The LO community risk indication score $CR_{lo} = 6$ is not assigned to any village. Table 12 summarizes the relative frequency of villages assigned to each class with respect to all four hazard types.

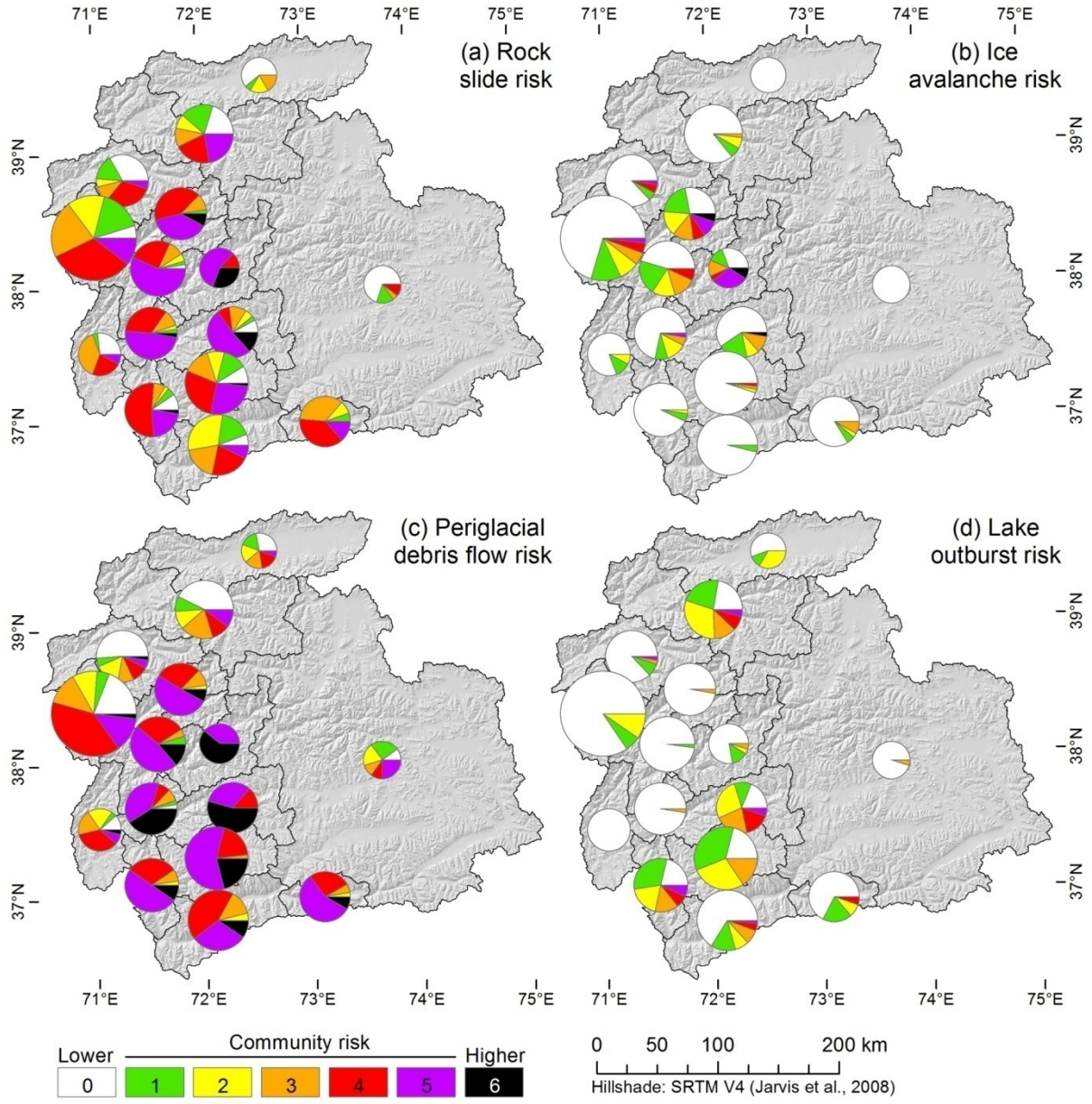

Fig. 13 Community risk, generalized to 15 regions. For each region, the pie chart illustrates the relative abundance of the different community risk indication scores. The size of each chart is proportional to the number of communities it represents.

A composite hazard and risk indication map is prepared for the entire study area. It provides a visual overlay of the hazard, impact hazard and community-based risk indication scores for each of the four process types considered in the study. Fig. 14 shows this map for a selected area

covering the Gunt Valley and its tributaries (see Fig. 1 for delineation). The area affected by the prehistoric Charthem rock slide (see Fig. 14a) is very well reproduced by the model, therefore a high RS risk is assigned to the nearby communities. However, also several other communities and lakes are possibly impacted by rock slides. The patterns of IA hazard and risk illustrate the isolated appearance of this type of hazard in the area (see Fig. 14b). Even though the main effect of the process is the possible impact on lakes, some communities in the main valley are at risk, but assigned rather low scores. Areas of PF hazard (see Fig. 14c) are strictly confined to steep slopes near the permafrost boundary which are however very common along the slopes of most valleys, confirming the broad-scale patterns shown in Fig. 11c. Therefore, most of the communities in the valleys are identified as at risk. The occurrence of periglacial debris flows in this area, often starting from the termini of rock glaciers, is evident in the field and from remotely sensed imagery (see Fig. 2c). The associated debris cones are located in zones of high impact hazard identified by the model. In contrast, most lakes are located where permafrost is assumed stable.

Table 12 Per cent of communities assigned to each class of the community risk indication score. RS = rock slides, IA = ice avalanches, PF = periglacial debris flows, LO = lake outburst floods.

Process type	Community risk indication score						
	0	1	2	3	4	5	6
RS	12.1%	9.7%	8.6%	15.3%	27.5%	23.9%	2.9%
IA	75.2%	8.9%	5.7%	4.8%	2.2%	2.4%	0.8%
PF	11.5%	3.7%	6.1%	9.2%	24.4%	31.4%	13.9%
LO	65.6%	12.3%	11.6%	6.2%	2.9%	1.4%	0.0%

Several lakes have developed near the termini of the glaciers of the tributary valleys (Mergili and Schneider, 2011; Mergili et al., 2013). Three of them are assigned the hazard indication score $H_{lo} = 5$ (see Fig. 14d). The debris flow travel distances predicted by the LO model are relatively short, only debris flows from two lakes could reach the communities of the main valley: the village of Varshedz is just located at the terminus of a possible debris flow starting from Lake Varshedz (see Fig. 2d; lake area 0.16 km², $S_{lo} = 5$, $H_{lo} = 5$). Lake Nimats, an erosion lake with $S_{lo} = 4$ and $H_{lo} = 5$, drains into a very steep channel heading directly down to the main valley. In the case of a (not very likely) sudden drainage, the nearby villages would most likely suffer substantial damage. The impact area of the distal floods resulting from the possible drainage of Lake Varshedz or Lake Nimats is characterized by lower to medium community risk indication scores of the possibly affected villages. The largest lake shown in Fig. 14d is Rivakkul (1.2 km², $S_{lo} = 4$, $H_{lo} = 5$). It is characterized by a very gently inclined downstream valley. As a result, the model predicts only a comparatively short travel distance of a possible outburst flood (4.6 km), being alleviated far upslope from the villages in the main valley.

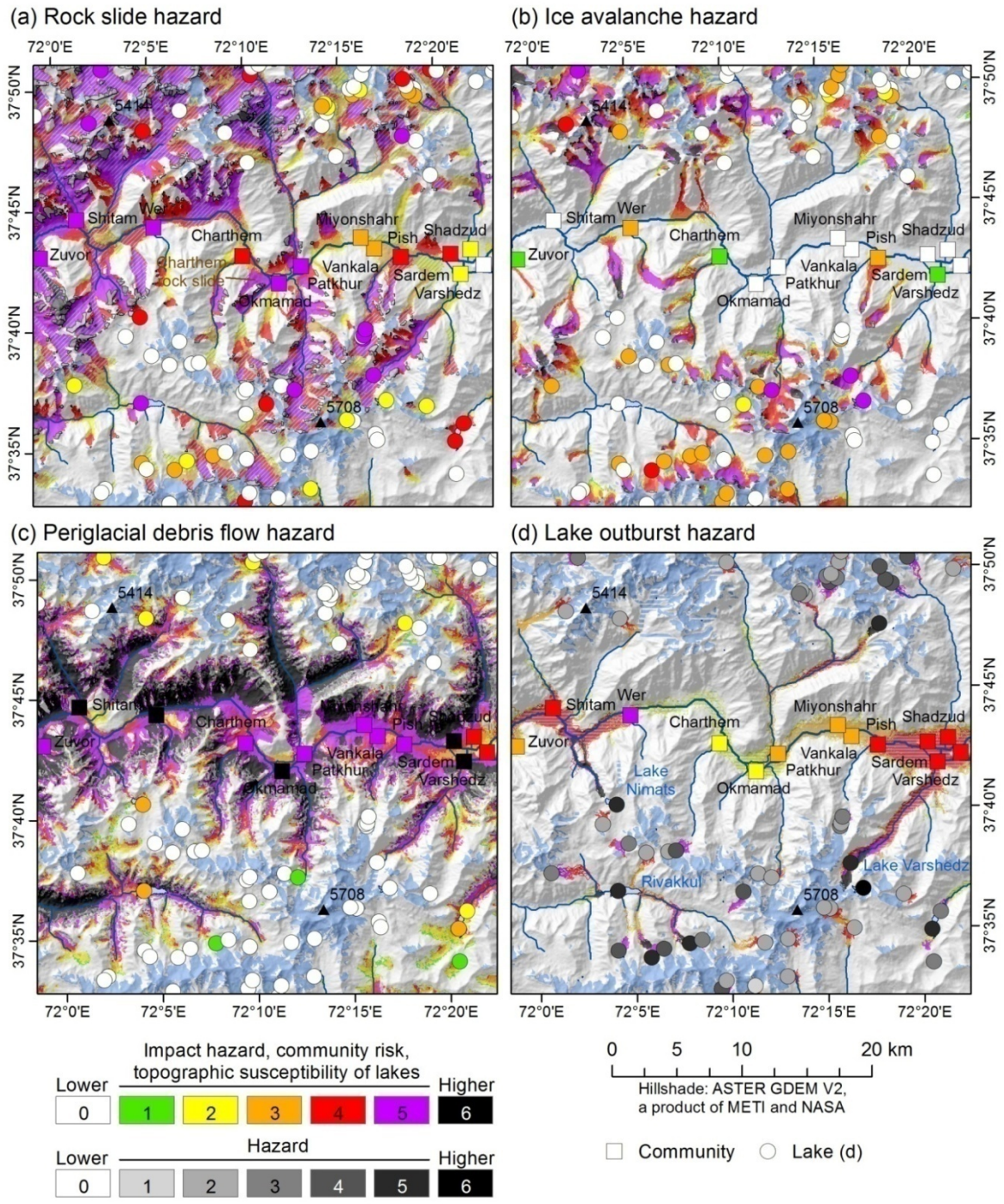

Fig. 14 Hazard, impact hazard, topographic susceptibility of lakes and community risk associated with each process type. (a) Rock slide, (b) ice avalanche, (c) periglacial debris flow, (d) lake outburst flood. The extent of the map is shown in Fig. 1.

6 Discussion

The purpose of the model approach introduced in the previous sections and the resulting hazard and risk indication maps is to provide a reproducible basis for targeted hazard and risk assessment studies and mitigation measures at the community scale. The approach chosen is thought to be useful for the study area in the Pamir for two reasons.

First, the general difficulty of establishing frequencies for rare or singular events in combination with sparse historical data in the study area makes strictly quantitative approaches such as statistical methods inapplicable. Therefore a hazard and risk indication scoring scheme has to be applied, even though such a concept introduces a certain degree of subjectivity.

Second, the vulnerability of the local population to these types of hazards is high, even though NGOs have launched programs to improve the awareness of and the preparedness for geohazard events in the previous decade. This situation is comparable to other high-mountain areas in developing countries (e.g., Carey, 2005). The results of the present study shall highlight high-risk areas and serve as a baseline for in-detail studies and risk mitigation procedures.

Consequently, the outcome of the study should not be seen as definite hazard and risk maps, but rather as conceptual hazard and risk indication maps. The hazard and risk indication score classes are therefore not given definite names such as Moderate hazard, Extremely high risk etc. Further, the interpretation of the model results on the basis of raster cells is appropriate for scientific discussion, but not for the design of risk mitigation measures. Here the scale of communities (see Fig. 14), catchments (see Fig. 12) or even regions (see Fig. 13) are much more suitable.

As far as a comparison with observed events is possible, it confirms the model results (e.g., Charthem rock slide, see Fig. 14a). In the case of large rock slides such as the 1911 Sarez event (see Fig. 2a) the comparison with the model results is of limited value due to the substantial change of the topography caused by such events. No records of ice avalanches in the study area are known to the authors whilst periglacial debris flows are very common. Their source and impact areas are well recognized by the model, but the false positive rate is high. The two lakes with recorded sudden drainage are not characterized by exceptionally high susceptibility scores – the prediction of lake outburst floods is therefore particularly challenging.

The quality of the model results strongly depends on the input data used. The detail and accuracy of the ASTER GDEM is considered sufficient for the purpose of the present study, even though the quality of the dam geometry estimates may suffer from artefacts and inaccuracies known for this type of DEM. Also the quality of the carefully mapped lake, glacier and land use data sets is largely considered sufficient. The potential permafrost areas were determined using a rule-of-thumb approach, adapting data obtained in the Alps (Haeberli, 1975; Mergili et al., 2012a). Even though the predicted conditions and scenarios are likely to be realistic, uncertainties are hard to quantify. The seismic hazard map used (Giardini et al., 1999) is a highly generalized global dataset. Other essential information such as the distinction bedrock – residual rock or the orientation and dip of the bedding planes of geological layers are hardly manageable at the scale relevant for a study of this type.

The scoring schemes used (see Table 2 to Table 7) are founded on expert knowledge. The interpretation of the model results have to consider the characteristics of the scheme used for each process. Necessarily, the schemes contain ±arbitrary thresholds such as those used for the event magnitude (see Table 3) or the 45° minimum slope for rock slides already used earlier by Hergarten (2012).

The modelling of the travel distance and the impact area of the considered processes is derived from the statistics of observed events. These statistics are reasonably robust for rock slides and

rock ice avalanches (Scheidegger , 1973; Evans and Clague, 1988; Bottino et al., 2002; Noetzli et al., 2006) and also for ice avalanches (Huggel et al., 2004a). However, they are based on observations from other mountain areas such as the Alps. Their application is based on the hypothesis that (i) the patterns observed there are comparable to those in the Pamir and (ii) that the – often rather small – datasets used for the derivation of the patterns and thresholds cover a representative sample of the reality. This is equally true for the slope-temperature curve shown in Fig. 7. The situation is even more difficult for periglacial debris flows (Huggel et al., 2004a) and particularly for lake outburst floods. The threshold of $\omega_{r,E} = 11°$ used by Huggel et al. (2004a, b) for debris flows from lake outburst events is not applicable to the Pamir as the 2002 Dasht event, where $\omega_{r,E} \sim 9.3°$, has shown (Mergili and Schneider, 2011). Also the parameterization of floods developing from lake outburst events is nothing more than a rough estimate so that the results (such as the short travel distance predicted for a sudden drainage of Rivakkul, see Fig. 14d) have to be interpreted with utmost care.

Further, the application of average slopes neglects the loss of energy due to changes of the flow direction. Strictly spoken, such concepts should only be used for straight flow paths. The criterion that the motion has to move away from the source with each step of the random walk partly accounts for this limitation.

Possible impact wave due to mass movements into lakes are explicitly accounted for by the model. Other types of interactions are included indirectly: The conversion of rock slides into rock-ice avalanches by the impact on glaciers is implicitly considered in the rock slide model, even though there are no means to estimate the entrainment of snow or ice. In the case of rock slides and rock-ice avalanches, the empirical relationships used implicitly include cascading effects such as the conversion into debris flows. Some process interactions are out of scope of the present study, such as the damming of lakes by mass movements and possible subsequent drainage. The same is true for the entrainment of debris, modelling of which remains a challenge particularly at the scale of the present study.

The approach used does not allow for an analytical overlay of the susceptibility, hazard, impact hazard and risk indication scores associated to each process type. Even though attempted as far as possible, a homogenization of the scoring schemes for the different processes proves highly problematic due to the missing physical basis. The data the analysis is based on differs between the processes: e.g., the possible magnitude of rock slides is given in maximum volumes whilst only the maximum involved surface area allowed under the assumptions taken is used for possible ice avalanches and lake outburst floods (see Table 3). Also the schemes for susceptibility can hardly be homogenized (see Table 5 to Table 7; Fig. 7), partly due to the varying level of detail of the available input data.

7 Conclusions

A regional-scale multi-hazard and -risk indication model was introduced, including four selected high-mountain processes: (i) rock slides and rock avalanches, (ii) ice-avalanches, (iii) periglacial debris flows and (iv) lake outburst floods. The model results for a very large area centred in the Pamir (Tajikistan) were presented and discussed. The model shall help to distinguish areas with

higher from those with lower risk, even though the possibilities for comparison with observed events are limited. The interpretation of the model results – preferably at the level of communities, catchments or regions – has to take into account the characteristics of the scoring schemes as well as the limitations of the input data and the methodology used.

Acknowledgements

The work presented is part of the project PAMIR supported by the European Commission (EC) and the Austrian Development Agency (ADA), as well as of the project TajHaz supported by FOCUS Humanitarian Assistance (an affiliate of the Aga Khan Development Network), the Swiss Agency for Development and Cooperation (SDC) and the UK Department for International Development (DFID). The Tajik Agency of Hydrometeorology has provided meteorological data. Special thanks for their support go to Matthias Benedikt, Johannes P. Müller and Jean F. Schneider, BOKU University, Vienna.

References

Alean, J.: Ice avalanches: some empirical information about their formation and reach. J. Glac., 31(109), 324–333, 1985.

Beniston, M.: Climatic Change in Mountain Regions: A Review of Possible Impacts. Clim. Change, 59(1–2), 5–31, 2003.

Bolch, T., Peters, J., Yegorov, A., Prafhan, B., Buchroithner, M. and Blagoveshchensky, V.: Identification of potentially dangerous glacial lakes in the northern Tien Shan. Nat. Haz., 59, 1691–1714, 2011.

Bottino, G., Chiarle, M., Joly, A.and Mortara, G.: Modelling Rock Avalanches and Their Relation To Permafrost Degradation in Glacial Environments. Permafr. Periglac. Proc., 13, 283–288, 2002.

Breien, H., DeBlasio, F. V., Elverhoi, A. and Hoeg, K.: Erosion and morphology of a debris flow caused by a glacial lake outburst flood, Western Norway. Landslides, 5(3), 271–280, 2008.

Carey, M.: Living and dying with glaciers: people's historical vulnerability to avalanches and outburst floods in Peru. Glob. Plan. Change, 47, 122–134, 2005.

Cenderelli, D. A. and Wohl, E. E.: Peak discharge estimates of glacial lake outburst floods and "normal" climatic floods in Mount Everest region, Nepal. Geomorphology, 40, 57–90, 2001.

Clarke, G. K. C.: Glacier outburst floods from 'Hazard Lake', Yukon Territory, and the problem of flood magnitude prediction. J. Glac, 28(98), 3–21, 1982.

Corominas, J., Copons, R., Vilaplana, J. M., Altamir, J. and Amigó, J.: Integrated Landslide Susceptibility Analysis and Hazard Assessment in the Principality of Andorra. Nat. Haz., 30, 421–435, 2003.

Costa, J. E.: Floods from Dam Failures. U.S. Geol. Surv. Open File Rep. 85-560, Denver, Colorado, 54 pp., 1985.

Costa, J. E. and Schuster, R.L.: The formation and failure of natural dams. Geol. Soc. Am. Bull., 100, 1054–1068, 1988.

Dussaillant A., Benito G., Buytaert W., Carling P., Meier C. and Espinoza F.: Repeated glacial-lake outburst floods in Patagonia: an increasing hazard? Nat. Haz., 54, 469–481, DOI 10.1007/s11069-009-9479-8, 2010.

Evans, S. G.: The maximum discharge of outburst floods caused by the breaching of man-made and natural dams. Can. Geotech.J., 23, 385–387, 1986.

Evans S. G. and Clague, J. J.: Catastrophic rock avalanchesin glacial environments. In: Bonnard, C. (ed.): Landslides, A.A. Balkema, Rotterdam, 2, 1153–1158, 1988.

Evans S. G. and Clague J. J.: Recent climatic change and catastrophic geomorphic processes in mountain environments. Geomorphology, 10(1-4), 107–128, 1994.

Evans, S. G., Bishop, N. F., Fidel Smoll, L., Valderrama Murillo, P., Delaney, K. B., Oliver-Smith, A: A re-examination of the mechanism and human impact of catastrophic mass flows originating on Nevado Huascarán, Cordillera Blanca, Peru in 1962 and 1970. Engin. Geol., 108, 96–118, 2009a.

Evans, S. G., Roberts, N. J., Ischuk, A., Delaney, K. B., Morozova, G. S., Tutubalina, O.: Landslides triggered by the 1949 Khait earthquake, Tajikistan, and associated loss of life. Engin. Geol., 109, 195–212, 2009b.

Giardini, D., Grünthal, G., Shedlock, K. and Zhang, P.: The GSHAP Global Seismic Hazard Map. Ann. Geophys., 42(6), DOI 10.4401/ag-3784, 1999.

GRASS Development Team: Geographic Resources Analysis Support System (GRASS) Software. Open Source Geospatial Foundation Project, http://grass.osgeo.org, 2013.

Haeberli, W.:Untersuchungen zur Verbreitung von Permafrost zwischen Flüelapass und Piz Grialetsch (Graubünden). Dissertation, University of Basel, 1975.

Haeberli, W.: Frequency and characteristics of glacier floods in the Swiss Alps. Ann. Glac., 4, 85–90, 1983.

Haeberli, W., Clague, J. J., Huggel, C. and Kääb, A.: Hazards from lakes in high-mountain glacier and permafrost regions: Climate change effects and process interactions. Avances de la Geomorphología en España, 2008-2010, XI Reunión Nacional de Geomorphología, Solsona, 439–446, 2010a.

Haeberli, W., Portocarrero, C. and Evans, S.: Nevado Hualcán, Laguna 513 y Carhuaz 2010 – Observaciones, evaluación y recomendaciones (un corto informe técnico luego de las reuniones y visita de campo en Julio 2010). Unpublished report on behalf of the Communidad Provincial de Carhuaz, 2010b.

Haritashya, U. K., Bishop, M. P., Shroder, J. F., Bush, A. B. G., Bulley, H. N. N.: Space-based assessment of glacier fluctuations in the Wakhan Pamir, Afghanistan. Clim. Change, 94, 5–18, 2009.

Harris, C., Arenson, L. U., Christiansen, H. H., Etzelmüller, B., Frauenfelder, R., Gruber, S., Haeberli, W., Hauck, C., Hölzle, M., Humlum, O., Isaksen, K., Kääb, A., Kern-Lütschg, M. A., Lehning, M., Matsuoka, N., Murton, J. B., Nötzli, J., Phillips, M., Ross, N., Seppälä, M.,

Springman, S. M., VonderMühll, D.: Permafrost and climate in Europe: Monitoring and modelling thermal, geomorphological and geotechnical responses. Earth-Sci. Rev., 92(3–4), 117–171, 2009.

Harrison, S., Glasser, N., Winchester, V., Haresign, E., Warren, C., Jansson, K.: A glacial lake outburst flood associated with recent mountain glacier retreat, Patagonian Andes. Holocene, 16, 611–620, 2006.

Hergarten, S.: Topography-based modelling of large rockfalls and application to hazard assessment. Geophys. Res. Lett., 39, L13402, DOI 10.1029/2012GL052090, 2012.

Hewitt, K.: Natural dams and outburst floods in the Karakorum Himalaya. In: Glen J. W. (ed.): Hydrological aspects of alpine and high-mountain areas. IAHS Publication 138, 259–269, 1982.

Hewitt, K., Clague, J.J. and Orwin, J.F.: Legacies of catastrophic rock slope failures in mountain landscapes. Earth-Sci. Rev., 87, 1–38, 2008.

Hewitt, K. and Liu, J.: Ice-dammed lakes and outburst floods, Karakoram Himalaya: historical perspectives on emerging threats. Phys. Geog., 31(6), 528–551, 2010.

Huber, U., Bugmann, H. and Reasoner, M.: Global Change and Mountain Regions. An overview of current knowledge. Advances in Global Change Research. Springer, Dordrecht, 2005.

Huggel, C.: Assessment of Glacial Hazards based on Remote Sensing and GIS Modeling. Dissertation at the University of Zurich, Schriftenreihe Physische Geographie Glaziologie und Geomorphodynamik, 2004.

Huggel, C., Kääb, A., Haeberli, W., Teysseire, P. and Paul, F.: Remote sensing based assessment of hazards from glacier lake outbursts: a case study in the Swiss Alps, Can. Geotech. J., 39, 316–330, 2002.

Huggel, C., Kääb, A., Haeberli, W. and Krummenacher, B.: Regional-scale GIS-models for assessment of hazards from glacier lake outbursts: evaluation and application in the Swiss Alps. Nat. Haz. Earth Syst. Sci., 3, 647–662, 2003.

Huggel, C., Haeberli, W., Kääb, A., Bieri, D. and Richardson, S.: Assessment procedures for glacial hazards in the Swiss Alps. Can. Geotech.J., 41(6), 1068–1083, 2004a.

Huggel, C., Kääb, A. and Salzmann, N.: GIS-based modeling of glacial hazards and their interactions using Landsat-TM and IKONOS imagery. Norwegian J. Geog., 58, 761–773, 2004b.

Huggel, C., Zgraggen-Oswald, S., Haeberli, W., Kääb, A., Polkvoj, A., Galushkin, I. and Evans, S.G.: The 2002 rock/ice avalanche at Kolka/Karmadon, Russian Caucasus: assessment of extraordinary avalanche formation and mobility, and application of QuickBird satellite imagery. Nat. Haz. Earth Syst. Sci., 5, 173–187, 2005.

ICIMOD: Glacial lakes and glacial lake outburst floods in Nepal. ICIMOD, Kathmandu, 2011.

IPCC: Climate Change 2007: The Physical Science Basis. Contribution of Working Group I to the Fourth Assessment Report of the Intergovernmental Panel on Climate Change [Solomon, S., Qin, D., Manning, M., Chen, Z., Marquis, M., Averyt, K. B.,Tignor, M., and Miller, H.L. (eds.)]. Cambridge University Press, Cambridge and New York, 2007.

Iverson, R. M.: The physics of debris flows. Rev. Geophys., 35, 245–296, 1997.

Jarvis, A., Reuter, H. I., Nelson, A. and Guevara, E.: Hole-filled seamless SRTM data V4. International Centre for Tropical Agriculture (CIAT), available from http://srtm.csi.cgiar.org, 2008.

Kääb, A., Huggel, C., Fischer, L., Guex, S., Paul, F., Roer, I., Salzmann, N., Schlaefli, S., Schmutz, K., Schneider, D., Strozzi, T. and Weidmann, Y.: Remote sensing of glacier- and permafrost-related hazards in high mountains: an overview. Nat. Haz. Earth Syst. Sci., 5, 527–554, 2005.

Kassam, K. A.: Viewing Change Through the Prism of Indigenous Human Ecology: Findings from the Afghan and Tajik Pamir. Hum. Ecol., 37, 677–690, 2009.

Khromova, T. E., Osipova, G. B., Tsvetkov, D. G., Dyurgerov, M. B. and Barry, R. G.: Changes in glacier extent in the eastern Pamir, Central Asia, determined from historical data and ASTER imagery. Rem. Sens. Environ., 102, 24–32, 2006.

Mahmood, S. A., Shahzad, F. and Gloaguen, R.: Remote Sensing Analysis of Recent Active Tectonics in Pamir Using Digital Elevation Model: River Profile Approach. Proceedings of the Geoscience and Remote Sensing Symposium IGARSS, 7 – 11 July 2008, II-1259–II-1262, 2008.

Makhmadaliev, B., Kayumov, A., Novikov, V., Mustaeva, N. and Rajabov, I. (eds.): The Second National Communication of the Republic of Tajikistan under the United Nations Framework Convention on Climate Change. State Agency for Hydrometeorology, Dushanbe, 2008.

Mergili, M. and Schneider, J. F.: Regional-scale analysis of lake outburst hazard in the southwestern Pamir, Tajikistan, based on remote sensing and GIS. Nat. Haz. Earth Syst. Sci., 11, 1447–1462, 2011.

Mergili, M., Kopf, C.,Müllebner, B. and Schneider, J. F.: Changes of the cryosphere in the high-mountain areas of Tajikistan and Austria: a comparison. Geog.Ann., A, 94(1), 79–96, 2012a.

Mergili, M., Fellin, W., Moreiras, S. M. and Stötter, J.: Simulation of debris flows in the Central Andes based on Open Source GIS: Possibilities, limitations, and parameter sensitivity. Nat. Haz., 61(3), 1051–1081, 2012b.

Mergili, M., Schratz, K., Ostermann, A. and Fellin, W.: Physically-based modelling of granular flows with Open Source GIS. Nat. Haz. Earth Syst. Sci., 12, 187–200, 2012c.

Mergili, M., Müller, J. P. and Schneider, J. F.: Spatio-temporal development of high-mountain lakes in the headwaters of the Amu Darya river (Central Asia). Glob. Plan. Change, DOI 10.1016/j.gloplacha.2013.04.001, 2013.

Müllebner, B.: Modelling of potential permafrost areas in the Pamir and Alai mountains (Tajikistan) using Remote Sensing and GIS techniques. Master thesis, BOKU University, Vienna, 2010.

Narama, C., Duishonakunov, M. , Kääb, A., Daiyrov M. and Abdrakhmatov, K.: The 24 July 2008 outburst flood at the western Zyndan glacier lake and recent regional changes in glacier lakes of the Teskey Ala-Too range, Tien Shan, Kyrgyzstan. Nat. Haz. Earth Syst. Sci., 10, 647–659, 2010.

Neteler, M. and Mitasova, H.: Open source GIS: a GRASS GIS approach. Springer, New York, 2007.

Noetzli, J., Huggel, C., Hoelzle, M. and Haeberli, W.: GIS-based modelling of rock-ice avalanches from Alpine permafrost areas. Computational Geosci., 10, 161–178, 2006.

Quincey D. J., Richardson S. D., Luckman A., Lucas R. M., Reynolds J. M., Hambrey M. J. and Glasser N. F.: Early recognition of glacial lake hazards in the Himalaya using remote sensing datasets. Glob. Plan. Change, 56(1-2), 137–152, 2007.

Risley, J. C., Walder, J. S. and Denlinger, R.: Usoi dam wave overtopping and flood routing in the Bartang and Panj rivers, Tajikistan. Nat. Haz., 38(3), 375–390, 2006.

Richardson, S. D. and Reynolds, J. M.: An overview of glacial hazards in the Himalayas. Quatern. Int., 65/66, 31–47, 2000.

Rickenmann, D.: Empirical Relationships for Debris Flows. Nat. Haz., 19, 47–77, 1999.

Scheidegger, A. E.: On the Prediction of the Reach and Velocity of Catastrophic Landslides. Rock Mech., 5, 231–236, 1973.

Schuster, R. L. and Alford, D.: Usoi Landslide Dam and Lake Sarez, Pamir Mountains, Tajikistan. Environ. &Engin. Geosci., 10(2), 151–168, 2004.

Tinti, S., Maramai, A. and Cerutti, A. V.: The Miage Glacier in the Valley of Aosta (Western Alps, Italy) and the extraordinary detachment which occurred on August 9, 1996. Phys. Chem. Earth (A), 24(2), 157–161, 1999.

Tweed, F. S. and Russell, A. J.: Controls on the formation and sudden drainage of glacier-impounded lakes: implications for jökulhlaup characteristics. Prog. Phys. Geog., 23(1), 79–110, 1999.

Vilímek, V., Zapata, M. L., Klimes, J., Patzelt, Z. and Santillán N.: Influence of glacial retreat on natural hazards of the Palcacocha Lake area, Peru. Landslides, 2(2), 107–115, 2005.

Walder J. S. and Costa J. E.: Outburst floods from glacierdammed lakes: the effect of mode of lake drainage on flood magnitude. Earth Surf. Proc. Landforms, 21, 701–723, 1996.

Walder, J. S. and O'Connor, J. E.: Methods for Predicting Peak Discharge of Floods Caused by Failure of Natural and Constructed Earth Dams. Water Resour. Res., 33, 10, 2337–2348, 1997.

Watanabe, T. and Rothacher, D.: The 1994 Lugge Tsho glacial lake outburst flood, Bhutan Himalaya. Mt. Res. Dev., 16, 77–81, 1996.

WGMS: Global Glacier Changes: Facts and Figures (Zemp, M., Roer, I., Kääb, A., Hoelzle, M., Paul, F., Haeberli, W., eds.), UNEP, World Glacier Monitoring Service, University of Zurich, Switzerland, free download from WGMS and UNEP websites, 2008.

Appendix 7

Impact of large landslides, mitigation measures

Submitted book chapter

Schneider, J.F., Gruber, F.E., Mergili, M.: Impact of large landslides, mitigation measures. Submitted to the Proceedings of the Vajont 2013 Conference, October 8–10, 2013, Padova, Italy.

Abstract

Besides existing landslide-dammed lakes there is evidence of former cases in the high-mountain areas of Europe, Asia and America. In the Holocene, large landslides have repeatedly dammed lakes. Numerous prehistoric, historic and recent cases are evident where the dams could not resist the pressure of the impounding water. The result were flood waves characterized by particularly high peak discharges and long travel distances, leading to disasters where interfering with populated lands downstream. Even though most dam failures occur in the early phase after formation, lakes may also drain suddenly at later stages. Case studies from Central Asia and Northern Pakistan are employed in order to exemplify the involved phenomena regarding dam formation, outburst mechanisms and flood wave propagation. A particular focus is put on discussing the options for disaster risk reduction and hazard mitigation.

Keywords

Attabad, Computer modelling, Flood wave, Hattian Bala, Lake outburst flood, Landslide dam, Siachen-Gayari, Spillway

1 Introduction

Natural dams of various types retain lakes in many areas of the world. Costa & Schuster (1988) point out that mainly landslide-dammed lakes, glacier ice-dammed lakes and late neo-glacial moraine dams are prone to fail and to produce potentially destructive lake outburst floods. Whilst much work has been done on glacial lake outburst hazards (Richardson & Reynolds, 2000), the present paper focuses on landslide-dammed lakes.

Landslides are common geomorphic processes in high mountain regions such as Central Asia. Whilst the direct impact of such phenomena on mountain communities is obvious, many landslides are only the starting point of process chains. The formation of landslide-dammed lakes is often a highly significant secondary effect (Clague & Evans, 1994; Casagli & Ermini, 1999). Such landslide dams may fail suddenly due to impact waves, internal or retrogressive erosion, resulting in potentially destructive flood waves downstream. Lakes may also drain stepwise or continuously, others persist for a long period of time. Costa & Schuster (1988, 1991) and Schuster & Evans (2011) have shown that most dam failures occur in the first few months after the landslide event. Afterwards, the dam is usually consolidated so far that outburst floods become less likely (Fig. 1). However, impact waves triggered by mass movements into the lake may occur a very long time after dam formation.

Whilst geomorphic evidence indicates the existence and sudden drainage of landslide-dammed lakes in earlier stages of the Holocene, very recent cases have illustrated the huge challenge such phenomena pose for the population and the authorities of (possibly) affected areas.

The present paper is understood as a contribution to the understanding of the dynamics of landslide-dammed lakes and the challenges for risk mitigation in order to minimize future losses. The lessons learned from three recent cases from northern Pakistan (Hattian Bala, Attabad and Siachen-Gayari) are combined with historical and geomorphologic evidence from past events in Tajikistan and eastern Afghanistan. Figure 2 shows the geographic location of the cases discussed below.

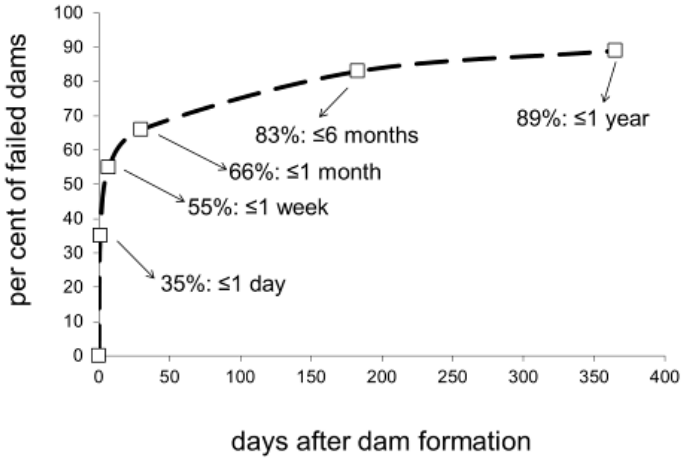

Fig. 1 – Percentage of failed dams plotted against the time after formation (after Schuster & Evans, 2011).

2 Evidence of former events

2.1 Landslide dams in the Tajik and Afghan Pamir

2.1.1 Lake Sarez

The highest natural dam known today, the Usoi Dam, has remained stable for more than 100 years now. It was formed by an earthquake-triggered landslide in 1911, blocking the Murghab Valley in the Tajik Pamir (see Fig. 2). Up to 600 m high, it impounded Lake Sarez, now 60 km long with a volume of 17 km³ (Schuster & Alford, 2004). Since seepage through the dam almost offsets the inflow into the lake, the lake level rises only approx. 0.2 m per year and has not yet reached the dam crest. Even though Schuster & Alford (2004) list several possible failure mechanisms, there is still disagreement upon the level of hazard emanating from Lake Sarez. The dam is rated rather stable due to the consolidated structure, huge dimensions and the existence of a preferential, non-eroding flow path through the dam (Ischuk, 2004, 2011). However, there is a creeping rock mass heading into the lake which, in case of sudden acceleration, could trigger an impact wave and consequent overtopping of the dam (Risley et alii, 2006). That rock mass, the dam and the Murghab River downstream are monitored and a flood early warning system was installed.

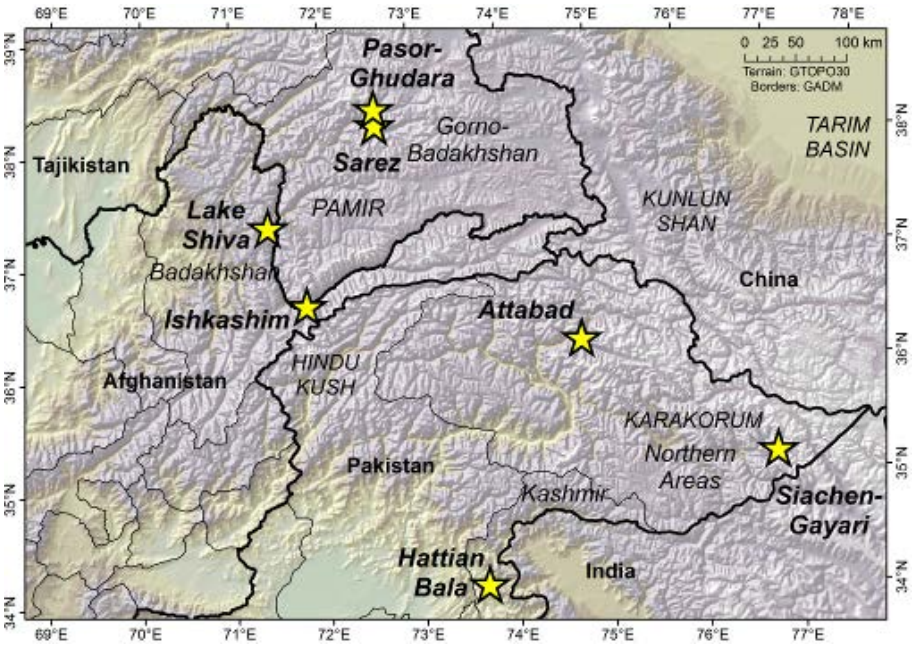

Fig. 2 – Case studies discussed in the article.

2.1.2 Lake Shiva

Lake Shiva has a maximum length of approx. 9 km and is located in the Shugnan District of north-east Afghanistan, at a distance of approx. 16 km from the south-west of Khorog, capital city of Gorno-Badakhshan, Tajikistan (see Fig. 2). It is impounded behind a natural composite dam across the valley of Arakht, a tributary of the river Panj which, in that region, constitutes the border between Afghanistan and Tajikistan.

A preliminary geological hazard assessment of the lake and dam was conducted by means of helicopter survey, satellite imagery interpretation and ground check in summer 2011. No

immediate hazard of sudden drainage was detected, but a partial collapse of the dam due to retrogressive and piping erosion cannot be completely ruled out. Subsequent flood wave modelling of two partial collapse scenarios have shown that in either case, in addition to all the villages on the way, the city of Khorog may be affected.

The dam retaining Lake Shiva is 1.6 km wide. Following Shroder & Weihs (2010) it is composed of the material of at least three landslides and a rock glacier. According to an assessment carried out by the authors the main part consists of a morainic dam, representing at least two late-glacial stages. This morainic dam, in its northern part, interdigitates with the deposit of a landslide which rushed down from the slopes to the north, presumably while the landscape had to accommodate the loss of its ice cover at the end of the last ice age. Perhaps a partial breach of the morainic dam did occur back then but if so, the gorge is now covered by landslide debris.

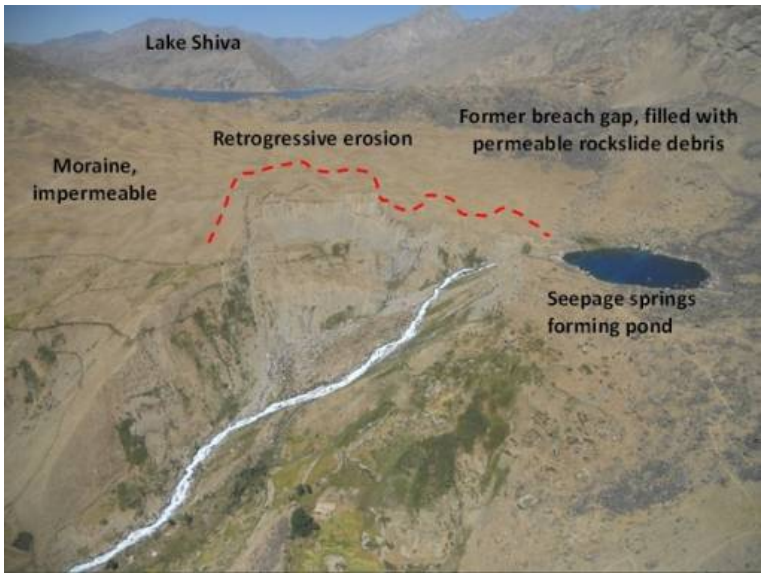

Fig. 3 – Lake Shiva composite dam, view to the W. The depression spring (circular lake, diameter approx. 200 m) and headwater of Arakht torrent in the foreground; to the left of the lake the unstable part of the downstream side of the dam, with a band of much smaller springs, conspicuous because of spots of green vegetation. Moraine deposit in the centre, rock slide deposit in the right part of the photograph, the source of the rock slide is farther right.

The dam has since consolidated, and obviously has never been overtopped by the impounded water in the shape it is now (after the possible first breakout). Instead, all the water supplied by the catchment is travelling through the dam by virtue of seepage, and for the most part is channelled through the permeable material supplied by the landslide. On the downstream side of the dam, part of the seeping water emerges in a stable depression spring, thereby creating a small circular lake (Fig. 3).

However, apart from the large spring with, stable piping, several additional springs have appeared on the downstream slope of the dam to the south of the main spring. This indicates seepage through the comparatively impermeable till constituting the main part of the dam. This has already led to retrogressive erosion of a currently rather small part of the dam affected by the seepage, and it is obvious that repeated slumping is taking place and retrogressive erosion is active (see Fig. 3). In case these instabilities continue, the dam – in the long run – could be

weakened by erosion of its narrowest part, and also be undermined by concentrated seepage (piping).

Furthermore, Shroder & Weihs (2010) describe the dam site as situated at the crossing of two active tectonic lines, which could trigger local earthquakes.

2.1.3 Pasor – Ghudara System

Whilst Lake Sarez and Lake Shiva are prominent examples of still rather intact natural dams, the Pamir also bears a lot of evidence for failed dams. Several valleys were temporarily blocked by huge, predominantly coarse-grained deposits. Fine sediments upstream indicate lakes that have disappeared either by sedimentation or by sudden or stepwise dam failure. Even though the origin of these deposits is not undisputed and some may represent Pleistocenic moraines, many of them are identified as landslide deposits. One such example is located in the upper Bartang Valley (Central Pamir, Fig. 4a). The Pasor landslide dam, approx. 300 m high, blocked the valley and impounded the up to 8 km long Ghudara Lake. The age of the lake sediments was determined as ≤4000 years using Optically Stimulated Luminescence (OSL). After accumulating several tens of metres of lake sediments, the lake drained in stages and the sediments were deeply eroded. The narrow gorge through the landslide deposit may have been blocked several times. Downstream alluvial deposits, which are partly eroded leaving only remnant large blocks, indicate at least one powerful outburst flood (see Fig. 4b).

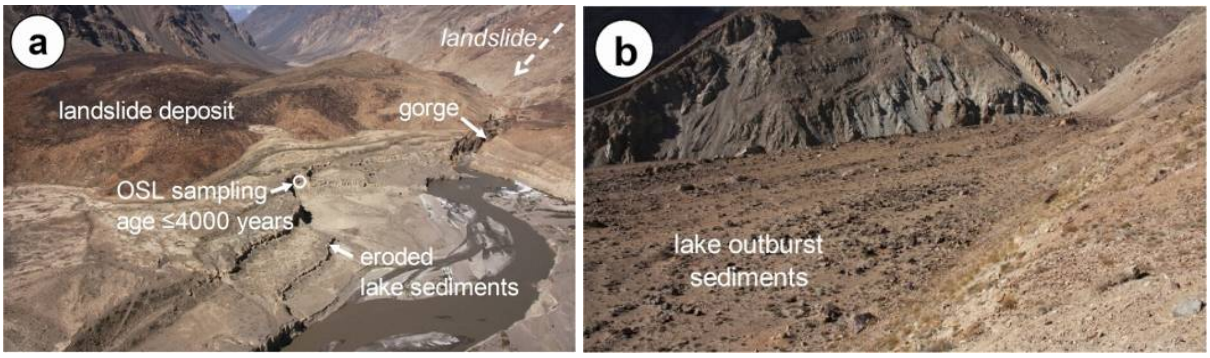

Fig. 4 – (a) Pasor landslide (background) and eroded lake sediments in the foreground. The lake level dropped in several stages. (b) Partly eroded lake outburst sediments directly downstream of the dam showing typical outburst flood structures.

2.1.4 Dasht-Sulayman System

The Panj Valley, forming the border between Tajikistan and Afghanistan (Wakhan Corridor), is partly blocked by the deposit of a debris avalanche at Dasht-Sulayman, upstream the town of Ishkashim (see Fig. 2). The origin of the landslide consisting of black slate is located in the mountain range south of the Panj River. Lake outburst sediments and residual boulders indicate a temporary blockage of the valley followed by sudden drainage, but historical evidence is missing. Ruins of a medieval fortification are situated on an older eastern lobe of the debris (Fig. 5). Detailed interviews in the near village uncovered legends about a "big flood long time ago". Such evidence is certainly purely speculative but can anyway give some indication of former events. More detailed geomorphological work is required in order to better understand this and other prehistoric events.

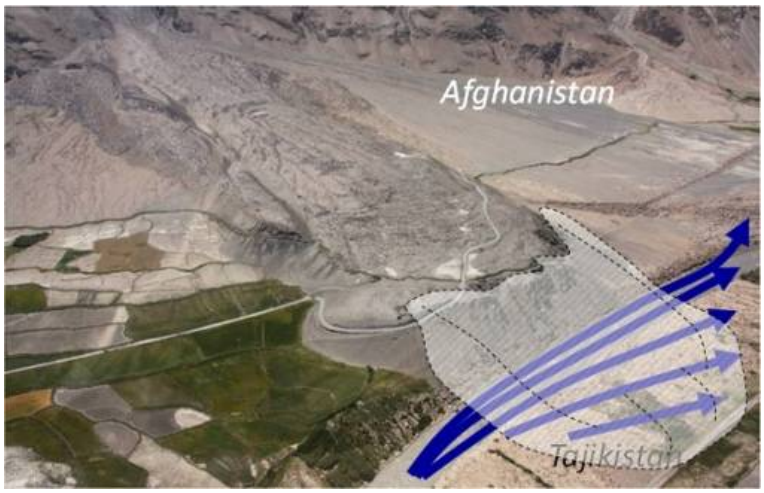

Fig. 5 – Debris avalanche at Dasht-Sulayman upstream Ishkashim in the Wakhan Corridor, Afghanistan. The Panj River eroded the lobe reaching Tajikistan, emptying a temporary lake impounded by the dam. A thin cover of lake sediments exists in the cultivated area on the lower left side and the ruins mentioned in the text are situated on the upper left of the photo. Washed out boulders cover the orographic right side of Panj River as remnants of the lake outburst flood. The eroded cliff on the orographic left side is approx. 50 m high.

2.2 Historical lake outburst floods in northern Pakistan

The Hunza and Indus Valleys of northern Pakistan, deeply incised and seismically active (Shroder, 1998), have a particular history of landslide-dammed lakes (Hewitt, 1982, 1998) with specific cases in 1841, 1858, 1962, 1974 and 2010.

The largest event is documented from the Indus valley near the Nanga Parbat. In December 1840 or January 1841 a giant earthquake-triggered landslide dammed the Indus River in the vicinity of Raikot Bridge. The exact location of this natural dam is still disputed, but it impounded a temporary lake with a length estimated between 30 (Shroder, 1998), 57 (Delaney & Evans, 2011) and 64 km (Mason,1929). In early June the barrier was overtopped and breached, leading to a tremendous flood wave down the river. The meagre historical records of this huge flood wave were compiled by Mason (1929). Approx. 3–5 billion m³ of water were released in less than 24 hours, 2 million m³ of solids were eroded within a short time. 430 km downstream, the wave front was described as "a wall of water, mud and rocks" which still had a height of approx. 25 m (Shroder, 1998; NESPAK, 2010). A Sikh army that had camped upstream of Attock was hit by the wave, with at least 500 casualties. The actual volume of water discharged by the Great Indus Flood is unknown and estimates vary similar to those regarding lake length, but Mason (1929) gives dimensions of the barrier that would indicate a volume of more than one cubic kilometre. The release of this volume within one day would indicate an average discharge of over 14,000 m³/s, but the height of the flood wave at Attock suggests an initial discharge several times higher. Cornwell & Hamidullah (1992) point out that the estimation of the peak discharge varies from 56,630 m³/s (Hewitt, 1964) to 509,000 m³/s (Shroder et alii, 1991). Delaney and Evans (2011) calculated a peak discharge of approx. 114,000 m³/s.

In 1858, another massive slope failure (Ghammessar landslide, 125 million m³) occurred just downstream of Attabad, close to the village of Sulmanabad. Its extensively eroded toe still

contains boulders 20–30 m in size (Shroder, 1998). The landslide blocked the Hunza River and impounded a lake, Delaney & Evans (2011) estimate a lake volume of 0.8 km³. In August 1858 the dam was overtopped and the resulting erosion, more than 300 m deep, led to retrogressive slumping of the toe of the landslide – on which the town of Sulmanabad is now located – into the river. Mason (1929) attributes a 20 m flood wave at Attock to the Ghammessar slope failure. According to NESPAK (2010) the flood led to a wave height of 16.5 m at Attock, the flood hydrograph adding up to a volume of 1.85 billion m³. This second Great Indus Flood destroyed several villages and forts downstream of the dam but the population was warned, remembering the 1841 great flood (Delaney & Evans, 2011).

Additionally to the Ghammessar slope failure, Shroder (1998) describe several other slope failures in the proximity of Attabad, for instance the older and the younger Serat slope failures just opposite of the 2010 Attabad landslide (see next chapter). An estimated volume of 1.5 million m³ of the younger Serat landslide was eroded by the river, presumably by an outburst flood. In October 1962 a mass movement was released from the scarp of the Ghammessar landslide, killing six men of the Public Works Department of the Government of Pakistan and impounding water up to Gulmit. When the lake drained suddenly after several months, it undercut remnants of the 1858 landslide, causing several houses of the village of Sulmanabad to drop into the Hunza River. However, they had not been occupied as the population was aware of the instability of that slope. NESPAK (2010) reports of another Hunza River blockage in the area of Gulmit in 1974: this dam failed due to overtopping a few months later, the resulting flood caused some minor damage.

The 2010 Attabad landslide and formation of Hunza Lake, with its far-reaching consequences for the region, is a further entry in the long list of events in that area. It is discussed in detail in the next chapter.

3 Case studies of recent events

Several landslide-dammed lakes have formed in the last 50 years. Examples include the events of Aini (Tajikistan, 1964), Mayunmarca (Peru, 1974), Val Pola (Italy, 1987), Tsatichu (Bhutan, 2003), Hattian Bala (Pakistan, 2005), Tangjiashan (China, 2008), Attabad (Pakistan, 2010) and Siachen-Gayari (Pakistan 2012). Some of these dams have failed. The cases of the failed dam of Hattian Bala as well as of Attabad and Siachen-Gayari where the dams were still intact in March 2013 shall be discussed in detail.

3.1 Case study 1: Hattian Bala Landslide

On October 8, 2005, a magnitude 7.6 earthquake struck Kashmir in northern Pakistan and caused many casualties as well as severe damage. Several mass movements were triggered. The Hattian Bala landslide, located at a tributary of Jehlum River southeast of Muzaffarabad (see Fig. 2 for location), was reactivated, resulting in a rock avalanche with a volume of approx. 65 million m³ (Dunning et alii, 2007; Schneider, 2009; Fig. 6). Consisting of sand-, silt- and mudstones of the Murree Formation, it destroyed a small village and several farms.

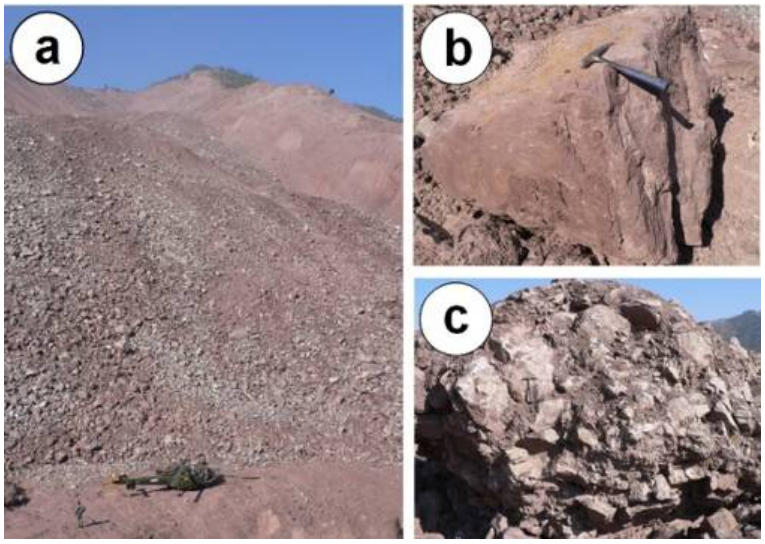

Fig. 6 – (a) Proximal base of the Hattian Bala rock avalanche, helicopter at the location of the future spillway channel. Karli Lake is situated at the left of the photograph. (b) Sandstone block of the Murree formation in the silt-to claystone landslide debris matrix. (c) Cemented debris of a former landslide at the same location.

An area of 1.8 km² was directly affected by the landslide, the deposit formed a dam with an area of 0.9 km² impounding Karli and Tung rivers and creating two lakes (Fig. 7a, b). Based on the geometry of the embankment, the maximum volume of the lakes, i.e. when the water level equals the elevation of the lowest saddle of the dam crest, was calculated: Karli (or Zalzal) Lake, the larger of the two, would grow to a volume of approx. 61.7 million m³, Tung (or Bani Hafiz) Lake to 3.6 million m³ (Schneider, 2009). The portion of the deposit impounding Karli Lake had a maximum depth of 230 m (Dunning et alii, 2007) to 350 m (Schneider, 2009). Large sandstone blocks were stabilizing the surface of the orographic right (distal) portion of the dam.

After detailed investigations, several measures to mitigate the hazard related to a possible dam failure were initiated (Schneider, 2009). Besides the installation of a monitoring system and the design of hazard maps and evacuation plans, it was decided to limit the water level of the lakes and to ensure controlled overflow by excavating reinforced spillways for Karli Lake and Tung Lake, with lengths of 425 m and 130 m, respectively. For Karli Lake the spillway was not built not over the saddle, representing the natural drainage path, but over the centre of the dam in order to avoid a destabilization of the adjacent slope. The spillway was partly completed in June 2006, but not reinforced. Its depth was 10 m and the clast size varied from sand to cobbles beneath a relatively thin, coarse bouldery surface layer (Dunning et alii, 2007). The level of Karli Lake reached the spillway at the end of March 2007. In June 2007 the spillway appeared stable, but was not lined. Seepage was observed in the lower, unchanneled section.

Due to the increasing consolidation of the dam, Schneider (2009) rated the probability of a failure as unlikely if the artificial spillway would be lined with sandstone blocks in order to avoid erosion. However, he also pointed out the scenario of impact waves triggered by the sudden acceleration of active slumps observed on the margins of Karli Lake, especially on the orographic left side (see Fig. 7b).

In February 2010, a process chain including spill over of the dam of Karli Lake and deep retrogressive erosion of the spillway occurred (Fig. 7c and Fig. 8). The following debris flow led to severe damage and one fatality downstream. Konagai & Sattar (2012) conclude that the breach can be attributed to the hydrologic situation (moderate rainfall after dry conditions) in combination with a deteriorating dam body due to weak weathering resistance of the material. Some landslides observed close to the lake were most likely caused by slope destabilization due to the suddenly lowered lake level and the resulting changes in pore water pressure. However, further investigations are required in order to fully understand the process chain that occurred here.

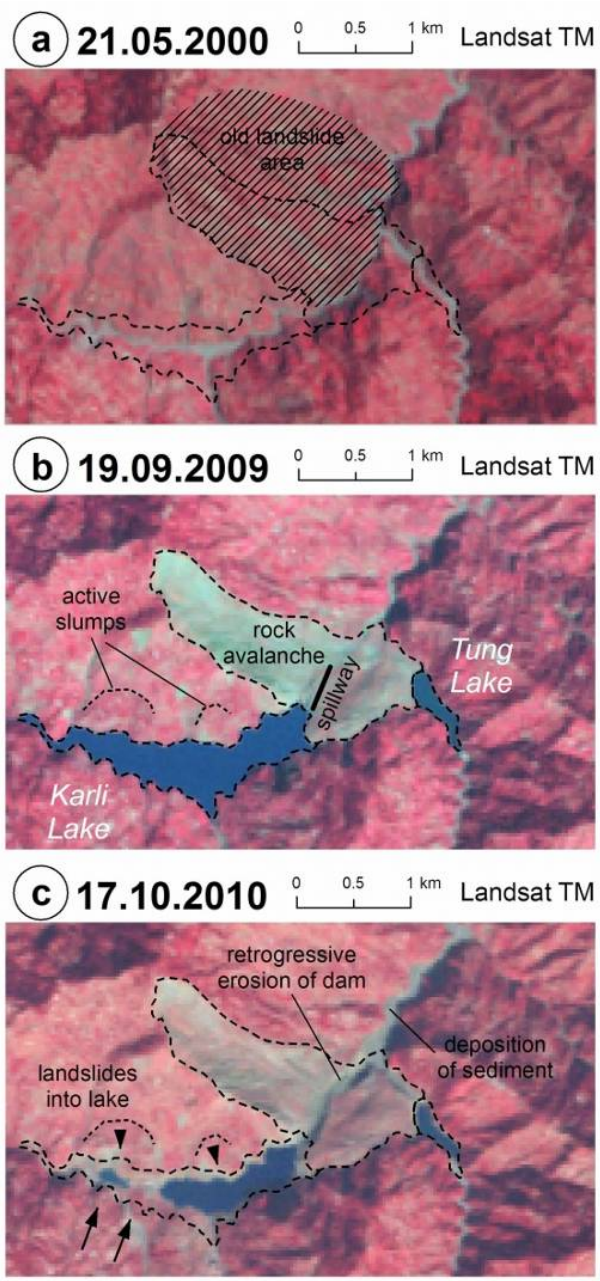

Fig. 7 – History of the Hattian Bala landslide and the related lakes: (a) Situation before the landslide. (b) Hattian Bala landslide, Karli Lake and Tung Lake before the breach of the dam. (c) Situation after the breach of the dam with remnants of Karli Lake and Tung Lake.

Fig. 8 – Eroded breach in the debris deposit of the Hattian Bala landslide below the artificial spillway. Note the landslide scars in the background and the former level of Karli Lake marked by the snow line. Photo taken on February 10, 2010 by Dr. Kausar from the Geological Survey of Pakistan.

3.2 Case study 2: Attabad Dam

The two Great Indus Floods of 1841 and 1858, as well as smaller events such as GLOFs, increased the awareness of the local population which is generally prepared against natural hazards. The village of Attabad registered cracks and slides over a period of several years. On January 4, 2010 a new 45 million m³ rock slide occurred on the orographic right side of the Hunza gorge, destroying part of the village of Attabad (see Fig. 2 for location). The landslide occurred in a tectonically very active region on a local fault just north of the Main Boundary Thrust and was certainly prepared by seismic destabilization. However, no obvious trigger for the rock slide is evident as the weather preceding the event was cold and dry and no significant seismic activity was measured. The area of western Attabad had been declared a high hazard area for a large-scale failure some years earlier and was therefore evacuated at the time of the event.

At the bottom of the valley, lake sediment presumably originating from the 1858 landslide dam lake was mobilized through undrained loading and possibly through liquefaction of clay, overtopping the rock avalanche deposit and leading to two secondary mudflows (NESPAK, 2010). One of them propagated upstream for a distance of approx. 1.5 km, the other travelled 3 km downstream. It hit the settlement of Sarat, claiming 19 lives. 141 houses became uninhabitable (Petley et allii, 2010).

As a consequence of the Attabad event, a huge debris deposit in the valley blocked the Hunza River. The length of the embankment along the river is approx. 2 km, the width up to 400 m.

As it is the case for most landslide dams, the highest point (210 m above the old valley bottom) is situated at the distal part of the deposit. This is where a large amount of the landslide material accumulated. The saddle is located close to the proximal northern slope of the valley, 126 m above the original riverbed. Following the saddle, the slope of the downstream face of the dam is 35° (NESPAK, 2010).

The grain size of the dam material ranges from clay and silt to sand, gravel and large boulders. A large amount of black clay with high organic content was observed in and on the deposit as well as up- and downstream of the dam (remnants of the secondary mudflows). Laboratory tests of

the lacustrine sediment mobilized by the landslide showed a plasticity limit of 21–22% and a liquid limit of 28%. The dam is partly covered by an up to 0.5 m thick layer of fine rock powder. The main part of the dam (the actual rock slide deposit) is gneiss, with intrusions of pegmatite and aplite. Whilst finer material dominates the area around the saddle, the coarser material and large boulders have accumulated at the orographic left (distal) side of the dam. The large boulders are not confined to the top of the embankment, but exist also inside the dam, highly contributing to its stability.

Seepage through the dam developed after about 2 months (Fig. 9) and then increased in a nonlinear way. At that point, internal erosion by seepage was considered a potential failure mechanism.

Fig. 9 – Rock slide dam of Attabad, looking SE. The rock slide originated from the lower left side of the photograph. The photo was taken on May 26, 2010, a few days before overflow started. Note the erosion channel from seeped water and the boundary between the dark lacustrine deposits and the brighter mass of gneiss rock slide debris.

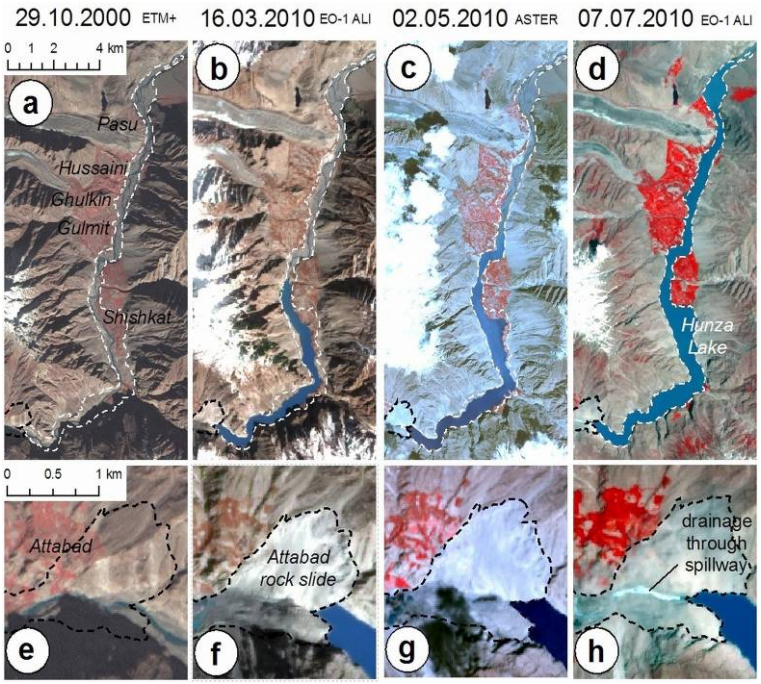

Fig. 10 – Attabad rock slide and the temporal development of Hunza Lake: (a) and (e) Situation before the Attabad rock slide. (b), (c), (f) and (g) Growth of the lake prior to overflow (d) lake extent after overflow. (h) Situation after overflow with drainage through the spillway. The white dashed line shows the extent of the lake on July 7, 2010, the black dashed line shows the extent of the Attabad rock slide. North is up.

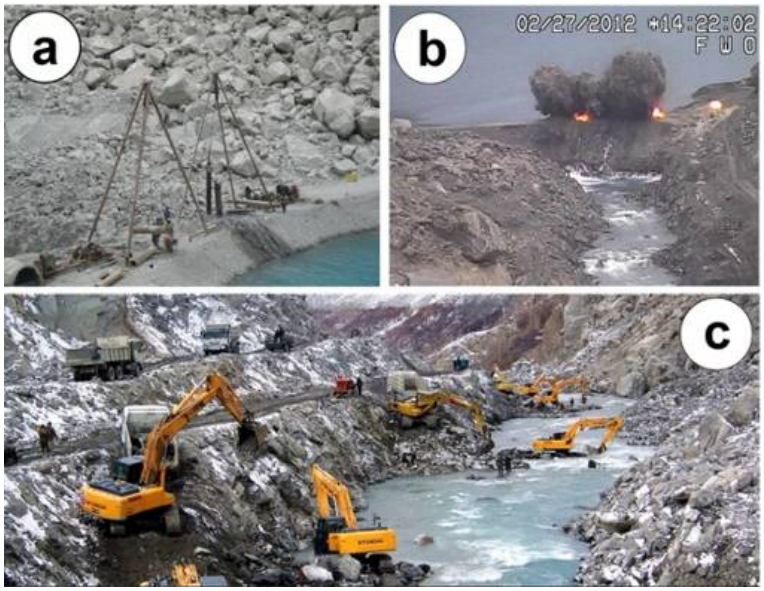

Fig. 11 – Attabad Dam: Front Works Organization (FWO) excavating the overflow channel in order to lower the lake level as well as the hazard of an outburst flood wave. (a) Coffer dam to hold lake water back with drilling rigs for installing explosives. (b) Blasting coffer dam to let the water erode the artificial channel. (c) Excavators working on deepening the channel. The work is slow despite the heavy machinery. It can be done stepwise only during the dry season. Note the large gneiss boulders in a clayey matrix of fine debris mixed with lake sediments, which prevent the channel being eroded. Photos courtesy of FWO.

In order to decrease the overall volume of the lake and to regulate the future flow over the dam, the National Disaster Management Authority of Pakistan (NDMA) oversaw the construction of an artificial spillway at the saddle of the embankment. The result was a narrow channel with a bottom width of about 1 m and a depth of 14 m, mainly in the silty clay of the lake deposit.

Figure 10 illustrates the temporal development of Hunza Lake, monitored by the NDMA. Due to the morphology of the valley, which broadens farther upstream of the dam, the filling rate of the lake was initially high and then decreased with time. A slight increase in the filling rate took place in spring 2010 due to snow and glacier melt. In the night of May 28 to May 29, 2010 the dam was overtopped and drained through the constructed spillway. At that point the lake level at the spillway was 111.41 m above the original valley bottom. Overflow increased slowly at first, still allowing for an increase in lake water level of up to 50 cm per day. The spillway underwent retrogressive erosion with almost no basal down cutting. On June 5, inflow and outflow of the lake reached a balance at a lake level of 115.21 m above the original valley bottom. In May 2011, erosion at the outflow of the lake was still controlled by large boulders in the dam. Blasting efforts did not significantly alter this situation (Fig. 11).

When overflow started, the lake had reached a length of 21 km and an approximate volume of 450 million m^3. In the middle of July 2010, Hunza Lake was about 22 km long, covered an area of 12 km^2 and had a volume of almost 600 million m^3 (Kargel et allii, 2010). The main reason for the further growth of the lake after the onset of the overflow was the higher inflow during summer.

Flooding of the area upstream of the dam led to the inundation of 240 houses in 5 villages. 23 km of the Karakorum Highway were destroyed. 25,000 people living upstream of the dam suffer from lack of economic activity and items of daily sustenance.

3.3 Case study 3: Siachen-Gayari Ice/Rock Avalanche

On 7 April 2011, a snow avalanche from the Saltoro Range hit a northern parent glacier below Bilafond Glacier in the Siachen Region in Jammu Kashmir, Pakistan (see Fig. 2 for location). The resulting ice avalanche entrained material from a lateral moraine and overran the Gayari military camp. 139 people were buried under the deposit of snow, ice, rock and debris which covered an area of more than 1 km² to a depth of up to sixty metres. Large blocks were embedded in a concrete-like matrix of ice and crushed rock with grain sizes down to silt fraction (Fig. 12, Fig. 13).

Several smaller avalanches from adjacent mountains followed after the main slide. Even though, due to their limited extent, they caused no additional damage, these slides hampered the search operations. The compacted debris cone impounded a lake with a surface area that over time increased to 25 ha. Excavating a drainage channel was necessary in order to reduce the hazard of an outburst flood putting the rescue works as well as the population and infrastructure downstream at risk (Fig. 14). The excavation efforts were successful and an outburst flood was avoided.

Due to a concerted effort by the Pakistani Army seconded by rescue teams from Germany, Norway, and Switzerland, the number of recovered bodies is increasing each day. Around 450 engineers and workers, with heavy equipment, were working around the clock whenever possible. Simultaneous efforts were undertaken to tackle effects of intruding water on site such as the inundation of rescue excavations, erosive cuttings and crevasses. This water was slowing down the pace of rescue efforts.

Fig. 12 – Siachen-Gayari ice/rock avalanche, looking NW: the remaining tongue of the glacier, the capped moraine, the ice/rock debris-cone/dam and the beginning of impounding are visible on this photograph. The buried camp is situated on the left side of the picture, where also the spillway was dug out. Photo taken by Pakistan Army shortly after the event.

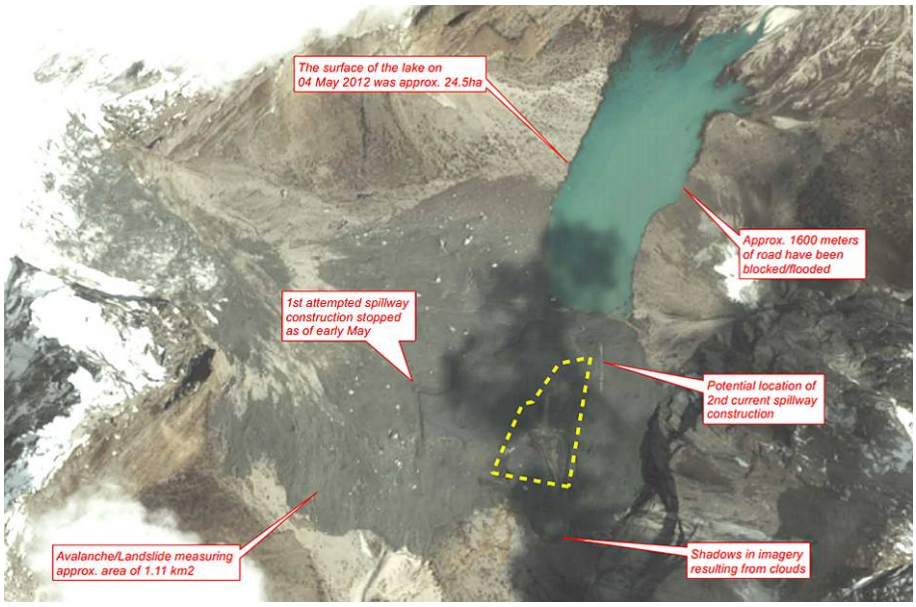

Fig. 13 – UNOSAT poster used as base for decision making. The avalanche originated in the firn area of the Saltoro Range on the left side of the scene, entraining ice from the seracs and till from the lateral moraine on the orographic right side of the valley. The debris cone/dam and the impounded lake are clearly visible on the post-event scene. Imagery: Ikonos, May 4, 2012.

Fig. 14 – Heavy equipment excavating human remains and the artificial spillway. Photo courtesy of ISPR. Note the compacted debris consisting of ice and crushed rocks. Blasting efforts were not successful.

The Gayari camp was considered a safe place since a 700 years old mosque at the camp site had not been affected by geohazard processes for centuries. However, with global warming, the subsequent retreat of permafrost and glaciers is putting many settlements and activities in high mountain valleys at risk. Therefore, places formerly deemed safe with regard to natural hazards need to be reinvestigated. A brief look at satellite images of Kashmir showed several hamlets, camps and infrastructures located below possibly hazardous glaciers or rock formations, thus being in situations similar to that which led to the tragedy at the Gayari Camp.

4 Challenges for risk mitigation

As demonstrated in the previous chapters, landslide-dammed lakes may drain after a few hours or days, but may also persist for millennia. Even though most dam failures occur in the first few months after their formation, lakes may represent hazards several years later (Karli Lake) or may be at least perceived as such even after 100 years (Lake Sarez). Each stage in the history of a dam requires specific risk mitigation strategies, including a combination of technical and non-technical measures.

Immediate emergency measures have to include the construction of erosion-resistant open spillways or drainage tunnels in order to constrain the lake water level. Such structures reduce upstream flooding and pressure on the dam, allowing for controlled drainage. The finding by Schuster (2006) that some spillways work fine while others fail is supported by the recent cases presented here: the Attabad spillway was still working one and a half years after coming into operation in spite of a rather negative prognosis before. It is often hard to predict the performance of spillways prior to the actual overflow due to a variety of uncertain parameters, particularly regarding the internal structure of the dam.

Furthermore, well-designed spillways still have a limited capacity and are not able to withstand powerful impact waves triggered by mass movements into lakes. In the case of Hattian Bala, such a wave initiated the retrogressive erosion of the dam because of the absence of rip rap or gabions.

Additional non-technical measures are always required. Such include the evacuation of people from possibly affected zones. NDMA reported that in the case of Attabad, 2,692 families living downstream in the district Hunza and Gilgit were evacuated to 25 camps. Since such action is very sensitive, the extent of the area to be evacuated has to be well defined. A quick method to categorize the susceptibility of downstream areas to inundation due to an outburst flood is to display their height above the river bed. Such a map can easily be derived using GIS and a digital elevation model, but it does not account for the specific characteristics of the possible flood (inundation height, velocity, travel time). Such parameters require the application of physically-based computer models for the propagation of floods and debris flows. Figure 15 shows the hazard indication map for a possible outburst flood of the Siachen-Gayari lake, based on the assumption of outburst hydrographs, subsequent physically-based modelling with FLO-2D and the height above river. Also in the case of Attabad, a combination of height above river and physically-based modelling was applied in order to support the selection of evacuation areas downstream of the dam.

Figure 16 illustrates a section of the resulting hazard indication map, giving a first impression of potentially affected areas. It has to be strongly emphasized that such maps have to be interpreted with utmost care and with the awareness of the specific capacities and shortcomings of the input data applied in the model as well as of the software used. The comparison of the results from more than one type of model is highly advisable.

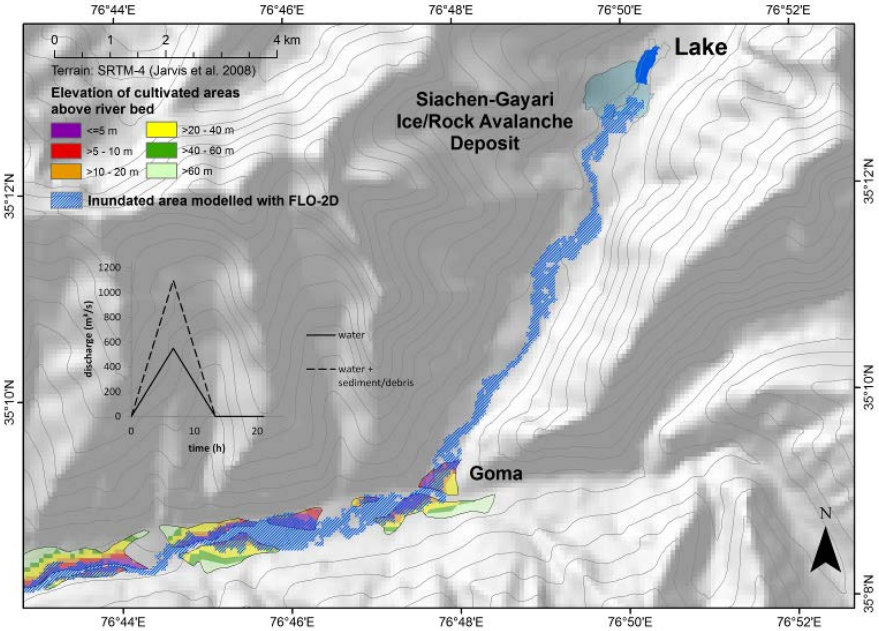

Fig. 15 – Hazard indication map showing the area downstream of the Siachen-Gayari ice/rock avalanche based on heights above river and FLO-2D. The hydrograph applied as input to the modelling of the flood wave propagation considers water bulked with sediment and debris.

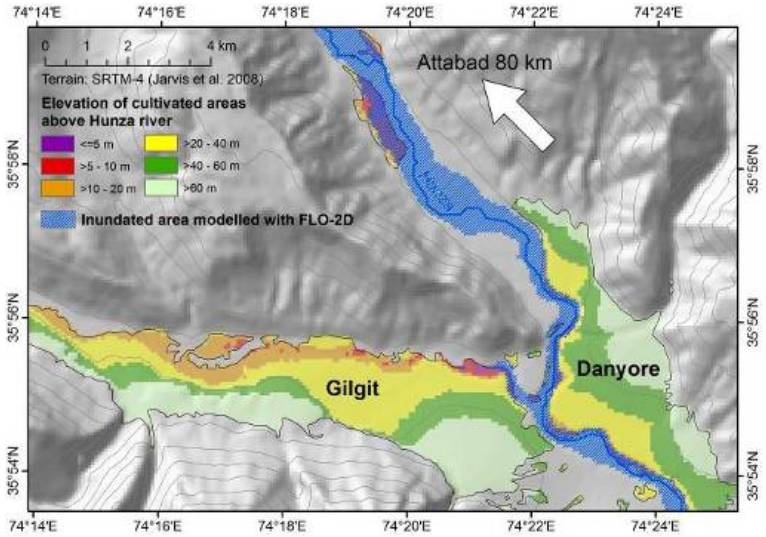

Fig. 16 – Example of a hazard indication map for a possible outburst of Hunza Lake covering a section of the valley approx. 80 km downstream of the dam, based on height above river and modelling with FLO-2D. The planes of Gilgit and Danyore are formed by lake sediments of the former Baktor dam.

Flood propagation modelling often simulates worst-case scenarios, assuming a specific initial situation. Long-term evacuation of downstream areas is generally neither desirable nor feasible from a socio-economic point of view, apart from the fact that the population of evacuation camps yearns to return to their houses. Therefore the prediction and early recognition of specific critical situations is essential, particularly in the case of dams persisting for more than a few weeks or months. However, such tasks have proven to be difficult. Continuous monitoring of possible triggers of dam failures (e.g., unstable slopes or inflow into the lake) in combination with the

installation of sensors for impact waves and flooding may be highly useful given that (1) the systems are maintained in an appropriate way, (2) they are connected to an operational emergency warning system and (3) the communities downstream are prepared and know how to react in case. Computer models can help to estimate travel times and therefore the period available for evacuation.

5 Conclusions

Landslides are common geomorphologic processes in mountain areas all around the world. Sometimes they block entire valleys and impound lakes which may drain suddenly. Steep and narrow valleys in seismically active zones (like the Pamir of Tajikistan and the Karakoram in Northern Pakistan) are particularly susceptible as geomorphologic and historical evidence has shown along with more recent cases.

Even though there are no means to prevent the formation of landslide dams, the prediction of possible dam failures remains a challenge. Adverse effects on people, property and infrastructures can be alleviated by applying a combination of appropriate risk mitigation strategies, including monitoring, awareness and preparedness building. Using the know-how from former events helps to understand the actual rapid landform change processes.

Acknowledgements

The first author of the present paper was invited to the sites discussed in the article by SDC (Switzerland), FOCUS (Tadjikistan), NDMA (Pakistan) and UN OCHA. Special thanks go to General Ahmed Nadim (NDMA), Kamran Shariff (UN OCHA), Dr. Kausar (Geological Survey of Pakistan) and Mustafa Karim (FOCUS).

References

Casagli N. & Ermini L. (1999) – Geomorphic analysis of landslide dams in the Northern Apennine. Transactions of the Japanese Geomorphological Union, 20: 219–249.

Clague J.J. & Evans S.G. (1994) – Formation and failure of natural dams in the Canadian Cordillera. Geological Survey of Canada Bulletin, 464: 1–35.

Costa J.E. & Schuster R.L. (1988) – The formation and failure of natural dams. Geological Society of America Bulletin, 100: 1054–1068.

Costa J.E. & Schuster R.L. (1991) – Documented historical landslide dams from around the world. U.S. Geological Survey Open-File Report, 91-239: 1–486.

Delaney K.B. & Evans S.G. (2011) – Rockslide Dams in the Northwest Himalayas (Pakistan, India) and the Adjacent Pamir Mountains (Afghanistan, Tajikistan), Central Asia. In: Evans S.G., Hermanns R.L., Strom, A., Scarascia-Mugnozza, G. (eds) – Natural and Artificial Rockslide Dams. Lecture Notes in Earth Sciences, 133: 205–242.

Cornwell K. & Hamidullah S. (1992) – Geomorphic evidence of catastrophic flooding along the middle Indus valley. Geological Bulletin University of Peshawar, 25: 113–121.

Dunning S.A., Mitchell W.A., Rosser N.J. & Petley D.N. (2007) – The Hattian Bala rock avalanche and associated landslides triggered by the Kashmir Earthquake of 8 October 2005. Engineering Geology, 93(3-4): 130–144.

Hewitt K. (1964) – The Karakoram Ice Dam. Indus, 5: 18–30.

Hewitt K. (1982) – Natural dams and outburst floods in the Karakorum Himalaya. In: Glen J. W. (ed.) – Hydrological aspects of alpine and high-mountain areas. IAHS Publication, 138: 259–269.

Hewitt K. (1998) – Catastrophic landslides and their effects on the upper Indus streams, Karakorum Himalaya, northern Pakistan. Geomorphology, 26: 47–80.

Ischuk A.R. (2004) – Usoy Natural Dam – Problem of Security (Lake Sarez, Pamir Mountains, Tajikistan). NATO – ARW Security of Natural and Artificial Rockslide Dams, June 8–13, 2004, Bishkek, Kyrgyzstan, Abstracts Volume.

Ishuk A.R. (2011) – Usoi Rockslide Dam and Lake Sarez, Pamir Mountains, Tajikistan. Natural and Artificial Rockslide Dams. In: Evans S.G., Hermanns R.L., Strom, A., Scarascia-Mugnozza, G. (eds) – Natural and Artificial Rockslide Dams. Lecture Notes in Earth Sciences, 133: 423–440.

Kargel J.S., Leonard G., Crippen R.E., Delaney K.B., Evans S.G. & Schneider J.F. (2010) – Satellite Monitoring of Pakistan's Rockslide-Dammed Lake Gojal. EOS, 91(43): 394–395.

Konagai K. & Sattar A. (2012) – Partial breaching of Hattian Bala Landslide Dam formed in the 8th October 2005 Kashmir Earthquake, Pakistan. Landslides, 9: 1–11.

Mason (1929) – Indus Floods and Shyok Glaciers. The Himalayan Journal, 1: 10–29.

NESPAK (2010): Dam Break Study of Hunza River near Atabad. Report to the National Disaster Management Authority, Pakistan.

Petley D., Rosser N.J., Karim D., Wali S., Ali N., Nasab N. & Shaban K. (2010) – Non-seismic landslide hazards along the Himalayan arc. In: Williams A.L., Pinches G.M., Chin C.Y., McMorran T.J. & Massey C.I. (eds) – Geologically Active. CRC Press, London: 143–154.

Richardson S.D. & Reynolds J.M. (2000) – An overview of glacial hazards in the Himalayas. Quaternary International, 65/66: 31–47.

Risley J.C., Walder J.S. & Denlinger R.P. (2006) – Usoi Dam wave overtopping and flood routing in the Bartang and Panj Rivers, Tajikistan. Natural Hazards, 38(3): 375–390.

Schneider J.F. (2009) – Seismically reactivated Hattian slide in Kashmir, Northern Pakistan. Journal of Seismology, 13(3): 387–398.

Schuster R.L. (2006) – Risk-reduction measures for landslide dams. Italian Journal of Engineering Geology and Environment, Special Issue I: 9–13.

Schuster R.L. & Alford D. (2004) – Usoi Landslide Dam and Lake Sarez, Pamir Mountains, Tajikistan. Environmental and Engineering Geoscience, 10(2): 151–168.

Schuster R.L. & Evans S.G. (2011) – Engineering Measures for the Hazard Reduction of Landslide Dams. In: Evans S.G., Hermanns R.L., Strom, A., Scarascia-Mugnozza, G. (eds) – Natural and Artificial Rockslide Dams. Lecture Notes in Earth Sciences, 133: 77–100.

Shroder J.F. (1998) – Slope failure and denudation in the western Himalaya. Geomorphology, 26(1-3): 81–105.

Shroder J.F. & Weihs B.J. (2010) – Geomorphology of the Lake Shewa landslide dam, Badakhshan, Afghanistan using remote sensing data. Geografiska Annaler, 92A(4): 469–483.

Shroder J.F., Cornwell K. & Khan M.S. (1991) – Catastrophic breakout Floods in the western Himalaya, Pakistan. Geological Society of America Abstracts with Programs, 23(5).

Appendix 8

Hazard and risk indication maps

The hazard and risk indication maps are provided separately in the format A0.

Appendix 8.1 Rock slide hazard and risk indication map

Appendix 8.2 Ice avalanche hazard and risk indication map

Appendix 8.3 Periglacial debris flow hazard and risk indication map

Appendix 8.4 Lake outburst hazard and risk indication map